UNIVERSIDADE FEDERAL DO PARÁ
INSTITUTO DE GEOCIÊNCIAS
PROGRAMA DE PÓS-GRADUAÇÃO EM GEOLOGIA E GEOQUÍMICA

TESE DE DOUTORADO Nº 184

A SUCESSÃO CAMBRIANA-SILURIANA DA BACIA DO PARNAÍBA E PROVÍNCIA MINERAL DE CARAJÁS: PALEOAMBIENTE, PROVENIÊNCIA E EXTENSÃO DA GLACIAÇÃO SILURIANA NO GONDWANA OESTE

Tese apresentada por:

IVAN ALFREDO ROMERO BARRERA
Orientador: Prof. Dr. Afonso Cesar Rodrigues Nogueira (UFPA)

BELÉM- PARÁ
2024

Dados Internacionais de Catalogação na Publicação (CIP) de acordo com ISBD
Sistema de Bibliotecas da Universidade Federal do Pará
Gerada automaticamente pelo módulo Ficat, mediante os dados fornecidos pelo(a) autor(a)

R763s Romero Barrera, Ivan Alfredo.

As sucessões Ordovicianas-Silurianas da Bacia do Parnaíba e da Província Mineral de Carajás: paleoambiente, proveniência e extensão da Glaciação Siluriana no Gondwana Oeste / Ivan Alfredo Romero Barrera. — 2024.

xxiii, 186 f. : il. color.

Orientador(a): Prof. Dr. Afonso César Rodrigues Nogueira

Tese (Doutorado) - Universidade Federal do Pará, Instituto de Geociências, Programa de Pós-Graduação em Geologia e Geoquímica, Belém, 2024.

1. Geologia estratigráfica - Paleozóico. 2. Glaciação Siluriana. 3. Drenagem transcontinental. 4. Supercontinente Gondwana. 5. Província Mineral de Carajás. I. Título.

CDD 551.72

Universidade Federal do Pará
Instituto de Geociências
Programa de Pós-Graduação em Geologia e Geoquímica

A SUCESSÃO CAMBRIANA-SILURIANA DA BACIA DO PARNAÍBA E PROVÍNCIA MINERAL DE CARAJÁS: PALEOAMBIENTE, PROVENIÊNCIA E EXTENSÃO DA GLACIAÇÃO SILURIANA NO GONDWANA OESTE

Tese apresentada por

IVAN ALFREDO ROMERO BARRERA

Como requisito parcial à obtenção de Grau de Mestre em Ciências na Área de GEOLOGIA e Linha de Pesquisa ANÁLISE D BACIAS SEDIMENTARES.

Data de Aprovação: 18 / 12 / 2024

Banca Examinadora:

Prof. Dr. Afonso Cesar R. Nogueira
(orientador - UFPA)

Documento assinado digitalmente
gov.br
GELSON LUIS FAMBRINI
Data: 18/12/2024 20:54:00-0300
Verifique em https://validar.iti.gov.br

Prof. Dr. Gelson Luis Fambrini
(membro- UFPE)

Documento assinado digitalmente
gov.br
RENATO SOL PAIVA DE MEDEIROS
Data: 19/12/2024 14:36:00-0300
Verifique em https://validar.iti.gov.br

Prof. Dr. Renato Sol Paiva de Medeiros (UFPA)
(membro - MPEG)

Documento assinado digitalmente
gov.br
FRANCISCO ROMERIO ABRANTES JUNIOR
Data: 19/12/2024 10:43:32-0300
Verifique em https://validar.iti.gov.br

Prof. Dr. Francisco Romério Abrantes Junior
(membro - UFF)

Prof. Dr. Candido Augusto Veloso Moura
(membro - UFPA)

Dedico esse trabalho a minha família,
pelo seu apoio e amor incondicional.

AGRADECIMENTOS

Agradeço primeiramente ao Deus tudo poderoso sempre por tudo, pela saúde e pela oportunidade de me permitir ter novas experiências, conhecer novas pessoas e diferentes locais durante a minha vida.

Expresso meus mais sinceros agradecimentos a todas as pessoas e entidades que tornaram esse trabalho possível.

A Coordenação de Aperfeiçoamento de Pessoal de Nível Superior (CAPES) pela bolsa concedida (Processo 88887.508135/2020-00).

Ao PPGG, à Universidade Federal do Pará, e ao Governo Brasileiro pelo suporte financeiro e estrutural durante o desenvolvimento desta pesquisa.

Ao Prof. Dr. Afonso Nogueira, pela orientação, sugestões, discussões, conselhos e, pela confiança dada para o desenvolvimento desta pesquisa.

Ao Laboratório de Análises Minerais da Superintendência Regional de Belém do Serviço Geológico do Brasil (LAMIN/CPRM), e à técnica Jenny Ortega, pela captura de imagens em catodoluminescência de zircões detríticos.

Ao Laboratório de Geocronologia da Universidade de Brasília, em nome do Prof. Dr. Elton Dantas.

Ao Laboratório de Geologia Isotópica da Universidade Federal do Rio Grande do Sul, em nome da Profa. Dra. Juliana Marques.

Ao Laboratório de Microssonda Eletrônica da Universidade Estadual Paulista (UNESP Campus Rio Claro), em nome do Prof. Dr. George Luiz Luvizotto.

Agradeço aos técnicos: Joelma Soares e Bruno Veras (Laboratório de Laminação), pela ajuda e boa disposição.

Aos Profs. Drs. João Milhomem e José Bandeira, pelas sugestões, discussões e apoio sempre que precisei.

Aos amigos e colegas do PPGG, Fábio Pereira, Renan Fernandes, Leandro Sepeda, Camila Vilar, Luisa Barros, Yasmin Ferro, Renata Veras, Pedro Guilherme, Taynara Martins, Argel Nunes e Meireanny Golçalves, pela amizade e acompanhamento durante o desenvolvimento desta pesquisa.

Agradeço especialmente a minha companheira e amiga Bruna Nogueira pelo carinho, por estar sempre ao meu lado contribuindo para meu aprendizado, e por me ajudar em todos os aspectos da minha vida.

Ao grande amigo que a vida me deu o Prof. Dr. Hugo Bertete Aguirre, pelo acompanhamento e o apoio durante os momentos difíceis.

Agradeço aos meus pais, Esperanza Barrera e Abraham Romero, pelo apoio, investimentos e ensinamentos. Ao meu irmão Manuel Romero por sempre caminhar do meu lado.

Agradeço a todos que, direta ou indiretamente, me auxiliaram a iniciar e concluir este trabalho, cujos nomes não caberiam em poucas páginas.

RESUMO

O registro sedimentar correspondente ao Paleozoico Inferior nas bacias sedimentares do Norte e Nordeste Brasileiro é bem exposto em afloramentos na Bacia do Parnaíba e de forma localizada na Província Mineral de Carajás (PMC). Estes depósitos considerados de idade Cambriano/Ordoviciano-Siluriano, baseado na identificação de estratos glaciais silurianos e idades máximas de deposição (U-Pb em zircão detrítico), representam uma janela de oportunidade para entender a evolução paleoambiental e paleogeográfica do Gondwana Ocidental. Os registros analisados neste trabalho incluem sequências siliciclásticas de 300-400 metros de espessura e extensões laterais que superam os 300.000 Km^2, representativos de depósitos aluviais, glacio-marinhos e deltaicos sobrepostos discordantemente às rochas cristalinas do embasamento. A sucessão basal compreende litoarenitos de granulação grossa e conglomerados fluviais que afloram em bacias intracratônicas e grabens isolados no nordeste do Brasil e na África central. No Brasil, essas unidades correspondem às formações Ipu, Cariri e Tacaratu, enquanto na África são representadas pelos grupos Inkisi, Banalia e Biano. Os conglomerados e arenitos da Formação Ipu, base do Grupo Serra Grande da Bacia do Parnaíba, são aqui correlacionados com os depósitos aluviais correspondentes à Formação Gorotire do Grupo Paredão, isolada em grabens na PMC. Estes depósitos estão recobertos em contato brusco por diamictitos maciços a estratificados, folhelhos carbonosos com estruturas *dumpstone* e *dropstone* e arenitos com estratificação cruzada sigmoidal pertencentes ao membro superior do Grupo Paredão na PMC e à Formação Tianguá na Bacia do Parnaíba. Durante o evento de amalgamação do supercontinente Gondwana no Neoproterozóico-Cambriano, a aglutinação das massas continentais foi controlada pelo desenvolvimento dos principais sistemas orogênicos, com deposição das primeiras sequências sedimentares em bacias tipo rifte. Esses extensos compartimentos geotectônicos subsidentes foram concomitantes com o rearranjo do padrão regional de drenagem e produção de grandes volumes de sedimentos dispersados por sistemas fluviais transcontinentais. No limite Cambriano- Ordoviciano, estes "*Big Rivers*", se estendiam ao longo de amplas peneplanícies por centenas de quilômetros, atravessando os limites das atuais bacias intracratônicas da margem noroeste do supercontinente, e alimentados por diversas áreas-fonte. A arquitetura deposicional destas sucessões consiste em leitos tabulares de conglomerados e arenitos maciços a estratificados lateralmente contínuos por quilômetros, às vezes preenchendo a geometrias concavas-canalizadas. Esses depósitos são organizados em ciclos granodecrescentes ascendentes em escala métrica que refletem a predominância do fluxo em lençol com incisões esporádicas de canal preenchidas por formas de leito bidimensionais e tridimensionais de pequena a grande escala. Fácies de leques aluviais para a Formação Ipu não

foram observados e sugerem erosão do registro da borda da depressão onde aconteceu a deposição destes registros. Da mesma forma, os dados de paleocorrentes unidirecionais preferencialmente para NNW, ultrapassam os limites atuais da Bacia do Parnaíba indicando que a área deposicional era maior do que a atualmente preservada. Durante a transição dos períodos Ordoviciano e Siluriano a porção oeste do supercontinente Gondwana foi submetida a um extenso período glacial, cujo máximo está registrado em rochas de idade Hirnantiana (~445 Ma), em bacias do norte da África. Sendo assim, o evento glacial que iniciou no Ordoviciano médio teria congelado porções continentais que representariam as cabeceiras dos grandes sistemas aluviais na África e no Brasil, dando começo ao declínio destas drenagens transcontinentais. A migração do supercontinente em direção ao Polo Sul foi concomitante com fatores astronômicos tais como mudanças da rotação da terra e diminuição da radiação solar, que favoreceram o crescimento dos lençóis de gelo. O término do evento glacial foi marcado pelo maior aumento do nível eustático do mar registrado na história da terra, gerando expressivas transgressões marinhas, que iniciaram no Llandovery (~443 Ma) e finalizaram no Ludlow (~423 Ma). A fase de degelo propiciou a instalação de sistemas glacio-marinhos pro-glaciais com ampla presença de icebergs, processos de ablação e aumento da zona anóxica dos mares que permitiu uma vasta preservação da matéria orgânica a nível global. A progradação de sistemas deltaicos de desgelo marco o final da deposição da sequência pós-glacial. Estas sucessões estariam bem representadas pelo membro superior do Grupo Paredão e pela Formação Tianguá. A partir da investigação dos registros sedimentares Ordovicianos do nordeste do Brasil e da África central por meio de análises detalhadas da arquitetura fluvial e idades U-Pb de zircão detrítico, surge uma narrativa convincente dos imensos sistemas de drenagem transcontinental que moldaram a paisagem após a amalgamação do supercontinente Gondwana. Adicionalmente, registros paleozoicos são descritos pela primeira vez na PMC, fornecendo assim uma chave fundamental para melhor entendimento estratigráfico, aumentando o entendimento das reconstruções paleoambientais, paleogeográficas e paleoclimáticas do Supercontinente Gondwana durante o Paleozoico Inferior.

Palavras-chave: Supercontinente Gondwana, Paleozoico Inferior, Provincia Mineral de Carajás, Bacia do Parnaíba, Grupo Paredão, Grupo Serra Grande, Glaciação Siluriana, Drenagem transcontinental.

ABSTRACT

The Lower Paleozoic sedimentary record corresponding to the northern and northeastern Brazilian sedimentary basins is well exposed in outcrops within the Parnaíba Basin and locally in the Carajás Mineral Province (CMP). These deposits, considered Cambrian/Ordovician-Silurian age, based on the Silurian glacial strata identification maximum depositional age (U-Pb in detrital zircon), represent a unique opportunity to understand the paleoenvironmental and paleogeographic evolution of Western Gondwana. The records analyzed in this study include siliciclastic sequences with thicknesses ranging between 300–400m and lateral continuity that exceeds 300,000 km², representing alluvial, glacio-marine, and deltaic deposits unconformably overlying crystalline basement rocks. The basal succession comprises coarse-grained lithoarenites and fluvial conglomerates exposed in intracratonic basins and isolated grabens in northeastern Brazil and central Africa. In Brazil, these units correspond to the Ipu, Cariri, and Tacaratu formations, while in Africa, they are represented by the Inkisi, Banalia, and Biano groups. The conglomerates and sandstones of the Ipu Formation, at the base of the Serra Grande Group in the Parnaíba Basin, are here correlated with the corresponding alluvial deposits of the Gorotire Formation in the Paredão Group within isolated grabens in the CMP. These deposits are sharply overlain by massive to stratified diamictites, carbonaceous shales with dumpstone and dropstone structures, and sandstones with sigmoidal cross-stratification belonging to the upper member of the Paredão Group in CMP and the Tianguá Formation in Parnaíba Basin. During the amalgamation of the Gondwana supercontinent in the Neoproterozoic-Cambrian periods transition, the coalescence of continental masses was controlled by the development of major orogenic systems, accompanied by the deposition of the first sedimentary sequences in rift-type basins. These extensive subsiding geotectonic compartments coincided with the reorganization of regional drainage patterns and the generation of large sediment volumes transported by transcontinental fluvial systems. At the Cambrian-Ordovician period boundary, these “Big Rivers” extended across vast peneplains for hundreds of kilometers, overcoming the current intracratonic basin limits along the northwestern margin of the supercontinent and fed by diverse source areas. The fluvial architecture of these successions consists of massive to stratified tabular beds of conglomerates and sandstones, laterally continuous over kilometers and sometimes filling concave-channel geometries. These deposits are arranged in metric-scale fining-upward cycles, reflecting the dominance of sheet flow processes with sporadic channel incisions filled by small- to large-scale two- and three-dimensional bedforms. Alluvial fan facies for the Ipu Formation were not observed, suggesting basinal edges erosion. In addition, unidirectional paleocurrent data predominantly oriented NNW extend beyond the Parnaíba

Basin current limits, indicating that the depositional area was more extensive than presently preserved. During the transition between the Ordovician and Silurian periods, the western portion of the Gondwana Supercontinent experienced an extensive glacial period, climaxing in the Hirnantian (~445 Ma), as recorded in rocks from northern African basins. Thus, the glacial event that began in the Middle Ordovician likely froze continental areas representing the headboard of large alluvial systems in Africa and Brazil, initiating the decline of these transcontinental drainages. The migration of the supercontinent toward the South Pole coincided with astronomical factors such as Earth rotational changes and decreased solar radiation, promoting ice sheet growth. The end of the glacial event was marked by the largest eustatic sea-level rise in Earth history, triggering significant marine transgressions starting in the Llandovery (~443 Ma) and ending in the Ludlow (~423 Ma). The melting phase promotes the development of proglacial glacio-marine systems with widespread icebergs, ablation processes, and an expansion of anoxic zones in seas, allowing extensive global organic matter preservation. The ice-melt deltaic systems progradation marks the end of the post-glacial sequence deposition. These events records are well represented in Paredão Group upper member and Tianguá Formation successions. Through the investigation of Ordovician sedimentary records from northeastern Brazil and central Africa, complemented with detailed analyses of fluvial architecture and U-Pb detrital zircon ages, a compelling narrative emerges of immense transcontinental drainage systems that shaped the landscape after the Gondwana Supercontinent amalgamation. Additionally, Paleozoic records are described for the first time in the CMP, providing a critical key for improved stratigraphic understanding and enhancing paleoenvironmental, paleogeographic, and paleoclimatic reconstructions of the Gondwana supercontinent during the Lower Paleozoic.

Keywords: Gondwana Supercontinent, Lower Paleozoic, Carajás Mineral Province, Parnaíba Basin, Paredão Group, Serra Grande Group, Silurian Glaciation, Transcontinental drainage.

LISTA DE ILUSTRAÇÕES

CAPÍTULO I INTRODUÇÃO

CAPÍTULO III UNRAVELING THE PALEOENVIRONMENT AND PROVENANCE OF CAMBRIAN-SILURIAN SEDIMENTARY SERIES IN THE SOUTHEASTERN AMAZONIAN CRATON: INSIGHTS FROM EARLY PALEOZOIC GEODYNAMIC EVOLUTION AND STRATIGRAPHIC REDEFINITION OF THE CARAJÁS MINERAL PROVINCE

CAPÍTULO V SEDIMENTOLOGY FROM A PRE-VEGETATIONAL BIG RIVER SYSTEM: AN EXAMPLE FROM EASTERN PARNAÍBA BASIN, BRAZIL

LISTA DE TABELAS

CAPÍTULO III UNRAVELING THE PALEOENVIRONMENT AND PROVENANCE OF CAMBRIAN-SILURIAN SEDIMENTARY SERIES IN THE SOUTHEASTERN AMAZONIAN CRATON: INSIGHTS FROM EARLY PALEOZOIC GEODYNAMIC EVOLUTION AND STRATIGRAPHIC REDEFINITION OF THE CARAJÁS MINERAL PROVINCE

SUPLEMENTARY MATERIAL

CAPÍTULO IV THE ORDOVICIAN TRANS-CONTINENTAL DRAINAGES RECOGNITION IN NORTHERN BRAZIL AND CENTRAL AFRICA: IMPLICATIONS FOR THE WESTERN GONDWANA EARLY PALEOZOIC PALEOGEOGRAPHY AND TECTONOSTRATIGRAPHIC EVOLUTION

SUMÁRIO

CAPÍTULO I INTRODUÇÃO

1.1 ORGANIZAÇÃO DA MONOGRAFIA

Esta monografia está organizada em seis capítulos, estruturada em argumentos introdutórios, artigos científicos e considerações finais. Os capítulos introdutórios estão divididos em duas partes; O Capítulo I apresenta a problemática discutida no trabalho, objetivos, área de estudo e as unidades geológicas estudadas; e o Capítulo II aborda as metodologias aplicadas na obtenção do arcabouço sedimentológico e litoestratigráfico das sucessões sedimentares analisadas. Os artigos científicos estão organizados sequencialmente segundo a sua importância. O primeiro artigo (Capítulo III), intitulado "*UNRAVELING THE PALEOENVIRONMENT AND PROVENANCE OF CAMBRIAN-SILURIAN SEDIMENTARY SERIES IN THE SOUTHEASTERN AMAZONIAN CRATON: INSIGHTS FROM EARLY PALEOZOIC GEODYNAMIC EVOLUTION AND STRATIGRAPHIC REDEFINITION OF THE CARAJÁS MINERAL PROVINCE*" aborda os aspectos sedimentológicos e estratigráficos de rochas siliciclásticas presentes na região da Serra do Paredão na PMC, posicionando estas dentro do arcabouço paleoambiental e paleogeográfico do Supercontinente Gondwana. O segundo artigo (Capítulo IV), intitulado "*THE ORDOVICIAN TRANS-CONTINENTAL DRAINAGES RECOGNITION IN NORTHERN BRAZIL AND CENTRAL AFRICA: IMPLICATIONS FOR THE WESTERN GONDWANA EARLY PALEOZOIC PALEOGEOGRAPHY AND TECTONOSTRATIGRAPHIC EVOLUTION*" discute os aspectos sedimentológicos, estratigráficos e de proveniência sedimentar do registro de drenagens transcontinentais Ordovicianas presentes no nordeste do Brasil e na África central, composta por uma espessa sucessão (~300-1000m) de conglomerados e arenitos. O terceiro artigo (Capítulo V) intitulado "*SEDIMENTOLOGY FROM A PRE-VEGETATIONAL BIG RIVER SYSTEM: AN EXAMPLE FROM EASTERN PARNAÍBA BASIN, BRAZIL*" debate a primeira análise de arquitetura deposicional realizada dentro do registro de um mega sistema fluvial no contexto do Supercontinente Gondwana. O Capítulo VI finaliza a monografia apresentando as considerações finais e conclusões do trabalho.

1.2 APRESENTAÇÃO

O supercontinente Gondwana foi conformado pela amalgamação de Gondwana Oriental e Ocidental perto do fim do Neoproterozóico como resultado da orogenia Transbrasiliana- Pan-Africana (Stern 1994, Burke *et al*. 2003, Collins & Pisarevsky 2005, Johnson *et al*. 2011). Os eventos orogênicos foram seguidos por soerguimentos de escala

continental, erosão de bacias intramontanas, formação de riftes, e o desenvolvimento de extensas peneplanícies nas margens oeste e norte do supercontinente (Stampfli & Borel 2002, Cocks & Torsvik 2002, Fernández-Suárez *et al*. 2002, Avigad *et al*. 2005, von Raumer & Stampfli 2008, Stampfli *et al*. 2011). Estas condições propiciaram a deposição de vastas camadas de arenito de idades Cambro-Ordovicianas com um volume estimado superior a 15 milhões de km^3 (Avigad *et al*. 2005). A subsidência térmica produzida após o rifteamento Neoproterozóico tardio (pós-orogênico) teria criado condições ideais para uma ampla geração de espaço de acomodação, permitindo a deposição dos arenitos quartzosos, estimados como a sequência detrítica mais disseminada já depositada na crosta continental (Burke *et al*. 2003). A integração de evidências de campo indica que a sedimentação é consistente com o transporte por meio de sistemas fluviais entrelaçados ao longo do supercontinente com uma direção geral de paleocorrente sul-norte para os depósitos do norte da África e nordeste do Brasil e norte-sul para as sucessões presentes na África central (Avigad *et al*. 2005, Squire *et al*. 2006, Meinhold *et al*. 2013, Timothée *et al*. 2023, Cerri *et al*. 2024). A intensa denudação no Supercontinente e a grande produção de arenitos fluviais coincidiram com mudanças globais significativas, como oscilações na química oceânica, um aumento significativo de pCO2 atmosférico e a explosão biótica cambriana (Knoll 1991, Jacobsen & Kaufman 1999, Berner & Kothavala 2001).

A movimentação do Supercontinente Gondwana para o polo Sul na passagem entre o Ordoviciano Superior para o Siluriano inferior, gerou grandes variações de temperatura a nível global, assim como grandes variações no nível eustático do mar (Munnecke *et al*. 2010, Melchin *et al*. 2012, Scotese 2016). A glaciação que afetou a porção central e oeste do supercontinente, e que iniciara no final do período Ordoviciano detonou o segundo maior evento de extinção (*ordovicianextinction*) já registrado na história da Terra, dizimando grande parte da fauna marinha (Ziegler *et al*. 1977, Finnegan *et al*. 2011, Scotese *et al*. 1999, Sheehan 2001, Barnes 2004).

No norte e nordeste do Brasil estes grandes eventos deposicionais, assim como as variações climáticas e do nível do mar, estão documentadas nas sucessões siliciclásticas dos grupos Paredão e Serra Grande na Provincia Mineral de Carajás e na Bacia do Parnaíba respectivamente. Importantes discussões acerca dos modelos deposicionais, idades e correlações dos registros glaciais depositados no Gondwana Oeste durante o Paleozoico Inferior, tem tomado grande relevância em reconstruções dos

modelos paleoambientais e paleogeográficos. Características como a natureza glacial definida para diamictitos depositados durante o Siluriano Inferior, além do diacronismo a escala continental destes depósitos, auxiliaram em reconstruções paleogeografícas como evidências do deslocamento do supercontinente através da zona polar (Díaz-Martínez & Grahn 2006).

Durante as últimas décadas, muitos trabalhos tiveram como objetivo principal propor o posicionamento estratigráfico dos grupos Paredão e Serra Grande, estes estudos estiveram baseados, majoritariamente em interpretações paleontológicas, correlações estratigráficas e análises de proveniência sedimentar, impulsados principalmente pelas indústrias mineiras e dos hidrocarbonetos (Caputo & Lima 1984, Ramos *et al*. 1984, Pinheiro 1997, Le Hérissé *et al*. 2001, Grahn *et al*. 2005, Cerri *et al*. 2021, Cerri *et al*. 2022).

Até o momento os depósitos siliciclásticos do Grupo Paredão carecem de estudos sedimentológicos e de proveniência sedimentar detalhados, que permitam um melhor entendimento do contexto estratigráfico no qual aconteceu a deposição desta sucessão. A presente pesquisa pretende estudar esta sequência na PMC com base principalmente em análises multe-enfoque de proveniência sedimentar, fácies e sistemas deposicionais. Trabalhos sobre proveniência sedimentar, assim como, trabalhos específicos com enfoque em análise de assembleia de minerais pesados ou geocronologia são raros ou até inexistentes na bibliografia especializada. Desta forma, o presente trabalho permitirá um melhor entendimento do suprimento sedimentar e áreas-fonte para a PMC no Paleozoico inferior, permitindo inclusive tecer considerações paleogeográficas.

A sequência ordoviciana-devoniana da Bacia do Parnaíba apesar de ter sido alvo de diferentes trabalhos de caráter regional nas últimas décadas, em decorrência principalmente da exploração de óleo e gás pela PETROBRAS (Góes *et al*. 1990), carece de estudos sedimentológicos, faciológicos, e de arquitetura deposicional de detalhe que permitam um melhor entendimento estratigráfico desses depósitos. O estudo que será empregado neste trabalho, com base em análise de fácies e arquitetura depoicional, permitirá uma compreensão litoestratigráfica operacional para esta sequência. Permitindo um entendimento mais refinado dos registros geológicos do Grupo Serra Grande na Bacia do Parnaíba, ligados a eventos extremos de temperatura, em um contexto global de

modificações paleoclimáticas e paleogeográficas vigentes durante a deriva do Supercontinente Gondwana.

1.3 LOCALIZAÇÃO E ACESSO À ÁREA DE ESTUDO

A área de estudo encontra se localizada nas regiões norte e nordeste do Brasil, pontualmente nos estados do Pará, Piauí e Ceará (Fig. I.1). No sudeste do Estado do Pará, na região de Bom Jesus, em proximidades do município de Parauapebas (Fig. I.1-C). Ao noroeste do Estado do Ceará, na Mesorregião do Noroeste Cearense, em imediações dos municípios de Ipueiras, Sobral e Santana de Acaraú (Fig. I.1-A). No sudeste do Estado do Piauí, na região da Serra da Capivara, na vizinhança dos municípios de São Raimundo Nonato e São João do Piauí (Fig. I.1-B). Os afloramentos ocorrem na borda geomorfológica leste da Bacia do Parnaíba, onde foram realizadas descrições em exposições do tipo corte de estrada e lajedo, em seções pertencentes ao Grupo Serra Grande. A caracterização dos depósitos sedimentares presentes em grabens isolados na região de Bom Jesus no Estado do Pará, foi realizada a partir da descrição de testemunhos de sondagem cedidos pela empresa Vale.

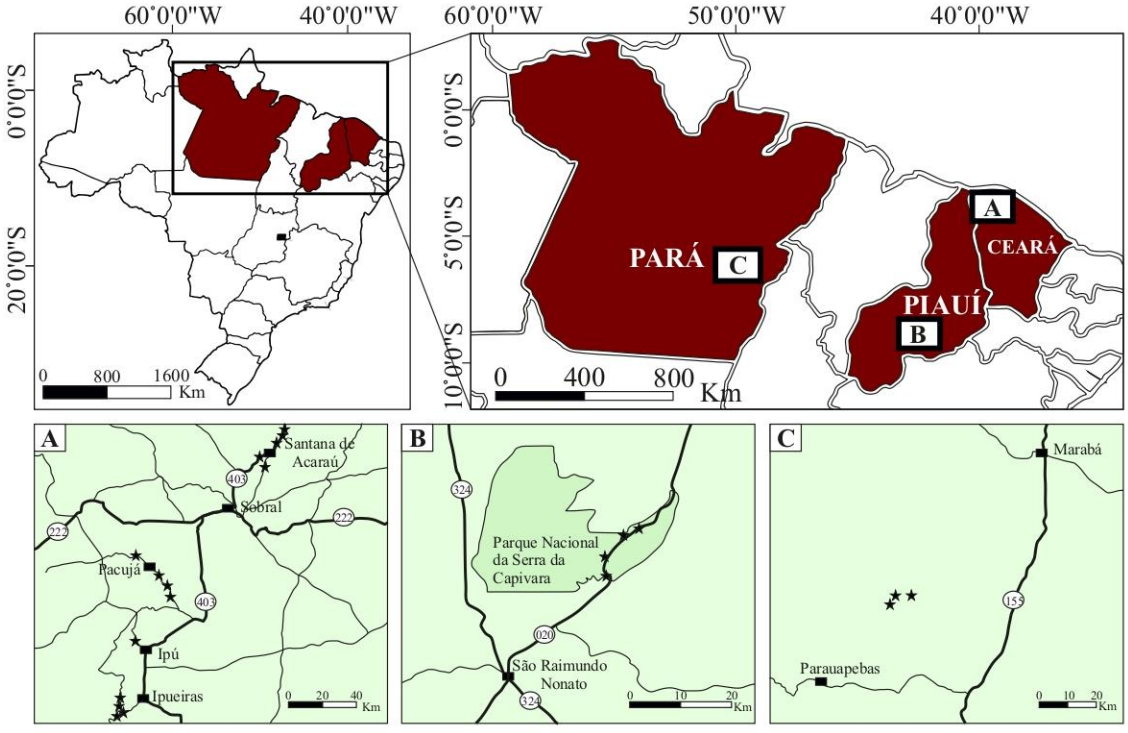

Figura I.1- Mapa de localização da área de estudo. Destacando os municípios, as estradas principais de acesso e a disposição geográfica dos afloramentos.

1.4 OBJETIVOS

Esta pesquisa tem como objetivo principal analisar os depósitos siliciclásticos das Sequências cambrianas/ordovicianas - silurianas da Bacia do Parnaíba e da PMC, com o intuito principal de contribuir no seu entendimento paleoambiental e paleogeográfico. Como objetivos específicos destacam-se:

i) Estudar os depósitos siliciclásticos cambrianos/ordovicianos-silurianos dos grupos Paredão e Serra Grande, utilizando estudos faciológicos e estratigráficos com o intuito de possibilitar a reconstituição paleoambiental;
ii) Correlacionar e tecer considerações paleogeográficas e paleoclimáticas durante o Paleozoico inferior no oeste do Gondwana para as sucessões analisadas;
iii) Definir as áreas-fontes de proveniência sedimentar na PMC durante o Paleozoico inferior;
iv) Inserir a sequência cambriana/ordoviciana-siluriana da PMC nos eventos globais de variações extremas de temperatura do início do Paleozoico;

1.5 CONTEXTO GEOLOGICO REGIONAL

1.5.1 A Provincia Mineral de Carajás

A PMC está localizada na porção oriental do Cráton Amazônico, Norte do Brasil (Almeida *et al*. 1981) (Fig. I.2). Esta província abriga minérios de ferro e óxido de ferro-cobre-ouro (IOCG) de classe mundial, bem como depósitos de manganês, níquel, tungstênio, estanho e ouro-PGE (Tallarico *et al*. 2005, Moreto *et al*. 2015, Bettencourt *et al*. 2016, Marangoanha 2018). A PMC é subdividida nos domínios Rio Maria e Carajás os quais apresentam uma evolução geológica complexa durante os períodos Meso-Neoarqueano a Paleoproterozóico (Machado *et al*. 1991, Feio *et al*. 2012, Feio *et al*. 2013, Tavares *et al*. 2018). A sucessão sedimentar do Domínio Carajás compreende as seguintes unidades da base ao topo: Grupo Grão Pará (formações Parauapebas, Carajás e Igarapé Bahia); Diamictitos Serra Sul; Conglomerados Tarzan; Grupo Águas Claras, dividido nas formações Igarapé Boa Sorte e Igarapé Azul; e o Grupo Paredão.

A Formação Parauapebas de idade Neoarqueana inclui uma ~2–3 km de espessura de rochas vulcânicas félsicas a máficas (Gibbs *et al*. 1986, Macambira 2003, Zucchetti 2007, Cabral *et al*. 2013, Martins *et al*. 2017). A Formação Carajás sobrejacente abrange níveis de formação ferrífera bandada (BIF) com espessura de ~250–300 m (Cabral *et al*.

2013, Luz & Crowley 2012). Ambas as unidades são consideradas de idade Neoarqueana (Olszewski *et al*. 1989, Trendall *et al*. 1998, Martins *et al*. 2017). Os depósitos BIF estão subjacentes a um conjunto de rochas vulcanoclásticas e estratos turbidíticos marinhos de águas profundas pertencentes à Formação Igarapé Bahia (Dreher 2004, Dreher *et al*. 2005, Dreher *et al*. 2008, Tallarico *et al*. 2005, Galarza *et al*. 2008).

Os diamictitos Serra Sul (Araújo & Nogueira 2019) sobrepõem-se de forma discordante ao Grupo Grão Pará. Os conglomerados Tarzan representam depósitos de leque submarino adjacentes aos diamictitos (Araújo & Nogueira 2019). Esta sucessão inclui diamictitos, ritmitos, arenitos e conglomerados depositados em um sistema de leques costeiros subglaciais a submarinos de idade Paleoproterozoica (Tallarico *et al*. 2005, Araújo & Nogueira 2019, Pinheiro 2019, Araújo 2020).

O Grupo Águas Claras, que se sobrepõe de forma discordante a unidades sedimentares mais antigas, compreende siltitos, arenitos e conglomerados. Essas rochas afloram na parte central do Domínio Carajás e apresentam metamorfismo de baixo grau (Araújo *et al*. 1988, Nogueira *et al*. 1995, Pinheiro 1997, Araújo Filho *et al*. 2020). Níveis de ritmitos enriquecidos com manganês, são descritos como Formação Igarapé Boa Sorte (Macambira *et al*. 1990, Macambira 2003). Dados U-Pb em zircão detrítico indicam uma idade máxima de deposição de 2,6 Ga para a Formação Igarapé Boa Sorte (Rossignol *et al*. 2022). A Formação Igarapé Azul consiste em arenitos, siltitos e conglomerados depositados em sistemas fluviais entrelaçados (Araujo & Maia 1991, Melo *et al*. 2019).

A Formação Gorotire e o Grupo Paredão representam sucessões sedimentares que sobrepõem de forma discordante unidades mais antigas no PMC e permanecem não metamorfizadas e sem mineralizações (Pinheiro 1997, Lima & Pinheiro 2001). O Grupo Paredão é predominantemente descrito como litoarenitos vermelhos e conglomerados polimíticos compostos principalmente de seixos de quartzo e seixos de quartzito depositados a partir de sistemas fluviais entrelaçados (Serique & Ramos 1984, Pinheiro 1997). A idade dessas rochas ainda está em discussão, com estimativas variando do Arqueano ao Proterozóico Médio ou mesmo ao Devoniano, baseadas principalmente em correlações estratigráficas com séries sedimentares presentes dentro e fora do PMC (Ramos *et al*. 1984, Pinheiro 1997). A idade de zircão detrítico disponível de 2,01 Ga obtida por Pereira (2009) para a Formação Gorotire sugere apenas a área fonte dos

depósitos. Por outro lado, o Grupo Paredão carece de análises geocronológicas de qualquer tipo.

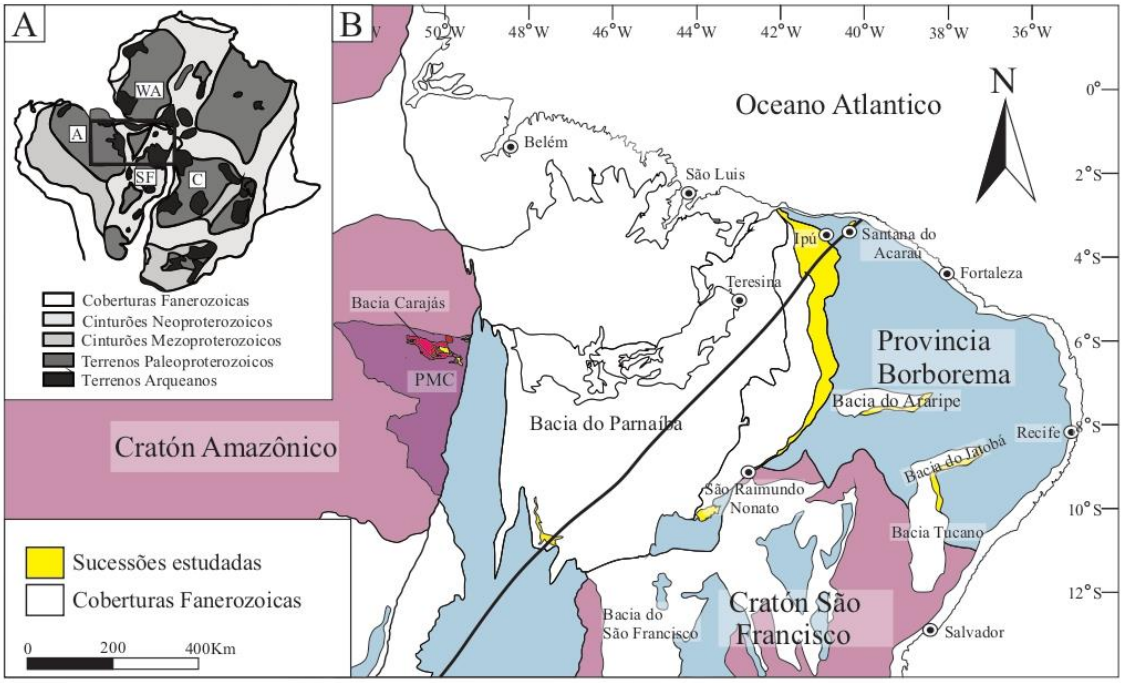

Figura I.2- Contexto geológico. A) Reconstrução pré-drift da América do Sul-África mostrando a localização dos crátons Oeste Africano (WA), Congo (C), Amazônico (A) e São Francisco (SF). B) Mapa geológico simplificado da região norte e nordeste do Brasil.

1.5.2 A Bacia do Parnaíba

A Bacia do Parnaíba, é classificada como uma bacia paleozoica do tipo intra-cratônica, localizada ao norte da Plataforma Sul-Americana, nordeste do Brasil, com área dimensionada em aproximadamente 600.000 Km2, podendo atingir de 3.4 a 3.5 km de espessura nos seus depocentros (Fig. I.2) (Caputo 1984, Daly *et al*. 2014, Vaz *et al.* 2007). Esta bacia, definida como do tipo *sag*, apresenta baixas e localizadas taxas de subsidência, controladas por ciclos orogênicos que não estão relacionados a limites de placas tectônicas (Daly *et al*. 2014). A origem e evolução da Bacia do Parnaíba estão relacionados, principalmente, a eventos tectonomagmáticos, que produziram o início da sedimentação durante o Paleozoico a partir de uma depressão Ordoviciana, provocada por ajustes isostáticos e resfriamento após a fusão de Gondwana (Brito Neves *et al*. 1984, De Castro *et al*. 2014). O embasamento da bacia está representado principalmente por rochas ígneas, metamórficas e sedimentares, com idades que vão desde o Arqueano até o Ordoviciano, formados e/ou retrabalhadas durante o Ciclo Brasiliano (Vaz *et al*. 2007).

Durante o Paleozoico inferior sobre o embasamento definido, teve lugar o desenvolvimento de uma grande superfície erosiva que representa a transição do

embasamento ao preenchimento sedimentar da Bacia do Parnaíba (Vaz *et al*. 2007, Daly *et al*. 2014, Porto *et al*. 2018). A estratigrafia desta bacia pode ser dividida em cinco sequências: Sequência Ordoviciana-Siluriana (Grupo Serra Grande); Sequência Devoniana (Grupo Canindé); Sequência Carbonífero-Triássica (Grupo Balsas); Sequência Jurássica (Grupo Mearim) e Sequência Cretácea (Formações Grajaú, Codó e Itapecuru) (Fig. I.3).

1.5.3 O Grupo Serra Grande

Small (1914) propôs o termo "Série Serra Grande" para englobar uma sucessão sedimentar com uma espessura de até 900 m, composta por calcários, arenitos e conglomerados. Este conceito foi examinado por Kegel (1953), que redefiniu estes limites e propôs o termo Formação Serra Grande, excluindo os calcários dobrados do embasamento, que ocorrem sotopostos e em discordância angular com camadas arenosas. Esta sucessão sedimentar foi elevada à categoria de Grupo por Carozzi *et al*. (1975). Finalmente Caputo & Lima (1984), com base em afloramentos presentes na borda leste da bacia e remanescentes do grupo na bacia de Jatobá, realizaram um posicionamento estratigráfico para o Grupo Serra Grande e separaram este em três formações: Ipu; Tianguá e Jaicós (Fig. I.3).

1.5.4 Formação Ipu

A Formação Ipu encontrasse depositada discordantemente sobre as rochas que compõem o embasamento da bacia e exibe um contato transicional com a Formação Tianguá (Caputo & Lima 1984). Estes depósitos estão compostos principalmente por arenitos, conglomerados, arenitos conglomeraticos e diamictitos, apresentando, na região nordeste da bacia, espessuras de até 300 m (Caputo & Lima 1984). Kegel (1953) descreveu alguns seixos facetados dentro de diamictitos localizados nas porções superiores da Formação Ipu, que tempo depois foram interpretados como de origem glacial. Caputo & Lima (1984), interpretaram os estratos basais da Formação Ipu, como depositados dentro de sistemas fluviais que alimentavam sistemas deltaicos desenvolvidos dentro de ambientes marinhos na porção oeste da bacia.

1.5.5 Formação Tianguá

Rodrigues (1967) utilizou o termo Tianguá para encerrar uma sucessão sedimentar composta por folhelhos negros, siltitos e arenitos finos, descrita em afloramentos dentro da região do município de Tianguá ao nordeste da bacia. Assim o membro Tianguá pertencente à antiga Formação Serra Grande (Kegel 1953), que foi elevado à categoria de formação por Carozzi *et al*. (1975). Caputo & Lima (1984), dividiram a formação em três diferentes membros: (1) folhelho preto a cinza escuro, bioturbado ou laminado e em algumas porções siltosa; (2) arenito fino a médio com intercalações de folhelho; e (3) folhelhos e siltitos intercalados, cinza escuros a verde. A Formação Tianguá tem uma espessura máxima de até 270 metros em subsuperfície e 150 metros medidos em afloramentos na borda leste da bacia (Caputo & Lima 1984). Estes depósitos foram interpretados como depositados dentro de sistemas marinhos rasos e representam grande importância para o posicionamento estratigráfico do Grupo Serra Grande devido à grande diversidade da microfauna presente nestes depósitos (Caputo & Lima 1984, Grahn & Caputo 1992, Grahn *et al*. 2005, Le Hérissé *et al*. 2001).

1.5.6 Formação Jaicós

A Formação Jaicós foi proposta por Plummer (1946), para designar arenitos grossos e conglomerados interpretados em escarpes da serra grande. Carozzi *et al*. (1975), utilizaram o nome Jaicós para designar a seção sedimentar sobreposta à Formação Tianguá que corresponde à porção superior da Formação Serra Grande proposta por Kegel (1953). Esta unidade está constituída principalmente por arenitos grossos a conglomeraticos, interpretados como depositados dentro de ambientes fluviais e deltaicos, com espessuras máximas de até 400 metros em subsuperfície e 200 metros em superfície (Caputo & Lima 1984, Vaz *et al*. 2007). A Formação Jaicós situa-se concordantemente sobrepondo a Formação Tianguá e na sua porção superior encontrasse limitada por uma discordância regional que a separa da Formação Itaim (Grupo Canindé) (Caputo & Lima 1984).

1.5.7 Restrições de idade

Durante as últimas décadas, muitas pesquisas tiveram como objetivo principal estabelecer a posição estratigráfica do Grupo Serra Grande. Esses estudos foram baseados principalmente em interpretações paleontológicas, impulsionadas principalmente pela indústria dos hidrocarbonetos (Caputo & Lima 1984, Le Hérissé *et al*. 2001, Grahn *et al*. 2005). Para as porções superiores Formação Ipu, Grahn *et al*. (2005) definiram uma idade

Llandovery médio, determinada principalmente pela presença de quitinozoários (Cingulochitina bouniensi; Pogonochitina tianguaense n. sp.; e Sphaerochitina palestinaense n. sp.). Análises realizadas nas porções basais da Formação Tianguá com base na identificação de palinomorfos e graptólitos (*Climacograptus cf. scalaris scalaris*) permitiram definir uma idade Llandovery médio (Le Hérissé *et al*. 2001, Grahn *et al*. 2005). Grahn *et al*. (2005), com base em interpretações de quitinozoários (Ramochitina sp.), presentes nas porções superiores da Formação Jaicós, definiram uma idade Praguiano (Devoniano Inferior), para os estágios finais da deposição. Com base nos dados apresentados, é fundamental destacar que a melhor idade definida dentro do Grupo Serra Grande para seu posicionamento estratigráfico é a interpretada para a Formação Tianguá. A ausência de material adequado para datação não tem permitido uma melhor definição da idade destas rochas, no entanto a presencia dos depósitos glaciogênicos na sucessão tem permitido separar estes registros em eventos pré- e pós-glaciais. Os depósitos pré-glaciais estão representados pelas porções inferior e média da Formação Ipu. Para estes depósitos uma idade máxima de deposição obtida a partir de análises U-Pb em zircão detrítico que varia entre 502-485 Ma (Cerri *et al*. 2024), e representa o melhor dado para o seu posicionamento estratigráfico até o momento.

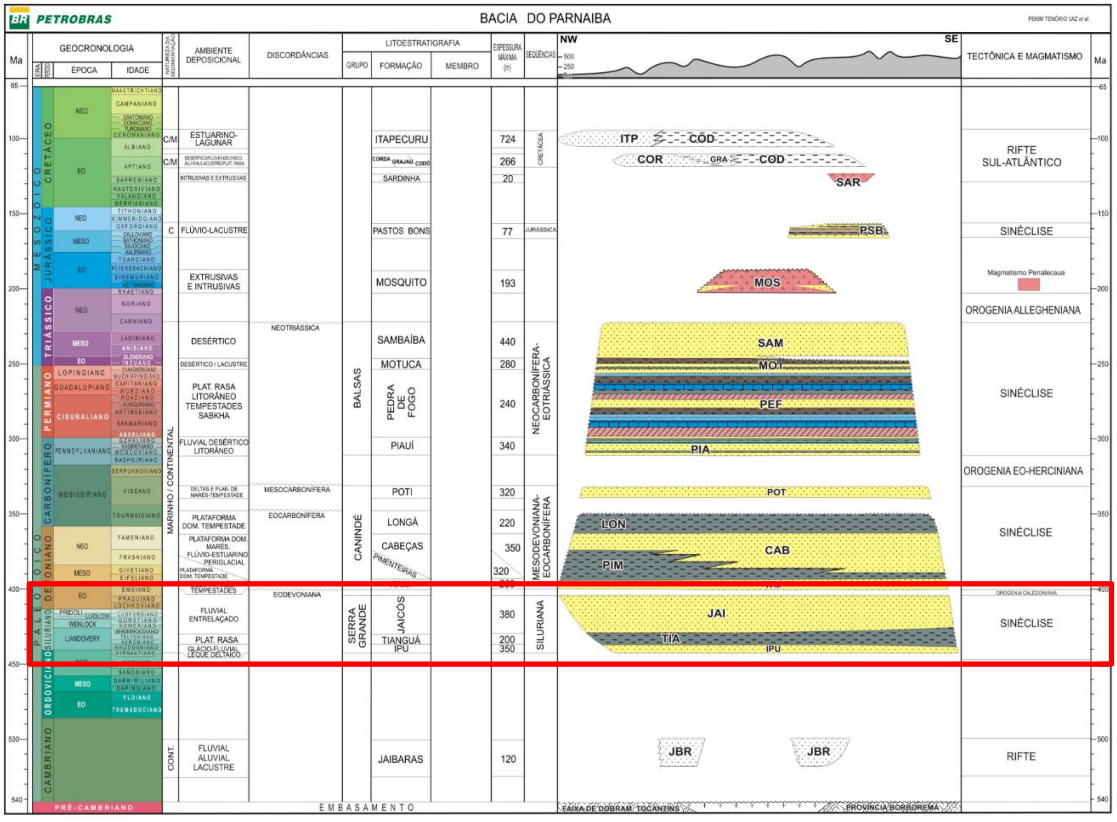

Figura I.3- Carta litoestratigráfica da Bacia do Parnaíba, em destaque o Grupo Serra Grande. Fonte: Vaz *et al*. (2007).

1.6 A GLACIAÇÃO ORDOVICIANA-SILURIANA

O evento glacial Ordoviciano-Siluriano no oeste de Gondwana teve uma duração aproximada de 35 Ma, subdividido em intervalos de crescimento de gelo e ciclos glaciais de derretimento de gelo (estilo glacial Cenozóico) (Ghienne *et al*. 2014, Sproson *et al*. 2022). Nas bacias africanas, dois principais eventos glaciais relacionados ao Ordoviciano Tardio são reconhecidos (Katian e Hirnantiano) (Ghienne *et al*. 2023). O evento glacial Hirnantiano representa o mais extenso e coincide com a segunda maior extinção em massa na história da Terra (Ghienne *et al*. 2014, Pohl *et al*. 2016). Reconstruções paleogeográficas do evento glacial do Ordoviciano tardio, tipicamente mostram um centro de manto de gelo localizado perto do norte da África com uma grande extensão cobrindo Gondwana do Polo Sul até as paleolatitudes médias a tropicais (Finnegan *et al*. 2011, Pohl *et al*. 2016). Dados sedimentológicos são concordantes com modelos paleogeográficos, mostrando um aumento progressivo na amplitude das condições glaciais no final do período Ordoviciano (Ghienne *et al*. 2014, Ghienne *et al*. 2023). Posteriormente, o derretimento do gelo no Hirnantiano, restaurou as condições pré-glaciais do nível do mar. Subsequentemente no Siluriano inferior, extensas transgressões que representam o máximo aumento do nível eustático do mar relacionado à glaciação afetaram a porção oeste do supercontinente (Ghienne *et al*. 2023).

O sequenciamento dos eventos da glaciação durante o Siluriano ainda é debatido, principalmente relacionado às bacias sul-americanas (Díaz-Martínez & Grahn 2006, Barrera *et al*. 2020). Sproson *et al*. (2022), usando dados isotópicos 187Os/188Os, δ7Li, δ13C, δ18O, combinados com um modelo dinâmico de carbono-ósmio-lítio e a resposta do nível do mar, definiram quatro períodos prolongados de alto precipitação de carbono orgânico, redução de CO2 atmosférico, resfriamento e expansão continental da glaciação para o Período Siluriano. Esses intervalos correspondem ao início do Sheinwoodiano, ao Homeriano, ao meio-Ludfordiano e ao final do Prídolí-início do Lochkoviano. Na Plataforma Sul-Americana, um evento glacial generalizado é reconhecido e posicionado no Llandovery inferior a medio, com base em descrições paleontológicas (Grahn 1991, Grahn & Caputo 1992, Grahn 1992, Grahn 2005, Grahn *et al*. 2005, Díaz-Martínez & Grahn 2006). Este evento foi descrito no Brasil nas bacias do Parnaíba (Formação Ipu), Amazonas (Formação Nhamundá) e Paraná (Formação Iapó) (Grahn 1991, Grahn & Caputo 1992, Grahn 1992, Grahn 2005, Grahn *et al*. 2005), e na Bacia Peru-Bolívia (estendendo-se pelo Peru, Bolívia e norte da Argentina) (Formação San Gabán no Peru,

Formação Cancañiri na Bolívia e Formação Zapla na Argentina) (Díaz-Martínez & Grahn 2006).

De acordo com dados paleontológicos de sucessões sedimentares proglaciais distais e pós-glaciais, a sedimentação glacial na América do Sul foi restrita ao início do Siluriano (Grahn 1991, Grahn & Caputo 1992, Grahn 1992, Grahn 2005, Grahn *et al*. 2005, Díaz-Martínez & Grahn 2006). No entanto, sequências glaciais como descritas neste trabalho, e a Formação Pimenta Bueno na Bacia Parecís (Afonso & Nogueira 2018) ainda precisam de mais análises geocronológicas e bioestratigráficas para a definição de sua posição estratigráfica e sua relação com a glaciação. Considerando um "estilo glacial Cenozóico" definido para a glaciação e os dados sedimentológicos e estratigráficos, acreditasse que as condições glaciais foram progressivamente mais significativas no final do Ordoviciano. Depois, no Siluriano, essas condições glaciais foram gradualmente desaparecendo. A transição entre os períodos Ordoviciano e Siluriano representa uma incerteza no declínio ou preservação dos lençóis de gelo. Assim, duas possibilidades de evolução para os mantos de gelo são: (1) os lençóis de gelo do Ordoviciano se derreteram completamente, com uma nova camada de gelo reformada na América do Sul no Siluriano inferior que não atingiu as bacias africanas, ou (2) os lençóis de gelo do Ordoviciano se derreteram parcialmente, abandonando uma camada de gelo reduzida e prolongada apenas na América do Sul. A primeira proposta é mais concordante com os registros transgressivos do Ordoviciano tardio sem influência glacial descritos nas bacias do Amazonas, Paraná e Peru-Bolívia (Grahn 1991, Grahn 1992, Grahn & Paris 1992, Díaz-Martínez & Grahn 2006).

No entanto, o número limitado de afloramentos e núcleos glaciais relacionados a esses eventos na América do Sul também representa um desafio para o desenvolvimento da compreensão da glaciação. Na Bacia do Amazonas, este evento está representado principalmente por diamictitos e arenitos foliados, depositados em ambientes subglaciais (Soares 1998). As análises de palinomorfos encontradas nos diamictitos presentes na Formação Nhamundá revelaram uma idade Llandovery-Wenlock para estes depósitos (Melo 1997, Melo & Steemans 1997). Na Bacia do Paraná, o registro glacial presente na Formação Iapó, está representado principalmente por diamictitos, conglomerados e siltitos (Adôrno 2014), interpretados como depositados a partir de geleiras em águas marinhas rasas (Assine *et al*. 1998). Adôrno (2014) descreve a interfase entre a Formação Iapó e a Formação Vila Maria como transicional, encontrando similaridades nas faunas

fósseis presentes em ambas as formações. Datações absolutas de Rb-Sr realizadas em folhelhos negros basais da Formação Vila Maria indica uma idade de 435,9 ± 7,8 Ma, para esses depósitos (Mizusaki *et al*. 2002).

Durante o Paleozóico Inferior, a Bacia Peru-Bolívia representava grande parte da zona marginal oeste do supercontinente Gondwana (Díaz-Martínez & Grahn 2006). Com ampla distribuição lateral, esta bacia estava presente em muitos países da América do Sul (Peru, Bolívia, Colômbia, Venezuela, Argentina e parte mais ocidental do Brasil) (Díaz-Martínez & Grahn 2006). Durante o Paleozoico inferior está bacia poderia estar conectada ao norte com a Bacia do Amazonas e ao sul com a Bacia do Paraná (Díaz-Martínez & Grahn 2006). Atualmente, registros glaciais do Paleozoico inferior foram identificados nessa extensa bacia sedimentar em países como Peru, Bolívia e Argentina, representados pelas formações San Gaban, Cancañiri e Zapla, respectivamente (Díaz-Martínez *et al*. 2001, Díaz-Martínez & Grahn 2006). Esses registros foram interpretados como inicialmente depositados por geleiras aterradas e posteriormente ressedimentados por fluxos gravitacionais, que transportaram esses sedimentos para as porções mais profundas da bacia (Rodrigo *et al*. 1977, Díaz-Martínez 1997, Díaz-Martínez 1998). Com base em uma análise da fauna de quitinozoários presente no registro glacial, Díaz-Martínez & Grahn (2006) definiram uma idade de Llandovery (Aeronian-Telychiano) para as formações Zapla e Cancañiri.

CAPÍTULO II MATERIAIS E MÉTODOS

2.1 ANÁLISE FACIOLÓGICA

Nas últimas décadas, o estudo acerca de análise de fácies para fins da interpretação paleoambiental ganhou um grande impulso devido principalmente à política adotada pelas empresas petrolíferas de liberar para a comunidade científica conceitos e técnicas de análise de fácies utilizadas para prospecção de hidrocarbonetos. Essa atitude permitiu a sistematização e aperfeiçoamento das técnicas de descrição e da aplicação do conceito de fáceis. O conceito de fácies pouco modificou desde *Gressly*, o primeiro a conceituar o termo em meados do século dezoito, e pode ser definido como as propriedades físicas, químicas e biológicas das rochas que coletivamente, permitem uma descrição objetiva, como também a distinção entre rochas de diferentes tipos (Walker 1992). Numa investigação geológica utilizando a técnica de análise faciológica, são necessários a utilização de dois processos: o descritivo, onde são observadas características físicas, químicas e biológicas das rochas; e o interpretativo, onde deve-se usar analogias com modelos modernos observados diretamente na natureza ou fruto de teorias ou experimentações. Neste trabalho será utilizada a proposta para descrição de fácies segundo Walker (1992), que englobam as principais evidências possíveis de serem detectadas em campo e que envolvem litologia, medidas de paleocorrentes obtidas a partir de estratificações cruzadas em sedimentos arenosos, granulometria, estruturas sedimentares, conteúdo fossilífero e geometria do corpo. Informações sobre a litologia associada a medidas de paleocorrente nos fornecem informações sobre a área-fonte dos sedimentos. Granulometria, grau de seleção, estruturas sedimentares e conteúdo fossilífero nos fornecem indícios sobre o transporte, deposição e ecologia, refletindo o nível de energia e separando, naturalmente, os processos sedimentares. Já a geometria do corpo está relacionada, ainda que parcialmente, à topografia do ambiente deposicional requerendo certo cuidado nas interpretações. A descrição de fácies será auxiliada por perfis estratigráficos e seções panorâmicas (cf. Wizevic 1991), esta última obtida a partir de fotomosaicos. Para localizar com precisão as diferentes localidades visitadas durante a etapa de campo será utilizado o aparelho GPS (*Global Posittioning System*), que determina as coordenadas geográficas e/ou UTM. As diferentes coordenadas das localidades visitadas serão plotadas em mapas de localização obtidos por meio de informações existentes em mapas geológicos da região estudada.

2.2 ANÁLISE DE ELEMENTOS ARQUITETURAIS

A análise de elementos arquiteturais foi originalmente desenvolvida em estudos de ambientes deposicionais aluviais, sendo o procedimento formalizado por Miall (1985, 1996) que define elemento arquitetural como: "(...) um componente de um sistema deposicional equivalente em tamanho ou menor do que o preenchimento de um canal [fluvial] e maior do que uma unidade de fácies individual, caracterizado por uma assembleia de fácies distintiva, geometria interna, forma externa e, em alguns casos, variação vertical [de fácies]".

Para a análise dos elementos arquiteturais será utilizada a metodologia proposta por Miall (1985, 1996) e Miall & Tyler (1991). O procedimento baseia-se no reconhecimento e hierarquização das superfícies limitantes dos estratos sedimentares, considerando parâmetros como: o tipo de contato (erosivo ou gradacional); a forma geométrica (plana, irregular, côncava, convexa); a extensão lateral e a assembleia das fácies associadas. As superfícies representam modificações ou interrupções dos processos de deposição, limitando corpos com geometria definida e significado genético. Esse procedimento é de grande utilidade para a análise de sistemas deposicionais, pois permite o reconhecimento de geometrias e a caracterização de processos não identificados pela simples análise de fácies em perfis. Permite também o agrupamento de associações de fácies segundo um critério descritivo, baseado no reconhecimento e hierarquização das superfícies observadas em afloramentos.

2.3 PROVENIÊNCIA SEDIMENTAR

2.3.1 Determinação da assembleia de minerais pesados

Minerais pesados são acessórios e sensíveis indicadores da proveniência de sedimentos, embora processos como intemperismo, abrasão, fracionamento hidrodinâmico e diagênese, que atuam durante o ciclo sedimentar, podem obscurecer a assinatura original (Morton & Hallsworth 1999, Morton 1985). A determinação de assembléias de minerais pesados seguirá as técnicas clássicas descrita em Mange & Maurer (1992). Os minerais pesados foram concentrados por bromorfórmio e avaliados em lâminas sob microscópio óptico. No estudo de proveniência dos minerais pesados, foram considerados vários fatores que estão intrinsecamente relacionados ao transporte (arredondamento, abrasão) e intemperismo (dissolução, hidratação).

2.3.2 Química Mineral – Microssonda Eletrônica

Duas amostras foram selecionadas para análise de minerais pesados e química mineral em granadas. A separação e preparação dos minerais pesados foram realizadas seguindo os procedimentos padrões descritos por Mange & Maurer (1992). Grãos detríticos de granada foram separados de amostras selecionadas, montados em resinas epóxi, e polidos para serem analisados na Microssonda Eletrônica. A análise quantitativa da granada foi realizada usando a Microssonda Eletrônica JEOL8230 (EPMA) no Departamento de Geologia da Universidade Estadual Paulista. A voltagem de aceleração foi ajustada para 15 kV e a corrente para 20 nA.

A porcentagem molecular de cada granada analisada pode ser calculada uma vez que as composições químicas são obtidas. A partir das composições de óxido medidas, as proporções moleculares foram calculadas com base em 12 oxigênios. O grupo granada contém seis membros finais, incluindo piropo (Prp), almandina (Alm), espessartina (Sps), grossular (Grs), andradita (Andr) e uvarovita (Uva). Morton *et al*. (2004) distinguiram os principais tipos de granada detrítica em sedimentos pela construção de um diagrama ternário de Prp - Alm + Sps - Grs (Mg - Fe + Mn - Ca) para discriminação de rocha fonte (Tipo A, B e C).

2.3.3 Paleocorrentes

A análise de paleocorrentes proporciona determinar o sentido do paleofluxo que reflete a localização do declive principal do terreno, além de contribuir em estudos de geometria dos corpos sedimentares e auxiliar na interpretação paleoambiental e fundamental na determinação da área fonte. A aquisição dos dados de paleocorrentes consistiu na medição da direção e inclinação dos estratos cruzados de estruturas direcionais tais como estratificação e laminação cruzada e estratificação inclinada seguindo as interpretações de fácies prévias. As medições são feitas com bússola magnética, tratadas estatisticamente e plotados em diagramas de roseta. Em relação às formas de leito de pequeno porte, as formas de leito que geram estratificações cruzadas de grande porte geralmente são movidas pelo fluxo principal e possui maior confiabilidade na medição do paleofluxo, não sendo preciso um grande número de medidas.

2.3.4 Geocronologia: Método U-Pb em Zircão detrítico

A datação U-Pb de grãos de zircão detríticos provenientes de sedimentos clásticos tem se tornado um método muito utilizado na correlação sedimentar e estudos de proveniência (Fedo *et al*. 2003). A datação foi realizada em grãos de zircão de arenitos e conglomerados do Grupo Serra Grande. As amostras foram lavadas e desagregadas para posterior separação dos minerais pesados a partir de peneiramento, densidade (bromofórmio) e métodos magnéticos (separador magnético isodinâmico Frantz). A separação dos grãos de zircão foi feita manualmente com auxílio de lupa binocular. Em seguida, os grãos foram colocados em discos com resina epóxi para posterior imageamento com CL e elétrons retroespalhados no microscópio eletrônico de varredura (MEV) no Laboratório de Microscopia Eletrônica de Varredura do Serviço Geológico do Brasil (SBG/CPRM), Belém. As imagens de elétrons retroespalhados e por CL foram obtidas para examinar as características morfológicas dos grãos de zircão, padrões de zoneamento interno e inclusões internas, fraturas ou áreas danificadas que podem prejudicar a leitura do sinal isotópico. Os detalhes da análise isotópica por LA-ICP-MS são descritos em Buhn *et al*. (2009) e Chemale Jr. *et al*. (2012). Normalmente, a precisão analítica fica entre 1,9 e 3,7% com uma exatidão de 0,6 a 3,8%. A correção de contribuição de chumbo comum, quando é efetuada, apoia-se no modelo de composição do Pb proposto por Stacey & Kramers (1975).

O Sistema U-Pb baseia-se no decaimento isotópico, sob taxas diferentes, de dois isótopos-pai (^{235}U e ^{238}U) que geram dois isótopos-filhos (^{207}Pb e ^{206}Pb, respectivamente). Trata-se de um sistema interdependente, bivariante. O mineral mais utilizado para datar rochas pelo sistema U-Pb é o zircão ($ZrSiO_4$), devido às seguintes propriedades: i) O mineral incorpora U, na sua estrutura, em substituição ao Zr, mas pouco ou nenhum ^{204}Pb (comum) durante a cristalização; ii) Tem ocorrência bem distribuída como mineral acessório na maioria das rochas ígneas, metamórficas e sedimentares; iii) Apresenta a propriedade de preservar tanto sua integridade cristalina quanto a assinatura isotópica até cerca de 800º C. A estrutura do zircão também acomoda ^{232}Th, que produz um isótopo de Pb (^{208}Pb) que não é utilizado na determinação de idades.

O princípio básico da representação do sistema baseia-se na curva de referência "Concórdia", a qual mostra em diagrama de eixos coordenados $^{207}Pb/^{235}U$ e $^{206}Pb/^{238}U$ (Wetherill 1956), as variações de razões isotópicas em função do tempo. Resultados analíticos que plotam exatamente sobre a concórdia têm idades 206Pb/238U, $^{207}Pb/^{235}U$

e $^{207}Pb/^{206}Pb$ iguais e podem representar um sistema isotópico fechado e, por essa razão, são chamadas de concordantes. Razões localizadas fora da curva são designadas de discordantes. Nesse caso, um distúrbio isotópico em uma amostra de idade uniforme gera um arranjo de resultados analíticos que definem uma linha reta (discórdia), cuja extrapolação (regressão) trunca a concórdia, nos casos mais simples em dois pontos, os quais correspondem aos interceptos superior e inferior, que assinalam as idades de formação e do distúrbio.

O Laser Ablation (LA) (laser New Wave UP ^{213}Nd: YAG (λ = 213 nm)) é um equipamento acessório ao espectrômetro de massas (ICP-MS) acoplado a um microscópio. Devido a essa característica, possui uma resolução espacial da mesma ordem de grandeza da técnica SHRIMP (Sensitive High Resolution Ion Microprobe) (25-40 μm), permitindo a escolha precisa do domínio pontual restrito do mineral que se pretende analisar. A extração dos íons da amostra é feita por um feixe de laser de alta energia (abrasão) o qual, por sua vez, gera um feixe molecular na forma de aerossol de sólidos e gases que alimentam uma célula de mistura para retenção do sinal, sendo a amostra então dissociada e ionizada em um plasma de alta temperatura, antes de ser analisada no espectrômetro de massa. Estas análises foram realizadas na Universidade de Brasília baixo a supervisão do Prof. Dr. Elton Luiz Dantas.

2.3.5 Estudo isotópico: Sm-Nd em rocha total

Os isótopos de Sm-Nd são reconhecidos como excelentes marcadores de origem sedimentar, proporcionando a caracterização do material detrítico em relação às suas rochas fontes, através do estabelecimento de sistemas isotópicos radiogênicos. A composição isotópica Sm-Nd de sedimentos não depende apenas do decaimento de ^{147}Sm a partir da deposição, mas também das idades das partículas que os compunham (Faure 1986). Estudos de McCulloch & Wasserburg (1978) demonstram que sedimentos tem as razões Sm/Nd muito constantes e similares às das rochas das quais foram derivadas. Concluindo assim, que durante os processos de intemperismo, transporte, deposição e diagênese, os sedimentos não sofrem alterações significativas nas razões Sm/Nd.

O princípio do método radiométrico Sm-Nd consiste na desintegração do ^{147}Sm em ^{143}Nd, através da emissão espontânea de uma partícula α +2 com uma meia vida de 106 Ga. O procedimento para análise inclui basicamente três etapas: dissolução de amostras; separação química e depósito dos elementos Sm e Nd nos filamentos. A etapa

de dissolução das amostras consiste, inicialmente em pesar aproximadamente 50 mg de amostra e misturá-la a 50 mg de traçador misto $^{149}Sm/^{150}Nd$ em um cadinho de Teflon Savillex para posteriormente serem atacadas utilizando os ácidos HNO_3, HF e HCl com o objetivo de recuperar os elementos terras raras (ETR), onde estão presentes os elementos Sm e Nd. A etapa seguinte consiste na extração dos elementos Sm e Nd a partir da solução de ETR anteriormente separada e evaporada, utilizando técnicas convencionais de troca catiônica em colunas de Teflon contendo resina Eichron® Ln-Spec. A última etapa consiste no depósito dos concentrados de Sm e Nd das amostras, os quais após a secagem são dissolvidos em uma solução de 1 ml de HNO_3 e, posteriormente, depositados em filamento duplo de Ta–Re. As análises Sm-Nd foram realizadas com um espectrômetro de massas multicoletor por ionização térmica (TIMS) Triton PlusTM da Thermo ScientificTM, na Universidade Federal do Rio Grande do Sul e em um espectrômetro de massa Finnigan MAT-262 na Universidade de Brasília. A reprodutibilidade dos resultados isotópicos tem sido avaliada por repetidas análises dos padrões de rocha internacionais BHVO-1 e BCR-1. A razão $^{143}Nd/^{144}Nd$ é normalizada para $^{146}Nd/^{144}Nd = 0{,}7219$, e a constante de decaimento usada foi $6{,}54 \times 10^{-12}$ para a correção de discriminação de massa.

2.3.6 Proveniência sedimentar macroscópica

A análise de proveniência sedimentar macroscópica foi realizada através da contagem de clastos dos conglomerados presentes no membro inferior do Grupo Paredão. Deste modo, foram identificados diferentes tipos de clastos de acordo com sua litologia. A finalidade principal desta análise foi identificar possíveis modificações nas áreas ao longo da sucessão. O método de contagem de clastos é uma ferramenta útil na caracterização e identificação de mudanças locais de áreas fonte, podendo ser diretamente correlacionado com litologias originais destas (e.g., Haughton *et al.* 1991, Howard 1993). Assim, a composição dos clastos presentes nas rochas sedimentares refletiriam principalmente áreas fontes locais (e.g., Ferguson *et al*. 1996, Allen & Heller 2011). Por exemplo, variações nos padrões de clastos podem refletir reativações tectônicas de falhas de borda durante a deposição (Whittaker *et al.* 2010).

Os dados de contagem de clastos foram coletados nas camadas de conglomerados, ao todo, foram contabilizados mais de 2700 clastos para o membro inferior do Grupo Paredão. Devido à dificuldade de remoção dos clastos da rocha para obter o valor do volume destes, optou-se apenas pela quantificação dos diferentes litotipos identificados.

2.3.7 Petrografia e caracterização textural

Amostras de arenitos serão analisadas para determinação de aspectos texturais e composicionais, contagem de 300 pontos, por meio de microscopia óptica (seções delgadas), sendo efetuados os seguintes estudos: (1) distribuição granulométrica, o grau de arredondamento e esfericidade; (2) classificação dos arenitos segundo Garzanti (2019); (3) determinação da composição de possível cimento carbonático (calcita e/ou dolomita), através de tingimento de metade da lâmina com uma solução de alizarina vermelha S e ferrocianeto de potássio utilizando o método de Adams *et al.* (1984).

A descrição de diamictito de origem glacial seguiu as metodologias descritas por Busfield & Le Heron (2013, 2018). A análise micromorfológica de diamictitos glaciais, que inclui o reconhecimento de elementos texturais diagnósticos da ação glacial, pode trazer informações importantes sobre a dinâmica glacial. Este tipo de análises auxilia na investigação de eventos glaciais antigos geralmente sujeitos a efeitos tectônicos e metamórficos. A descrição micromorfológica dos litotipos é crucial para identificação e separação de texturas glaciais e efeitos tectônicos secundários.

CAPÍTULO III UNRAVELING THE PALEOENVIRONMENT AND PROVENANCE OF CAMBRIAN-SILURIAN SEDIMENTARY SERIES IN THE SOUTHEASTERN AMAZONIAN CRATON: INSIGHTS FROM EARLY PALEOZOIC GEODYNAMIC EVOLUTION AND STRATIGRAPHIC REDEFINITION OF THE CARAJÁS MINERAL PROVINCE

Artigo submetido em: Journal of Sedimentary Research (05/08/2024)

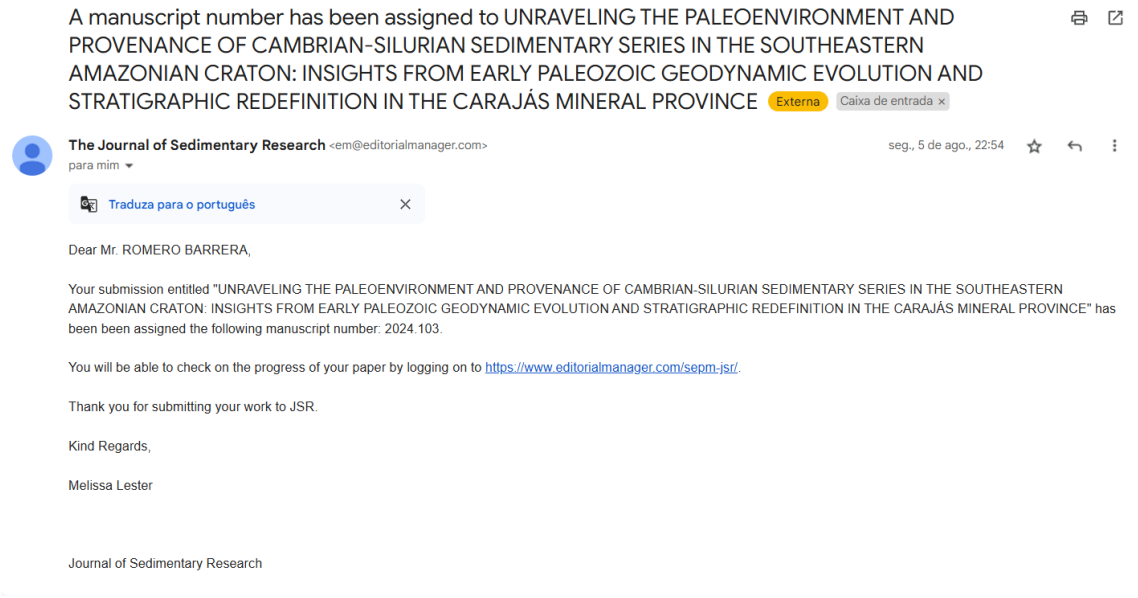

A manuscript number has been assigned to UNRAVELING THE PALEOENVIRONMENT AND PROVENANCE OF CAMBRIAN-SILURIAN SEDIMENTARY SERIES IN THE SOUTHEASTERN AMAZONIAN CRATON: INSIGHTS FROM EARLY PALEOZOIC GEODYNAMIC EVOLUTION AND STRATIGRAPHIC REDEFINITION IN THE CARAJÁS MINERAL PROVINCE Externa Caixa de entrada ×

The Journal of Sedimentary Research <em@editorialmanager.com> seg., 5 de ago., 22:54

para mim

Traduza para o português

Dear Mr. ROMERO BARRERA,

Your submission entitled "UNRAVELING THE PALEOENVIRONMENT AND PROVENANCE OF CAMBRIAN-SILURIAN SEDIMENTARY SERIES IN THE SOUTHEASTERN AMAZONIAN CRATON: INSIGHTS FROM EARLY PALEOZOIC GEODYNAMIC EVOLUTION AND STRATIGRAPHIC REDEFINITION IN THE CARAJÁS MINERAL PROVINCE" has been been assigned the following manuscript number: 2024.103.

You will be able to check on the progress of your paper by logging on to https://www.editorialmanager.com/sepm-jsr/.

Thank you for submitting your work to JSR.

Kind Regards,

Melissa Lester

Journal of Sedimentary Research

UNRAVELING THE PALEOENVIRONMENT AND PROVENANCE OF CAMBRIAN-SILURIAN SEDIMENTARY SERIES IN THE SOUTHEASTERN AMAZONIAN CRATON: INSIGHTS FROM EARLY PALEOZOIC GEODYNAMIC EVOLUTION AND STRATIGRAPHIC REDEFINITION OF THE CARAJÁS MINERAL PROVINCE

Ivan Alfredo Romero Barrera[1], Afonso César Rodrigues Nogueira[1], José Bandeira[1], João Marinho Milhomem Neto[1], George Luvizotto[2], Elton Dantas[4], Renan Fernandes dos Santos[1], Juliana Charão Marques[5], Fernando Mattos[3].

[1] Programa de Pós-Graduação em Geologia e Geoquímica, Faculdade de Geologia, Instituto de Geociências, Universidade Federal do Pará, 66075-110, Belém, PA, Brazil, (ivan.barrera@ig.ufpa.br).

[2] Instituto de Geociências e Ciências Exatas, Universidade Estadual Paulista - Unesp, Avenida 24-A, Bela Vista, 178, Rio Claro, SP, 13506-900, Brazil.

[3] Management of Geology and Drilling of Iron Deposits, Vale S.A., 68516-000 Parauapebas, Brazil

[4] Instituto de Geociências, Universidade de Brasília, Campus Universitário, Asa Norte, 70910-900, Brasília, DF, Brazil.

[5] Instituto de Geociências, Universidade Federal do Rio Grande do Sul, 90010-150, Porto Alegre, RS, Brazil.

ABSTRACT

Multiple deformation and mineralization stages are defined in the southeastern Amazonian Craton. They are related to the geodynamic evolution of the Carajás and Bacajá domains and their relationship with the Araguaia Belt. These tectonic evolutionary events began in the Archean (~2.87 Ga) with the collision of the Carajás and Rio Maria domains and concluded in the Cambrian (~490 Ma) with the collapse of the Araguaia orogen. In the Carajás Domain region, a series of unmineralized and low to un-metamorphosed sedimentary successions represent an anomaly compared to the surrounding Paleoproterozoic basement. Published structural data suggests these records were deposited in different geodynamic contexts, but this differentiation has yet to be specified and remains controversial. To address these issues, we conducted core-based sedimentologic, isotopic (Sm-Nd), petrographic, macroscopic provenance, and heavy mineral studies on Gorotire Formation and Paredão Group sedimentary rocks in the Carajás Domain area. From our findings and prior analyses, we propose the following stratigraphic evolution of the region. The Gorotire Formation, ~400-meter-thick, encompasses meter-scale fining-upward cycles of fluvial sandstones and conglomerates. The Paredão Group is here subdivided into two members. The sequence can be divided into lowermost sediments derived from local basement material erosion and subsequent sedimentation whose isotopic signature is incompatible with the basement. This subdivision corresponds to ~90-meter-thick alluvial fan massive conglomerates for the lower member and ~140-meter-thick glaciomarine massive diamictite and laminated sandstone that change vertically to deltaic sandstone and siltstone organized in meter-scale coarsening-upward cycles for the upper member. Multiproxy provenance analyses show sediment source areas restricted to the Carajás Domain for the Gorotire Formation. Contrastingly, the data suggest the Carajás Domain, Araguaia Belt, and Goiás Magmatic Arc as possible source areas for the Paredão Group. Ratifies the Araguaia Orogen collapse age (~490 Ma) as the maximum depositional age for the sedimentary successions investigated here. In the Carajás Domain region, during the Early Paleozoic, the Araguaia Orogen collapse was followed by an extensional-transtensional episode that allowed the installation of rift basins near the margins of the Amazonian Craton. Provenance and sedimentological data from the fluvial and alluvial fan deposits indicate concomitant palaeogeographical deposition in a rift basin context. Stratigraphic and isotopic data show a drastic transition between the continental and marine settings, suggesting a progressive expansion of basin limits (rift to sag basin?). For the first time, Paleozoic sedimentary

successions are described in the Carajás Domain region. They now provide a fundamental key to better stratigraphic understanding, expanding the tectonic evolution of the Amazonian Craton to the Early Gondwana supercontinent scenario.

Keywords: Amazonian Craton; Carajás Domain; Araguaia Belt; Gondwana Supercontinent; Sm/Nd isotope.

1. INTRODUCTION

Non-orogenic sedimentary successions contain sedimentologic, petrographic, and isotopic information fundamental to discussing the provenance and paleogeography of terranes that are stable and involved in orogenic events (Dickinson and Suczek, 1979; Johnsson, 1993). Provenance studies of siliciclastic sedimentary rocks are traditionally based on paleocurrent analysis and petrographic data (Dickinson and Suczek, 1979; Dickinson et al., 1983; McLennan et al., 1993; Garzanti, 2017). Sometimes, these techniques are inconclusive when applied to sediments lacking flow indicators (e.g., cores) or having undergone extensive diagenetic processes. In cases where the detrital composition is inconclusive, isotopic variations of the Sm/Nd system can be used to make inferences about provenance indicators (Nelson and De Paolo, 1988; Fuenlabrada et al., 2020). It is widely accepted that the Sm/Nd ratio in crustal rocks remains unchanged mainly by chemical weathering, transport, deposition, diagenesis, or anything other than high-grade metamorphism (Taylor and McLennan, 1985). Therefore, the Sm/Nd characteristics of sediments are taken to reflect accurately those of their protoliths and to aid in characterizing source areas (Nelson and DePaolo, 1988; McLennan et al., 1989; McLennan and Hemming, 1992; Fuenlabrada et al., 2020). Reworking sediment with average upper crustal Sm/Nd isotope characteristics considerably diluted the representativity of juvenile detritus (Thorogood, 1990). Consequently, Sm/Nd model ages could be considered a weighted average for the ages of extraction from a mantle reservoir of the protoliths of a detrital component (Fuenlabrada et al., 2020).

The Carajás Mineral Province (CMP) represents an extensive geological compartment subdivided into the Rio Maria and Carajás domains (Dall'Agnol et al., 2013) (Fig. III.1). In this work, we adopt the terminology "domain" and not "basin" for the sinistral strike-slip structure with the occurrence of Precambrian volcano-sedimentary

deposits that reflect the Serra dos Carajás morphology. The term "domain" is justified because the Carajás region comprises several sedimentary successions with distinct lithologies and paleoenvironmental interpretations, indicating that this area was the site of more than one isolated basin.

Isolated sedimentary deposits filling small graben structures are features commonly found in the Amazonian Craton (Araujo et al., 1988). The lack of appropriate dating material and poor age constraints allowed for the inclusion of these deposits in lithostratigraphic contexts without any genetic relationship. Examples of these units are the conglomerate and sandstone succession considered as a Proterozoic cover of the CMP, representative of the Gorotire/Caninana Formation and the Paredão Group (Pinheiro, 1997; Pereira, 2009; Nascimento & Oliveira, 2015) (Fig. III.1). U-Pb detrital zircon analysis in the Caninana Formation indicates 2.0 Ga as the maximum depositional age for these deposits (Pereira, 2009). In contrast, the Paredão Group was previously considered Paleoproterozoic to Paleozoic in age (Pinheiro, 1997; Vasquez et al., 2008). However, the stratigraphic position and geodynamic context in which these sediments were deposited remain controversial.

Core-based facies analysis of the Gorotire Formation and Paredão Group in the Serra do Rabo and Serra do Paredão regions, respectively, allowed the redescription and redefinition of these units and the identification, for the first time, of occurrences of Paleozoic strata in the CMP (Fig. III.1). Facies analysis was combined with multiproxy provenance analysis, based on new whole-rock Sm-Nd isotope data, sandstone petrography, heavy minerals, garnet mineral chemistry, and macroscopic provenance interpretation. Our results suggest that the analyzed sedimentary series are not genetically related to the Archean-Neoproterozoic evolution of the southeastern Amazonian Craton, significantly challenging CMP Proterozoic stratigraphy. The new lithostratigraphic framework also includes the record of glacial events of global significance that affected Western Gondwana during the Early Paleozoic.

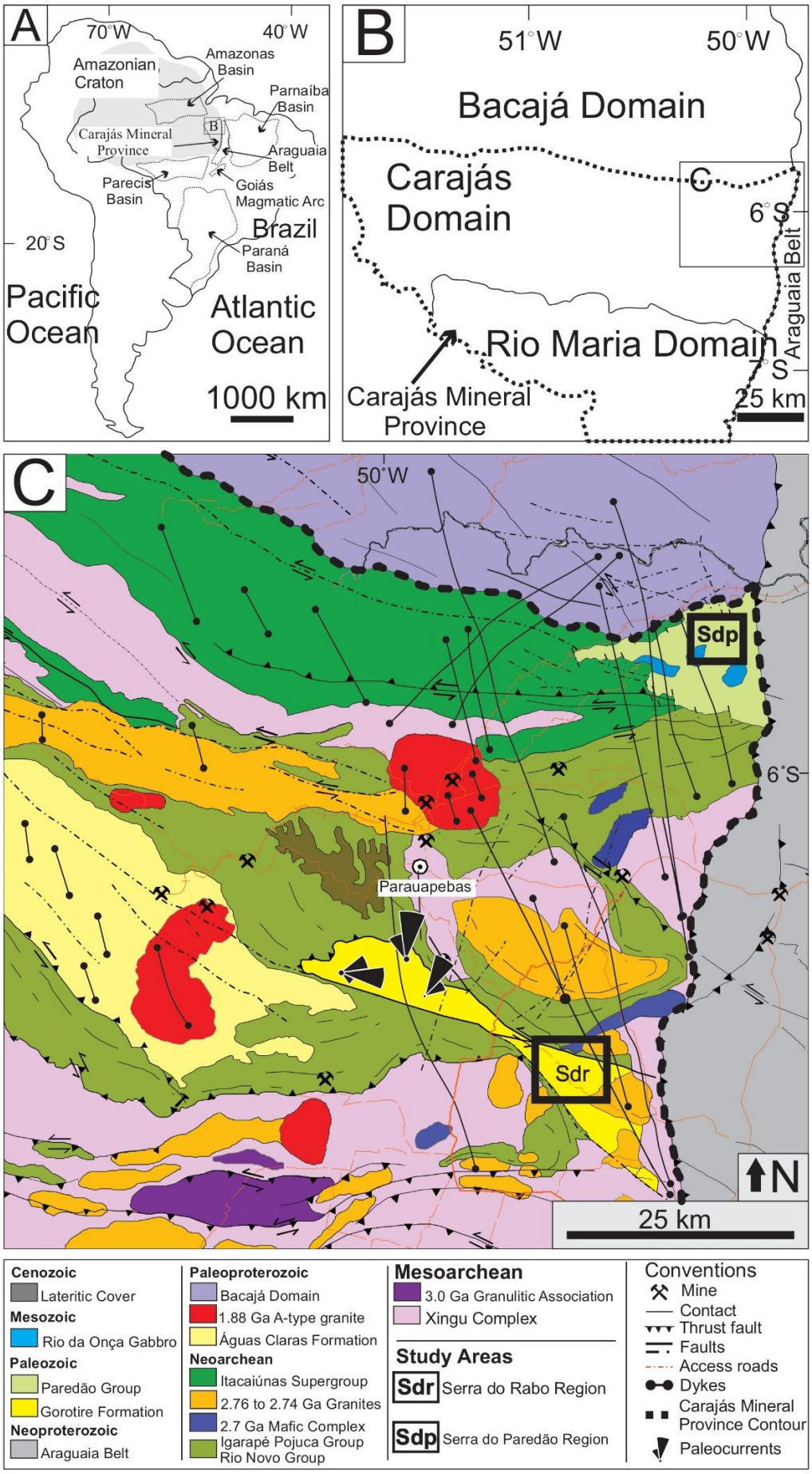
A
70°W
40°W
Amazonian Craton
Amazonas Basin
Parnaíba Basin
Carajás Mineral Province
B
Araguaia Belt
Parecis Basin
Goiás Magmatic Arc
Brazil
20°S
Paraná Basin
Pacific Ocean
Atlantic Ocean
1000 km
B
51°W
50°W
Bacajá Domain
Carajás Domain
C
6°S
Araguaia Belt
Rio Maria Domain
7°S
Carajás Mineral Province
25 km
C
50°W
Sdp
6°S
Parauapebas
Sdr
N
25 km
Cenozoic
Lateritic Cover
Mesozoic
Rio da Onça Gabbro
Paleozoic
Paredão Group
Gorotire Formation
Neoproterozoic
Araguaia Belt
Paleoproterozoic
Bacajá Domain
1.88 Ga A-type granite
Águas Claras Formation
Neoarchean
Itacaiúnas Supergroup
2.76 to 2.74 Ga Granites
2.7 Ga Mafic Complex
Igarapé Pojuca Group
Rio Novo Group
Mesoarchean
3.0 Ga Granulitic Association
Xingu Complex
Study Areas
Sdr Serra do Rabo Region
Sdp Serra do Paredão Region
Conventions
Mine
Contact
Thrust fault
Faults
Access roads
Dykes
Carajás Mineral Province Contour
Paleocurrents

Figure III.1- Location map of the study area. A) South America map showing the location of the Amazon craton, Carajás Mineral Province, Parnaíba Basin, Paraná Basin, Amazonas Basin, and Parecís Basin, in Brazil. B) The Carajás Mineral Province map shows the location of the Carajás Domain. C) The Carajás Domain geological map shows the location of the study area. Modified from Vasquez et al. (2008b). Gorotire Formation Paleocurrents data from Nascimento & Oliveira, (2015).

2. GEOLOGICAL SETTING

The CMP is in the eastern portion of the Amazonian Craton, Northern Brazil (Almeida et al., 1981) (Fig. III.1A). The CMP is bordered to the west by the Proterozoic rocks of the Uatumã Supergroup (Juliani & Fernandez, 2010; Fernandes et al., 2011; Ferreira & Lamarão, 2013); to the east by the Neoproterozoic-Cambrian Araguaia Belt; to the north by the Archean-Paleoproterozoic Bacajá Domain (Santos, 2003; Vasquez et al., 2008); and to the south by the Archean Santana do Araguaia Domain (Vasquez et al., 2008; Corrêa & Macambira, 2014) (Fig. III.1B). This province hosts world-class iron and iron oxide-copper-gold ores (IOCG), as well as deposits of manganese, nickel, tungsten, tin, and gold-PGE (Tallarico et al., 2005; Moreto et al., 2015; Bettencourt et al., 2016; Marangoanha, 2018) (Fig. III.1C).

The Rio Maria and Carajás domains of the CMP underwent a complex geological evolution during the Meso-Neoarchean to Paleoproterozoic periods (Machado et al., 1991; Feio et al., 2012, 2013; Tavares et al., 2018). One of the critical issues concerning the stratigraphy of this region is the diversity of stratigraphic interpretations, with some studies designating the same rock sets by different names (e.g., Docegeo, 1988; Araújo et al., 1988; Araújo & Maia, 1991; Pinheiro, 1997; Tavares et al., 2018; Araujo, 2020) (Fig. III.2). Using the lithostratigraphic procedure respecting term priority and considering zircon detrital age data as maximum depositional ages, we integrate previous tectonic interpretations (Pinheiro, 1997) and modify the latest lithostratigraphic proposal of Araújo et al. (2021).

Despite this study focusing on the youngest conglomerate deposits, we tentatively redefine the sedimentary succession of the underlying Carajás Domain, which now comprises the following units from the base to the top (Fig. III.2): Grão Pará Group (Parauapebas, Carajás, and Igarapé Bahia formations); Serra Sul Diamictites (not "Serra Azul Formation," as these rocks correspond to an isolated succession without a defined stratigraphic position); Tarzan Conglomerates, related to part of the upper Igarapé Cigarra Formation; Águas Claras Group, divided into the Igarapé Boa Sorte and Igarapé Azul formations; and the Gorotire Formation, understood here as the lower part of the Paredão Group. Figure III.2 shows the correspondences with previous lithostratigraphic schemes.

The Carajás Domain comprises ~2.85 Ga Mesoarchean igneous and metamorphic basement corresponding to the Xingu Complex (Machado et al., 1991). The Neoarchean Parauapebas Formation includes a ~2–3-km-thick pile of felsic to mafic volcanic rocks (Gibbs et al., 1986; Macambira, 2003; Zucchetti, 2007; Cabral et al., 2013; Martins et al., 2017). The overlying Carajás Formation encompasses banded iron formation (BIF) strata with a thickness of ~250–300 m (Cabral et al., 2013; Luz & Crowley, 2012). Both units were deposited coevally at ca. 2.75–2.74 Ga (Olszewski et al., 1989; Trendall et al., 1998; Martins et al., 2017). The BIF deposits underlie a set of volcaniclastic rocks and subordinate deep-water marine turbidite strata of the Igarapé Bahia Formation (Dreher, 2004; Dreher et al., 2005, 2008; Tallarico et al., 2005; Galarza et al., 2008).

The Serra Sul diamictites (Araújo and Nogueira, 2019) unconformably overlie the Grão Pará Group. Tarzan conglomerates have been positioned as submarine fan deposits adjacent to diamictites (Araújo and Nogueira, 2019). This succession includes diamictites, rhythmites, sandstones, and conglomerates deposited in a coastal subglacial to submarine fan system (ca. 2.58–2.06 Ga) (Tallarico et al., 2005; Araújo & Nogueira, 2019; Pinheiro, 2019; Araújo, 2020).

The Águas Claras Group, which unconformably overlies older sedimentary units, comprises mudrocks, sandstones, and conglomerates. These rocks crop out in the central part of the Carajás Domain, are commonly folded and faulted, and show very low-grade metamorphism (Araújo et al., 1988; Nogueira et al., 1995; Pinheiro, 1997; Araújo Filho et al., 2020). A rhythmite stratum, locally enriched in manganese, is described as the Igarapé Boa Sorte Formation (Macambira et al., 1990; Macambira, 2003). These rocks include mudrocks and fine-grained sandstone with shale partings rich in organic matter, oxides, and hydroxides of manganese, marl, and manganiferous carbonate (Costa et al., 2005; Costa, 2017). U-Pb dating of detrital zircon grains indicates a maximum depositional age of 2.6 Ga for the Igarapé Boa Sorte Formation (Rossignol et al., 2022). The Igarapé Azul Formation consists of sandstones and siltstones with minor conglomerates (Araujo and Maia, 1991; Melo et al., 2019). It was deposited in a braided fluvial system (Araujo and Maia, 1991; Nogueira et al., 1995; Araújo Filho et al., 2020). Paleocurrent reconstruction suggests a westward migration of the channel belt for the Proterozoic fluvial deposits (Nogueira et al., 1995; Araujo and Maia, 1991). Available zircon data limit the maximum depositional age for the Carajás domain successions to 1.88 Ga from the Carajás Granite (Machado et al., 1991; Teixeira et al., 2018). The 2.6

Ga age represents the maximum depositional age for the Águas Claras deposits found on sandstone, as replicated by various authors (Araújo, 2020; Rossignol et al., 2022). In some areas of the CMP, the Águas Claras Formation unconformably overlies the Grão Pará Group (Fig. III.1). It is younger than 2575 ± 12 Ma, the age provided by monazite dating from the matrix of ore-bearing magnetite breccias belonging to the Igarapé Bahia Formation (e.g., Tallarico et al., 2005).

The Transamazonian cycle (~2.0 Ga) caused the segmentation of the Carajás Domain into different compartments with a complex history of deformation and metamorphism (Macambira et al., 2009; Tavares et al., 2018). Anorogenic granites and dike swarms (~1.88 Ga) (Machado et al., 1991; Teixeira et al., 2018) crosscut the Carajás Domain and represent an essential stratigraphic limit, segregating sedimentary successions deposited before and after this event (Fig. III.2). Geological cross-sections introduced by Tavares et al. (2018) of the Carajás Domain show multistage deformation. However, the deposits ascribed to the Gorotire Formation appear undeformed, overlapping the bulk of deformed and metamorphosed rocks, suggesting a younger age for these deposits. The Gorotire Formation includes sandstones and conglomerates interpreted as alluvial to fluvial deposits (Lima & Pinheiro, 2001).

The Gorotire Formation and Paredão Group represent sedimentary successions that unconformably overlay older units in the CMP and remain low- to unmetamorphosed and unmineralized (Pinheiro, 1997; Lima & Pinheiro, 2001). The Paredão Group is predominantly described as reddish lithoarenites and polymictic conglomerates composed mainly of quartz pebbles and quartzite cobbles deposited in a braided fluvial system (Serique & Ramos, 1984; Pinheiro, 1997). The age of these rocks is still under discussion, with estimates ranging from the Archean to the Middle Proterozoic or even the Devonian, based mainly on stratigraphic correlations with sedimentary series present within and outside the CMP (Fig. III.2) (Ramos et al., 1984; Pinheiro, 1997). The available detrital zircon age of 2.01 Ga obtained by Pereira (2009) for the Gorotire Formation only suggests the source area. On the other hand, the Paredão Group lacks geochronological analysis of any kind.

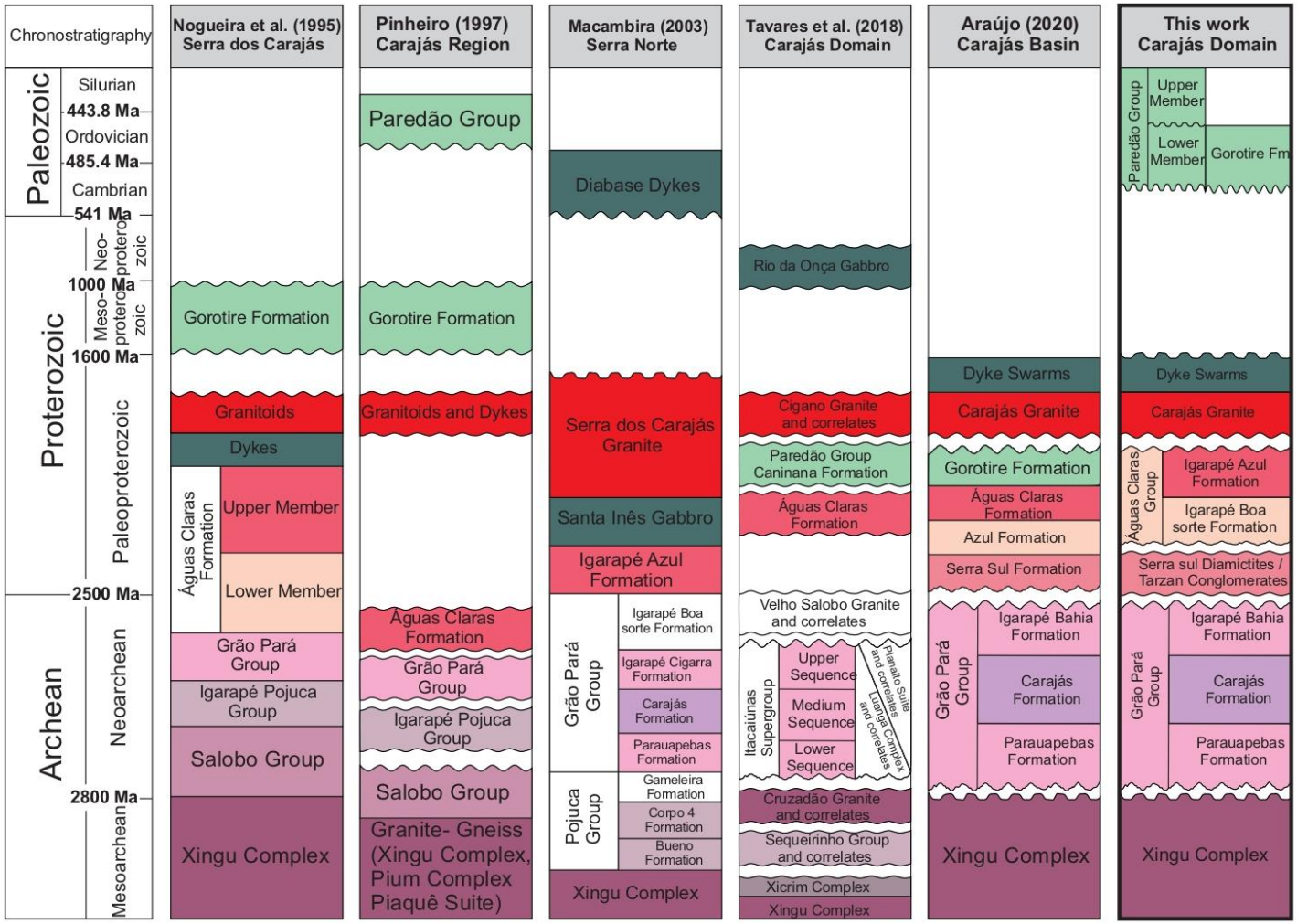

Figure III.2- Comparison between the main stratigraphic proposals for the Carajás region (southeast of the Amazon Craton, Brazil).

The Carajás Domain has been interpreted as a strike-slip, intracratonic, and foreland basin (Araújo et al., 1988; Pinheiro, 1997; Araújo et al., 2021). The foreland basin model requires further discussion, as diagnostic structures such as nappes have not been described so far, and oblique thrust faults and folds have been associated with local transpression related to the Carajás Fault (Pinheiro & Holdsworth, 1997; Holdsworth & Pinheiro, 2000).

3. MATERIAL AND METHODS

In this study, we conducted a drill core-based stratigraphic and provenance analysis from the Gorotire Formation (well-162, ~400m-deep) and Paredão Group (well-Pkc, ~293m-deep) in the Serra do Rabo and Serra do Paredão regions, respectively (Fig. III.1C). Vale S.A., a mining company in Parauapebas County in northern Brazil, made the drill cores available. We selected the drill cores with more lithologic heterogeneities and clear bed contacts. Each sedimentary succession was logged bed by bed using outcrop-based facies analysis techniques (lithologies, sedimentary structures, and vertical variations). The bed thicknesses were categorized as follows: very thin-bedded (<1 cm), thin-bedded (1–10 cm), medium-bedded (10–30 cm), thick-bedded (30–100 cm), and very thick-bedded (>100 cm) (Ingram, 1954). The facies analysis followed the methodology proposed by Walker (1992, 2006). Paleoenvironmental reconstructions are proposed based on the detailed study of the sedimentary facies, understanding the depositional processes, and recognizing genetically related sets of facies, subsequently organized in facies associations that reflect different depositional systems. The facies were categorized mainly based on lithologies, and the sedimentary processes were analyzed through the structures and textures observed in the different lithofacies.

We sampled 24 small rock pieces from the investigated drill cores to assess vertical grain-size variation. Petrographic and Sm-Nd isotopic analyses were carried out to enhance the field description. The thin sections were prepared and analyzed in the Laboratory of Petrography of the Federal University of Pará. The quantification and characterization of the primary and authigenic mineralogies of the sandstones were based on the petrography of thin sections under an optical microscope (Galehouse, 1971). In addition, the presence of glaciotectonic microstructures in diamictites, such as alignment, crushing, and rotation of grains, micro-faults, and micro-folds, was tested (see Van der Meer, 1993; Menzies et al., 2016; Busfield & Le Heron, 2018).

Two samples were selected for heavy mineral analysis. Separation and preparation of the heavy minerals were performed by following standard procedures described by Mange & Maurer (1992). Detrital garnet grains were separated from selected samples, mounted in epoxy resins, ground, and polished for electron probe micro-analyzer. Quantitative analysis of garnet was carried out using a JEOL8230 Electron Probe Microanalyzer (EPMA) at the Department of Geology of the São Paulo State University, Brazil. The acceleration voltage was set to 15 kV and the current to 20nA. The analyzed elements, operating conditions, and detection limits are presented in Table III.1.

Table III.1-Summary of EPMA operating conditions. Count times were equally distributed between peak and background positions. L alpha lines were used for all elements.

Element	Standard	Analyzing Crystal	Count time (s)	Detection Limit (ppm)
Si	Orthoclase	TAP	10	280
Al	Anorthite	TAP	20	165
Mg	Olivine	TAP	20	145
Ca	Wollastonite	PET	20	210
Ti	Rutile	PET	30	140
Cr	Cr2O3	PET	20	180
Fe	Fe2O3	LIF	10	380
Mn	Rhodonite	LIF	20	270

For the Nd isotope analysis, 24 samples were collected to cover the stratigraphic record, considering facies variations. Conglomerate and diamictite matrix, siltstones, and sandstone samples were selected whenever possible because coarse-grained samples often yield biased isotopic compositions (e.g., Frost & Winston, 1987; Evans et al., 1991). The analysis was conducted at the Geochronological Laboratories of the Federal University of Rio Grande do Sul, Brazil, and at the University of Brasília, Brazil. Samples were crushed, powdered, and dissolved in an HF-HNO_3 mixture in high-pressure Teflon vessels. A ^{150}Nd–^{149}Sm tracer was added to determine Nd and Sm concentrations. The REEs were then extracted by cation exchange chromatography, and Sm and Nd were subsequently separated following Gioia and Pimentel (2000) procedure. The total procedural blanks are less than 100 pg. Sm and Nd analyses were performed using a triple filament assembly in a Thermo ScientificTM TRITON thermos-ionization mass spectrometer (TIMS) at Universidade Federal do Rio Grande do Sul and in a Finnigan MAT-262 mass spectrometer at Universidade de Brasília. The Nd and Sm isotopes were measured in static mode. The Sm and Nd concentrations and the $^{147}Sm/^{144}Nd$ ratios have

an accuracy of 0.5% (SE), which corresponds to an average error on the initial ε_{Nd} value of ±0.5 epsilon units based on repeated measurements of standard JNdi and BHVO-2. The age model was calculated using the values proposed by DePaolo (1981) for the depleted mantle. Considering the revised stratigraphical scheme adopted here, the εNd values were recalculated for the Gorotire Formation and Paredão Group (Fig. III.2).

4. STRATIGRAPHY AND PROVENANCE ANALYSIS

The Paredão Group represents the first unit of the cover sequence (below Mesozoic and Cenozoic strata). It is defined in the Serra do Paredão Region, where lower and upper members are differentiated. A single unit, the Gorotire Formation, has been described in the Serra do Rabo Region. The sedimentologic, stratigraphic, and provenance data related to these sequences are presented below.

4.1 GOROTIRE FORMATION SEDIMENTOLOGICAL ASPECTS

Description. −The Gorotire Formation is ~400m thick (Fig. III.3). This sedimentary succession overlaps discordantly with the BIF deposits from the Carajás Formation. It comprises finning-upward cycles, with thicknesses ranging from 2m to 20m (Fig. III.3). Conglomerates at the cycling base that radiatively pass for sandstones (Fig. III.3). An upward progressive cycle thickness reduction was identified from tens of meters to a maximum of 7 meters with sharp contacts between individual cycles. Levels of clast-supported polymictic conglomerates with thicknesses ranging from 0.5-2 m exhibit massive bedding (Fig. III.3). The clasts vary in size from granule to boulder, with a matrix constituted of coarse-grained sand (Fig. III.4). The clasts mainly comprise quartz, BIF, granite, gneiss, quartzite, schist, sandstone, and mudrock from the underlying units (Fig. III.4A to E). The clast shapes are generally rounded. Medium to coarse-grained sandstone intervals, up to 15m-thick, exhibit trough crossbedding, tabular crossbedding, low-angle cross-bedding, and even parallel plane stratification (Fig. III.4 F to J). The sandstones are moderately well-sorted. The rock framework presents sub-angular to sub-rounded grains with low sphericity. The grains comprise quartz, feldspars, quartzite, slate, BIF fragments, granites, silex, schist, gneiss, sandstones, and mudrocks (Fig. III.4K to N). The cement compositions are mainly silica and clay minerals; however, coats of iron oxide and hydroxides surrounding quartz grains are also present (Fig. III.4K and N). Mudrock beds and small-scale structures were not found.

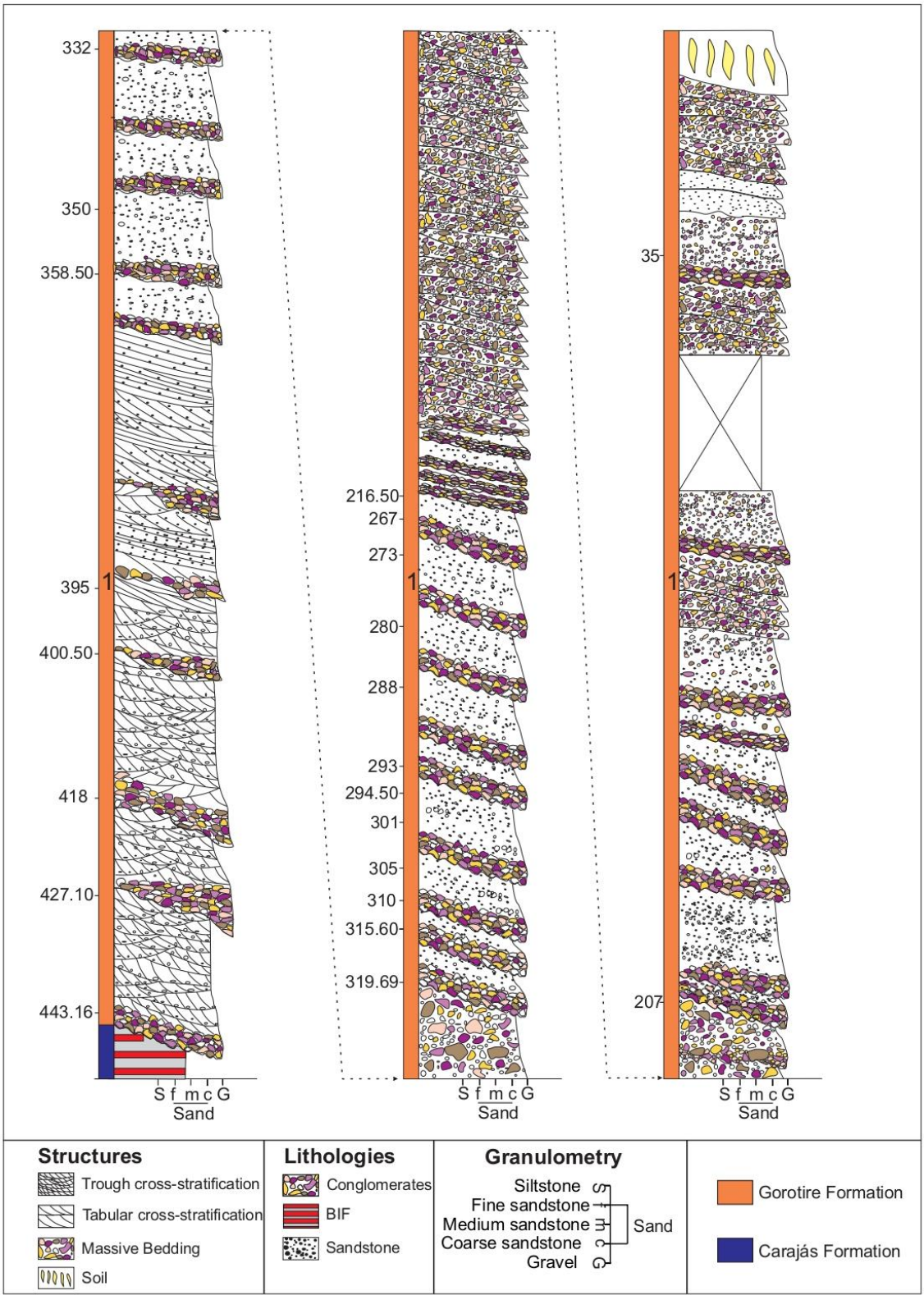

Figure III.3- Sedimentary log and facies descriptions of the Gorotire Formation in the Serra do Rabo region, Carajás Domain, North Brazil.

Interpretation. −The Gorotire Formation lithofacies indicate coarse-grained bed-load transport in energetic underwater currents by dune and bar migration (Cotter, 1978; Davies et al., 2011; Ielpi & Rainbird, 2015). The conglomeratic facies show massive

bedding, suggesting rapid deposition from high-energy traction currents in a lower flow regime associated with high water discharge rates and sediment concentration (Lowe, 1975; Hjellbakk, 1997; Miall, 2006). Cross-bedded sandstones indicate a migration of two- and three-dimensional dune and/or bars under a lower flow regime (Hjellbakk, 1997; Ielpi & Rainbird, 2015). The overall upward cycle thickness reduction indicates the progressive diminution of accommodation space (Schumm, 1968; Cotter, 1978; Fuller, 1985; MacNaughton et al., 1997; Long, 2004; Davies & Gibling, 2010). The absence of fine-grained sediments and small-scale sedimentary structures at the top of the cycles indicates poor preservation or extreme fluvial erosion, which confirms the high-energy conditions within a bed-load fluvial system (Long, 1978; Bridge, 2006; Davies et al., 2011; Ielpi & Rainbird, 2015). Although fluvial facies rarely show a predictable vertical stacking pattern, the record described coincides with previous features defined for pre-vegetation braided rivers (Cotter, 1978; Hjellbakk, 1997; Davies et al., 2011). The absence of vegetation is a controlling factor for the channel morphology, increasing the migratory tendency, with implications for the geometry of bedforms (Miall, 1981; Bridge, 2006; Davies & Gibling, 2010; Davies et al., 2011). The slight variation in granulometry and the occurrence of one or two types of main structures make it challenging to identify a cyclicity, features typically described in pre-Silurian river systems (e.g., Barrera et al., 2020).

4.2 GOROTIRE FORMATION PROVENANCE ASPECTS

4.2.1 Sandstone Petrography

The clastic compositions and representative photomicrographs of the 9 Gorotire Formation sandstone samples are shown in Fig. III.4K to N. The sandstones are medium to coarse-grained and moderately sorted, with occasional granules. The samples are dominated by quartz (9–13%), feldspars (22–28%), and lithic fragments (59–66%) (Table III.2). The quartz exhibits angular to subangular grains represented by polycrystalline quartz and monocrystalline quartz. Feldspar plagioclase, orthoclase, and microcline grains are angular to subangular. Plagioclases may show zoning, with dissolved edges and deformed grains with undulating extinction and high fracturation.Plagioclases may show zoning, with dissolved edges and deformed grains with undulating extinction and high fracturation.Lithic fragments are plutonic, metamorphic, BIF, and sedimentary (Fig. III.4K to N), including granitic fragments with porphyritic texture; quartzite fragments,

which are highly oriented polycrystalline quartz with strong undulating extinction and sutured internal contacts, schist characterized by the predominance of oriented micas, gneiss, and chert grains; mudrocks that display irregular shapes, eventually deformed and flattened, generating pseudomatrix, and rounded fine-grained sandstone. Based on the framework component modal proportions, the sandstone was classified into quartzo-feldspatho-lithic (qFL) and feldspatho-lithic (FL) (Fig. III5).

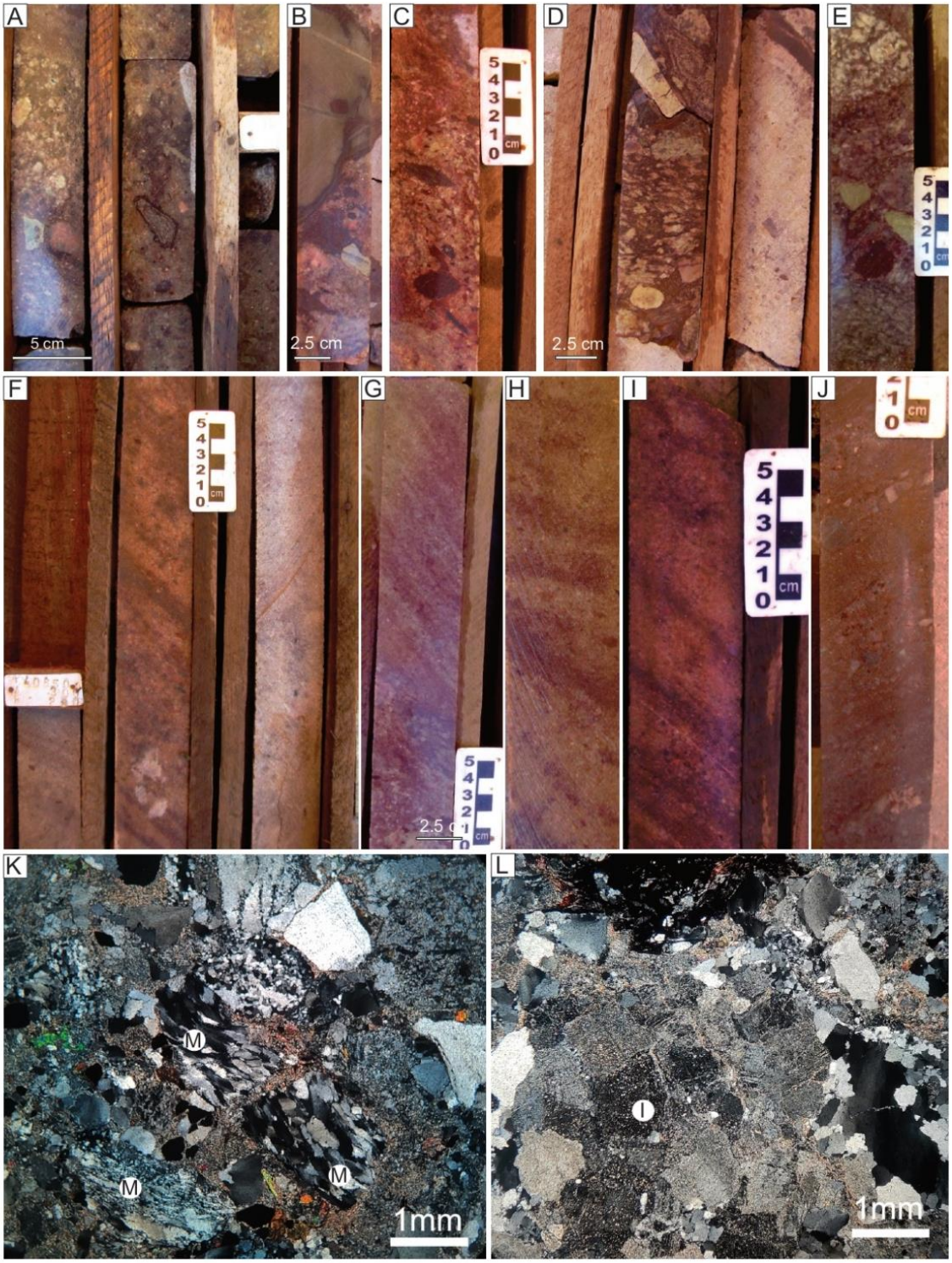

Figure III.4- Facies aspects of the Gorotire Formation in the Serra do Rabo region. A to E) Polymictic massive conglomerates facies. Note the widespread rounded clast morphologies and the broad range of clast size. F to J) Cross-bedding coarse sandstone facies; note the wide vertical clast size variation in tabular cross-stratification (J). K and L) Representative photomicrographs of the lithic-rich sandstones. Igneous fragments (I) and metamorphic fragments (M).

Table III.2- Detrital framework grain compositions of Gorotire Formation sandstones from the Carajás Domain. Qm: monocrystalline quartz, Qp: polycrystalline quartz, P: plagioclase, Lv: volcanic lithic fragments, Lm: metamorphic lithic fragments, Ls: sedimentary lithic fragments, MC: matrix and cement, O: others.

Raw point count								Volume percentage of QFL (%)				
Sample	Qm	Qp	P	Lv	Lm	Ls	MC	O	Total	Q	F	L
162-2	14	22	70	85	95	8	15	5	314	9.15	26.64	65.19
162-3	20	15	68	80	93	7	22	8	313	12.4	24.02	63.6
162-4	13	21	80	75	90	5	7	3	294	12	28.16	59.85
162-5	11	20	75	79	91	6	13	0	295	11	26.59	62.45
162-6	8	28	73	82	88	5	6	9	299	12.7	25.7	61.61
162-7	9	20	65	85	83	3	19	7	291	11.1	24.8	64.5
162-8	12	21	60	90	89	4	9	2	287	12	21.73	66.3
162-9	8	29	62	78	93	7	8	4	289	10.1	23.22	66.66
162-10	10	27	61	88	90	3	12	3	294	13.4	22.1	64.49

Quartz-poor fluvial origin sandstones plotting in the qFL field are typical from sources of undissected orogenic domains, including volcanic regions (cf. Garzanti, 2019). Fine-grained sedimentary rock fragments throughout the succession may indicate proximal sources due to them not supporting mechanical wear and disappearing with the sediment-source area distance increase (see Garzanti, 2017). Lithic fragments described in the sandstone samples exhibit similar compositions to the Archean to Paleoproterozoic rocks of the Carajás Domain, which suggest that these act as both basement and source for the Gorotire Formation.

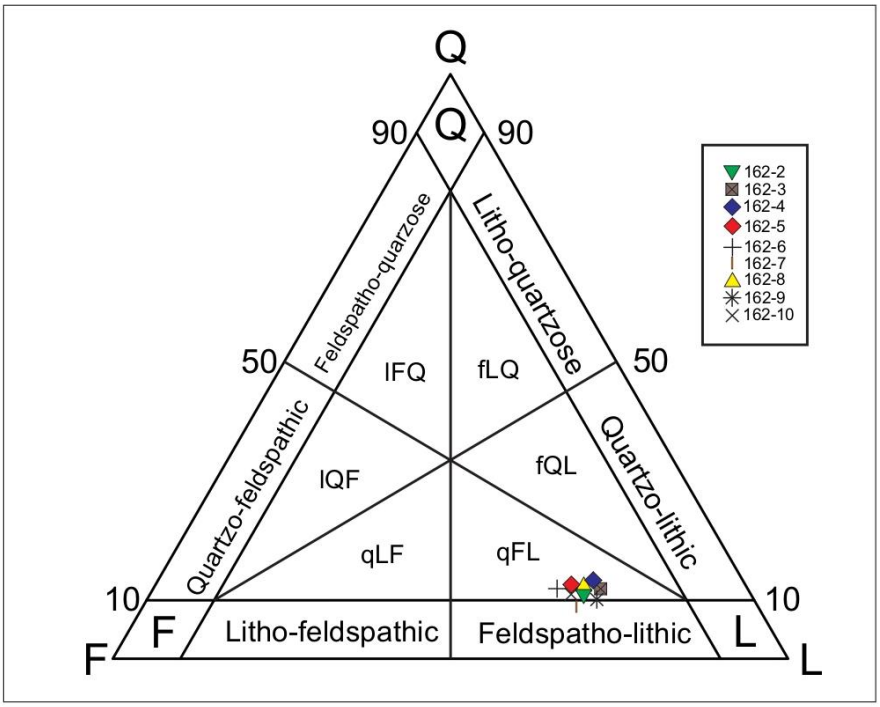

Figure III.5- Interpretation of the sandstone composition from the petrography of nine sections of the Gorotire Formation based on the schemes proposed by Garzanti (2019). Standard plots: Quartz, Feldspar, Lithic grains (Q, F, L), showing quartzo-feldspatho-lithic (fQL) and feldspatho-lithic (FL) nature of the sandstone.

4.3 PAREDÃO GROUP LOWER MEMBER SEDIMENTOLOGICAL ASPECTS

Description. −The Paredão Group lower member is ~90m thick, measured in cores that have not reached the basement (Fig. III.6). It is composed mainly of 2–18m thick beds of massive clast-supported conglomerates, interbedded with centimetric lenses of massive coarse to very coarse-grained sandstones. Low-angle cross-stratified sandstones occur locally with abrupt contact with overlaying conglomerates. Clasts are mostly subangular to sub-rounded (Fig. III.7). Maximum particle size is typically boulder grade and is roughly proportional to bed thickness. The composition of the pebbly to granular matrix is similar to that of the larger clasts (Fig. III.7). The beds are typically unstratified and ungraded (Fig. III.7A). Granulometric variations were identified within the conglomeratic facies, with more significant proportions of cobbles in the lower and middle portions of the association and larger volumes of pebbles in the upper part. Locally disproportionate clasts occur in the finer conglomeratic facies. These deposits form lithosomes from meters to decameters thick with minimal internal facies variations (Fig. III.6). Clast composition mainly comprises quartz, BIF, granite, gneiss, quartzite, schist, silexite, mafic volcanic, and basic volcanic rock fragments (Fig. III.7B to L).

Interpretation. −These deposits are interpreted as gravitational sediment flow. Clast-supported conglomerates without internal organization suggest the deposition of low- to non-cohesive debris flows (Nemec & Steel, 1984; Blair & McPherson, 1994a, 1994b). The conglomerate thick-bedded, poorly organized texture of the deposits and general lack of stratification represent a non-selective deposition style. The correlation between maximum particle size and bed thickness suggests that the transporting flow's competence was directly proportional to its thickness (Went, 2005). These features are commonly attributed to sediments deposited by the frictional freezing of non-cohesive sediment gravity flows (Lowe, 1976, 1979). The thin lenses of stratified sandstone represent more dilute flows and inter-surge or inter-flow deposits. Conglomerate textural characteristics are consistent with flows of high sediment concentration and express common clast interactions (Went, 2005). Clasts were likely supported during transport by dispersive pressure and buoyancy (Enos, 1977; Went, 2005). This condition at least has prevailed in the latter stages of the flow, immediately before deposition. The bed

thickness scale suggests deposition in major fan head channels tens of meters deep (Went, 2005).

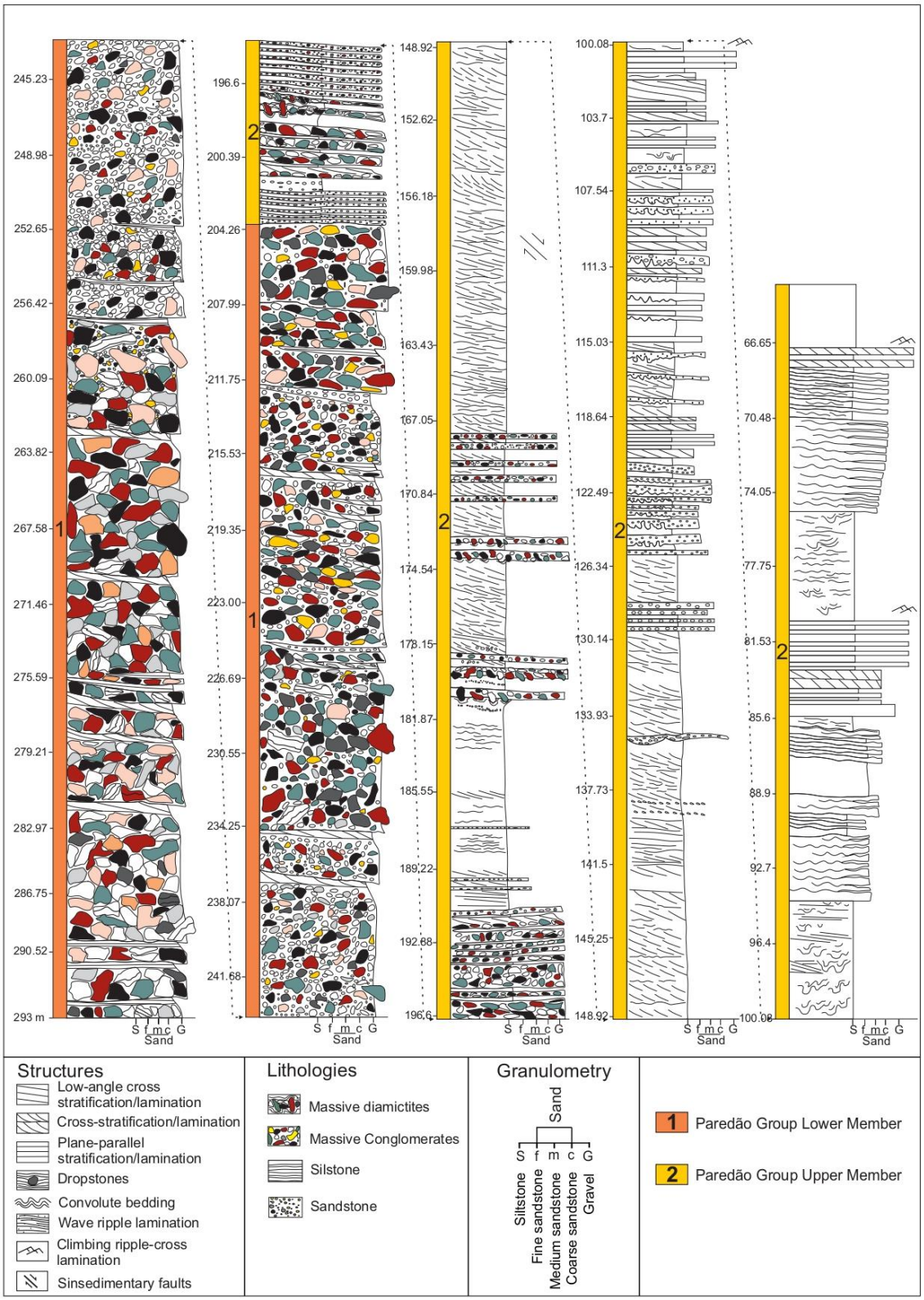

Figure III.6- Sedimentary log and facies descriptions of the Paredão Group in the Serra do Paredão region, Carajás Domain, North Brazil.

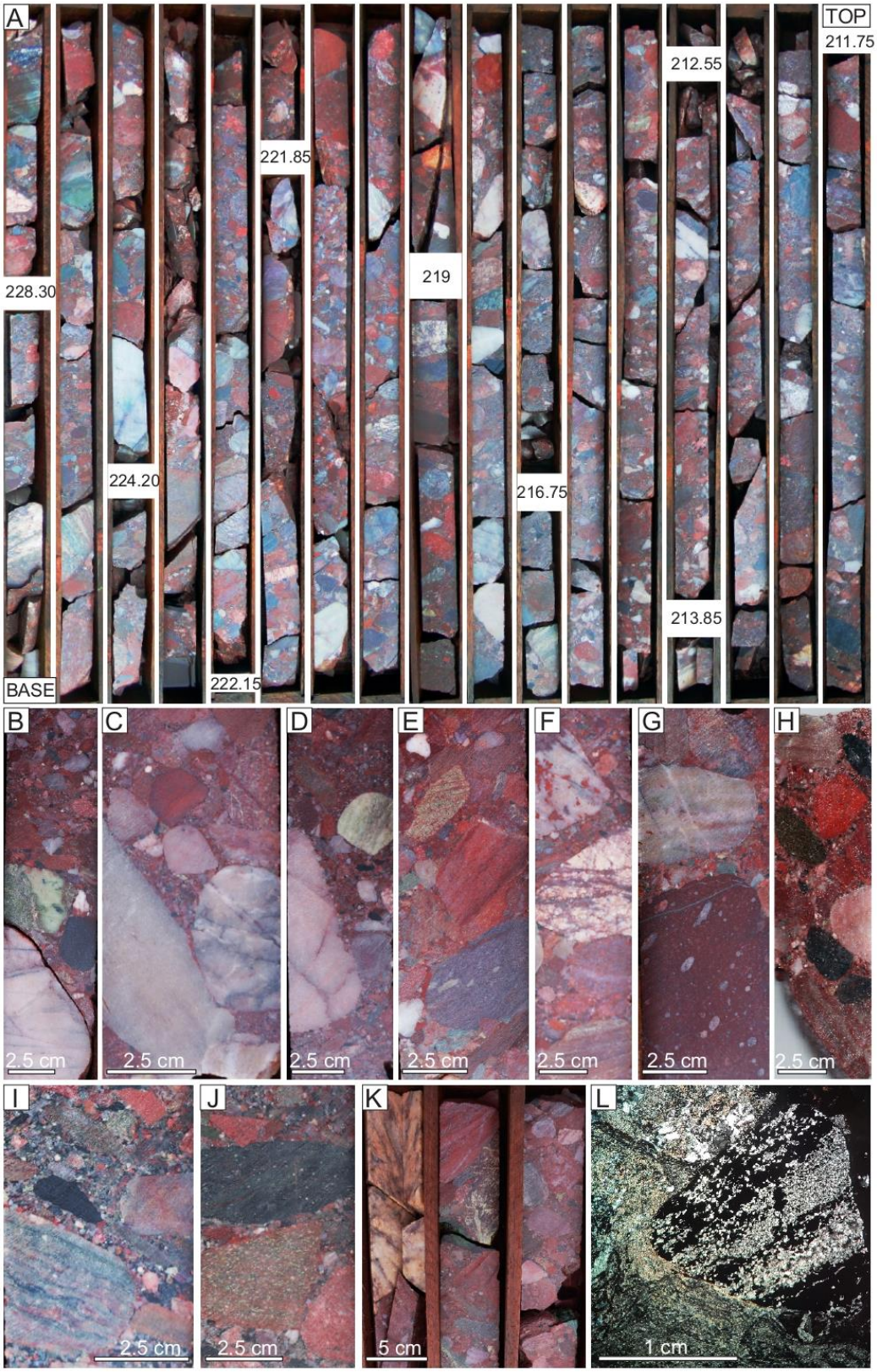

Figure III.7- Facies aspects of the Paredão Group Lower Member. A) Part of the drill core shows a general overview of the conglomerates and cross-bedded sandstone. B to L) Images of the main variety of composition clasts in the polymictic clast-supported conglomerate's facies; note the widespread rounded clasts morphologies, the broad range of clast size, and massive bedding. The main clasts comprise quartz, quartzite, slate, BIF fragments, granites, silex, schist, gneiss, sandstones, and mudrocks.

4.4 PAREDÃO GROUP LOWER MEMBER PROVENANCE ASPECTS

4.4.1 Macroscopic Provenance

The macroscopic provenance analysis in the conglomerates of the Paredão Group lower member (gravel, pebble, and cobble granulometry), totalizing ~2700 clast, reveals that the seven most abundant lithotypes in these deposits are vein quartz (~14,48%), mafic volcanic (~13,85%), schist (~13,22%), BIF (~12,96%), quartzite (~12,33%), basic volcanic (~11,70%), and gneiss (~10,70). In contrast, other lithotypes are much less significant (all below 5%), which include acid volcanic, marble, mudrocks, and silexite (Fig. III.7). The distribution of these lithotypes is homogeneous through the core. The polymictic conglomerate composition and the sedimentological data from the Paredão Group lower member suggest a neighboring source-area region probably related to the Carajás Domain and Araguaia Belt rocks.

4.4.2 Heavy Minerals

The heavy mineral spectra of the analyzed samples (n = 2, Table III.3.1, in supplementary material) are primarily dominated by opaque magnetic minerals, with an average of 85%. These opaque magnetic minerals have the BIF as a source. Garnet and epidote exhibit the contents with averages of 5,5% (maximum 6,1%) and 1,1% (maximum 1,5%), respectively. This mineral group is derived from metamorphic source rocks (Deer et al., 1992). Due to this mineral's high sensitivity to corrosion characteristics, garnet grains show euhedral morphologies that suggest a short distance to the source areas (Morton and Hallsworth, 1994). The stable detrital heavy mineral, tourmaline, and rutile (Morton and Hallsworth, 1999) display an average of 8,45%. This mineral assemblage is typical in acidic to intermediate granitoid rocks, as well as in mature siliciclastic sediments and some metamorphic rocks.

In the analyzed samples, zircon displays the highest concentration of ZTR (zircon > tourmaline > rutile) minerals. Based on the heavy minerals group present in the studied samples, the ZTR and garnet-zircon index (GZi) ratios were calculated. The dominance of the ultra-stable heavy minerals is shown in the ZTR index of 55 on average (Table III.3.1, in supplementary material). On the other hand, the high proportions of garnets are reflected in the Gzi, with a value of 43 on average. The high values of the ZTR and GZi index indicate that these sediments are mainly related to recycled metasedimentary rocks that limit the heavy mineral spectrum to ultra-stable and metamorphic origin.

Metasedimentary sequences from the Carajás Domain and Araguáia Belt represent the basement and neighboring for the Paredão Group rocks and most likely correspond to a source for these deposits.

4.4.3 Detrital Garnet Chemistry

The molecular percentage of every analyzed garnet can be calculated once chemical compositions are obtained. From the measured oxide compositions, molecular proportions were calculated on the basis of 12 oxygens. The garnet group contains six endmembers, including pyrope (Prp), almandine (Alm), spessartine (Sps), grossular (Grs), andradite (Andr), and uvarovite (Uva). Morton et al. (2004) distinguished the major detrital garnet types in sediments by the construction of a ternary diagram of Prp - Alm + Sps - Grs (Mg – Fe + Mn – Ca) for source rock discrimination (Type A, B and C. Fig. III.8).

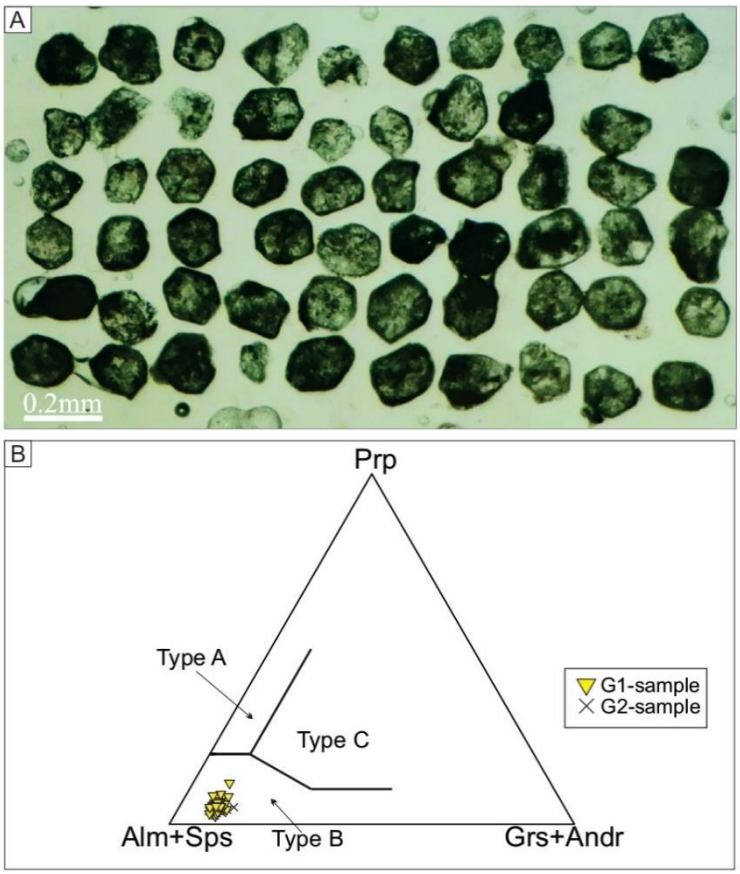

Figure III.8- Analyzed garnets to the Serra do Paredão Lower Member. A) Representative photomicrographs of the garnet grains. B) Ternary plot of the detrital garnet composition by Morton et al. (2004).

Detrital garnets of the two samples reveal a pale green color under plane-polarized light and are mainly angular in shape (Fig. III.8A). A calculation of end members

indicated that the garnets exhibit minor variations in chemical compositions (Table III.3.2, in supplementary material). The average component of the 106 analyzed detrital garnets from the Paredão Group, lower member is as Alm15,31 Prp5,00 Sps70,27 Grs9,41. According to the discrimination diagram of Morton et al. (2004), all analyzed grains display Type B garnet enrichment (Fig. III.8B). These garnets are most likely derived from low- to medium-grade metasedimentary rocks (cf. Morton et al., 2004, 2005). Garnet mineral chemistry and the discrimination of the origin rock type allowed the definition of the Buritirama Formation as the plausible source. The Buritirama Formation exhibits manganiferous marbles with euhedral, fine-grained (~0.05 mm) spessartine crystals (Salgado et al., 2019b). It represents part of the basement over which rest the deposits of the Paredão Group. The presence of these garnets also supports a basement that acts as a continuous source for these deposits.

4.5 PAREDÃO GROUP UPPER MEMBER SEDIMENTOLOGICAL ASPECTS

Description. −The Paredão Group upper member is ~140m thick (Fig. III.6). It consists of interbedded clast to matrix-supported diamictite, sandstone, and siltstones in the first forty meters, which change vertically for a 100 m thick succession of stacked coarsening-upward cycles, with individual thicknesses ranging from 10m to 20m, including sandstones, siltstones, and rhythmites.

Diamictites comprise 0.2- 0.9 m thick beds, usually massive or subordinately with faint boundaries (Fig. III.6 and III.9A). The chaotic rock framework exhibits clasts with predominantly angular to subangular morphologies and low sphericity, often faceted, varying in size from granule to boulder (Fig. III.9B to D). Crushing clasts were also identified (Fig. III.9E). Rock constituents are mainly BIF, metamorphic, and igneous rock fragments (~87 - 92% of whole rock composition) and, to a lesser extent, quartz within a coarse-grain sandy to siliceous matrix. These deposits exhibit compositional similarities with the Paredão Group lower member conglomerates. However, these diamictites present faceted and crushing clasts that imply different genetic depositional processes and contexts for the two sequences.

Lonestones are described along the entire association, inserted in the layers of diamictites that abruptly cover laminated siltstones and sandstone beds (Fig. III.9F-G, III.10). Vertically within each coarsening upward cycle, the deposits range from siltstones at the base through alternating sandstone and siltstone beds to sandstones at the top of the

succession (Fig. III.6). The beds exhibit centimetric to metric thicknesses. The contacts between the lithofacies are undulating, and soft sediment deformations were identified (Fig. III.11A). Rhythmic intercalations of sandstones and siltstones are observed in the upper portions of the succession, stacked in centimeter-to-metric-scale coarsening-upward cycles (Fig. III.11 B to D). Fine to coarse sandstone layers exhibit sedimentary structures ranging from cross-lamination, climbing ripple cross-lamination (restricted to the coarsening upward cycles top), and tabular and low-angle cross-bedding to massive bedding (Fig. III.11 E to H). Sandstone presents sub-angular grains with medium sphericity, composed mainly of igneous and metamorphic clasts, quartz, and feldspars. Sandstone cement compositions are mostly microcrystalline silica and, to a lesser extent, iron oxides and hydroxides. The siltstone layers range from planar-, wavy-, and crossed-laminations to massive bedding (Fig. III.11 I to K). Soft sediment deformation structures are widespread in contact between sandy and silt laminations (Fig. III.11 L to M).Micro-fault structures are described in siltstone beds. In the siltstone lithofacies, the grains are compounds of quartz and feldspar, sub-rounded with medium sphericity. Micro-faults and convolute bedding are restricted to siltstone beds. No glacio-tectonic deformation was observed throughout the entire succession.

Interpretation. −This sedimentary succession is interpreted as being deposited in a glaciomarine environment that gradually evolved into a deltaic setting. Despite the lack of glaciotectonic structures, characteristics such as faceted and chorusing clasts, combined with the sedimentary structures presented here, represent a robust framework for interpreting a glacial event.

The glacial deposits are probably related to the retreat phase of the ice sheets, which released large amounts of water and debris feeding this system (Lønne, 1995; Miller, 1996; Visser, 1997). Diamictites represent deposits generated by debris flows with significant inputs of pebbles and cobbles, which were established during the retreat of the ice margins (Visser, 1997). The viscosity of debris flow with low water content was controlled by low energy currents, causing poor sediment segregation, ranging from massive bedding to faint stratification (see Barrera et al., 2020). During the ice-melting, ice-rafted debris processes generated various structures characteristic of subaquatic systems, such as dropstones and dumpstones (Boulton & Deynoux, 1981; Eyles, 1993; Hart & Roberts, 1994; Miller, 1996; Zecchin et al., 2015). Sediment plumes deposited sandstones and siltstones on meltwater in a marine environment influenced by glaciers

(Pickering et al., 1989; Visser, 1991). The presence of cross- and wavy-laminations indicates the action of unidirectional and oscillatory flows, the product of subaqueous deposition by tractive flows alternating with periods of decantation (Le Heron et al., 2013). Deformational structures are related to highly concentrated muddy gravitational flows (Pickering et al., 1989; Vessely, 2006).

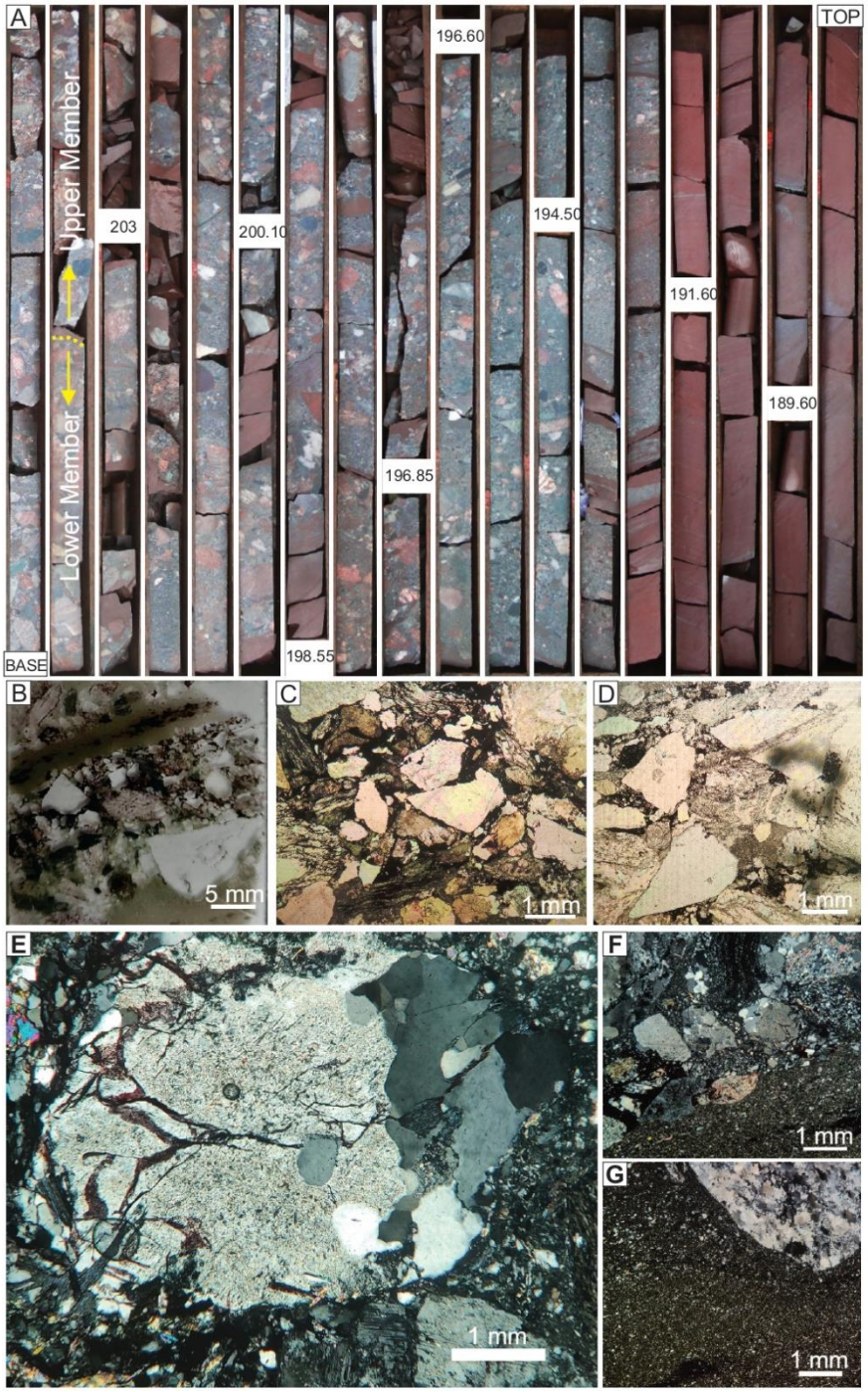

Figure III.9- Facies and petrographic aspects of the Paredão Group Upper Member. A) Part of the drill core showing a general overview of the laminated siltstones and massive diamictites and contact between lower and upper members of the Paredão Group. The dotted yellow line indicates the contact. B to G) Representative photomicrographs of the glacial deposits showing faceted clasts (B, C, and D), crushing clasts (E), and lonestones deforming basal siltstone laminations (F and G).

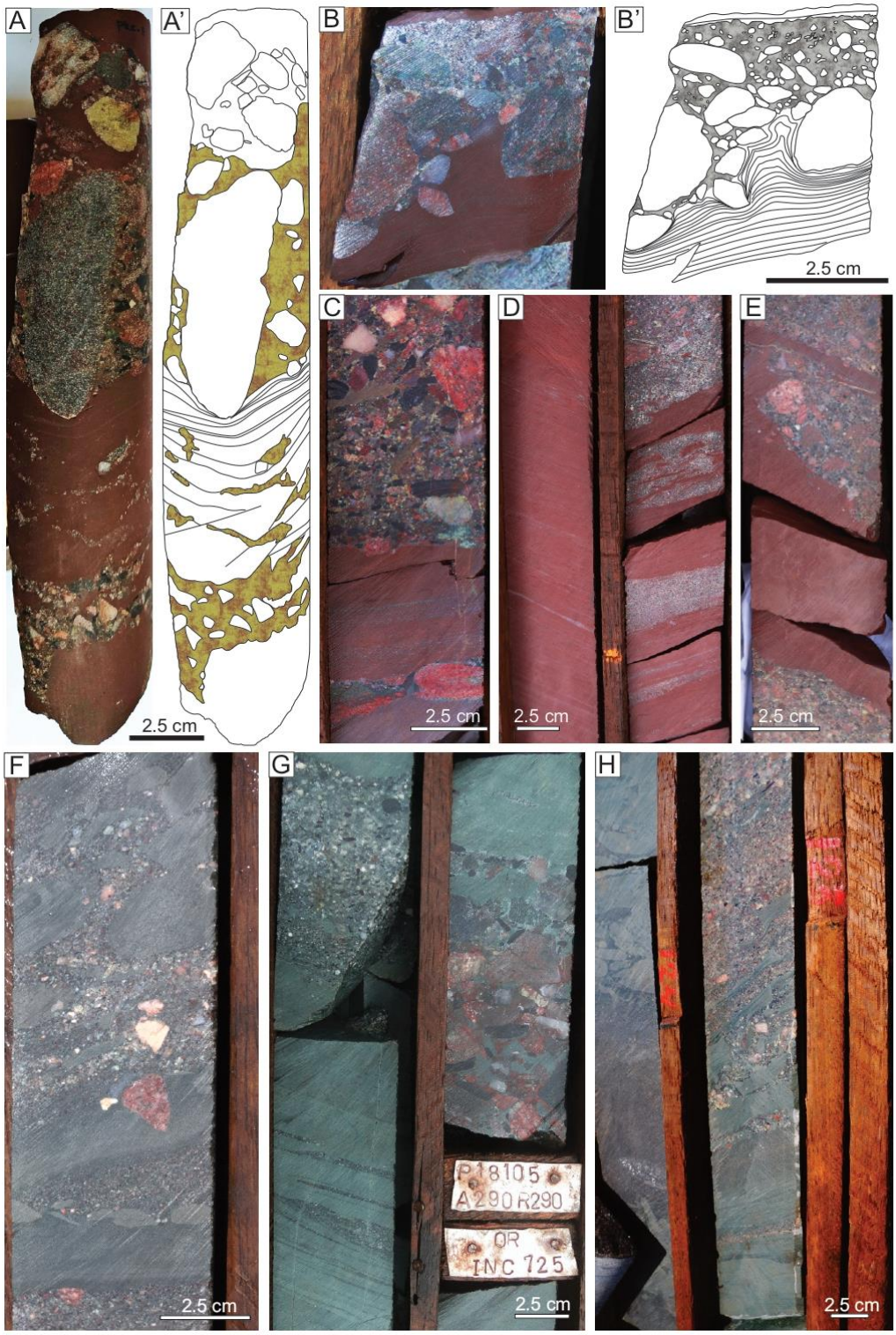

Figure III.10- Facies aspects of the Paredão Group Upper Member. A-A' and B-B') Dropstones and dumpstones are deforming basal strata in laminated siltstones. C) Massive diamictites interbedded with laminated siltstones. D) Cross-laminated siltstones to the right and massive coarse-sandstones/diamictites interbedded with laminated siltstones to the left; note the load cast deformation in the massive diamictites and laminated siltstones boundary and the siltstones rip-up clast in massive coarse-sandstones. E) Centimetric lenses of massive to incipient-stratified diamictites interbedded with massive siltstone beds. F) Details of the contacts between massive pebbly sandstone and siltstone with microfault and convolute bedding. Note the small-scale dropstones deforming the basal siltstone lenses. G) Details of the contact between massive diamictite and sandstone with laminated siltstone. H) Details of the massive pebbly sandstone with siltstone lenses to the right and deformed and reworked siltstone beds to the left. Note the microfault and convolute bedding in siltstone.

The decantation of the fine fraction, combined with the fall of clasts from icebergs, generates the intercalation described between siltstones and diamictites (Vessely, 2006). The vertical variations in the granulometry of these deposits suggest an active ice sheet margin, producing an accumulation of poorly immature sediment in moderately deep waters devoid of strong currents. This hydrodynamic behavior indicates a variable grounding line during deposition (Powell, 1990). The progressive decrease in the density of glaciogenic depositional processes suggests that the glacial influence was progressively disappearing.

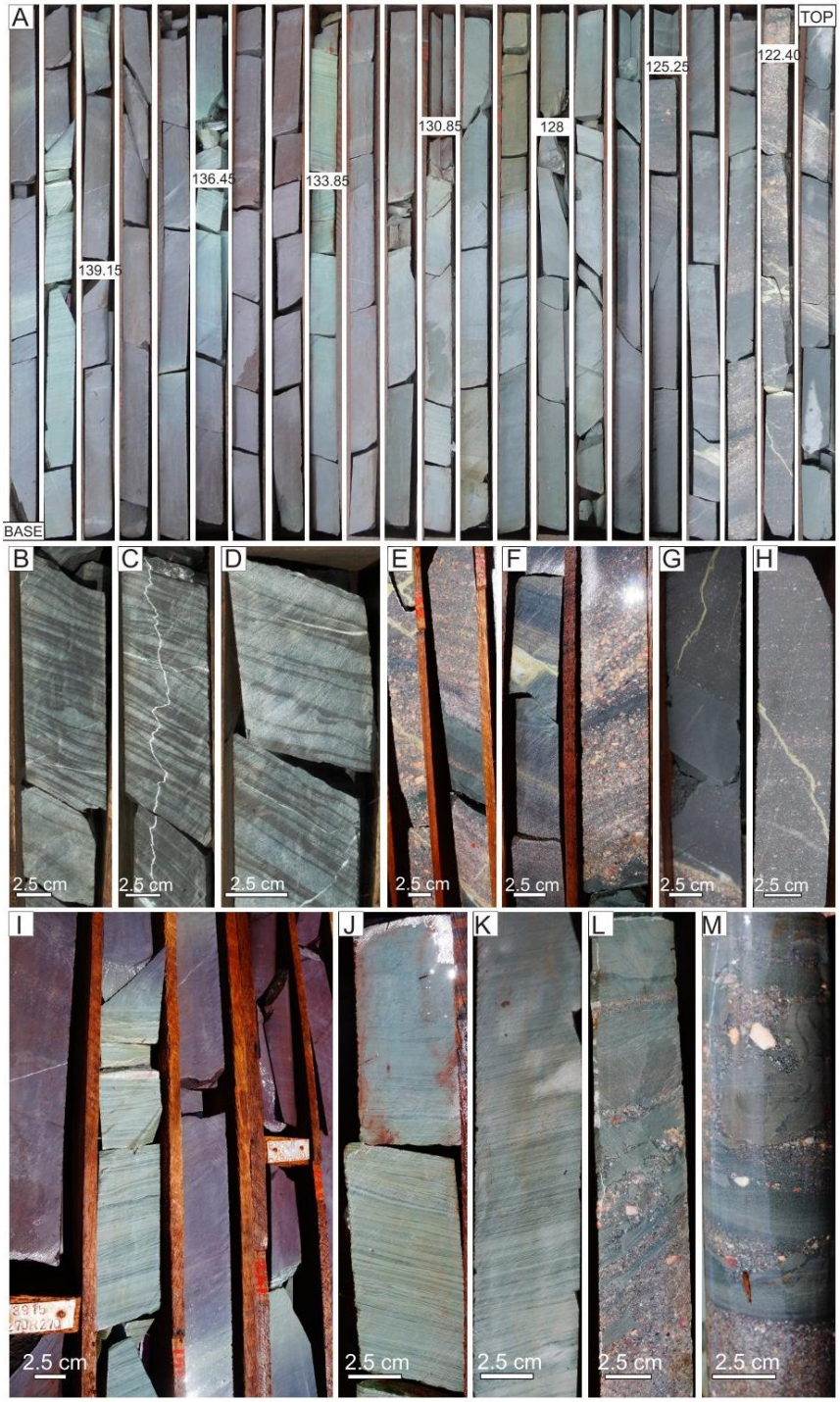

Figure III.11- Facies aspects of the Paredão Group Upper Member. A) Part of the drill core shows a general overview of the laminated siltstones and cross-bedded sandstone. B to D) Rhythmic intercalations of sandstones and siltstone facies. E to G) Cross-bedded sandstone facies; note the abrupt vertical grain size variation. H) Fine sandstones with even parallel- to low-angle cross-stratification facies. I to K) Siltstone facies with structures ranging from planar-, wavy-, and crossed-laminations to massive bedding. L and M) Soft sediment deformation structures between the contact of sandstones and siltstone facies; note the micro-fault, dumpstone, and dropstone structures restricted to siltstone facies.

The decrease of the glacial influence allows the installation of a deltaic environment in a marine setting, with the coastal influence of tidal and wave processes. The continuous progradation of sand-silt mouth bars produces the coarsening-upward pattern, characteristic of deltaic successions (Bhattacharya, 2006). Accelerated and prolonged input of water-saturated sediments and their deposition results in total or partial liquefaction and fluidization, which produce massive stratification and water escape structures, respectively (Lowe, 1975; Owen, 2003). Convoluted beds and deformed laminations are consistent with waterscape structures (Frey et al., 2009). The successive progradation of the sandy-bars bodies contributes to the deformation of the underlying deposits. A climbing ripple cross-lamination in the top of the coarsening upward cycles within metric-scale sandstone beds suggests long-duration hyperpicnal flows and high rates of sand fall (Dietrich et al., 2017). The predominance of sandstone and low siltstone strata towards the top of the association indicates increasing proximity to the coastline, possibly interpreted as a delta front or tidal bars within a distal delta front (Galloway, 1975; Scasso et al., 2012; Dietrich et al., 2017).

4.6 THE GLACIAL INFERENCE

Glacial records are recognized as excellent stratigraphic markers that allow the correlation of glaciogenic successions worldwide. The Paredão Group, upper member succession, is interpreted here as glaciogenic sediments. Precambrian glacial deposits have been described between the Grão Pará Group and Águas Claras deposits, denominated of Serra Sul Formation (Fig. III.2). The stratigraphic position of these Precambrian deposits occurs some kilometers below the Paredão succession. The broad glaciotectonic characteristics, the restricted main clast constituents associated with this record (banded iron formation and volcanic rocks), and the tectonic and geological context discard any stratigraphic correlation with the Paleoproterozoic Serra Sul glaciation. The Paredão glaciogenic to deltaic sedimentary series shows clast compositions that suggest the Carajás Domain and Araguaia Belt as the main source areas. This provenance data implies a younger than Paleoproterozoic stratigraphic position of the Paredão succession devoided glaciotectonic features, indicating a younger

glaciation. Additionally, we discard the Neoproterozoic glaciations characterized by the occurrence of cap carbonates described worldwide (e.g., Hoffman et al., 1998; Nogueira et al., 2003), never found in the Carajás domain. Considering the MDA for the Paredão Group, lower member (~490Ma), the Paredão glacial succession can be regarded as one of the records of Paleozoic glacial events.

Paleozoic glaciations include two events that affected the western portion of the Gondwana Supercontinent: The Ordovician-Silurian glaciation (Hambrey, 1985; Caputo, 1984; Ghienne et al., 2007, 2023) and the Devono-Permo-Carboniferous glaciation (Vessely, 2006; Caputo et al., 2008; Barbosa, 2014). The proximity to the geographic south pole controls the exclusively siliciclastic composition of these glaciogenic deposits (Vessely, 2006; Barbosa, 2014; Ghienne et al., 2018; Barrera et al., 2020). The Devono-Permo-Carboniferous glacial event can be discarded because its occurrence implies a record of very thick succession to reach the upper Paleozoic strata. In addition, Paredão Group deposits overlie Precambrian metamorphic rocks, and the glaciogenic succession is superimposed to Cambro-Ordovician continental deposits, more compatible with the Early Paleozoic initial phase of deposition in Brazil (Brito Neves et al., 1984; Brito Neves, 2002). This constatation coincides with the previous suggestion of Pinheiro (1997) and Vasquez et al. (2008a) regarding the Ordovician-Silurian age for the Paredão Group.

The record of the Ordovician - Silurian glacial event in Brazil consists of siliciclastic successions, represented mainly by pro-glacial glaciomarine environments without glaciotectonic evidence (Adôrno, 2014; Barrera et al., 2020). These successions are composed of sandy-matrix massive to stratified diamictites, sandstones, and siltstones, with a wide presence of dropstone and dumpstone structures (Adôrno, 2014; Barrera et al., 2020). Locally, thin beds of sandy matrix tilites are restricted to the Amazonas Basin (Soares, 1998). Glacial units are represented by the Ipu Formation in Parnaíba Basin (Barrera et al., 2020), the Nhamundá Formation in Amazonas Basin (Soares, 1998), and the Iapó Formation in Paraná Basin (Adôrno, 2014). Paleontological descriptions suggest a Llandovery depositional age (~440 Ma) for these records (Grahn & Caputo, 1992; Grahn, 1992; Grahn et al., 2005). These glacial deposits are gradually transitioned to marine and deltaic facies. Organic matter-rich black shales correspond to the record of post-glacial transgressions that exhibit a typical fossil assemblage (Llandovery – Early Silurian) (Grahn & Caputo, 1992; Steemans & Pereira, 2002; Grahn et al., 2005; Grahn, 2005; Adôrno, 2014).

5. SM/ND ISOTOPIC DATA

Comparing the isotopic Sm/Nd pattern of the analyzed sedimentary series with the isotopic characteristics of potential source rocks yields information about the source areas. The Sm/Nd isotope results (Table III.4) represent a mixture of contributions from juvenile and crustal materials, thus providing additional arguments on the nature and relative contribution of each source area. This can constrain identifying the paleogeographical context of the Gorotire Formation and Paredão Group source rocks during sediment deposition.

5.1 GOROTIRE FORMATION

Eleven samples of conglomerate matrix and sandstones from the Gorotire Formation were separated and analyzed for Sm-Nd isotopes (Fig. III.12). The results are listed in Table III.4, together with ε_{Nd}-values and depleted mantle Nd-T_{DM} model ages. These unmetamorphosed deposits represent a record of a post-Proterozoic Carajás Domain tectonic reactivation, probably related to extensional tectonics that allows rift basin installation (cf. Teixeira et al., 2019) associated with the orogenetic collapse of the Araguaia Belt (~490-500 Ma) (Dias et al., 2017). Samples from the Gorotire Formation yield negative ε_{Nd} (490) values ranging between −22.6 and −30. Nd-T_{DM} Model ages show Meso- to Neo-Archean distribution between 2.56 and 2.98 Ga (Fig. III.12A).

Comparing the isotopic Sm-Nd pattern of the Gorotire Formation with isotopic characteristics of potential source rocks yields information about the source areas (Fig. III.12B). These sedimentary deposits display negative ε_{Nd} values and ancient Nd-T_{DM} ages, indicating a contribution of crustal materials, probably derived from sources in a neighboring continental cratonic region. The isotopic signature indicates a dominant old continental crustal source compatible with the Carajás Domain rocks. The dominantly Mesoarchean Nd-T_{DM} ages from the Gorotire Formation are consistent with provenance from the cratonic Carajás Domain areas (Fig. III.12B). 2.8 Ga younger Nd-T_{DM} ages occur in the minority (only four analyses), probably representing uncertainties inherent in calculating model ages.

Table III.4- Whole rock Sm-Nd isotope data of the Gorotire Formation and the Paredão Group in the Carajás Domain.

Formation	Rock Type	Sample	Sm (ppm)	Nd (ppm)	$^{147}Sm/^{144}Nd$	$^{143}Nd/^{144}Nd$	$\varepsilon_{Nd\,(0)}$	ε_{Nd}		T_{DM} (Ga)
								490 Ma	440 Ma	
Gorotire Formation	Conglomerate matrix	162-2A	3.13	15.96	0.118677	0.511242	-27.22	-22.37		2.92
	Conglomerate matrix	162-2B	3.02	16.87	0.10829	0.511239	-27.3	-21.78		2.63
	Conglomerate matrix	162-3A	3	15.27	0.11895	0.511194	-28.16	-23.33		3.01
	Conglomerate matrix	162-3B	2.85	15.83	0.10905	0.511173	-28.6	-23.12		2.75
	Conglomerate matrix	162-4A	1.92	11.45	0.101379	0.510953	-32.85	-26.93		2.86
	Conglomerate matrix	162-4B	1.78	11.52	0.09324	0.511012	-31.7	-25.27		2.59
	Sandstone	162-6A	1.95	12.42	0.095293	0.510816	-35.54	-29.23		2.90
	Sandstone	162-6B	1.83	12.58	0.08806	0.510776	-36.3	-29.56		2.77
	Sandstone	162-7A	1.84	11.16	0.099834	0.510913	-33.65	-27.62		2.88
	Sandstone	162-8A	2.11	12.99	0.098198	0.510813	-35.59	-29.47		2.98
	Sandstone	162-8B	2	13.33	0.09089	0.51081	-35.7	-29.07		2.80
Paredão Group Lower Member	Conglomerate matrix	PKC-1A	4.68	22.9	0.12368	0.511607	-20.11	-15.56		2.44
	Conglomerate matrix	PKC -1B	3.9	20.68	0.11407	0.511594	-20.4	-15.21		2.22
	Sandstone	PKC-2A	2.64	14.22	0.112475	0.511355	-25.02	-19.78		2.56
	Sandstone	PKC-2B	2.76	15.85	0.1053	0.511279	-26.5	-20.81		2.49
	Sandstone	PKC-3A	3.59	19.31	0.112435	0.511466	-22.85	-17.61		2.38
	Sandstone	PKC-3B	3.79	21.91	0.10474	0.511427	-23.6	-17.89		2.27
	Conglomerate matrix	PKC-4A	1.69	7.88	0.129869	0.511483	-22.53	-18.37		2.87
	Conglomerate matrix	PKC-4B	1.76	8.43	0.12594	0.511401	-24.1	-19.72		2.89
Paredão Group Upper Member	Diamictite matrix	PKC-7A	8.42	41.21	0.123525	0.511985	-12.73		-8.63	1.79
	Diamictite matrix	PKC-7B	7.53	39.25	0.11602	0.511984	-12.8		-8.23	1.65
	Silstone	PKC-10A	7.8	39.03	0.120812	0.512013	-12.19		-7.93	1.69
	Sandstone	PKC12A	5.57	30.48	0.110502	0.511661	-19.06		-14.23	2.04
	Sandstone	PKC-12B	6.59	34.79	0.114483	0.511802	-16.29		-11.70	1.91

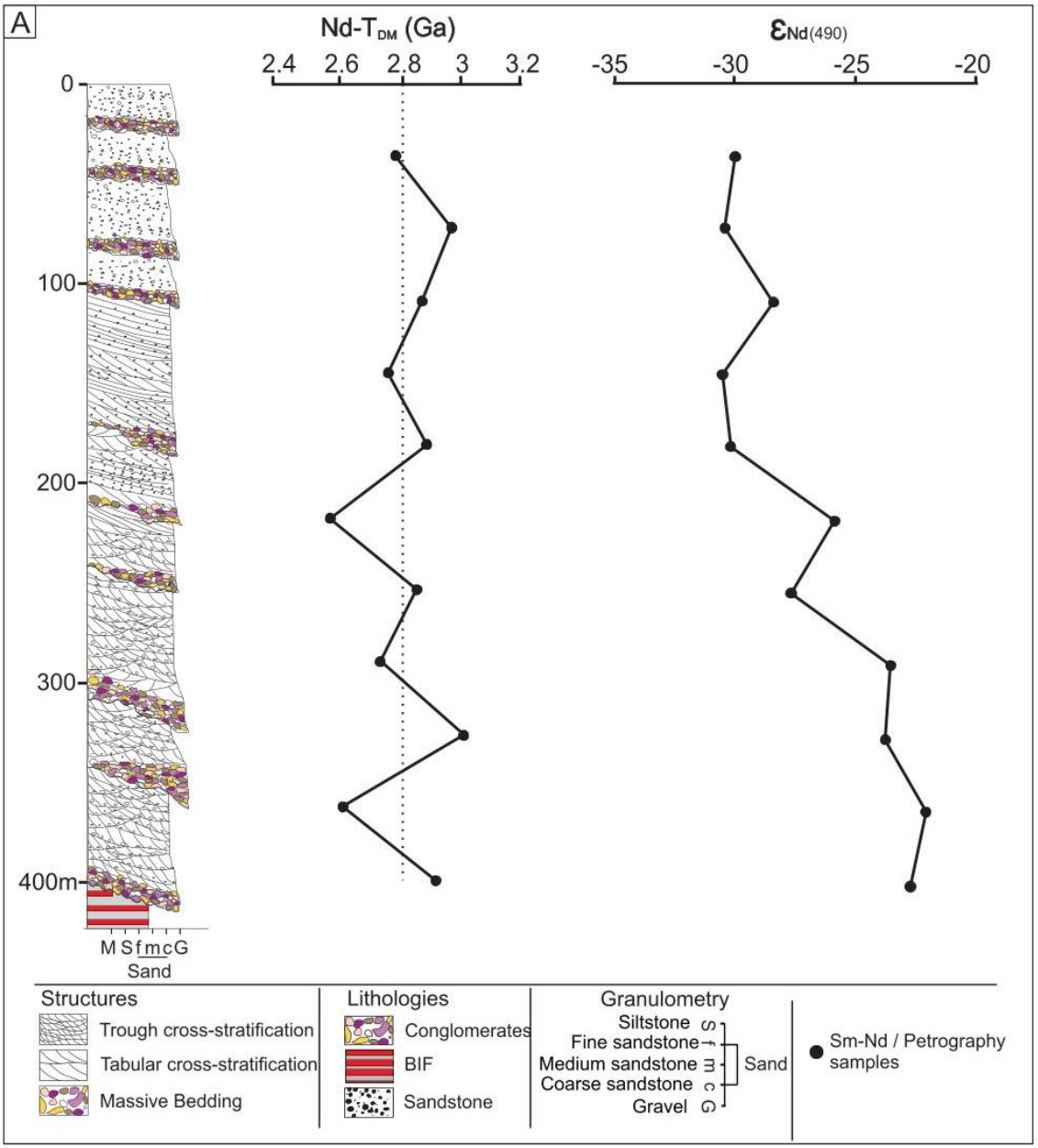
A
Nd-T$_{DM}$ (Ga)
2.4 2.6 2.8 3 3.2
ε$_{Nd(490)}$
-35 -30 -25 -20
0
100
200
300
400m
M S f m c G
Sand
Structures
Trough cross-stratification
Tabular cross-stratification
Massive Bedding
Lithologies
Conglomerates
BIF
Sandstone
Granulometry
Siltstone
Fine sandstone
Medium sandstone
Coarse sandstone
Gravel
S
F
M
C
G
Sand
Sm-Nd / Petrography samples

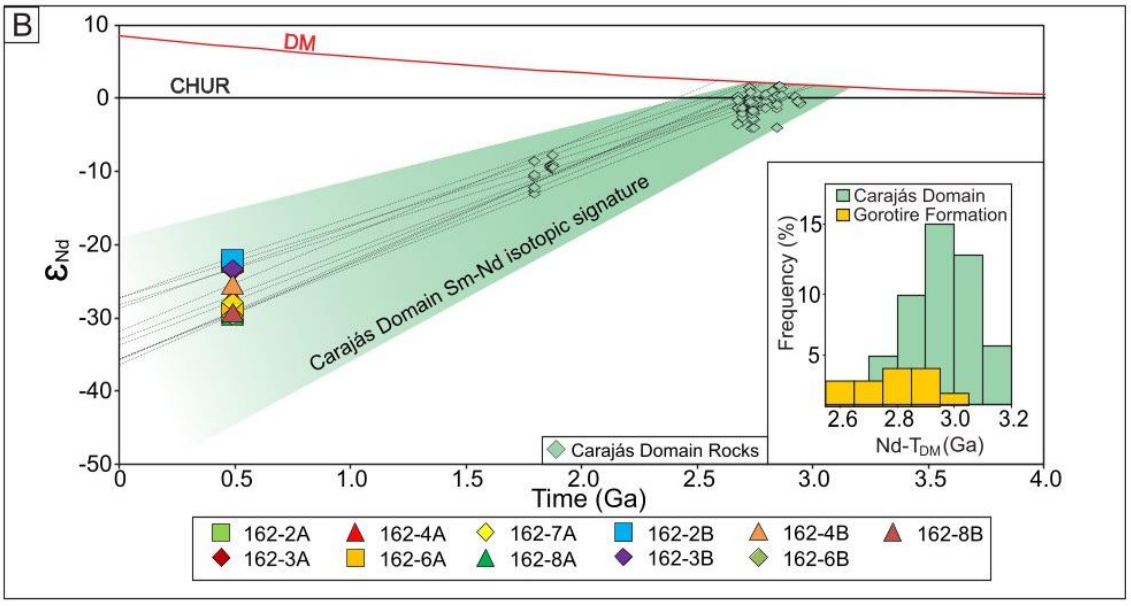
B
DM
CHUR
ε$_{Nd}$
10
0
-10
-20
-30
-40
-50
Carajás Domain Sm-Nd isotopic signature
Carajás Domain Rocks
Carajás Domain
Gorotire Formation
Frequency (%)
15
10
5
2.6 2.8 3.0 3.2
Nd-T$_{DM}$ (Ga)
0 0.5 1.0 1.5 2.0 2.5 3.0 3.5 4.0
Time (Ga)
162-2A
162-3A
162-4A
162-6A
162-7A
162-8A
162-2B
162-3B
162-4B
162-6B
162-8B

Figure III.12- Sm/Nd isotopic data from the Gorotire Formation. A) Schematic stratigraphic logs of the Gorotire Formation, showing the relative stratigraphic position of each sample selected for Sm/Nd analysis and vertical distribution of Nd-TDM and ƐNd(490 Ma). B) ƐNd(t) vs. Age (Ma) evolution diagram for the Gorotire Formation rocks. The field of the Sm/Nd isotope signature of the Carajás Province incorporates data from rocks reported by Mellito (1998), Santos et al. (2000), Leite (2001), Teixeira et al. (2002), Galarza (2002), Galarza & Macambira (2002), Pimentel et al. (2003), Barros et al. (2004), Dall'Agnol et al. (2005), Feio et al. (2012), Feio et al. (2013), Santos et al. (2013), Teixeira et al. (2017), Galarza et al. (2017), Martins et al. (2017), Marangoanha et al. (2020), Martins (2021).

5.2 PAREDÃO GROUP LOWER MEMBER

Eight samples of the conglomerate matrix and sandstone from the Paredão Group lower member were separated and analyzed for Sm-Nd isotopes (Fig. III.13). The results are listed in Table III.4 together with $\varepsilon_{(Nd)}$-values and depleted mantle Nd-T_{DM} model age. These unmetamorphosed deposits are geographically transitioning between the Araguaia Belt, Bacajá, and Carajás domains. Previously, these successions were defined as an isolated remnant of the Ordovician sequence of the Parnaíba Basin (cf. Pinheiro, 1997). However, the sedimentological and provenance characteristics presented here show proximal alluvial facies from a restricted system. Thus, we interpreted these deposits as a time-equivalent system developed in the same tectonic context (post-Araguaia Orogen collapse) as the Gorotire Formation. Samples from the Paredão Group lower member yield negative $\varepsilon_{Nd(490\ Ma)}$ values ranging between −15.2 and −20.8. Nd-T_{DM} model ages show distribution among Paleoproterozoic to Archean ranging between 2.2 and 2.8 Ga (Fig. III.13A).

Comparing the isotopic Sm-Nd pattern of the Paredão Group lower member with isotopic characteristics of potential source rocks yields information about the source areas (Fig. III.13B). These sedimentary deposits display negative ε_{Nd} values, indicating a contribution of crustal materials. However, the Paleoproterozoic Nd-T_{DM} ages are incompatible with the idea of the Carajás Domain rocks as a unique sediment source. Due to the geographical proximity with the Araguaia Belt, the basement and other igneous rocks that comprise this orogenic belt were considered as possible sources (Fig. III.13B). Two crustal growth events from the Carajás Domain (2.7 to 3.0 Ga) and Araguaia Belt (1.9 to 2.1 Ga) respectively, were observed (Fig. III.13B, references therein). The Paredão Group lower member samples show evolutionary trends that plot in the range between the crustal growth intervals mentioned above (Fig. III.13B). The Nd isotopic signature of these samples indicates the sources mixing from the older continental crust (Carajás Domain and Araguaia Belt basement; Fig. III.13B). Bacajá Domain was discarded as a

possible source because sedimentologic and isotopic data suggest that alluvial fans developed westward, from the Araguia Belt to the Carajás Domain.

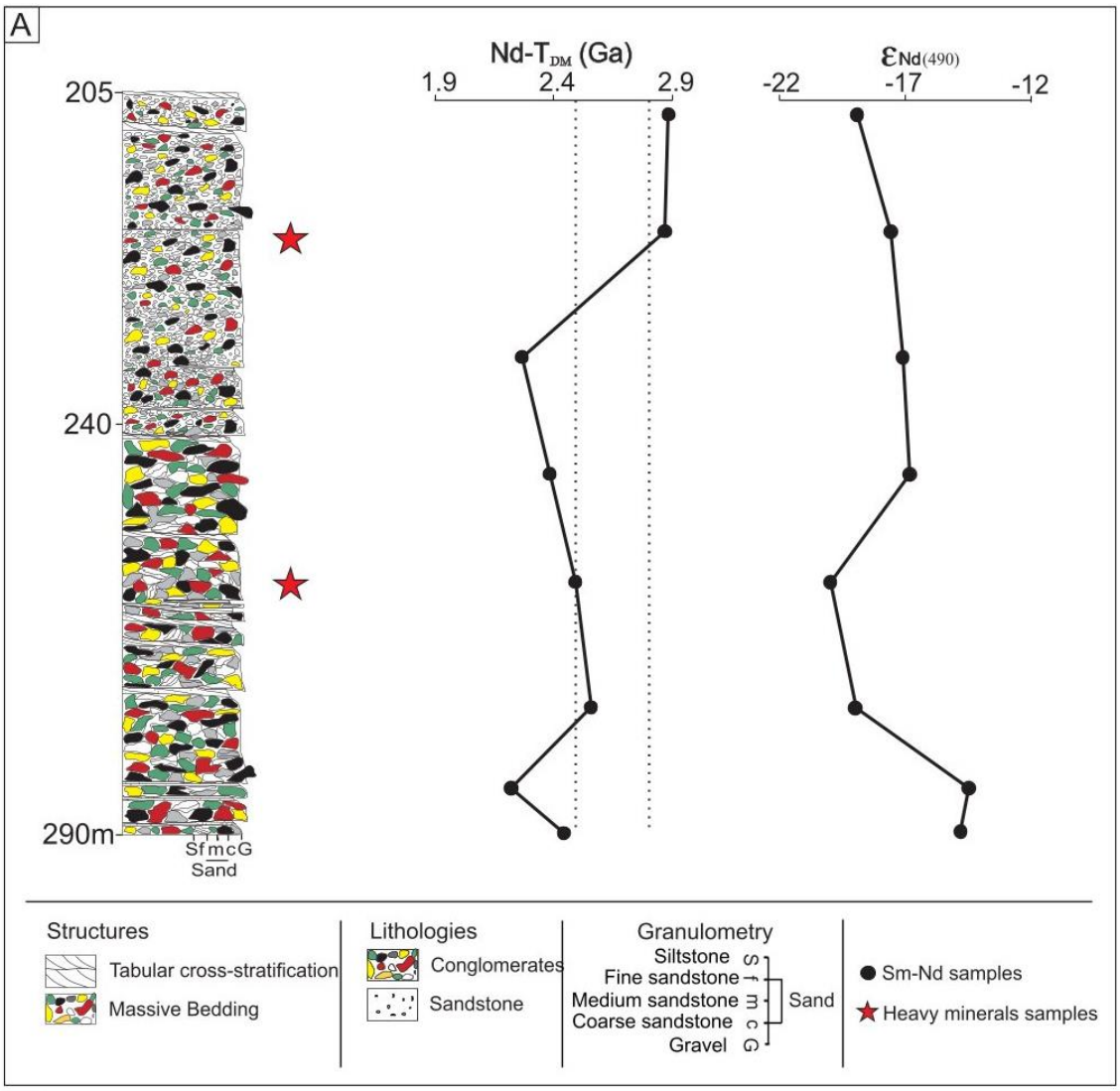

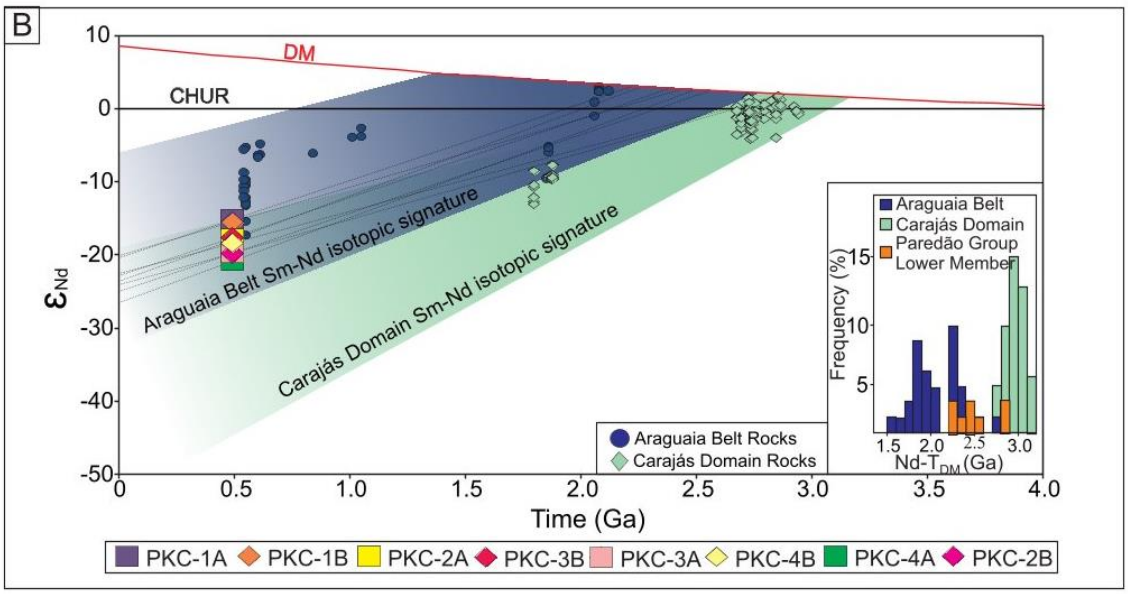

Figure III.13- Sm/Nd isotopic data from the Paredão Group Lower Member. A) Schematic stratigraphic logs of the Paredão Group Lower Member, showing the relative stratigraphic position of each sample selected for Sm/Nd analysis and vertical distribution of Nd-TDM and ƐNd(490 Ma). B) ƐNd(t) vs. Age (Ma) evolution diagram for the Paredão Group Lower Member rocks. The field of the Sm/Nd isotope signature of the Carajás Province incorporates data from rocks reported by Mellito (1998), Santos et al. (2000), Leite (2001), Teixeira et al. (2002), Galarza (2002), Galarza & Macambira (2002), Pimentel et al. (2003), Barros et al. (2004), Dall'Agnol et al. (2005), Feio et al. (2012), Feio et al. (2013), Santos et al. (2013), Teixeira et al. (2017), Galarza et al. (2017), Martins et al. (2017), Marangoanha et al. (2020), Martins (2021). The field of the Sm-Nd isotope signature of the Araguaia Belt incorporates data from rocks reported by Lisboa (2003), Paixão (2009), Arcanjo et al. (2013), Silva Neto (2018), Gorayeb et al. (2019).

5.3 PAREDÃO GROUP UPPER MEMBER

Five samples of the diamictite matrix, sandstones, and siltstones from the Paredão Group upper member were separated and analyzed for Sm-Nd isotopes (Fig. III.14). The results are listed in Table 4 together with $\varepsilon_{(Nd)}$-values and depleted mantle Nd-T_{DM} model age. Samples from the Paredão Group upper member yield negative $\varepsilon_{Nd(440\ Ma)}$ values varying between −8 and −14.3. Nd-T_{DM} model ages show Paleoproterozoic distribution ranging between 1.6 to 2.0 Ga (Fig. III.14A).

Comparing the isotopic patterns of Sm-Nd in the upper member of the Paredão Group with isotopic characteristics of potential source rocks provides information about the source areas (Fig. III.14B). These sedimentary deposits display negative ε_{Nd} values, indicating a contribution of crustal materials. However, the Paleoproterozoic Nd-T_{DM} ages younger than 1.9 Ga are incompatible with the idea of the Carajás Domain and Araguaia Belt rocks as a unique sediment source. In addition to the Carajás Domain and Araguaia Belt, the defined igneous sources for the metasedimentary rocks from the Araguaia Belt were also examined (cf. Pinheiro et al., 2011) (Fig. III.14B). Three episodes of continental crust formation in the Carajás Domain (2.7 to 3.2 Ga), Araguaia Belt (~2.1 Ga) and Goiás Magmatic Arc (0.9 to 1.1 Ga) are shows in the Fig. III.14B (references therein). The Paredão Group upper member samples show evolutionary trends that plot in the range between the Araguaia Belt and Goiás Magmatic Arc intervals (Fig. III.14B). The isotopic signature of these samples suggests the source-sediments mixing of older continental crust from the Carajás Domain, Araguaia Belt, and from the juvenile Meso-Neoproterozoic basement of Goiás Magmatic Arc (Fig. III.14B).

5.4 DATA ACCURACY

The Sm/Nd model age study in sedimentary rocks provenance has added to understanding crustal growth and geodynamic evolution (cf. Fuenlabra et al., 2020). It is widely accepted that the Sm/Nd ratio in crustal rocks remains unchanged mainly by chemical weathering, transport, deposition, diagenesis, or anything other than high-grade

metamorphism (Taylor and McLennan, 1985). Therefore, the Sm/Nd characteristics of sediments are taken to reflect accurately those of their protoliths and to aid in characterizing source areas (Nelson and DePaolo, 1988; McLennan et al., 1989; McLennan and Hemming, 1992; Fuenlabrada et al., 2020). Despite any differences in precise interpretation, Sm/Nd model ages could be considered a weighted average for the ages of extraction from a mantle reservoir of the protoliths of a detrital component (McLennan et al., 1989; Thorogood, 1990; Fuenlabrada et al., 2020). Analysis carried out in same horizon sand-mud pairs on modern deep-sea turbidites shows marked differences in the Sm/Nd ratio associated with separating components of different source areas during sediment transport and sorting (cf. McLennan et al., 1989). Therefore, failing to account for all grain sizes can lead to an incomplete understanding of the provenance of sediments.

The present study introduces isotopic data from continental and marine settings in different tectonic contexts (Fig. III.15). The analysis attempts to cover the most significant number of lithologies in these sedimentary series. Average variations between the samples were as substantial as three epsilon Nd units, corresponding to the Sm/Nd model age, which differed by up to 0,26 Ga (Table III.4). Figure III.15 exhibits a comparative resume of the isotopic Sm/Nd data. Considering that previous research shows variations in model age up to 0,44 Ga and seven epsilon Nd units in different grain size samples from the same horizons (cf. McLennan et al., 1989), the data from the studied sedimentary series present each one consistent source areas along the measured sedimentary logs (Fig. III.15 A). The variance among the sedimentary processes and transport mechanisms in each depositional setting influences differences between the isotopic data of the analyzed sedimentary series (Fig. III.15B). Reworking sediment with average upper crustal Sm/Nd isotope characteristics considerably dilutes the representativity of juvenile detritus (Thorogood, 1990). In this way, the isotopic signature of the Gorotire Formation was probably defined by the autocyclic processes that characterize pre-vegetational braided rivers (e.g., cannibalization of channel belts).

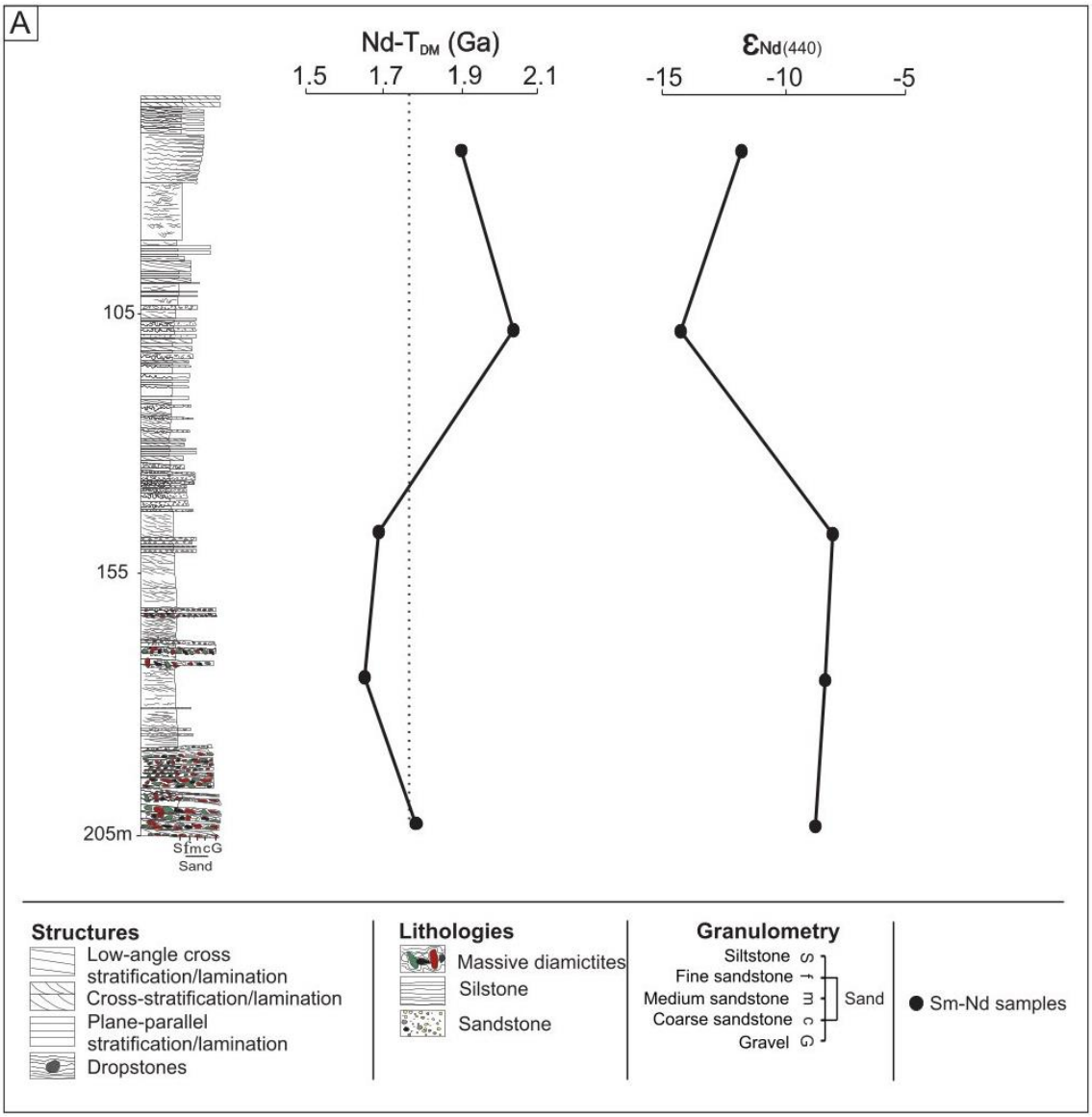
A
Nd-T$_{DM}$ (Ga)
1.5 1.7 1.9 2.1
εNd(440)
-15 -10 -5
105
155
205m
SfmcG
Sand
Structures
Low-angle cross stratification/lamination
Cross-stratification/lamination
Plane-parallel stratification/lamination
Dropstones
Lithologies
Massive diamictites
Silstone
Sandstone
Granulometry
Siltstone
Fine sandstone
Medium sandstone
Coarse sandstone
Gravel
S
F
M
C
G
Sand
Sm-Nd samples

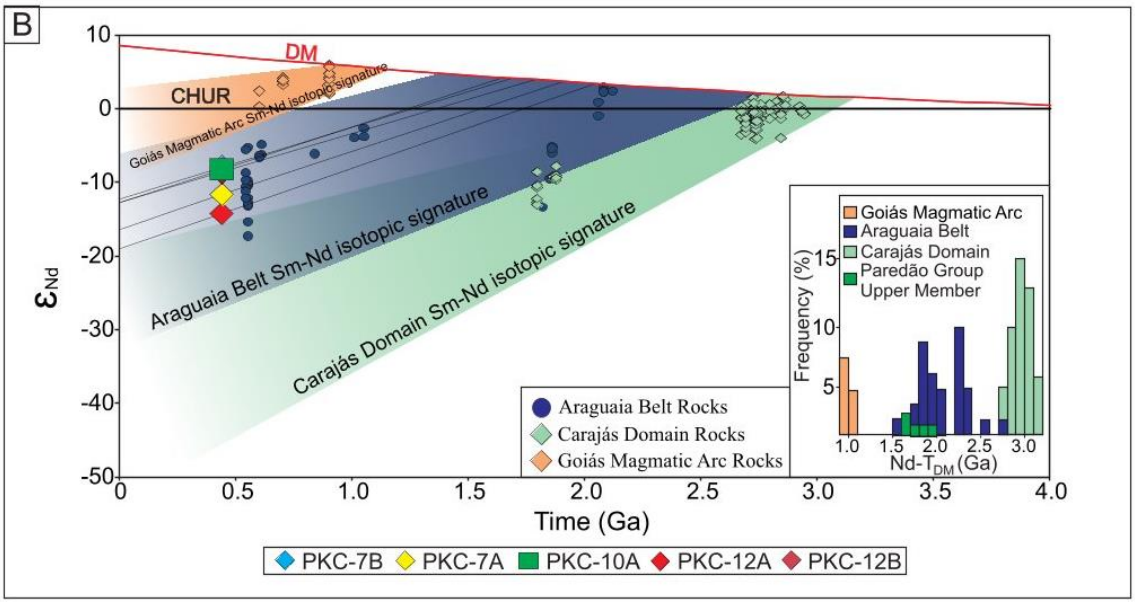
B
DM
CHUR
Goiás Magmatic Arc Sm-Nd isotopic signature
Araguaia Belt Sm-Nd isotopic signature
Carajás Domain Sm-Nd isotopic signature
εNd
Time (Ga)
Araguaia Belt Rocks
Carajás Domain Rocks
Goiás Magmatic Arc Rocks
Goiás Magmatic Arc
Araguaia Belt
Carajás Domain
Paredão Group
Upper Member
Frequency (%)
Nd-T$_{DM}$ (Ga)
PKC-7B PKC-7A PKC-10A PKC-12A PKC-12B

Figure III.14- Sm/Nd isotopic data from the Paredão Group Upper Member. A) Schematic stratigraphic logs of the Paredão Group Upper Member, showing the relative stratigraphic position of each sample selected for Sm/Nd analysis and vertical distribution of Nd-TDM and ƐNd(440 Ma). B) ƐNd(t) vs. Age (Ma) evolution diagram for the Paredão Group Upper Member rocks. The field of the Sm/Nd isotope signature of the Carajás Province incorporates data from rocks reported by Mellito (1998), Santos et al. (2000), Leite (2001), Teixeira et al. (2002), Galarza (2002), Galarza & Macambira (2002), Pimentel et al. (2003), Barros et al. (2004), Dall'Agnol et al. (2005), Feio et al. (2012), Feio et al. (2013), Santos et al. (2013), Teixeira et al. (2017), Galarza et al. (2017), Martins et al. (2017), Marangoanha et al. (2020), Martins (2021). The field of the Sm-Nd isotope signature of the Araguaia Belt incorporates data from rocks reported by Lisboa (2003), Paixão (2009), Arcanjo et al. (2013), Silva Neto (2018), Gorayeb et al. (2019). The field of the Sm-Nd isotope signature of the Goiás Magmatic Arc incorporates data from rocks reported by Pimentel & Fuck (1992).

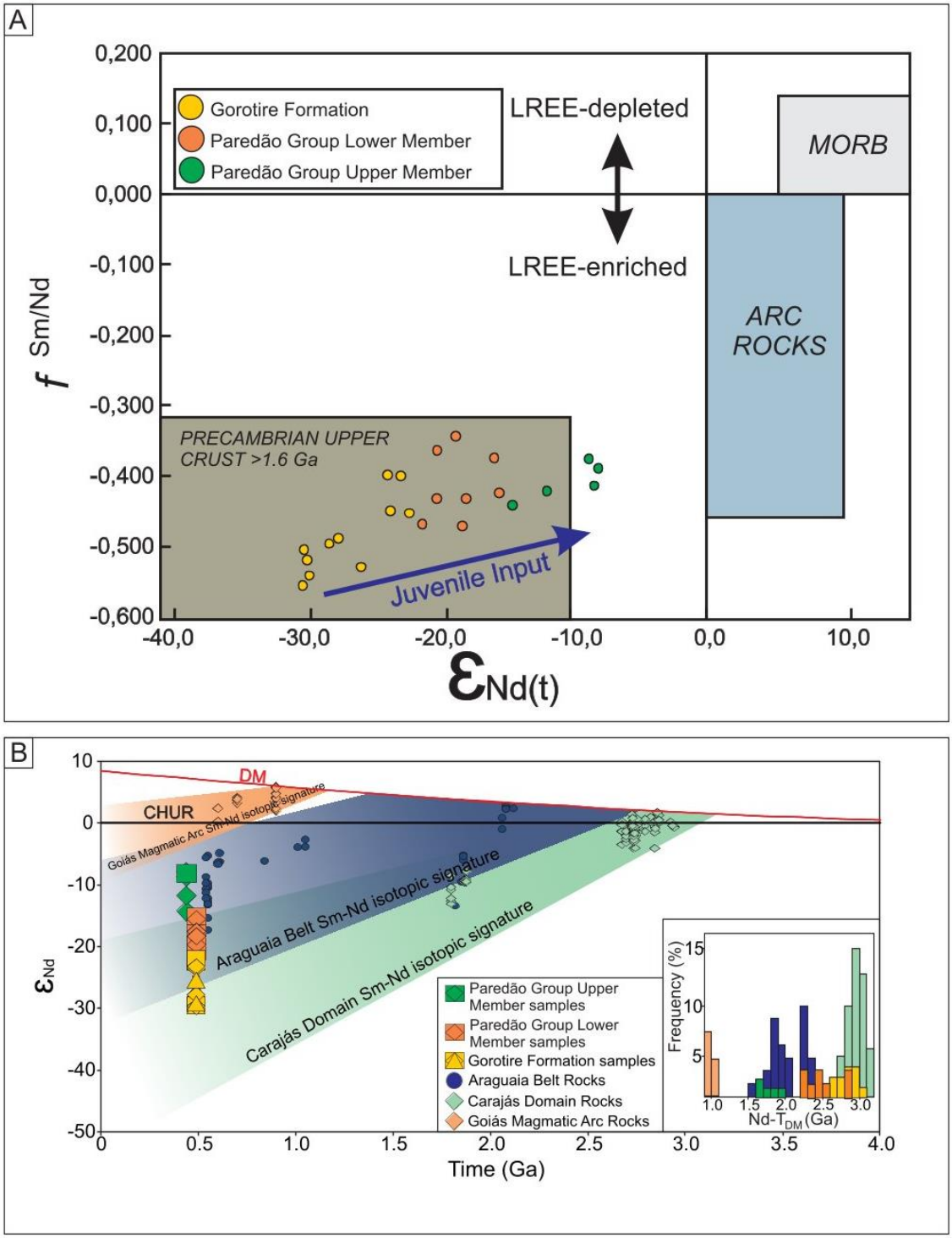

Figure III.15- Sm/Nd isotopic data from the Gorotire Formation and Paredão Group. A) fSm/Nd vs. εNd discrimination by McLennan et al. (1993) illustrates the MORB, Arc rocks, Passive margin/Craton, and Active margin fields. Plotted εNd values were calculated according to the inferred depositional ages of the Gorotire Formation and Paredão Group. B) εNd (t) vs. Age (Ma) evolution diagram for the Gorotire Formation and Paredão Group rocks.

On the other hand, the short transport and the restricted sediment dispersion that identify the alluvial fans system allow the preservation of the isotopic source areas signature in the lower member of the Paredão Group. Glaciomarine to delta settings interpreted for the upper member of the Paredão Group enable the conservation of source area signatures due to the poor ice transport sorting and the deficient proglacial and ice-melting currents that do not dilute the representative of juvenile detritus. Additionally, it is essential to note that these findings show that the classic provenance analyses based only on petrography and sedimentology are still open to doubt, and further research is needed to understand sediments provenance fully.

6. TECTONIC SETTING OF THE GOROTIRE FORMATION AND PAREDÃO GROUP.

Multiple deformation stages are defined in the southeastern Amazon Craton, related to the geodynamic evolution of the Carajás and Bacajá domains and their relationship with the Araguaia Belt (cf. Grainger et al., 2008; Tavares et al., 2018; Oliveira, 2018; Teixeira et al., 2019). These tectonics evolutionary events started in the Archean (~2.87 Ga) with the Carajás and Rio Maria domains collision (Tavares et al., 2018) and ended in the Cambrian (~490 Ma) with the collapse of the Araguaia orogen (Gorayeb et al., 2020).

Basin inversion during the development of the Araguaia belt generated a regional metamorphic event (528 Ma) (Moura et al., 2008). It was followed by extensional tectonics that led to the collapse of the Araguaia orogen (~0.49 Ga) (Gorayeb et al., 2020). In the Carajás Domain region, this extensional-transtensional episode (Teixeira et al., 2019) allows the rift basin installation in the craton margin (NNW-SSE) parallel the Araguaia Belt. A series of dykes (NNW-SSE) emplaced in Paleoproterozoic rocks in the Eastern Carajás Domain margin in proximities to the Serra do Paredão and Serra do Rabo regions reveals an early Cambrian intraplate mafic magmatism episode (535-485 Ma) (Amaral, 1974; Gomes et al., 1975; Santos et al., 2002; Teixeira et al., 2019). This magmatic event probably represents a response to the rift basin installation.

The transition from rift to post-rift stages in the Paredão Group is a key aspect of the geological record. As indicated by the sedimentary stacking patterns and the provenance data, this transition suggests a progression and evolution in the geological record. The Gorotire Formation, previously interpreted as the result of the Carajás Fault Paleoproterozoic reactivation, is now seen in a new light. The paleocurrent pattern of these sediments suggests a more extensive deposition area than the one limited by the Carajás Fault splays (cf. Nascimento & Oliveira, 2015). In addition, despite these sedimentary sequences being in a world-class mineral province, ore bodies or mineralization traces were never described. Moreover, the possible coexistence of the Gorotire Formation and the Paredão Group lower member paleoenvironments are more compatible with the deposition in a rift basin (Fig. III.16). Multiproxy provenance analysis data presented here for the Gorotire Formation and the Paredão Group lower member suggest a restricted deposition region with source areas related to the Carajás Domain and the Araguaia Belt (Fig. III.15 and III.16A). The sedimentary stacking patterns for the Gorotire formation show finning upward cycles with thicknesses up to 20m, indicating a record of a possible largest river. However, although one of the best clues to the scale of fluvial depositional systems is the size of the depositional architecture (Miall, 2006), the limited outcrops surface and provenance data restrictions are incompatible with an extensive river record (see. Potter, 1978). Thus, the Gorotire Formation fluvial deposits may reflect an accelerated subsidence stage rather than the contribution of a single extensive drainage system. These subsidence conditions are also observed in the proximal alluvial fan facies from the Paredão Group lower member and the Gorotire Formation (Lima & Pinheiro, 2001), represented by conglomeratic beds with thicknesses up to 30m. The sedimentary stacking patterns and the provenance data suggest that the deposition of these units is related to the syn-rift to rift stages, with high rates of accommodation space creation.

The glaciomarine to deltaic deposits from the Paredão Group upper member represent the post-rift stages (Fig. III.16B). Sedimentologic and stratigraphic data show a drastic transition between the continental and marine settings into the lower and upper members of the Paredão Group, suggesting a progressive basin limits expansion. In addition, the isotopic data (Sm/Nd) shows a vertical ascending input increase of juvenile sources, reinforcing the hypothesis of the growth of basin limits (Fig. III.15) (rift to sag basin?). The discontinuity surface that separates the Paredão Group members is

interpreted as the product of no deposition or, more probably, glacial erosion. The glacial record described here is interpreted as a possible record of the Silurian Glaciation, dating in the Brazilian intracratonic basins as Llandovery (~440 Ma) (Grahn & Caputo, 1992; Grahn et al., 2005; Grahn, 2005; Adôrno, 2014). However, more geochronological and biostratigraphical analysis is still needed to define the stratigraphic position and the relationship of the Paredão series with the glaciation.

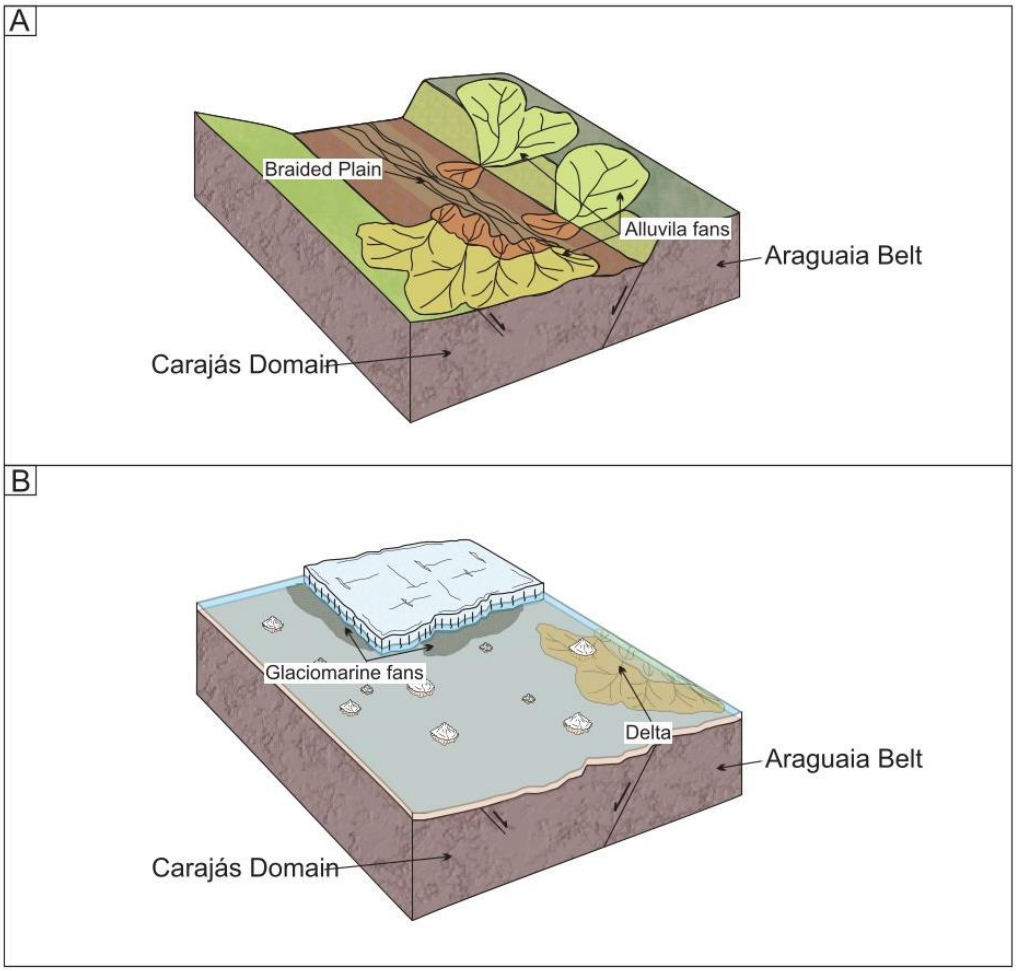

Figure III.16- Schematic reconstruction of the Southeastern Amazon Craton active margin during Cambrian-Silurian times (not to scale). A) The rift phase shows the alluvial and fluvial systems from the Gorotire Formation and Paredão Group Lower Member. B) Glacial conditions showing a basin expansion.

The reactivation of the South American Platform resulting from the fragmentation of the Gondwana Supercontinent during the Mesozoic, complemented by the continental separation between Africa and South America, influenced major tectonic events (Milani & Thomaz Filho, 2000; Zalán, 2004). In the Carajás region, this neotectonic framework corresponds to a transcurrent regime induced by the overlapping of extensional environments responsible for the Atlantic Ocean opening and compressive Andes Mountains installation (Pinheiro, 1997; Bemerguy et al., 2000; Braga, 2016). The Carajás

and Cinzento systems constituted this regimen and represented a regional reactivation event that affected the basement fabric (Pinheiro & Holdsworth, 2000). Regional orientation of the Archean mylonitic fabric of the basement follows a process of structural inheritance controlled by the geometry of structures generated during the tectonic events (Pinheiro & Holdsworth, 2000). The importance of this fabric as a controlling element of the geometry of late structures and reactivation along the transcurrent systems is represented by the preservation of narrow depocenters in the craton firm crust due to the brittle extension of the upper crust, which allowed the preservation of Paleozoic sequences such as those described in Serra do Paredão and Serra do Rabo regions (Pinheiro, 1997; Pinheiro & Holdsworth, 1997).

7. CONCLUSIONS

An integrated approach, combining sedimentological, stratigraphic, and multiproxy provenance analyses, led to the definition of a new stratigraphic framework for the Paredão Group and the Gorotire Formation in the Carajás Domain. The new stratigraphic evolutionary proposal for these deposits comprises the redefined Gorotire Formation and the Paredão Group subdivided into two members. The Gorotire Formation ~400m-thick includes a set of conglomerates and sandstone strata deposited in a bedload fluvial system. The Paredão Group corresponds to ~90m-thick alluvial fans massive conglomerates for the lower member and ~140m-thick glaciomarine massive diamictite and laminated sandstone that change vertically for deltaic sandstone and siltstone organized in meter-scale coarsening-upward cycles for the upper member. Provenance analyses for the Gorotire Formation and Paredão Group consist of whole-rock Sm-Nd isotopic data, sandstone petrography, heavy minerals, garnet mineral chemistry, and macroscopic provenance interpretation. These data reinforce the understanding that these sedimentary successions are not genetically related to the Archean-Neoproterozoic evolution of the CMP, and the deposition of these rocks only started when the southeastern Amazonian Craton was a stable continental substrate after the Neoproterozoic age. Additionally, it is essential to note that these findings show that the classic provenance analyses based only on petrography and sedimentology are still open to doubt, and further research is needed to understand sediments provenance fully.

Sedimentological and vertical stratigraphic attributes associated with marine conditions concomitant with glacial sedimentation, described in the glaciogenic deposits studied in this research and those related to the Ordovician-Silurian glacial event, led to

the recognition of a possible correlation between these records. The occurrence of Paleozoic deposits in an area considered exclusively Precambrian opens the perspective of understanding this part of the Amazonian craton as subsiding in different time intervals, allowing the preservation of different superimposed basinal phases. The South American Platform Mesozoic-reactivation controlled the Archean-Paleoproterozoic fabric movimentation. The importance of this fabric is represented by the preservation of narrow depocenters in the craton firm crust due to the brittle extension of the upper crust, which allowed the preservation of Paleozoic sequences such as the Paredão Group and Gorotire Formation. The discovery of Cambrian-Silurian strata in the CMP promotes new insight into the stratigraphy and the ore-mineral prospection. The simplification of the stratigraphy modifies the Proterozoic evolution, eliminating these problematic sedimentary sequences in the Carajás domain, which was never addressed adequately. This work also withdrew the Paredão Group and Gorotire Formation from the hall of possible prospective targets of the CMP since these successions were not affected by the Precambrian mineralization events.

ACKNOWLEDGMENTS

The authors are very grateful to Vale S.A. for making the drill cores available to study. This paper is a part of the Ph.D. thesis of the first author, who is thankful to the Programa de Pós-Graduação em Geologia e Geoquímica (PPGG) of the Federal University of Pará (UFPA) for logistic and financial support. The first author acknowledges the CAPES – Fundação Coordenação de Aperfeiçoamento de Pessoal de Nível Superior (Brazil) - Grant 88887.508135/2020-00.

REFERENCES

Adôrno R. R. 2014. Estudo cronobioestratigráfico da Formação Vila Maria: litoestratigrafia e paleontologia do limite ordoviciano-siluriano da Bacia do Paraná, estados de Goiás e de Mato Grosso, Brasil Central. MS Dissertation, Universidade de Brasília, Brasília, Brazil, pp. 94.

Afonso, J., Nogueira, A., 2018. Sedimentology and stratigraphy of Neoproterozoic-lower Paleozoic carbonate-siliciclastic succession of the southwesternmost Amazon Craton,

state of Rondônia, Brazil. Brazilian Journal of Geology. 48. 10.1590/2317-4889201820170002.

Almeida F.F.M., Hasui Y., Brito Neves B.B., Fuck R.A. 1981. Brazilian Structural Provinces: An introduction. Earth-Science Reviews, 17: 1–29.

Amaral, G. 1974. Geologia pré-cambriana da região amazônica. PhD Thesis, Universidade de São Paulo, Brazil, pp. 217.

Araújo, O.J.B., Maia, R.G.N., Silva, J.J.X., Costa, J.B.S., 1988. A megaestruturação da folha Serra dos Carajás. In: Congresso Latino Americano de Geologia. vol. 7. pp. 324–333.

Araújo, O.J.B., Maia, R.G.N., 1991. Serra dos Carajás, folha SB.22-ZA, Estado do Pará. In: Programa Levantamentos Geológicos Básicos do Brasil. Companhia de Pesquisa de Recursos Minerais, pp. 164p.

Araújo Filho, R.C., Nogueira, A.C.R., Araújo, R.N., 2020. New stratigraphic proposal of a paleoproterozoic siliciclastic succession: implications for the evolution of the Carajás Basin, Amazonian craton, Brazil. J. S. Am. Earth Sci. 102665 https://doi.org/ 10.1016/j.jsames.2020.102665.

Araújo, R., & Nogueira, A., 2019. Serra sul diamictite of the Carajás Basin (Brazil): a paleoproterozoic glaciation on the Amazonian Craton. Geology 47, 1166–1170. https://doi.org/10.1130/G46923.1.

Araújo, R., 2020. Estratigrafia e eventos da transição Neoarqueano-Paleoproterozóico da Bacia de Carajás, sudeste do Cráton Amazônico. PhD Thesis, Universidade Federal do Pará, Brazil, pp. 215.

Arcanjo, S.H.S., Abreu, F.A.M., Moura, C.A.V., 2013. Evolução geológica das sequências do embasamento do Cinturão Araguaia na região de Paraíso do Tocantins (TO), Brasil. Braz. J. Genet. 43, 501–514.

Barbosa, R.C.de M., 2014. Paleoambiente e proveniência da formação cabeças da bacia do Parnaíba: evidências da glaciação famenniana e implicações na potencialidade do reservatório. Phd Thesis, Universidade Federal do Pará, Belém, Brasil, pp. 124.

Barrera I.A.R., Nogueira A.C.R., Bandeira J. 2020. The Silurian glaciation in the eastern Parnaíba Basin, Brazil: paleoenvironment, sequence stratigraphy and insights for the evolution and paleogeography of West Gondwana. Sedimentary Geology, 406-105714.

Bhattacharya, J.P., 2006. "Deltas". In: Posamentier, H.W., Walker, R.G., (Eds.), Facies Models Revisited. SEPM Society for Sedimentary Geology, pp. 237-293.

Barros, C.E.M., Macambira, M.J.B., Barbey, P., Scheller, T., 2004. Dados isotópicos Pb–Pb em zircão (evaporação) e Sm–Nd do Complexo Granítico Estrela, Província Mineral de Carajás, Brasil: implicações petrológicas e tectônicas. Rev. Bras. Geociencias 34, 531–538.

Bemerguy R.L, Espírito Santo C. V., Costa J. B. S., Rozal E. O., 2000. Aspectos Morfoestruturais e Neotectônicos da Região da Serra dos Carajás (Sudeste do Estado do Pará). UNESP, Geociências, São Paulo, 19(1): 35-49.

Bettencourt, J.S., Juliani Xavier, R.P., Monteiro, L.V.S., Bastos-Neto, A.C., Klein, E.L., Assis, R.R., Leite-Jr, W.P., Moreto, C.P.N., Fernandes, C.M.D., Pereira, V.P., 2016. Metallogenetic systems associated with granitoid magmatism in the Amazon Craton: an overview of the present understanding and exploration significance. J. S. Am. Earth Sci. 68, 22–49.

Blair, T.C., McPherson, J.G., 1994a. Alluvial fan processes and forms. In: Abrahams, A.D., Parsons, A. (Eds.), Geomorphology of Desert Environments. Chapman & Hall, London, pp. 354-402.

Blair, T. C., & McPherson, J. G. 1994b. Alluvial fans and their natural distinction from rivers based on morphology, hydraulic processes, sedimentary processes, and facies assemblages. Journal of Sedimentary Research; 64 (3a): 450–489. doi: https://doi.org/10.1306/D4267DDE-2B26-11D7-8648000102C1865D

Boulton G.S. & Deynoux M. 1981. Sedimentation in glacial environments and identifying tills and tillites in ancient sedimentary sequences. Precambrian Res., 15: 397–422. Doi: https://doi.org/10.1016/0301-9268(81)90059-0.

Braga, A. A., 2016. Influência estrutural sobre cavernas em formações ferríferas, Carajás-PA. Master dissertation. Universidade Federal do Paraná, Curitiva, Brazil, pp. 70.

Bridge, J.S., 2006. Fluvial facies models: Recent developments, in Posamentier, H.W., and Walker, R.G., eds., Facies models revisited: SEPM (Society for Sedimentary Geology) Special Publication 84, p. 85–170.

Brito Neves, B.B., Fuck, R.A., Cordani, U.G., Thomaz F, A., 1984. Influence of basement structures on the evolution of the major sedimentary basins of Brazil: a case of tectonic heritage. J. Geodyn. 1, 495–510. https://doi.org/10.1016/0264-3707(84)90021-8.

Brito Neves, B. B., 2002. Main Stages of Development of the Sedimentary Basins of South America and their Relationship with the Tectonics of Supercontinents. Gondwana Research. 4. 175-196. 10.1016/S1342-937X(05)70901-1.

Busfield M.E. & Le Heron D.P. 2018. Snowball Earth under the microscope. Journal of Sedimentary Research, 88:659-677.

Cabral, A.R., Creaser, R.A., Nagler, T., Lehmann, B., Voegelin, A.R., Belyatsky, B., Pasava, J., Seabra Gomes Jr., A.A., Galbiatti, H., Bottcher, M.E., Escher, P., 2013. Trace element and multi-isotope geochemistry of late-archean black shales in the Carajás iron-ore district, Brazil. Chem. Geol. https://doi.org/10.1016/j.chemgeo.2013.08.041.

Caputo, M. V. 1984. Stratigraphy, tectonics, paleoclimatology, and paleogeography of Northern Basins of Brazil.Thesis (doctorate) – University of Califórnia, Santa Bárbara. 586p.

Caputo, M. V., Streel, M., Isbell, J., 2008. Late Devonian and Early Carboniferous glacial records of South America. Special Paper of the Geological Society of America. 441. 161-173. 10.1130/2008.2441(11).

Costa, M.L., Fernandez, O.J.C., Requelme, M.E.R., 2005. Depósito de Manganês do Azul, Carajás: estratigrafia, mineralogia, geoquímica e evolução geológica. In: Caracterização de depósitos minerais em distritos mineiros da Amazônia. DNPM-CT/Mineral-ADIMB,231-333.

Costa, F.F.O. 2017. A Sucessão Siliciclástica paleoproterozoica associada ao depósito de manganês do Azul da Serra dos Carajás. MS Dissertation. Universidade Federal do Pará, Brazil, pp. 62.

Cotter, E., 1978. The evolution of fluvial style, with special reference to the Central Appalachian Paleozoic. In: Miall, A.D. (Eds.), Fluvial Sedimentology. Canadian Society of Petroleum Geologists Memoir 5, pp. 361–383.

Dall‟Agnol, R., Teixeira, N.P., Rämö, O.T., Moura, C.A.V., Macambira, M.J.B., Oliveira, D.C. 2005. Petrogenesis of the Paleoproterozoic rapakivi A-type granites of the Archean Carajás metallogenic province, Brazil. Lithos, 80(1): 101-129.

Dall'Agnol, R., Oliveira, D.C., Guimarães, F.V., Gabriel, E.O., Feio, G.R.L., Lamarão, C.N., Althoff, F.J., Santos, P.A., Teixeira, M.F.B., Silva, A.C., Rodrigues, D.S., Santos, M.J.P., Silva, C.R.P., Santos, R.D., Santos, P.J.L., 2013. Geologia do Subdomínio de Transição do Domínio Carajás – Implicações para a evolução arqueana da Província Carajás - Pará. SBG. In: Simpósio de Geologia da Amazônia 13. CD-ROM, Anais, Belém, in Portuguese.

Davies, N. S., Gibling, M. R., 2010. Paleozoic vegetation and the Siluro-Devonian rise of fluvial lateral accretion sets. Geology, 38(1), 51–54. doi:10.1130/g30443.1.

Davies, N.S., Gibling, M.R., Rygel, M.C., 2011. Alluvial facies evolution during the Palaeozoic greening of the continents: case studies, conceptual models and modern analogs. Sedimentology 58, 220–258. https://doi.org/10.1111/j.1365-3091.2010.01215.x.

DePaolo D.J. 1981. A neodymium and strontium isotopic study of the Mesozoic calc-alkaline granitic batholiths of the Sierra Nevada and Peninsular Ranges, California. Journal of Geophysical Research, 86 (B11): 10470-10488.

Deer, W.A., Howie, R.A., Zussman, J., 1992. An Introduction to Rock-forming Minerals. Longman Group Limited, Hong Kong. 696 pp.

Dias, A.N.C., Moura, C.A.V., Milhomem Neto, J.M., Chemale Jr., F., Girelli, T.J., Masuyama, K.M., 2017. Geochronology and thermochronology of the gneisses of the brasiliano/Pan-African Araguaia belt: records of exhumation of West Gondwana and Pangea break up. J. S. Am. Earth Sci. 80, 174–191.

Díaz-Martínez, E., Grahn, Y., 2006. Early Silurian glaciation along the western margin of Gondwana (Peru, Bolivia, and northern Argentina): Paleogeographic and geodynamic setting. Paleogeography, Paleoclimatology, Paleoecology. 245, 62–81. https://doi:10.1016/j.palaeo.2006.02.018.

Dickinson, W.R., Suczek, C.A., 1979. Plate tectonics and sandstone composition. Am. Assoc. Pet. Geol. Bull. 63 (12), 2164–2172.

Dickinson, W.R., Beard, L.S., Brakenridge, G.R., Erjavee, J.R., Ferguson, R.C., Inman, K.F., 1983. Provenance of North American phanerozoic sandstones in relation to plate tectonic setting. Geol. Soc. Am. Bull. 94 (2), 222–235.

Dietrich, P., Ghienne, J.-F., Schuster, M., Lajeunesse, P., Nutz, A., Deschamps, R., Duringer, P., 2017. From outwash to coastal systems in the Portneuf-Forestville deltaic complex (Québec North Shore): Anatomy of a forced regressive deglacial sequence. Sedimentology, 64(4), 1044–1078. doi:10.1111/sed.12340

Docegeo (Rio Doce Geologia e Mineração). 1988. Revisão litoestratigráfica da Província Mineral de Carajás, Pará. In: Congresso Brasileiro de Geologia, 35. Belém, 1988. Anexo aos Anais, p. 11-54.

Dreher A.M. 2004. O depósito primário de Cu-Au de Igarapé Bahia, Carajás: rochas fragmentárias, fluidos mineralizantes e modelo metalogenético. PhD Thesis, Campinas, SP, pp. 221.

Dreher, A.M., Xavier, R.P., Martini, S.L., 2005. Fragmental rocks of the Igarape Bahia Cu-Au deposits, Carajás mineral Province, Brazil. Revista Brasileira de Geociências 35, 359–368.

Dreher, A.M., Xavier, R.P., Taylor, B.E., Martini, S.L., 2008. New geologic, fluid inclusion, and stable isotope studies on the controversial Igarap´e Bahia Cu-Au deposit, Carajás Province, Brazil. Miner. Deposita 43, 161–184. https://doi.org/10.1007/s00126-007-0150-6.

Enos, P., 1977. Flow regimes in debris flow. Sedimentology, 24, 133–144.

Evans, J.A., Stone, P., Floyd, J.D., 1991. Isotopic characteristics of Ordovician greywacke provenance in the Southern Uplands of Scotland. In: Morton, A.C., Todd, S.P., Haughton, P.D.W. (Eds.), Developments in Sedimentary Provenance Studies. Geological Society Special Publication, 57, pp. 161–172.

Eyles N. 1993. Earth's glacial record and its tectonic setting. Earth-Science Reviews., 35: 1–248.

Feio, G.R.L., Dall'Agnol, R., Dantas, E.L., Macambira, M.J.B., Gomes, A.C.B., Sardinha, A. S., Oliveira, D.C., Santos, R.D., Santos, P.A., 2012. Geochemistry, geochronology, and origin of the Neoarchean Planalto Granite suite, Caraj´as, Amazonian craton: Atype or hydrated charnockitic granites? Lithos 151, 57–73. https://doi.org/10.1016/j.lithos.2012.02.020.

Feio, G.R.L., Dall‟Agnol, R., Dantas, E.L., Macambira, M.J.B., Santos, J.O.S., Althoff, F.J., Soares, J.E.B. 2013. Archean granitoid magmatism in the Canaã dos Carajás area: implications for crustal evolution of the Carajás province, Amazonian craton, Brazil. Precambrian Research 227: 157-185.

Fernandes, C.M.D., Juliani, C., Monteiro, L.V.S., Lagler, B., Misas, C.M.E., 2011. High-K calc-alkaline to A-type fissure-controlled volcanoplutonism of the São Félix do Xingu region, Amazonian craton, Brazil: exclusively crustal sources or only mixed Nd model ages? J. S. Am. Earth Sci. 32 (4), 351–368.

Ferreira, A.T.R., Lamarão, C.N., 2013. Geologia, petrografia e geoquímica das rochas vulcânicas Uatumã na área sul de São Félix do Xingu (PA), Província Carajás. Braz. J. Genet. 43 (1), 152–167.

Finnegan, S., K. Bergmann, J. M., Eiler, D. S., Jones, D. A., Fike, I., Eisenman, N. C., Hughes, A. K., Tripati, W., Fischer, W., 2011. The magnitude and duration of Late Ordovician-Early Silurian glaciation, Science, 331(6019), 903–906.

Frey, S.E., Gingras, M.K., and Dashtgard, S.E., 2009, Experimental studies of gas scape and water-escape structures: Mechanisms and morphologies: Journal of Sedimentary Research, v. 79, p. 808–816.

Frost, C.D., Winston, D., 1987. Nd isotopic systematic of coarse- and fine-grained sediments: examples from the Middle Proterozoic Belt Purcell Super Group. Journal of Geology 95, 309–327.

Fuenlabrada, J. M., Arenas, R., Martínez, S. S., Fernández, R. D., Pieren, A. P., Pereira, M. F., Silva, J. B., 2020. Geochemical and isotopic (Sm/Nd) provenance of Ediacaran-Cambrian metasedimentary series from the Iberian Massif. Paleoreconstruction of the North Gondwana margin. Earth-Science Reviews, 103079.

Fuller, A.O., 1985. A contribution to the conceptual modeling of pre-Devonian fluvial systems: Geological Society of South Africa Transactions, v. 88, p. 189–194.

Galarza M.A. 2002. Geocronologia e geoquímica isotópica dos depósitos de Cu-Au Igarapé Bahia e Gameleira, Província Mineral de Carajás, Brasil. PhD Thesis, Universidade Federal do Pará, Belém, Brazil, pp. 223.

Galarza, M.A., Macambira, M.J.B., 2002. Geocronologia e evolução crustal da área do depósito de Cu-Au Gameleira, Província Mineral de Carajás (Pará), Brasil. Revista do Instituto de Geociências da USP 2, 143–159.

Galarza, M.A., Macambira, M.J.B., Villas, R.N., 2008. Dating and isotopic characteristics (Pb and S) of the Fe oxide-Cu-Au-U-REE Igarapé Bahia ore deposit, Carajás mineral

province, Pará state, Brazil. J. S. Am. Earth Sci. 25, 377–397. https://doi.org/10.1016/j.jsames.2007.07.006.

Galarza M.A., Oliveira D.C., Rodrigues E.A., Santos A.N., Martins A.C., Marangoanha B. 2017. Neoarchean granitoids (2.73–2.74 Ga) intrusive and associated with the Pium Diopside- Norite, Canaã dos Carajás, Carajás Province (PA). In: Lima A.M & Gorayeb P. (eds.). Contribuições à geologia da Amazônia, SBG-Núcleo Norte, 10:225–246.

Galehouse, J. S., 1971. Sedimentation analysis. In: Procedures in sedimentary petrology; (eds) Carver, R. E., New York: Wiley-Interscience. Pp. 65–94.

Galloway, W., 1975. Process framework for describing the morphologic and stratigraphic evolution of deltaic depositional system. Society of Economic Paleontologists and Mineralogist (SEPM), Special Publication. 31, 127-156.

Garzanti, E. 2017. The Maturity Myth In Sedimentology and Provenance Analysis. Journal of Sedimentary Research. 87. 353-365. 10.2110/jsr.2017.17.

Garzanti, E. 2019. Petrographic classification of sand and sandstone. Earth-Science Reviews. 192. 10.1016/j.earscirev.2018.12.014.

Ghienne, J.-F., Le Heron, D.P., Moreau, J., Denis, M. and Deynoux, M. 2007. The Late Ordovician glacial sedimentary system of the North Gondwana platform. In: Hambrey, M.J., Christoffersen, P., Glasser, N.F. and Hubbard, B. (eds) Glacial Sedimentary Processes and Products. International Association of Sedimentologists, Oxford, Special Publications, 39, 290–319.

Ghienne, J.-F., Desrochers, A., Thijs, R.A., Vandenbroucke, A.A., Asselin, E., Dabard, M-P., Farley, C., Loi, A., Paris, F., Wickson, S., Veizer, J., 2014. A Cenozoic-style scenario for the end-Ordovician glaciation, Nat. Commun., 5, 4485.

Ghienne, J.-F., Benvenuti, A., El Houicha, M., Girard, F., Kali, E., Khoukhi, Y., Langbour, C., Magna, T., Míková, J., Moscarielllo, A. and Schulmann, K. 2018. The impact of the end-Ordovician glaciation on sediment routing systems: a case study from the Meseta (northern Morocco). Gondwana Research, 63, 169–178.

Ghienne, J-F., Abdallah, H., Deschamps, R., Guiraud, M., Gutiérrez-Marco, J. C., Konaté, M., Meinhold, G., Moussa, A., and Rubino, J-L. 2023. The Ordovician record of North and West Africa: unravelling sea-level variations, Gondwana tectonics, and the glacial impact. Geological Society, London, Special Publications, 533, 199 – 252.

Gibbs, A.K., Wirth, K.R., Hirata, W.K., Olszewski Jr., W.J., 1986. Age and composition of the Grão Pará groups volcanic, Serra dos Carajás. Revista Brasileira de Geociências 16, 201–211.

Gioia, S.M.C.L., Pimentel, M.M., 2000. The Sm–Nd isotopic method in the Geochronology Laboratory of the University of Brasília. Anais da Academia Brasileira de Ciências 72 (2), 219–245.

Gomes, C.B., Cordani, U.G., Basei, M.A.S., 1975. Radiometric ages from the Serra dos Carajás Area, Northern Brazil. Bull. Geol. Soc. Am. 86, 939–945.

Gomes, R. S., 2020. Geocronologia U-Pb em zircão detrítico e proveniência de arenitos pré-cambrianos da Região de Itupiranga-PA. Universidade Federal do Pará, Belém, Brazil, pp. 72.

Gorayeb, P. S. S., Santos, W. P., Moura, C. A. V., Sousa, L. H., 2019. Petrologia, geoquímica e geocronologia do Granodiorito Presidente Kennedy: contextualização na evolução do Cinturão Araguaia. Geologia USP. Série Científica, v. 19, p. 89-116.

Gorayeb, P. S. S., Cordani, U. G., Silva Neto, J. J., Sato, K., & Maurer, V. C. 2020. U–Pb SHRIMP zircon ages of Ediacaran-Cambrian granitic bodies in central Brazil: Implications for the tectonic evolution of the Araguaia belt. Journal of South American Earth Sciences, 102804. doi:10.1016/j.jsames.2020.102804

Grahn, Y., 1991. The Ordovician-Devonian biostratigraphy of Brazil. An. Acad. Bras. Cicnc. Resumo Comun. 94.

Grahn, Y. 1992. Revision of Silurian and Devonian strata of Brazil. Palynology, 16:35-61.

Grahn, Y., Caputo, M.V., 1992. Early Silurian glaciations in Brazil. Palaeogeography, Palaeoclimatology, Palaeoecology. 99, 9–15. https://doi.org/10.1016/0031-0182(92)90003-N.

Grahn, Y., Paris, F., 1992. Age and correlation of the Trombetas Group, Amazonas Basin, Brazil. Revue de Micropaléontologie 35, 197–209.

Grahn, Y., De Melo, J.H.G., Steemans, A.P., 2005. Integrated chitinozoan and miospore zonation of the Serra Grande group (Silurian-Lower Devonian), Parnaíba Basin, northeast Brazil. Rev. Espanola Micropaleontol. 37, 183–204.

Grahn, Y., 2005. Ordovician and Silurian chitinozoan biozones of western Gondwana. Geological Magazine - GEOL MAG. 143. 10.1017/S001675680600207X.

Grainger, C.J., Groves, D.L., Tallarico, F.H.B., Fletcher, I.L., 2008. Metallogenesis of the Carajás Mineral Province, Southern Amazon Craton, Brazil: varying styles of Archean through Paleoproterozoic to Neoproterozoic base- and precious-metal mineralization. Ore Geol. Rev. 33 (3–4), 451–489.

Hambrey, M.J., 1985. The late Ordovician-early Silurian glacial period. Palaeogeography, Palaeoclimatology, Palaeoecology, 51, 273-289.

Hart J.K. & Roberts D.H. 1994. Criteria to distinguish between subglacial glaciotectonic and glaciomarine sedimentation. I. Deformational styles and sedimentology. Sedimentary Geology, 91: 191-214.

Hjellbakk, A., 1997. Facies and fluvial architecture of a high-energy braided river: the Upper Proterozoic Seglodden Member, Varanger Peninsula, northern Norway. Sedimentary Geology. 114, 131-161. https://doi.org/10.1016/S0037-0738(97)00075-4.

Holdsworth, R.E., Pinheiro, R.V.L., 2000. The anatomy of shallow-crustal transpressional structures: insights from the Archaean Carajás fault zone, Amazon, Brazil. J. Struct. Geol. 22 1105-1023.

Hoffman P.F., Kaufman A.J., Halverson G.P., Scharg D.P. 1998. A Neoproterozoic Snowball Earth, Science, 281:1342-1346.

Ielpi, A., & Rainbird, R., 2015. Architecture and morphodynamics of a 1.6 Ga fluvial sandstone: Ellice Formation of Elu Basin, Arctic Canada. Sedimentology. 62, 1950-1977. https://doi.org/10.1111/sed.12211.

Ingram, R.L., 1954. Terminology for the thickness of stratification and parting units in sedimentary rocks. Geology Society Bulletin, 65, 937-938. https://doi.org/10.1130/0016-7606(1954)65[937:TFTTOS]2.0.CO;2.

Johnsson, M.J., 1993. The system controlling the composition of clastic sediments Geological Society of America Special Papers, 284, 1–20.

Juliani, C., Fernandez, C.M.D., 2010. Well-preserved Late Paleoproterozoic volcanic centers in the São Félix do Xingu region, Amazonian craton, Brazil. J. Volcanol. Geoth. Res. 191, 167–179.

Le Heron, D., Busfield, M., Kamona, F., 2013. An interglacial on snowball Earth? Dynamic ice behavior revealed in the Chuos Formation, Namibia. Sedimentology. 60, 411-427. https://doi.org/10.1111/j.1365-3091.2012.01346.x.

Leite A.A.S. 2001. Geoquímica, petrogênese e evolução estrutural dos granitoides arqueanos da região de Xinguara, SE do Cráton Amazônico. Tese de Doutorado. Centro de Geociências. Universidade Federal do Pará, Belém, 330p.

Lima F.D., & Pinheiro R.V.L. 2001. Formação Gorotire: Considerações Sobre uma Unidade Siliciclástica Particular da Serra dos Carajás - PA. In: Reis N.J. e Monteiro M.A.S. (orgs.) - Contribuições à Geologia da Amazônia, 1. Manaus, SBG/NO, 2: 201-224.

Lønne, I., 1995. Sedimentary facies and depositional architecture of ice-contact glaciomarine systems. Sediment. Geol. 98, 13–43. https://doi.org/10.1016/0037-0738(95)00025-4.

Long, D.G.F., 1978. Proterozoic stream deposits: some problems of recognition and interpretation of ancient sandy fluvial systems. In: Miall, A.D. (Ed.), Fluvial Sedimentology. Can. Soc. Pet. Geol., Mem., vol. 5, pp. 313–341.

Long, D.G.F., 2004, Precambrian Rivers, in Eriksson, P.G., et al., eds., The Precambrian Earth: Tempos and events: Developments in Precambrian Geology 12: Amsterdam, Elsevier, p. 660–663.

Lowe, D., 1975. Water escape structures in coarse grained sediment. Sedimentology. 22, 157 - 204. https://doi.org/10.1111/j.1365-3091.1975.tb00290.x.

Lowe, D.R., 1976. Grain flow and grain flow deposits. J. Sed. Petrol., 46, 188–199.

Lowe, D.R., 1979. Sediment gravity flows II: depositional models with special reference to deposits of high density turbidity currents. J. Sed. Petrol., 52, 279–297.

Luz B.R., Crowley J.K. 2012. Morphological and chemical evidence of stromatolitic deposits in the 2.75 Ga Carajás banded iron formation, Brazil. Earth and Planetary Science Letters, 355:60-72.

Macambira J.B., Ramos J.F.F., Assis J. F. P., Figueiras A. J. M. 1990. Projeto Serra Norte. Conv. Seplan/DOCEGEO/UFPa. Projeto Pojuca. Convênio DNPM/DOCEGEO/UFPa. Relatório final, pp. 150.

Macambira J.B. 2003. O ambiente deposicional da Formação Carajás e uma proposta de modelo evolutivo para a Bacia Grão-Pará. PhD Thesis, Campinas, SP, Brazil, pp. 217.

Macambira, M.J.B., Vasquez, M.L., Silva, D.C.C., Galarza, M.A., Barros, C.E.M., Camelo, J.F., 2009. Crustal growth of the central-eastern Paleoproterozoic domain, SW Amazonian craton: juvenile accretion vs. reworking. J. S. Am. Earth Sci. 27, 235–246.

Machado, N., Lindenmayer, Z., Krogh, T.E., Lindenmayer, D., 1991. U-Pb geochronology of Archean magmatism and basement reactivation in the Caraj´as area, Amazon shield, Brazil. Precambr. Res. 49, 329–354. https://doi.org/10.1016/0301-9268(91)90040-H.

Mange, M.A., Maurer, H.F.W., 1992. Heavy Minerals in Color. Chapman and Hall, London.

Martins P.L.G., Toledo, C.L.B., Silva A.M., Chemale Jr F., Santos J.O.S., Assis L.M. 2017. Neoarchean magmatism in the southeastern Amazonian Craton, Brazil: Petrography, geochemistry and tectonic significance of basalts from the Carajás Basin. Precambrian Research, 302:340–357.

Martins, P. L. G., Paleogeografia e ambiente tectônico de formação da Bacia Carajás: uma análise a partir de estudos geoquímicos, paleomagnéticos e isotópicos nas rochas vulcânicas do Grupo Grão-Pará. PhD Thesis, Belém, Brazil, pp. 262.

Marangoanha, B. 2018. Petrologia e evolução crustal da porção central do Domínio Canaã Dos Carajás, Província Carajás. Phd Thesis, Belém, PA, Brazil, pp. 224. (in português and English).

Marangoanha B., Oliveira D.C., Galarza M.A., Marques G.T. 2020. Crustal anatexis and mantle-derived magmas forming Neoarchean A-type granitoids in Carajás Province, northern Brazil: petrological evidence and tectonic control. Precambrian Research, 338:105585.

Mclennan, S.M., McCulloch, M.T., Taylor, S.R., Maynard, J.B., 1989. Effects of sedimentary sorting on neodymium isotopes in deep-sea turbidites. Nature 337, 547–549.

McLennan, S.M., Hemming, S., 1992. Samarium/neodymium elemental and isotopic systematics in sedimentary rocks. Geochim. Cosmochim. Acta 56 (3), 887–898.

McLennan, S.M., Hemming, S., McDaniel, D.K., Hanson, G.N., 1993. Geochemical approaches to sedimentation, provenance, and tectonics. In: Johnsson, M.J., Basu, A. (Eds.), Processes Controlling the Composition of Clastic Sediments. Geological Society of America, Boulder, CO, USA, pp. 21–40 Special Paper.

Mellito, K. M., 1998. Aplicação dos sistemas Rb-Sr, Pb-Pb e Sm-Nd no deposito polimetálico do Salobo 3ª, Provincia Mineral de Carajás, Pará. Master dissertation. Universidade Federal do Pará, Belém, Brazil, pp. 124.

Miall A.D. 1981. Analysis of fluvial depositional systems. Education Course Note Series. American Association of Petroleum Geologists. 20:1-75.

Miall, A.D. 2006. How do we identify big rivers? And how big is big? Sedimentary Geology. 186: 39–50.

Milani, E.J., Thomaz-Filho, A., 2000. Sedimentary basins of South America. In: Cordani, U. G., E. J. Milani, A. Thomaz-Filho & D. A. Campos (Eds). Tectonic evolution of South America. 31st International Geological Congress. Rio de Janeiro, Academia Brasileira de Ciências e Departamento Nacional da Produção Mineral (DNPM), Pp. 389–449.

Miller J.G.M. 1996. Glacial sediments. In: Reading H.G. (eds.). Sedimentary environments: processes, facies and stratigraphy. 3rd ed. [S.l], published by Wiley. 454-483.

Menzies J., van der Meer J.J.M., Ravier E. 2016. A Kinematic Unifying Theory of Microstructures in Subglacial Tills. Sedimentary Geology. 344: 57-70. Doi: https://doi.org/10.1016/j.sedgeo.2016.03.024.

Moreto C.P.N., Monteiro L.V.S., Xavier R.P., Creaser R.A., DuFrane S.A., Tassinari C.C.G., Sato K., Kemp A.I.S., Amaral W.S. 2015. Neoarchean and Paleoproterozoic iron oxide-copper-gold events at the Sossego Deposit, Carajas Province, Brazil: Re-Os and U-Pb geochronological evidence. Econ. Geol. 110: 809-835.Morris R.C. 1993. Genetic modeling for banded iron-formation of the Hamersley Group, Pilbara Craton, Western Australia. Precambrian Research, 60(1-4): 243-286.

Morton, A.C., Hallsworth, C.R., 1994. Identifying provenance-specific features of detrital heavy mineral assemblages in sandstones. Sedimentary Geology 90, 241–256.

Morton, A.C., Hallsworth, C.R., 1999. Processes controlling the composition of heavy mineral assemblages in sandstones. Sedimentary Geology 124, 3–29.

Morton, A.C., Hallsworth, C.R., Chalton, B., 2004. Garnet compositions in Scottish and Norwegian basement terrains: a framework for interpretation of North Sea sandstone provenance. Marine and Petroleum Geology 21, 393–410.

Morton, A.C., Whitham, A.G., Fanning, C.M., 2005. Provenance of Late Cretaceous to Paleocene submarine fan sandstones in the Norwegian Sea: integration of heavy mineral, mineral chemical and zircon age data. Sedimentary Geology 182, 3–28.

Nascimento, M.S., Oliveira, D.A., 2015. Ambiente deposicional e proveniência da Formação Gorotire, Província Carajás, sudeste do Cráton Amazônico. In: Gorayeb P., Meiguins A. (Eds.). Contribuições `a Geologia da Amazônia, 9, Belém, SBG-Norte (in Portuguese).

Nelson, B.K., DePaolo, D.J., 1988. Comparison of isotopic and petrographic provenance indicators in sediments from Tertiary continental basins of New Mexico. J. Sediment. Petrol. 58, 348–357.

Nemec, W., Steel, R.J., 1984. Alluvial and coastal conglomerates: their significant features and some comments on gravelly mass flow deposits. In: Koster, E.H., Steel, R.J. (Eds.), Sedimentology of Gravels and Conglomerates. Canadian Society of Petroleum Geologists Memoir 10, pp. 1-31.

Nogueira, A.C.R., Truckenbrodt, W., Pinheiro, R.V.L., 1995. Formação Águas Claras, Pré- Cambriano da Serra dos Carajás: redescrição e redefinição litoestratigráfica. Boletim Museu Paraense Emílio Goeldi 7, 177–277.

Nogueira A.C.R., Riccomini, C., Sial, A. N., Moura C. V., Fairchild, T., 2003. Soft-Sediment deformation at the base of the Neoproterozoic Puga cap carbonate (Southwestern Amazon Craton, Brazil): confirmation of rapid icehouse to greenhouse transition in snowball earth, Geology, 31(7):613-616.

Oliveira, J.R.; Silva Neto, C.S.; Costa, E.J.S. 1994. Serra Pelada; folha SB.22.X.C. Estado do Pará, escala 1:250.000. Brasília: CPRM, 220 p., il. Programa Levantamentos Geológicos Básicos do Brasil (PLGB).

Oliveira, R. G. 2018. Insights on the framework of the Carajás Province, Amazonian Craton, Brazil, and on the three-dimensional shape of the Carajás Basin, based on gravity data. Journal of the Geological Survey of Brazil vol 1, no 3, 101-112.

Olszewski, W.J., Wirth, K.R., Gibbs, A.K., Gaudette, H.E., 1989. The age, origin, and tectonics of the Grão Pará Group and associated rocks, Serra dos Carajás, Brazil: archean continental volcanism and rifting. Precambr. Res. 42, 229–254. https://doi.org/10.1016/0301-9268(89)90013-2.

Owen, G., 2003. Load structures: Gravity-driven sediment mobilization in the shallow subsurface. Geological Society, London, Special Publications. 216, 21-34. https://doi.org/10.1144/GSL.SP.2003.216.01.03.

Paixão, M. A. P., 2009. Complexo Ofilitico Quatipuru, Pará, Brasil. PhD Thesis. Universidade de Brasilia, Brasilia, Brazil, pp. 135.

Pereira, R. M. P., 2009. Geologia da Região Sul da Serra Norte e Características do Minério de Ferro do Depósito N8, Província Mineral Carajás. MS dissertation, Universidade Federal de Minas Gerais, Brazil, pp.131.

Pickering, K.T., Hiscott, R.N. & Hein, F.J. 1989. Deep Marine Environments: Clastic Sedimentation and Tectonics. Ed. London, Unwin Hyman, 416 p.

Pimentel, M., Lindenmayer, Z.G., Henrique, L. J., Armstrong, R., Araújo, J., 2003. Geochronology and Nd isotope geochemistry of the Gameleira Cu-Au deposit, Serra dos Carajás, Brazil: 1.8-1.7 Ga hydrothermal alteration and mineralization. Journal of South American Earth Sciences, 15(7):803–813.

Pinheiro R.V.L., 1997. Reactivation history of the Carajás and Cinzento Strike Slip Systems, Amazon, Brazil. PhD Thesis, Durham, Inglaterra, pp. 408.

Pinheiro, R.V.L., Holdsworth, R.E., 1997. The structure of the Carajás N-4 ironstone deposit and associated rocks: relationship to Archaean strike-slip tectonics and basement reactivation in the Amazon region, Brazil. J. S. Am. Earth Sci. 10, 305–319.

Pinheiro, B. L. S., 2005. Proveniência das rochas metassedimentares do Cinturão Araguaia, com base em datações em idades modelo sm-nd em rocha total e datação pb-pb em zircão. Master dissertation, Universidade Federal do Pará, Belém, Brazil, pp. 136.

Pinheiro, R. S., 2019. Evolução paragenética e regime de fluidos no sistema Cu-Co Tarzan, Província Carajás. MS dissertation, Universidade Estadual de Campinas, pp. 122.

Pohl, A., Donnadieu, Y., Le Hir, G., Ladant, J.-B., Dumas, C., Alvarez-Solas, J., Vandenbroucke, T.R.A., 2016. Glacial onset predated Late Ordovician climate cooling, Paleoceanography, 31, 800–821, doi:10.1002/2016PA002928.

Potter, P.E., 1978. Significance and origin of big rivers. Journal of Geology 86, 13 – 33.

Powell, R.D., 1990. Glacimarine processes at grounding-line fans and their growth to ice-contact deltas. In: Glacimarine Environments: Processes and Sediments (Eds J.A. Dowdeswell and J.D. Scourse), Geol. Soc. London Spec. Publ., 53, 53–73. https://doi.org/10.1144/GSL.SP.1990.053.01.03.

Ramos, J.F. da F., Moura, C.A.V., Melo, CF., Pereira, J.L. Serique, J.S.C., Rodrigues, R.M., 1984. Uma discussão sobre sequencias sedimentares tidas como Formação Rio Fresco, Sudeste do Para. Anais 33B Congresso Brasileiro de Geologia, Rio de Janeiro, 2, 862-872.

Rossignol, C., Antonio, P., Narduzzi, F., Siciliano Rego, E., Teixeira, L., Almeida de Souza, R., Ávila, J., Silva, M., Lana, C., Trindade, R., Philippot, P., 2022. Unraveling one billion years of geological evolution of the southeastern Amazonian Craton from detrital zircon analyses. Geoscience Frontiers. 13. 101202. 10.1016/j.gsf.2021.101202.

Salgado, S.S., Caxito, F.A., Figueiredo e Silva, R.C., Lana, C., 2019a. The provenance of the Buritirama Formation reveals the Paleoproterozoic assembly of the Bacaj´a and Caraj´as blocks (Amazon Craton) and the chronocorrelation of Mn-deposits in the Transamazonian/Birimian system of northern Brazil/West Africa. J. S. Am. Earth Sci. 96, 102364.

Salgado, S. S., Caxito, F. de A., Queiroga, G. N., & Castro, M. P. de., 2019b. Stratigraphy, petrography, and tectonics of the manganese-bearing Buritirama Formation, Northern Carajás Domain, Amazon Craton. Brazilian Journal of Geology, 49(1). doi:10.1590/2317-4889201920180106

Santos, J. O. S., Hartmann, L. A., Gaudette, H. E., Groves, D. I., Mcnaughton, N. J., Fletcher, I. R., 2000. A New Understanding of the Provinces of the Amazon Craton Based

on Integration of Field Mapping and U-Pb and Sm-Nd Geochronology. Gondwana Research, 3(4), 453–488. doi:10.1016/s1342-937x(05)70755-3

Santos, J.O.S., Hartmann, L.A., McNaughton, N.J., Fletcher, I.R., 2002. Timing of mafic magmatism in the Tapajós Province (Brazil) and implications for the evolution of the Amazon Craton: evidence from baddeleyite and zircon U-Pb SHRIMP geochronology. J. S. Am. Earth Sci. 15, 409–429.

Santos J.O.S. 2003. Geotectônica dos escudos das Guianas e Brasil-Central. In: Bizzi, L. A.; Schobbenhaus, C.; Vidotti, R. M.; Gonçalves, J. H. Geologia, tectônica e recursos minerais do Brasil. Brasília, DF: CPRM, p. 169-361.

Santos, M.J.P., Galarza, M.A., Oliveira, D. C., 2013. Geologia, geoquímica e geocronologia do Diopsídio-Norito Pium, Província Carajás. Boletim do Museu Paraense Emílio Goeldi-Ciências Naturais, 8(3):355–382.

Scasso, R.A., Aberhan, M., Ruiz, L., Weidemeyer, S., Medina, F. A. & Kiessling, W. 2012. Integrated bio- and lithofacies analysis of coarse-grained, tide-dominated deltaic environments across the Cretaceous/Paleogene boundary in Patagonia, Argentina. Cretaceous Research, 36, 37–57.

Schumm, S. A., 1968. Speculations concerning paleohydrologic controls of terrestrial sedimentation. Geol. Soc. Am. Bull. 79, 1573-1588. https://doi.org/10.1130/00167606(1968)79[1573:SCPCOT]2.0.CO;2.

Serique, J.S.C.B, & Ramos, J. F. da F., 1984. Aspectos petrograficos dos sedimentos Precambrianos da Serra do Paredao. Anais 33s Congresso Brasileiro de Geologia, Rio de Janeiro, 2, 886-893.

Silva Neto, J. J. A., 2018. Petrologia e geocronologia do magmatismo granítico do Cinturão Araguaia. Ms dissertation, Universidade Federal do Pará, Belém, Brazil, pp. 118.

Soares E. A. A. 1998. Fáceis litorâneas glaciais da formação Nhamundá (Siluriano inferior), na região de Presidente Figueiredo, AM, Bacia do Amazonas. MS Dissertation, Universidade Federal do Pará, Belém, Brazil, pp. 122.

Spencer C.J., Kirkland C.L., Taylor R.J.M. 2016. Strategies towards statistically robust interpretations of in situ U-Pb zircon geochronology. Geoscience Frontiers, 7(37):581-589.

Sproson, A., Pogge, S., Selby, D., Jarochowska, E., Fryda, J., Hladil, J., Loydell, D., Slavík, L., Calner, M., Maier, G., Munnecke, A., Lenton, T., 2022. Osmium and lithium isotope evidence for weathering feedbacks linked to orbitally paced organic carbon burial and Silurian glaciations. Earth and Planetary Science Letters. 577. 117260. 10.1016/j.epsl.2021.117260.

Tallarico F.H.B., Figueiredo B.R., Groves D.I., Kositcin N., McNaughton N.J., Fletcher I.R., Rego J.L. 2005. Geology and SHRIMPU–Pb Geochronology of the Igarapé Bahia Deposit, CarajásCopper–Gold Belt, Brazil: an Archean (2.57 Ga) example of iron–oxide Cu–Au–(U–REE) mineralization. Economic Geology, 100:7-28.

Tavares, F.M., Trouw, R.A.J., da Silva, C.M.G., Justo, A.P., Oliveira, J.K.M., 2018. The multistage tectonic evolution of the northeastern Caraj´as Province, Amazonian Craton, Brazil: revealing complex structural patterns. J. S. Am. Earth Sci. 88, 238–252. https://doi.org/10.1016/j.jsames.2018.08.024.

Taylor, S.R., McLennan, S.M., 1985. The Continental Crust: Its Composition and Evolution. Blackwell, London 312 pp.

Teixeira, N., Bettencourt, J., Moura, C., Dall'Agnol, R., Macambira, E., 2002. Archean crustal sources for Paleoproterozoic tin-mineralized granites in the Carajás Province, SSE Pará, Brazil: Pb–Pb geochronology and Nd isotope geochemistry. Precambrian Research, 119. 257-275. 10.1016/S0301-9268(02)00125-0.

Teixeira M.F.B., Dall‟Agnol R., Santos J.O.S., Sousa L.A.M., Lafon J.M. 2017. Geochemistry, geochronology and Nd isotopes of the Gogó da Onça Granite: a new Paleoproterozoic A-type granite of Carajás Province, Brazil. Journal of South American Earth Sciences, 80: 47–65.

Teixeira M.F.B., Dall‟Agnol R., Santos J.O.S., Oliveira, D. C., Lamarão, C. N., McNaughtond, N. J., 2018. Crystallization ages of Paleoproterozoic A-type granites of Carajás province, Amazon craton: Constraints from U-Pb geochronology of zircon and titanite. Journal of South American Earth Sciences, 88: 312–331.

Teixeira, W., Hamilton, M. A., Girardi, V. A. V., Faleiros, F. M., & Ernst, R. E., 2019. U-Pb baddeleyite ages of key dyke swarms in the Amazonian Craton (Carajás/Rio Maria and Rio Apa areas): Tectonic implications for events at 1880, 1110 Ma, 535 Ma and 200 Ma. Precambrian Research. doi:10.1016/j.precamres.2018.02.0

Thorogood, E.J., 1990. Provenance of the pre-Devonian sediments of England and Wales: Sm/Nd evidence. J. Geol. Soc. Lond. 147, 591–594.

Trendall, A.F., Basei, M.A.S., De Laeter, J.R., Nelson, D.R., 1998. SHRIMP zircon U-Pb constraints on the age of the Carajas formation, Grao Para Group, Amazon Craton. J. S. Am. Earth Sci. 11, 265–277. https://doi.org/10.1016/S0895-9811(98)00015-7.

Vasquez, L.V., & Rosa-Costa, L. T., 2008a. Geologia e recursos minerais do Estado do Pará. Sistema de informações geográficas: texto explicativo dos mapas geológico e tectônico e de recursos minerais do Estado do Pará. Escala 1:1.000.000. Belém: CPRM.

Vasquez, L.V., Sousa C.S., Carvalho J.M.A. 2008b. Mapa geológico e de recursos minerais do Estado do Pará. Escala: 1:1000.000. Programa geologia do Brasil (PGB). Integração, atualização e difusão de dados da geologia do Brasil. Mapas geológicos estaduais. CPRM- Serviço Geológico do Brasil- Superintendência regional de Belém.

Van der Meer J.J.M. 1993. Microscopic evidence of subglacial deformation. Quaternary Science Reviews. 12: 553-587.

Vessely, F.F., 2006. dinâmica sedimentar e arquitetura estratigráfica do grupo itararé (carbonífero-permiano) no centro-leste da bacia do paraná. PhD Thesis, Curitiba, Brazil, pp. 238.

Visser, J.N.J., 1991. Self-destructive collapse of the Permo-Carboniferous marine ice sheet in the Karoo Basin: evidence from the southern Karoo. S. Afr. J. Geol., 94, 255-262.

Visser J.N.J. 1997. Deglaciation sequences in the Permo-Carboniferous Karoo and Kalahari basins of southern Africa: a tool in the analysis of cyclic glaciomarine basin fills. Sedimentology. 44: 507 - 521. Doi: https://doi.org/10.1046/j.1365-3091.1997.d01-35.x.

Walker, R.G. 1992. Facies models and modern stratigraphic concepts. In: R.G. Walker, e N.P. James. Eds. Facies Models - Response to Sea Level Change. Geological Association of Canada, Ontario, Canada, 1-14 p.

Walker, R.G. 2006. Facies models revisited: an introduction. In: H.W. Posamentier R.G. Walker Facies Models Revisited. SEPM vol. 84 Society for Sedimentary Geology -SEPM Special Publications, Tulsa, Oklahoma. 1-18 p.

Went, D.J., 2005. Pre-vegetation alluvial fan facies and processes: an example from the Cambro-Ordovician Rozel Conglomerate Formation, Jersey, Channel Islands. Sedimentology 52, 693-713.

Zalán, P.V., 2004. Evolução Fanerozóica das Bacias Sedimentares Brasileiras. In: MANTESSO-NETO, V. et al. (orgs.). Geologia do Continente Sul-Americano: evolução da obra de Fernando Flávio Marques de Almeida. São Paulo: Beca, p. 595-612.

Zecchin, M., Octavian, C., Rebesco, M., 2015. High-resolution sequence stratigraphy of clastic shelves IV: High-latitude settings. Marine and Petroleum Geology. 68, 427-437. https://doi.org/10.1016/j.marpetgeo.2015.09.004.

Zucchetti, M. 2007. Rochas máficas do Grupo Grão-Pará e sua relação com a mineralização de ferro dos depósitos N4 e N5, Carajás, PA. PhD Thesis, Belo Horizonte, MG, Brazil, pp. 125.

SUPLEMENTARY MATERIAL

Table III.3.1- Detrital heavy mineral components of the Paredão Goup Lower Member samples from the Carajás Domain.zrn: zircon, tur: tourmaline, rt: rutile, ep: epidote, grt: garnet, opm: opaque magnetic minerals. ZTR Index = 100 × (zrn + tur + rt)/ total of nonopaque minerals, GZi = 100 × grt/(grt + zrn).

Sample	zrn	tur	rt	ep	grt	opm	ZTR	Gzi	Mineral chemistry
G-1	8.3	0.8	0.1	1.5	6.1	83.2	54.76	42.36	Garnet
G-2	7.1	0.6	0	0.7	5.5	86.1	55.39	43.65	Garnet

Table III.3.2- Chemical compositions and calculated results of detrital garnets of the Paredão Group Lower Member samples from the Carajás Domain. Prp: pyrope, Alm: almandine, Sps: spessartine, Grs: grossular, Andr: andradite, Uva: uvarovite (in molecular poroportions).

	SiO2(mole%)	Al2O3(mole%)	MgO(mole%)	CaO(mole%)	iO2(mole%	Cr2O3(mole%)	FeO(mole%)	MnO(mole%)	Total(mole%)	Prp %	Grs %	Alm %	Sps %	Andr %	Uva %
G1-1	42.7159	14.2159	2.0835	3.1614	0.139	0.0008	10.2034	27.4801	100	4.774553565	9.165989	23.08599	62.97346	0	0
G1-2	42.7808	14.1815	3.4656	2.9949	0.1302	-0.0003	6.1465	30.3008	100	7.944212087	8.68591	13.9112	69.45867	0	0
G1-3	42.6218	14.5072	1.7228	3.0629	0.1299	-0.001	8.5549	29.4016	100	3.965369188	8.919535	19.44143	67.67367	0	0
G1-4	42.5502	14.2369	2.1946	3.2278	0.1191	0.0047	5.9213	31.7454	100	5.002492441	9.308899	13.32639	72.36222	0	0
G1-5	42.6939	14.2871	2.2436	3.0829	0.1659	0.0081	5.8305	31.6881	100	5.147187496	8.948384	13.20671	72.69771	0	0
G1-6	42.5491	14.3267	2.8793	3.3366	0.1369	0.0083	2.6981	34.0651	100	6.569273559	9.631528	6.077891	77.72131	0	0
G1-7	42.5804	14.2279	2.3482	3.0427	0.1525	0.0103	8.968	28.6699	100	5.370732568	8.804774	20.25156	65.57293	0	0
G1-8	42.5946	14.244	2.1293	2.8617	0.14	-0.0072	5.0441	32.9936	100	4.869893368	8.280705	11.39018	75.45922	0	0
G1-9	42.5411	14.2711	2.1003	3.3638	0.1555	0.0066	6.6935	30.8681	100	4.791593307	9.709333	15.07705	70.42203	0	0
G1-10	42.414	14.2676	1.786	3.7418	0.1869	0.0029	11.054	26.5468	100	4.060850073	10.76407	24.81529	60.35978	0	0
G1-11	42.5675	14.308	1.9797	3.6301	0.1597	0.0116	7.1892	30.1542	100	4.517298611	10.47994	16.19662	68.80615	0	0
G1-12	42.8603	14.3928	2.0657	2.787	0.1259	0.0044	6.4153	31.3485	100	4.773494972	8.148296	14.63695	72.44126	0	0
G1-13	42.6506	14.2966	2.4984	3.1402	0.1779	0.0052	6.8478	30.3834	100	5.728190879	9.109058	15.5014	69.66135	0	0
G1-14	42.4328	14.3952	2.5923	2.764	0.0962	0.009	7.7614	29.949	100	5.931843296	8.002083	17.53513	68.53095	0	0
G1-15	42.5629	14.2526	2.2778	3.5022	0.2287	0.0032	5.3075	31.8652	100	5.19876201	10.11314	11.96021	72.72789	0	0
G1-16	42.4577	14.3057	2.1109	3.1996	0.1378	-0.0021	8.9386	28.8518	100	4.815422394	9.234705	20.13264	65.81724	0	0
G1-17	42.6643	14.1833	2.322	2.8075	0.1772	0.0064	4.703	33.1362	100	5.319137235	8.136907	10.63698	75.90697	0	0
G1-18	42.9669	14.3862	2.0869	2.742	0.1018	0.0068	7.2316	30.4777	100	4.833718627	8.035406	16.53783	70.59305	0	0
G1-19	43.0726	14.1726	2.1048	4.6878	0.0705	0.0006	12.5311	23.36	100	4.808969307	13.55099	28.26798	53.37207	0	0
G1-20	42.443	14.29	1.849	2.9333	0.14	0.003	13.0613	25.2804	100	4.227590368	8.485415	29.48539	57.80161	0	0
G1-21	42.5279	14.3885	1.8016	2.7679	0.1184	0.0078	5.1713	33.2165	100	4.129660446	8.027254	11.70362	76.13947	0	0
G1-22	42.8785	14.2821	2.6351	2.8862	0.12	0.0099	7.7042	29.4839	100	6.074842459	8.418311	17.53597	67.97087	0	0
G1-23	42.6951	14.1387	1.5964	3.1227	0.1431	0.002	2.2084	36.0935	100	3.642986984	9.015852	4.975744	82.36542	0	0
G1-24	42.7254	14.1412	1.9933	3.072	0.1563	0.0074	8.9117	28.9927	100	4.564299959	8.899864	20.14775	66.38809	0	0
G1-25	42.6316	14.2933	2.0318	3.0653	0.1224	0.0108	4.5494	33.2954	100	4.649724664	8.875236	10.27933	76.19571	0	0
G1-26	42.728	14.2079	2.4941	3.2389	0.1581	0.0076	8.0682	29.0972	100	5.713181746	9.386903	18.24758	66.65234	0	0
G1-27	42.5797	14.0372	1.3785	3.4964	0.2103	0.0043	4.6746	33.6188	100	3.130368086	10.04547	10.48087	76.34329	0	0
G1-28	42.6513	14.1886	2.0452	3.4029	0.1848	0.0078	6.5753	30.9441	100	4.670826258	9.832586	14.82648	70.67011	0	0
G1-29	42.5204	14.2464	1.9642	3.2546	0.139	0.0068	2.0936	35.7749	100	4.471823342	9.374696	4.706056	81.44743	0	0
G1-30	42.8041	14.3047	1.7832	4.2418	0.1014	0.0031	10.9487	25.8129	100	4.07375573	12.26043	24.69573	58.97008	0	0
G1-31	42.8985	14.2526	2.4901	3.0913	0.1356	0.0005	5.1828	31.9485	100	5.728729001	8.997944	11.77254	73.50078	0	0
G1-32	42.6941	14.2723	2.3412	3.214	0.0993	0.0001	9.1523	28.2267	100	5.361037685	9.31144	20.69212	64.6354	0	0

G1-33	43.0319	14.2161	2.1907	2.8006	0.1492	0.0005	7.8753	29.7358	100	5.065742494	8.193546	17.98008	68.76063	0	0
G1-34	42.8273	14.4703	1.6257	2.8524	0.1159	-0.0042	3.9006	34.2121	100	3.754688483	8.33498	8.89466	79.01567	0	0
G1-35	42.7602	14.1251	2.9135	3.1015	0.1461	0.0065	3.4958	33.4511	100	6.660927381	8.971232	7.890975	76.47687	0	0
G1-36	42.7717	14.106	1.7898	3.2762	0.1614	0.0064	6.2498	31.6385	100	4.091531936	9.475726	14.10626	72.32648	0	0
G1-37	42.4004	14.1713	2.1407	3.3816	0.1423	0.0097	10.4414	27.3126	100	4.860712185	9.714646	23.40816	62.01648	0	0
G1-38	42.6242	14.452	2.2863	2.6774	0.1023	0.0067	7.605	30.2462	100	5.264498469	7.800055	17.2897	69.64575	0	0
G1-39	42.5311	14.2381	2.5141	3.1025	0.1294	0.0053	5.9871	31.4923	100	5.734328962	8.95308	13.48283	71.82976	0	0
G1-40	42.7097	14.1326	1.0863	3.4747	0.1349	0.003	8.2946	30.1642	100	2.478085964	10.0287	18.68213	68.81108	0	0
G1-41	42.7245	14.1599	1.9804	3.353	0.1736	0.0049	6.0028	31.6008	100	4.526607609	9.69648	13.54685	72.23007	0	0
G1-42	42.8807	14.1429	1.8915	3.5086	0.146	0.0027	9.5387	27.8889	100	4.334586021	10.17269	21.58216	63.91057	0	0
G1-43	41.0438	15.1882	1.7117	3.4261	0.1058	0.0056	7.6421	30.8767	100	3.849247931	9.747851	16.96779	69.43511	0	0
G1-44	42.5523	14.1614	1.4701	3.4437	0.2071	0.0036	5.7937	32.3681	100	3.347564835	9.921288	13.02574	73.7054	0	0
G1-45	42.5843	14.2225	2.0879	3.2251	0.1658	0.006	3.5183	34.1901	100	4.763398571	9.309172	7.925096	78.00233	0	0
G1-46	42.8706	14.3736	2.5038	2.7342	0.1063	-0.0002	2.7822	34.6295	100	5.777166663	7.981898	6.33823	79.90271	0	0
G1-47	43.015	14.4529	2.1884	3.5965	0.0862	0.0219	11.2051	25.434	100	5.061535534	10.52437	25.58796	58.82613	0	0
G1-48	42.6597	14.1831	2.2093	3.3226	0.12	0.002	6.8346	30.6687	100	5.040633831	9.591116	15.396	69.97225	0	0
G1-49	42.5792	14.1581	1.8896	3.2943	0.1105	0.0038	7.8289	30.1357	100	4.302073393	9.489246	17.5984	68.61028	0	0
G1-50	42.6866	14.2681	2.5256	3.3169	0.16	-0.0022	4.3977	32.6473	100	5.777890122	9.600585	9.933327	74.6882	0	0
G1-51	42.8238	14.4696	1.543	2.8631	0.1407	0.0018	4.8819	33.2761	100	3.566675462	8.373265	11.14169	76.91837	0	0
G1-52	42.715	14.4901	1.6313	2.6879	0.1152	-0.0032	5.2582	33.1054	100	3.764910969	7.848644	11.98181	76.40464	0	0
G1-53	42.82	14.201	1.3864	3.9649	0.1298	0.0048	10.5875	26.9056	100	3.16805876	11.46298	23.88705	61.48191	0	0
G1-54	42.8914	14.0638	2.5532	3.3827	0.1621	0.0037	6.4429	30.5001	100	5.843311036	9.794861	14.55861	69.80322	0	0
G1-55	42.6534	14.1997	2.3918	3.2302	0.1655	0.0023	5.4307	31.9263	100	5.464862763	9.337797	12.25109	72.94625	0	0
G1-56	42.8148	14.35	2.0417	2.8532	0.1588	0.0093	9.8863	27.886	100	4.715387556	8.337163	22.54362	64.40383	0	0
G2-1	43.9766	13.831	1.8991	3.1158	0.145	0.0047	5.559	31.4689	100	4.437282546	9.210845	12.8242	73.52767	0	0
G2-2	42.6054	14.1246	1.961	3.3956	0.1765	0.007	8.9682	28.7618	100	4.469664129	9.792069	20.18213	65.55614	0	0
G2-3	42.7597	14.078	2.7769	3.2852	0.1277	0.0054	7.6915	29.2757	100	6.339500744	9.48893	17.33685	66.83472	0	0
G2-4	42.6062	14.1645	1.98	3.1515	0.1496	0.0053	3.5426	34.4002	100	4.513826357	9.089868	7.973816	78.42249	0	0
G2-5	42.923	14.1804	2.0299	3.1844	0.1365	0.0017	3.7805	33.7637	100	4.660529672	9.250152	8.569871	77.51945	0	0
G2-6	42.9784	14.3356	1.8534	3.8105	0.1091	0.009	10.9792	25.9249	100	4.266623101	11.09833	24.95458	59.68047	0	0
G2-7	38.397	13.0693	5.7659	3.5156	0.0518	-0.0042	10.9604	28.2441	100	11.70039439	9.025962	21.95959	57.31405	0	0
G2-8	42.8389	14.3678	1.8129	4.1584	0.1203	0.0058	10.9952	25.7007	100	4.155095326	12.05852	24.88139	58.90499	0	0
G2-9	42.6486	14.2361	1.2678	3.298	0.115	0.0057	2.749	35.6799	100	2.892240654	9.51908	6.191884	81.3968	0	0
G2-10	42.8799	14.2852	1.8872	3.5604	0.192	-0.0099	5.728	31.4772	100	4.335950076	10.34965	12.99373	72.32067	0	0
G2-11	42.7613	14.2147	2.5051	3.1132	0.1028	-0.0001	8.2529	29.0501	100	5.740059008	9.025244	18.67077	66.56392	0	0
G2-12	42.7114	14.1293	2.097	3.2559	0.1514	0.0042	4.3995	33.2512	100	4.786430093	9.402535	9.914733	75.8963	0	0
G2-13	42.5625	14.1505	1.0271	3.5329	0.2222	0.0002	3.7442	34.7604	100	2.336754853	10.16933	8.41054	79.08337	0	0
G2-14	42.7003	14.179	2.8586	3.0451	0.1544	0.0045	2.7332	34.3247	100	6.5362501	8.80922	6.170368	78.48416	0	0
G2-15	42.7651	14.1808	2.1918	3.7461	0.1291	0.0055	11.6141	25.3675	100	5.008010152	10.8294	26.20078	57.96181	0	0
G2-16	42.7275	14.1934	2.0683	3.3732	0.1567	0.0017	6.9046	30.5746	100	4.729938835	9.759885	15.58996	69.92022	0	0
G2-17	42.7973	14.1116	2.5242	2.9856	0.1123	0.0015	6.0822	31.3854	100	5.777237713	8.645472	13.74427	71.83302	0	0

G2-18	42.5655	14.0985	2.1382	3.3123	0.1424	0.0009	9.3574	28.3849	100	4.864772668	9.534645	21.02005	64.58053	0	0
G2-19	42.8599	14.0362	2.3843	3.0826	0.1363	0.0089	5.1512	32.3406	100	5.454693893	8.922515	11.63543	73.98736	0	0
G2-20	42.6218	14.2945	1.2896	3.5106	0.1609	0.0024	8.1368	29.9834	100	2.947766895	10.15267	18.36353	68.53604	0	0
G2-21	42.6374	14.2274	1.7284	3.5627	0.1689	0.0018	8.7129	28.9605	100	3.94620956	10.29143	19.64097	66.12139	0	0
G2-22	42.752	14.1703	1.6454	3.0227	0.1036	-0.0038	2.4944	35.8154	100	3.761091336	8.741744	5.62954	81.86763	0	0
G2-23	42.8112	14.2215	3.7351	2.9044	0.112	-0.0036	2.8605	33.3589	100	8.568132476	8.429484	6.478736	76.52365	0	0
G2-24	47.0604	15.2506	3.0959	2.0294	0.0961	-0.0027	5.0699	27.4003	100	8.132233175	6.744522	13.14882	71.97443	0	0
G2-25	42.9881	14.1504	2.4022	3.3696	0.1127	0.0105	12.03	24.9365	100	5.524893792	9.805139	27.31774	57.35222	0	0
G2-26	42.1076	14.0403	2.1184	3.3885	0.1674	0.0034	4.9679	33.2063	100	4.758650279	9.630391	11.01826	74.5927	0	0
G2-27	42.8394	14.2903	2.4424	3.2723	0.1782	-0.002	5.756	31.2234	100	5.616129405	9.519937	13.06789	71.79604	0	0
G2-28	42.8033	14.151	2.3744	3.6029	0.1591	-0.0024	9.587	27.3246	100	5.43055363	10.42565	21.64898	62.49482	0	0
G2-29	43.0344	14.2694	2.5555	3.1068	0.1263	0.0092	7.5512	29.3473	100	5.90333385	9.080199	17.22272	67.79374	0	0
G2-30	44.8377	13.9989	1.2502	2.7904	0.0913	0.0025	2.7657	34.2633	100	2.992727819	8.451131	6.53668	82.01946	0	0
G2-31	42.9133	14.3107	2.5012	3.2165	0.1712	0.0024	3.6018	33.2829	100	5.761831048	9.374676	8.192116	76.67138	0	0
G2-32	42.7538	14.2593	2.1439	3.277	0.1462	0.0079	6.5985	30.8134	100	4.915138562	9.505354	14.93623	70.64328	0	0
G2-33	42.8012	14.173	1.9266	3.4072	0.1676	0.0069	6.6688	30.8486	100	4.411689787	9.871239	15.07737	70.6397	0	0
G2-34	42.8172	14.1417	2.4193	3.1977	0.112	-0.0037	8.984	28.3319	100	5.540319255	9.264957	20.31324	64.88148	0	0
G2-35	42.7489	14.0779	2.5044	3.5171	0.0889	0.0091	7.1594	29.8943	100	5.70253974	10.13235	16.09554	68.06957	0	0
G2-36	41.8884	14.0817	2.589	3.8513	0.1605	0.003	4.6636	32.7626	100	5.775303203	10.86953	10.27137	73.0838	0	0
G2-37	42.8252	14.2704	2.254	3.316	0.1021	0.0053	6.1833	31.0438	100	5.169937739	9.622913	14.00284	71.20431	0	0
G2-38	43.1641	14.2241	3.4189	3.6483	0.1374	0.0067	4.6794	30.721	100	7.882030539	10.6415	10.65139	70.82508	0	0
G2-39	42.7685	14.1474	1.8991	3.2946	0.1585	0.0085	9.4813	28.2421	100	4.34867647	9.544926	21.43589	64.6705	0	0
G2-40	42.5954	14.1952	2.561	3.3016	0.1598	0.0172	9.9219	27.2479	100	5.849391134	9.54083	22.37486	62.23492	0	0
G2-41	42.8485	14.2495	2.1342	3.3087	0.1885	0.0068	7.1856	30.0784	100	4.906954382	9.624871	16.31189	69.15628	0	0
G2-42	42.9977	14.2115	2.3849	3.1734	0.1338	-0.0049	5.3164	31.7872	100	5.490585966	9.243447	12.08455	73.18141	0	0
G2-43	42.6243	14.1288	1.5173	3.5479	0.1877	0.0003	8.6058	29.3879	100	3.456986882	10.22724	19.35896	66.95682	0	0
G2-44	42.696	14.2938	2.1511	3.3341	0.1328	0.0144	8.839	28.5388	100	4.929727832	9.66722	20	65.40306	0	0
G2-45	42.975	14.3628	2.0779	2.6055	0.1198	0.0115	2.5118	35.3356	100	4.811069947	7.632534	5.742044	81.81435	0	0
G2-46	42.7422	14.1115	2.1436	3.5641	0.1958	0.0033	5.0693	32.1702	100	4.890913839	10.28861	11.4198	73.40067	0	0
G2-47	42.7677	14.3146	2.6455	3.0412	0.127	-0.0023	7.731	29.3751	100	6.081410145	8.845088	17.54675	67.52676	0	0
G2-48	42.675	14.1982	2.2998	3.117	0.1625	0.0077	4.508	33.0317	100	5.259565376	9.018976	10.17907	75.54239	0	0
G2-49	42.8249	14.2168	2.2097	3.4996	0.1511	-0.0004	9.2539	27.8443	100	5.065980695	10.15101	20.94688	63.83613	0	0
G2-50	42.8467	14.2132	2.2206	3.0922	0.1263	0.0104	4.0548	33.4357	100	5.096391091	8.978848	9.188112	76.73665	0	0

CAPÍTULO IV THE ORDOVICIAN TRANS-CONTINENTAL DRAINAGES RECOGNITION IN NORTHERN BRAZIL AND CENTRAL AFRICA: IMPLICATIONS FOR THE WESTERN GONDWANA EARLY PALEOZOIC PALEOGEOGRAPHY AND TECTONOSTRATIGRAPHIC EVOLUTION

Artigo submetido em: Geology (05/10/2024)

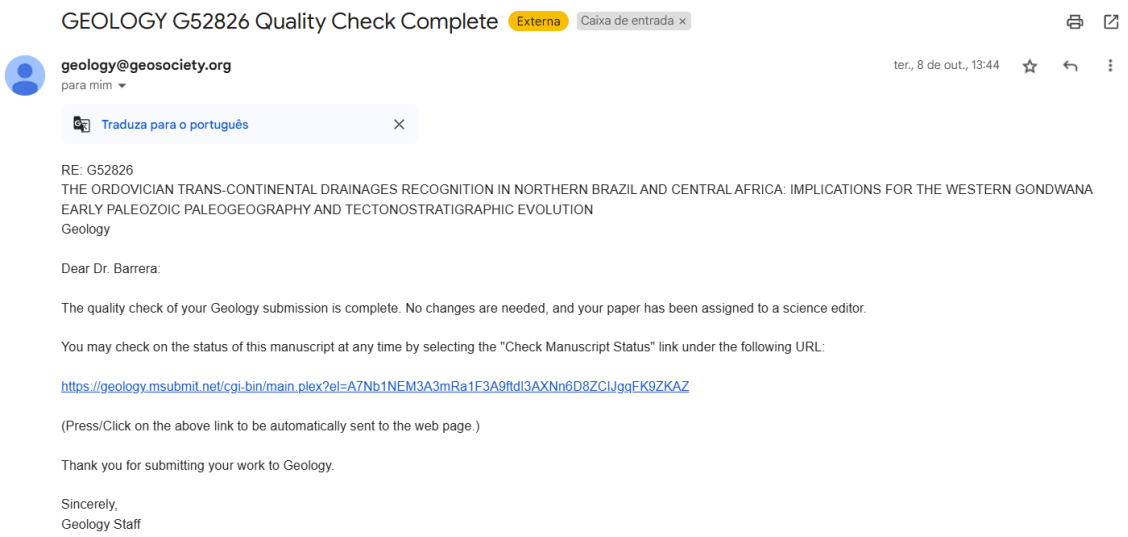

GEOLOGY G52826 Quality Check Complete Externa Caixa de entrada ×

geology@geosociety.org
para mim

ter., 8 de out., 13:44

Traduza para o português

RE: G52826
THE ORDOVICIAN TRANS-CONTINENTAL DRAINAGES RECOGNITION IN NORTHERN BRAZIL AND CENTRAL AFRICA: IMPLICATIONS FOR THE WESTERN GONDWANA EARLY PALEOZOIC PALEOGEOGRAPHY AND TECTONOSTRATIGRAPHIC EVOLUTION
Geology

Dear Dr. Barrera:

The quality check of your Geology submission is complete. No changes are needed, and your paper has been assigned to a science editor.

You may check on the status of this manuscript at any time by selecting the "Check Manuscript Status" link under the following URL:

https://geology.msubmit.net/cgi-bin/main.plex?el=A7Nb1NEM3A3mRa1F3A9ftdI3AXNn6D8ZClJgqFK9ZKAZ

(Press/Click on the above link to be automatically sent to the web page.)

Thank you for submitting your work to Geology.

Sincerely,
Geology Staff

THE ORDOVICIAN TRANS-CONTINENTAL DRAINAGES RECOGNITION IN NORTHERN BRAZIL AND CENTRAL AFRICA: IMPLICATIONS FOR THE WESTERN GONDWANA EARLY PALEOZOIC PALEOGEOGRAPHY AND TECTONOSTRATIGRAPHIC EVOLUTION

Ivan Alfredo Romero Barrera[1], Afonso César Rodrigues Nogueira[1], José Bandeira[1], João Milhomem Neto[1], Elton Dantas[2], Ana Maria Góes[3].

[1] Programa de Pós-Graduação em Geologia e Geoquímica, Faculdade de Geologia, Instituto de Geociências, Universidade Federal do Pará, 66075-110, Belém, PA, Brazil, (ivan.barrera@ig.ufpa.br).

[2] Instituto de Geociências, Universidade de Brasília, Campus Universitário, Asa Norte, 70910-900, Brasília, DF, Brazil.

[3] Universidade de São Paulo, Instituto de Geociências, São Paulo, SP, Brazil

ABSTRACT

The landmass extension for hundreds of kilometers in West Gondwana was a site for developing large Ordovician rivers, widely preserved as siliciclastic successions. These records include a 300-1000-meter-thick sequence comprising coarse-grained lithoarenites and conglomerate beds that outcrop on intracratonic basins and isolated grabens in Africa and Brazil. In Brazil, these units correspond to the Ipu, Cariri, and Tacaratu formations, while in Africa, they are represented by the Inkisi, Banalia, and Biano groups. The fluvial depositional architecture of these successions corresponds to meters-scale thickness tabular bodies laterally continuous for hundreds of kilometers. These sequences display remarkably similar detrital-zircon U–Pb age spectra patterns, suggesting that these two areas feed from similar sourcelands in an intracontinental tectonic stability context. The first integrated detrital zircon U-Pb age dataset from these Early Paleozoic transcontinental drainages is presented here. Recognizing these Big Rivers provides insights into the Western Gondwana paleogeographic and tectonostratigraphic evolution in response to the cessation of continent-continent collision after the supercontinent assembly.

1. INTRODUCTION

Understanding the geological evolution of the Gondwana supercontinent and its sedimentary environments during the Early Paleozoic is paramount in deciphering Earth history and paleogeographic dynamics. The dramatic changes in global plate motion in response to tectonic stability and the appearance of biota in the soils promoted rapid chemical weathering during the Ordovician period, resulting in the highest erosion and sedimentation rates in the geological record (Avigad et al., 2005; Squire et al., 2006). Alluvial systems mainly manage sediment transport. In this context, we correlated the early Paleozoic quartz-rich sedimentary rocks throughout Northeastern Brazil and Central Africa to assess the tectonic implications of the Western Gondwana sediment-dispersion system (Fig. IV.1A-B). Here, we synthesized collected and new U-Pb zircon detrital age data to refine our understanding of the source areas and the relationship between these sequences. Ultimately, this study seeks to significantly contribute to the paleogeographic and tectonic reconstruction of Western Gondwana during the Ordovician, offering valuable perspectives on the sedimentary events that shaped the supercontinent evolution.

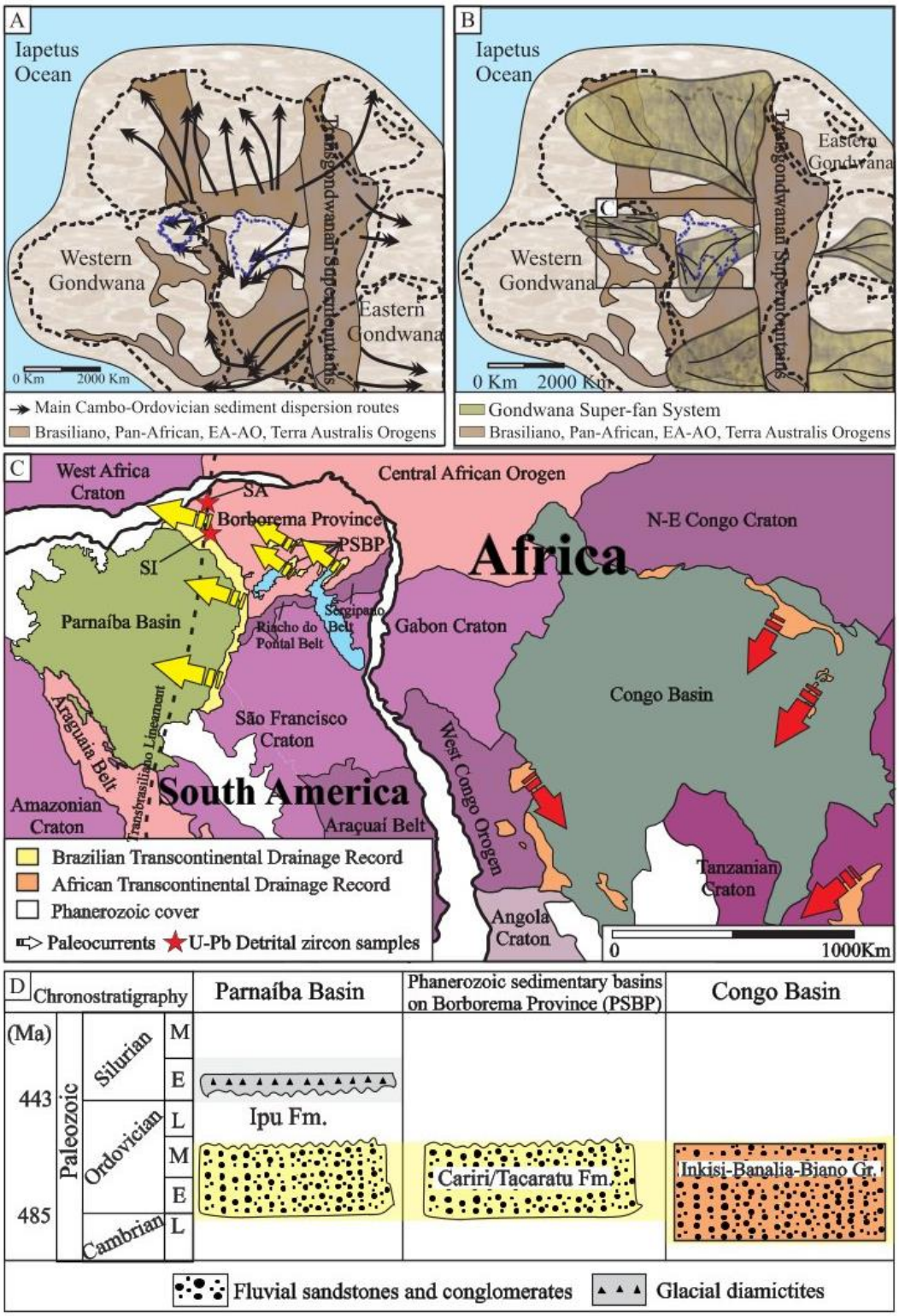

Figure IV.1- A-B: Ordovician Western Gondwana reconstruction showing the main sediment dispersion routes distribution of quartzose sandstones; mountainous areas and possible river systems are indicated. Modified from Burke et al. (2003). C: Simplified geological map of Northeastern Brazil and Central Africa (adapted from Straathof, 2011), highlighting the location of the U-Pb detrital zircon samples and paleocurrents. D: Correlation between the Ordovician BTDR and ATDR sedimentary successions.

2. GEOLOGICAL SETTINGS

The study area encompasses regions in Northeastern Brazil and Central Africa (Fig. IV.1C). During the Early Paleozoic, these territories were merged and constituted Western Gondwana. After the Brasiliano/Pan-African Orogeny, an expressive intracratonic thermal subsidence cycle was followed by the reorganization of drainages and the implantation of continental-scale Alluvial systems (Cerri et al., 2024). In this scenario, the studied siliciclastic sequences correspond to the first sedimentation pulse in Northern Brazil and Central Africa after the supercontinent assembly. These continental-scale rivers drained Proterozoic and Cambrian terranes, representing one of the most spectacular examples of transcontinental drainages. In Brazil, these sequences are composed of the Ipu, Cariri, and Tacaratu formations in the Parnaíba and Phanerozoic sedimentary basins on Borborema Province (PSBP) and constitute the Brazilian Transcontinental Drainage Record (BTDR) (Fig. IV.1D). This record with 200-400m-thick is represented mainly by coarse-grained sandstone and conglomerate, with cross-strata sets organized in finning-upward cycles (Barrera et al., 2020; Cerri et al., 2024). These sedimentary units are superimposed to a significant erosion surface that crosscut the Precambrian metamorphic basement (Daly et al., 2014).

In Africa, the fluvial sequence has been considered equivalent to post-Pan-African early Paleozoic red arkoses of the Northern African portion ("Red beds"), with outcrops at the periphery of the Congo Basin (Delvaux et al., 2021). The Inkisi Group in the Republic of Congo and Northern Angola (Straathof, 2011; Affaton et al., 2016), the Banalia Group in the Lindi region (Tait et al., 2011), the Biano Group in Katanga (Cailteux and De Putter, 2019), and the Upper Nama Group in Namibia (Blanco et al., 2011) that constitutes the African Transcontinental Drainage Record (ATDR). These sequences with 700-1000m thickness are constituted by medium to coarse-grained sandstones and conglomerates organized in finning-upward cycles (Timothée et al., 2023). These sedimentary deposits are superimposed to Pan-African unconformity that crosscut the basal Neoproterozoic sedimentary sequences (Delvaux et al., 2021).

3. MATERIALS AND METHODS

A sedimentologic and stratigraphic study was undertaken based on detailed descriptions of Ipu Formation outcrops from the Parnaíba Basin (Fig. IV.2). Six sandstone samples were collected and analyzed for U-Pb detrital zircon age. The samples were analyzed at the Universidade de Brasilia (UnB); 238U-206Pb (grains younger than 1,5

Ga) or 207Pb-206Pb (grains older than 1,5 Ga) ages were obtained for 120 zircons from each sample. Additionally, a compilation of new and previously published detrital zircon U-Pb ages (2719 grains from 55 samples) from Brazilian and African stratigraphic units within the transcontinental drainages contexts (Fig. IV.3). The Data Repository summarizes sample locations, stratigraphic context, analytical methods, and ages tables.

4. TRANSCONTINENTAL DRAINAGE RECONSTRUCTION

Identifying big rivers in the ancient record can be difficult. These systems typically carry the water and sediment load from vast areas of a continent or significant mountain range. Tectonic setting and sedimentological evidence can offer some guidance, including clues from provenance studies and the size of architectural elements (Miall, 2006; Fielding, 2007). The characteristics enclosing the sedimentary deposits discussed in the first Western Gondwana Big Rivers record are below. Note that we do not intend to discuss the primary origin of the detrital zircon grains since previous studies have already done this (see Cerri et al., 2024; Straathof, 2011).

4.1 THE SCALE OF DEPOSITIONAL ELEMENTS

Fluvial architecture is an elementary component of sedimentologic investigation because the scale of depositional elements in channel belts is related to the system scale. Due to the lack of definitive evidence on the relationship between bedform vertical scale and channel depth, it is essential to use 2D and 3D facies data. The channel-fill scale is a good indicator of channel depth. The ATDR exhibits thickness ranging between 700-1000 meters with broad lateral and width continuity in seismic profiles and well data (Delvaux et al., 2021). Timothée et al. (2023) present the unique architectural element analyses carried out in the ATDR and show an expressive record with channel fill thickness from 6,8m in multistory vertically amalgamed sandstone bodies. The multistoried description and the progressive lateral thickness variation of the lithosomes interpreted as unit bars are more compatible with a superposition of barchanoid dunes described in larger drainages.

The BTDR shows expressive outcrops mainly related to the Ipu Formation. This unit includes a 300-400-meter-thick succession comprising laterally continuous coarse-grained lithoarenites and conglomerate beds that outcrop in the Parnaíba Basin Eastern border (Fig. IV.2). Fluvial depositional architecture is dominated by bodies laterally

continuous for kilometers. The record comprises erosional-based 15 to 25-m thick fining-upward sandstone successions (Fig. IV.2A-B).

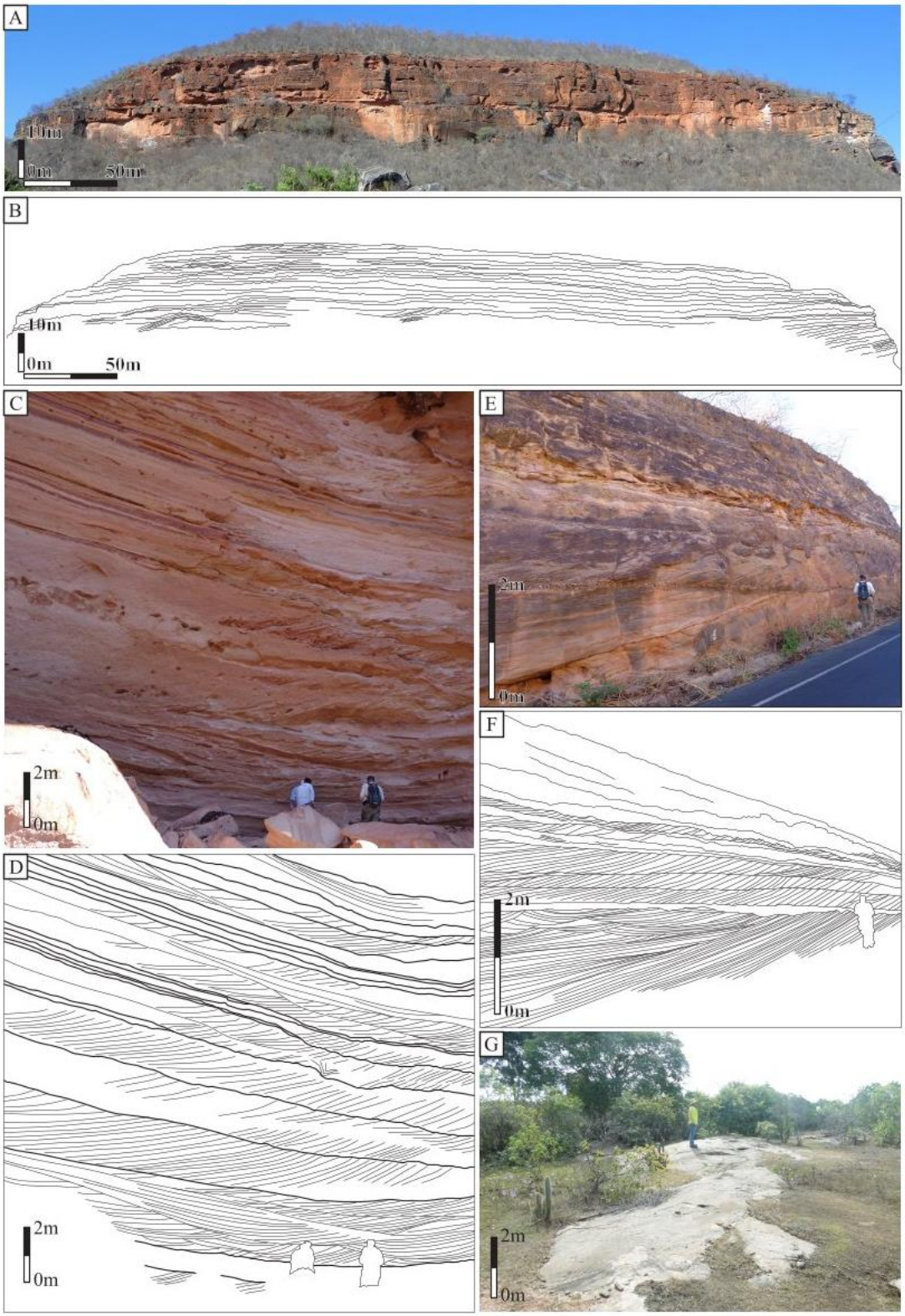

Figure IV.2- Sedimentologic aspects of the Ipu Formation in the Parnaíba Basin. A-B: Cross-strata sandstone cosets interpreted as deposits of large barchanoid dunes. C-D: Cross-strata sandstone sets interpreted as deposits of compound barchanoid dunes. E-F. Metric-scale trough cross-strata sandstone sets interpreted as deposits of unit bars. G: Metric-scale preserved dune morphology.

In the cycles base abundant 1 to 2.5 m-thick trough cross-strata pass laterally to and from trough-shaped cross-strata sets composed of 0.5 to 0.9 m-thick tabular and trough cross-strata (Fig. IV.2C-D). Locally, decimeter conglomerate beds and sandstone cosets with trough and tabular cross-strata cover meter-scale cross-strata sandstone bodies (Fig. IV.2E-F). Additionally, metric-scale preserved dune morphology was observed (Fig. IV.2G).

The presence of two distinct large-scale cross-strata sets in a local area indicates the presence of periodic bedforms. This overall structuration is consistent with the model for depositing large-scale barchanoid compound dunes in Big Rivers thalwegs (see. Almeida et al., 2016; Galeazzi et al., 2018). Also, the decimetric-scale cross-stratified cosets that compound the finning upward cycles built by superimposed dunes are probably the most common bedform record of large-river channels (cf. Galeazzi et al., 2018). Recognizing these architectural elements and the recorded lateral kilometric continuity suggests sediment deposition in massive channels in a Big River context.

4.2 DETRITAL ZIRCON U-PB AGES

U-Pb analyses for the BTDR and ATDR are presented as Kernel Density Estimates (KDEs) for all considered sedimentary basins (Fig. IV.3). All samples show the most prominent zircon groups between 0.75 and 0.5 Ga, with varying individual age probability peaks. The second prominent set is 1.2–0.85 Ga, with 2.2–1.7 and 2.8–2.5 Ga zircon age groups. The presence of ca. 1.0 Ga zircons accompanied by ca. 2.7–2.5 and 2.15–1.75 Ga zircons in Ordovician sandstones is an essential fingerprint for paleo-source area and paleogeographic reconstructions of Gondwana (Meinhold et al., 2013). A comparison of the detrital zircon age spectra and the CA-DA curve from BTDR and ATDR indicates that these two areas were fed from similar sourcelands in an intracontinental extensional tectonic context (Fig. IV.3 and IV.RD-3). The Gondwana supercontinent assembly involved a series of arc terrane accretions (ca. 820–650 Ma) followed by orogenic collisions and related magmatism (ca. 650–530 Ma) (Torsvik and Cocks, 2011). As a result of these orogenies, the East African Orogen (Trans-Gondwanan Supermountains) and the Brasiliano-Pan African Orogeny were built (Squire et al., 2006; Torsvik and Cocks, 2013; Wang et al., 2020). The uplift of these mountain ranges caused an increase in sediment production that fed the continental-

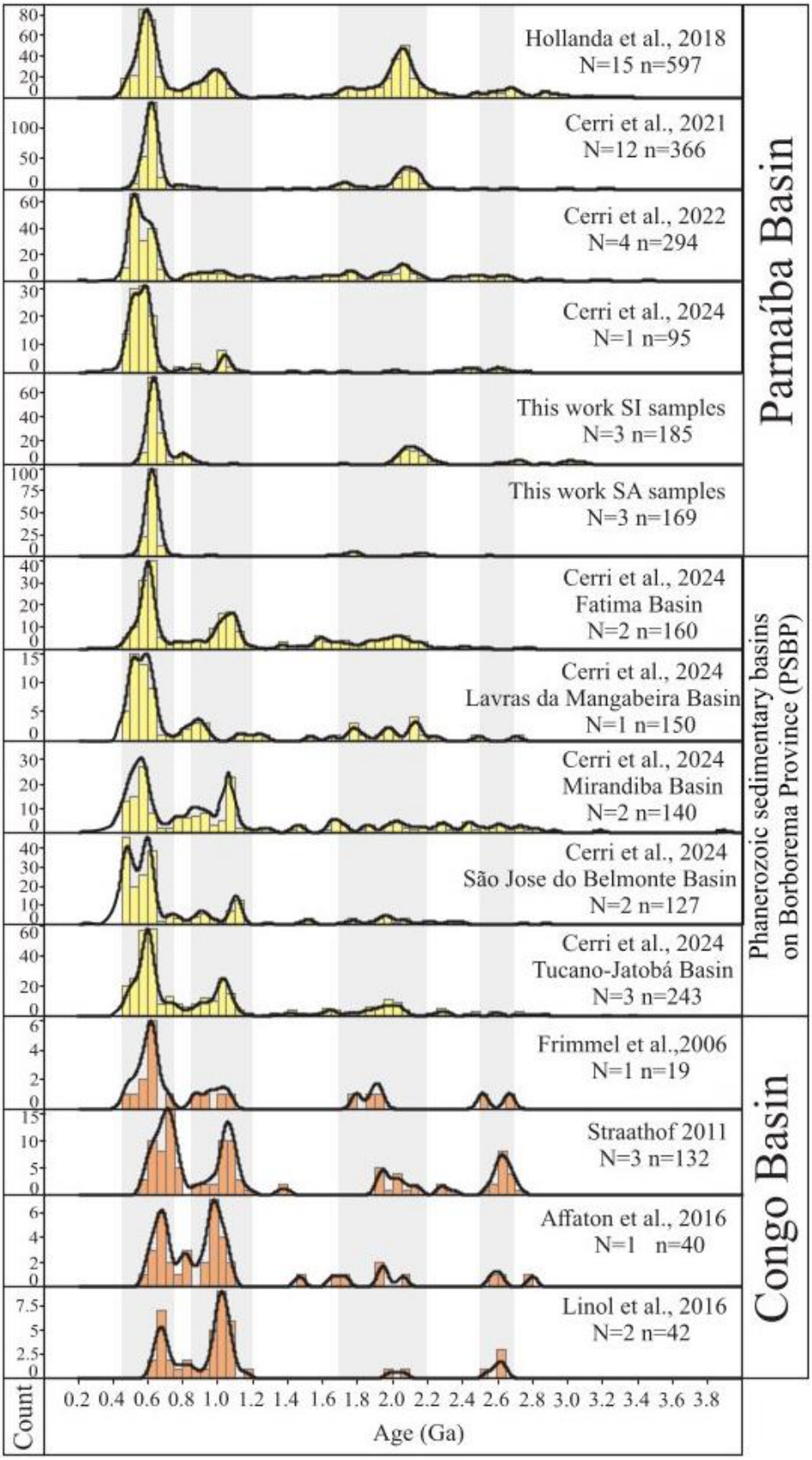

Figure IV.3- Kernel Density Estimates plots of the full age spectra of detrital zircon U–Pb ages from Ordovician sandstones of Western Gondwana.

scale alluvial systems flowing towards the West and East margins of Gondwana (Squire et al., 2006; Cerri et al., 2024). In Northern Africa, these sequences are enclosed between the Transgondwanan Superfan System (TSS) (Squire et al., 2006). It represents one of the most voluminous siliciclastic sequences ever deposited on a continental crust (Burke and Kraus, 2000). Based on sedimentological and stratigraphical data, Timothée et al. (2023) suggested that the ATDR was deposited in the same paleogeographic context as TSS. Additionally, U-Pb detrital zircon data shows remarkable similarities between the BTDR, ATDR, and TSS, indicating a simultaneous deposition for these records (see Delvaux et al., 2021).

BTDR previous provenance data suggest metamorphic belts adjacent to the Parnaíba Basin present-day southeastern contour as the unique land source. This hypothesis is based on the U-Pb detrital zircon data from the BTDR. However, possible sources-lands within this age range are also abundant within the mobile belts and cratons in present-day Southeast Brazil and Central Africa (see Meinhold et al., 2013; Veevers, 2017; Tavares et al., 2020; Delvaux et al., 2021). The integrated detrital zircon U-Pb age dataset from the BTDR and ATDR records reveal a probable concomitant Ordovician deposition that does not imply a consistent sediment route between Central Africa and Northeastern Brazil or fluvial systems connexion (Fig. IV.3 and IV.4).

4.3 TECTONOSTRATIGRAPHIC EVOLUTION

The Gondwana Supercontinent amalgamation was followed by post-orogenic extension and denudation. These rearranged drainage patterns dispersed large volumes of sediments by continental-scale fluvial systems (Fig. IV.4) (e.g., Squire et al., 2006). The BTDR and ATDR sedimentary piles often display 300–1000 m thicknesses. Maximum subsidence is recorded in basinal areas, while minimum rates typify proximal grabens surrounding basins present-day limits. Fluvial sandstones prevail in both cases, indicating sediment oversupply over time. Accretion of large terranes in complex orogens can also create conditions for large rivers to develop, commonly following tortuous paths around and across sutures (Miall 2006).

During the ATDR deposition, the Congo Basin depocenter migrated towards a central NW-SE oriented depression, open to the north with a maximum of 1.2 km of sediment thickness (Delvaux et al., 2021). The ATDR outcrops border the western-southern and eastern sides of the Congo Basin (Delvaux et al., 2021). For the ATDR

record, only continental environments were reported. Evidence that the deposition of the ATDR was interrupted or influenced by the late Ordovician or Early Silurian glaciation and ice sheet, which affected most of Northern Africa and South America, was not found (e.g., Ghienne et al., 2007; Barrera et al., 2020). The subsidence mechanism of the Congo Basin during the Paleozoic period is not precise. Seismic profiles indicate that the deformation during the Pan-African orogeny was localized, and the basin remained mostly undisturbed tectonically during this time interval (Delvaux et al., 2021). Instead, a general extensional context was established after the final Gondwana assembly.

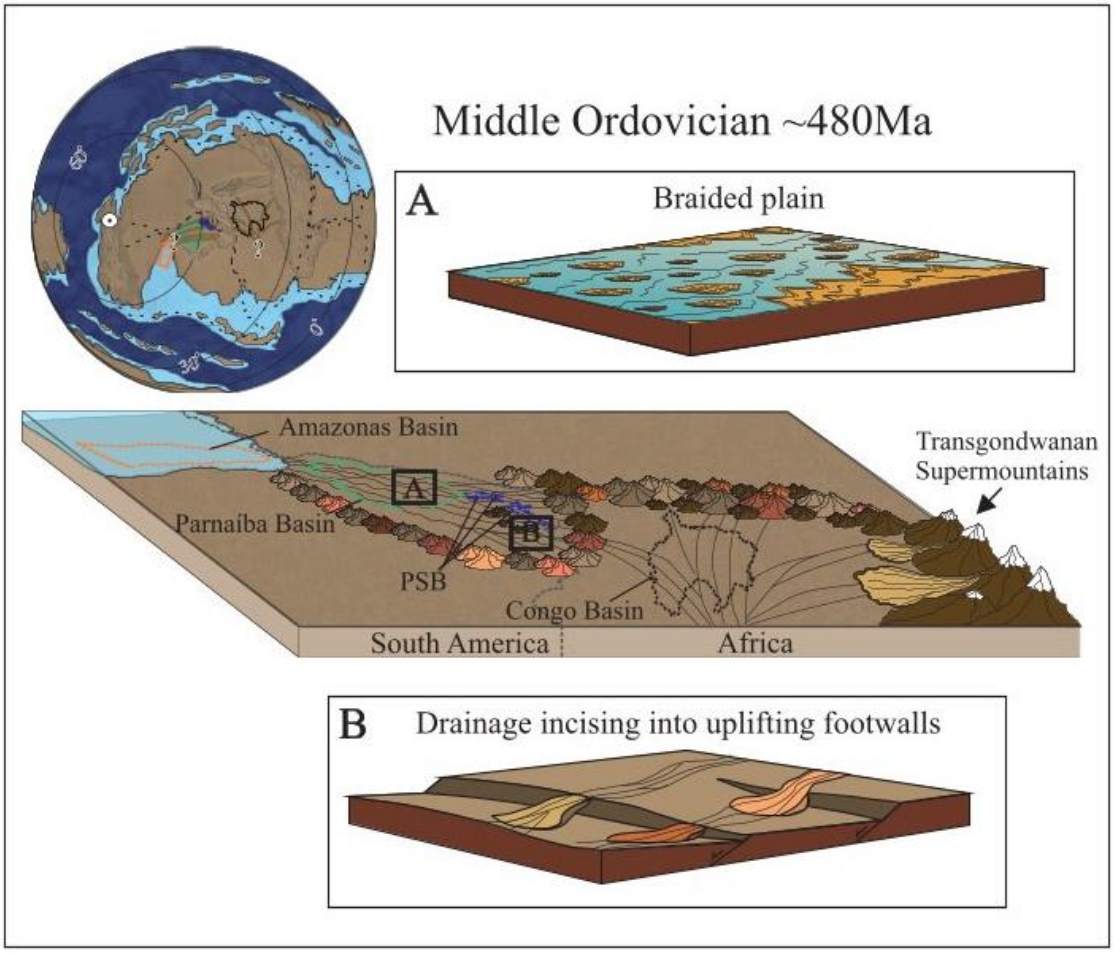

Figure IV.4- Ordovician Western Gondwana paleogeographic reconstruction: The supercontinent amalgamation promoted the development of large-scale pre-vegetation alluvial systems that drain mountain regions. Paleogeographic Maps were modified from Bakley (2008) and Torsvik & Cocks (2013).

Cerri et al. (2024) recently presented a robust data framework that allows the correlation of diverse Ordovician fluvial records of Northern Brazil, which we refer to as BTDR. They also propose a paleogeographic and tectonostratigraphic evolution model for this siliciclastic succession, suggesting that the alluvial system headboard was in the West Gondwana Orogen (Ganade et al., 2013) (Sergipano Belt). However, related alluvial

fan facies were never found, and the interpreted braided plain succession is present in several isolated grabens inserted into these metamorphic belts for thousands of kilometers (e.g., Figueiredo et al., 2015; Carvalho et al., 2018). Unidirectional paleocurrent data indicate that the depositional area was more extensive than currently preserved. Despite their mineralogical maturity, the Ordovician sandstones of BTDR and ATDR were principally derived directly from Neoproterozoic basement rocks that were themselves emplaced shortly before deposition. Reported U–Pb detrital zircon ages from Cambrian and Ordovician provide evidence that these mature quartz-rich sandstones are essentially first-cycle sediments.

The dataset suggests that drainages flowed towards the western/southwestern marine settings of Western Gondwana through a gently inclined platform or ramp (e.g., Torsvik and Cocks, 2013; Cerri et al., 2022). These circumstances allow the fluvial system proliferation and the establishment of sediment routes across the Western Gondwana (Fig. IV.4). In this palaeogeographical scenario, the ATRD and BTRD represent the legacies of concomitant different massive depositional depressions later individualized in the present-day basins and grabens by tectonics and erosion (Fig. IV.1 and IV.4). Silurian glacial diamictites covered the fluvial deposits of the Ipu Formation, marking the decline of the BTDR Big River. Fluvial sedimentary succession preservation may be related to the Atlantic Ocean opening extensional tectonics, which created a sizeable subsiding area with accommodation space and rift-basin installation (e.g., Figueiredo et al., 2015).

5. CONCLUSIONS

The investigation into the Ordovician sedimentary records of Northeastern Brazil and Central Africa sheds light on the ancient geological dynamics of Western Gondwana. Through detailed analyses of fluvial depositional architecture and detrital zircon U-Pb ages, a compelling narrative emerges of the immense transcontinental drainage systems that shaped the landscape after the assembly of the Gondwana supercontinent. The recognition of these massive drainage systems provides fascinating insights into the paleogeographical and tectonic evolution of Western Gondwana during the Early Paleozoic.

ACKNOWLEDGMENTS

This paper is a part of the Ph.D. thesis of the first author, who is thankful to the Programa de Pós-Graduação em Geologia e Geoquímica (PPGG) of the Federal University of Pará (UFPA) for logistic and financial support. The first author acknowledges the CAPES – Fundação Coordenação de Aperfeiçoamento de Pessoal de Nível Superior (Brazil) - Grant 88887.508135/2020-00.

REFERENCES

Affaton, P., Kalsbeek, F., Boudzoumou, F., Trompette, R., Thrane, K., Frei, R., 2016. The Pan-African West Congo belt in the Republic of Congo (Congo Brazzaville): stratigraphy of the Mayombe and West Congo Supergroups studied by detrital zircon geochronology. Precambrian Res. 272, 185–202.

Almeida, R. P. de, Galeazzi, C. P., Freitas, B. T., Janikian, L., Ianniruberto, M., & Marconato, A. 2016. Large barchanoid dunes in the Amazon River and the rock record: Implications for interpreting large river systems. Earth and Planetary Science Letters, 454, 92–102.

Avigad, D., Sandler, A., Kolodner, K., Stern, R.J., McWilliams, M., Miller, N., Beyth, M., 2005. Mass-production of Cambro-Ordovician quartz-rich sandstones as a consequence of chemical weathering of Pan-African terranes: environmental implications. Earth Planet. Sci. Lett. 240, 818–826.

Blakey, R. C. 2008. Gondwana paleogeography from assembly to breakup—A 500 m.y. odyssey. Special Paper 441: Resolving the Late Paleozoic Ice Age in Time and Space, 1–28.

Barrera, I.A.R., Nogueira, A.C.R., Bandeira, J., 2020. The Silurian glaciation in the eastern Parnaíba Basin, Brazil: paleoenvironment, sequence stratigraphy and insights for the evolution and paleogeography of West Gondwana. Sedimentary Geology 105714.

Blanco, G., Germs, G.J.B., Rajesh, H.M., Chemale Jr., F., Dussin, I.A., Justino, D., 2011. Provenance and paleogeography of the Nama Group (Ediacaran to early Palaeozoic, Namibia): Petrography, geochemistry and U–Pb detrital zircon geochronology. Precambrian Res. 187, 15–32.

Burke, K., Kraus, J.U., 2000. Deposition of immense Cambro-Ordovician sandstone bodies, now exposed mainly in North Africa and Arabia, during the aftermath of the final assembly of Gondwana. Geol. Soc. Am. Abstr. Programs 32, 249.

Burke, K., MacGregor, D.S., Cameron, N.R., 2003. Africa's petroleum systems: four tectonic ‘Aces’ in the past 600 million years. Geological Society of London Special Publications 207, 21–60.

Cailteux, J.L.H., De Putter, T., 2019. The Neoproterozoic Katanga Supergroup (D. R. Congo): State-of-the-art and revisions of the lithostratigraphy, sedimentary basin and geodynamic evolution. J. Afr. Earth Sci. 150, 522–531.

Cerri, R.I., Warren, L.V., Varejão, F.G., Silva, A.J.C.A., Lana, C., Assine, M.L., 2021. So close and yet so far: U-pb geochronological constraints of the Jaibaras Rift Basin and the intracratonic Parnaíba Basin in SW Gondwana. Geological Magazine, 121.

Cerri, R.I., Warren, L.V., Spencer, C.J., Varejão, F.G., Promenzio, P., Luvizotto, G.L., Assine, M.L., 2022. Using detrital zircon and rutile to constrain sedimentary provenance of Early paleozoic fluvial systems of the Araripe Basin, Western Gondwana. Journal of South American Earth Sciences 116, 103821.

Cerri, R.I., Warren, L.V., Luvizotto, G.L., Spencer, C.J., Assine, M.L., 2024. The Early Paleozoic sedimentary record in northeastern Brazil: Unravelling the sedimentary provenance and evolution of fluvial systems after the Western Gondwana assembly. Gondwana Research 131, 237-255.

Daly, M.C., Andrade, V., Barousse, C.A., Costa, R., McDowell, K., Piggott, N., Poole, A.J., 2014. Brasiliano crustal structure and the tectonic setting of the Parnaíba basin of NE Brazil: results of a deep seismic reflection profile. Tectonics 33, 2102–2120.

Delvaux, D., Maddaloni, F., Tesauro, M., Braitenberg, C., 2021. The Congo Basin: stratigraphy and subsurface structure defined by regional seismic reflection, refraction and well data. Global Planet. Change 198, 103407.

Fielding, C.R., 2007. Sedimentology and stratigraphy of Large River Deposits: recognition in the ancient record, and distinction from 'Incised Valley Fills'. In: Gupta, A. (Ed.), Large Rivers: Geomorphology and Management. John Wiley and Sons, pp.97–113. Chapter 7.

Frimmel, H., Tack, L., Basei, M., Nutman, A., Boven, A., 2006. Provenance and chemostratigraphy of the Neoproterozoic West Congolian Group in the Democratic Republic of Congo. Journal of African Earth Sciences 46 (3), 221–239.

Galeazzi, C. P., Almeida, R. P., Mazoca, C. E. M., Best, J. L., Freitas, B. T., Ianniruberto, M., … Tamura, L. N. 2018. The significance of superimposed dunes in the Amazon River: Implications for how large rivers are identified in the rock record. Sedimentology.

Ghienne, J.-F., Boumendjel, K., Paris, F., Videt, B., Racheboeuf, P., Salem, H. A. 2007. The Cambrian–Ordovician succession in the Ougarta Range (Western Algeria, North Africa) and interference of the late ordovician glaciation on the development of the lower Palaeozoic transgression on northern Gondwana. Bulletin of Geosciences, 82(3), 183–214.

Hollanda, M.H.B., Góes, A.M., Negri, F.A., 2018. Provenance of sandstones in the Parnaíba Basin through detrital zircon geochronology. In Cratonic Basin Formation: A Case Study of the Parnaíba Basin of Brazil (eds M.C. Daly, R.A. Fuck, J. Julià, D.I.M.

Macdonald and A.B. Watts), pp. 181–97. Geological Society of London, Special Publication no. 472.

Linol, B., de Wit, M.J., Barton, E., deWit, M.J.C., Guillocheau, F., 2016. U–Pb detrital zircon dates and source provenance analysis of Phanerozoic sequences of the Congo Basin, central Gondwana. Gondwana Res. 29, 208–219.

Meinhold, G., Morton, A.C., Avigad, D., 2013. New insights into peri-Gondwana paleogeography and the Gondwana super-fan system from detrital zircon U–Pb ages. Gondwana Res. 23, 661–665.

Miall, A.D., 2006. How do we identify big rivers? And how big is big? Sediment. Geol.186, 39–50.

Squire, R.J., Campbell, I.H., Allen, C.M., Wilson, C.J.L., 2006. Did the Transgondwanan Supermountain trigger the explosive radiation of animals on Earth? Earth Planet. Sci. Lett. 250, 116–133.

Straathof, G.B., 2011. Neoproterozooic Low Latitude Glaciations: An African Perspective. PhD thesis. University of Edinburg (285 pp.).

Tait, J., Delpomdor, F., Pr´eat, A., Tack, L., Straathof, G., Nkula, V.K., 2011. Neoproterozoic sequences of the West Congo and Lindi/Ubangi Supergroups in the Congo Craton, Central Africa. In: Arnaud, E., Halverson, G.P., Shields-Zhou, G. (Eds.), The Geological Record of Neoproterozoic Glaciations, Geological Society Memoir, 36, pp. 185–194.

Tavares, T. D., Martins, M. de S., Alkmim, F. F., & Lana, C. 2020. Detrital zircons from the Upper Três Marias Formation, São Francisco basin, SE Brazil: Record of foreland deposition during the Cambrian? Journal of South American Earth Sciences, 97, 102395.

Timothée, M., Florent, B., Hardy Meddry Dieu-Veill, N., Damien, D. 2024. The Cambro-Ordovician Gondwana alluvial megafan in Central Africa: Insights from the Paleozoic sandstones of the Inkisi group, Congo Republic and Democratic Republic of the Congo. Journal of African Earth Sciences, 209, art. no. 105109.

Torsvik, T.H., Cocks, L.R.M., 2013. Gondwana from top to base in space and time. Gondwana Res. 24 (3–4), 999–1030.

Torsvik, T.H., Cocks, L.R., 2011. The Paleozoic paleogeography of central Gondwana. In: Van Hinsbergen, D.J., Buiter, S.J.H., Torsvik, T.H., Gaina, C., Webb, S.J. (Eds.), The Formation and the Evolution of the Africa: A Synopsis of 3.8 Ga of Earth History, 357. Geological Society, London, Special Publications, pp. 137–166.

Veevers, J. J. 2017. West Gondwanaland during and after the Pan-African and Brasiliano orogenies: Downslope vectors and detrital-zircon U–Pb and T DM ages and εHf/Nd pinpoint the provenances of the Ediacaran–Paleozoic molasse. Earth-Science Reviews, 171, 105–140.

Wang, Q., Spencer, C.J., Hamdidouche, R., Zhao, G., Evans, N.J., McDonald, B.J., 2020. Detrital zircon U-Pb–Hf data from cambrian sandstones of the Ougarta Mountains Algeria: implication for palaeoenvironment. Geological Journal 55, 7760–7774.

SUPPLEMENTARY MATERIAL

Serra do Ibiapaba (SI) and Santana de Acaraú (SA) regions sample locations and stratigraphic context.

Samples were collected from Ipu Formation fluvial sandstone within the Parnaíba Basin and Santana de Acaraú Graben (Fig. IV.S1). These records consist of stacks of laterally continuous tabular bodies, with thicknesses ranging from 40 cm to 180 cm. The deposits show fining-upward cycles composed of sandstone and conglomerate beds (Fig. IV.S2). The contacts between the sandstone beds are mainly flat/non-erosional, and subordinate erosive contacts have been identified. Medium-to-coarse-grained sandstone and clast-supported conglomerate with medium- to coarse sandy matrix with granules exhibit tabular cross-bedding to low-angle stratification and even parallel stratification (Fig. IV.S2). Subordinate levels of massive conglomerates change laterally to pebbly sandstone. The cross-strata dips show preferential paleocurrent trends towards the N-NW (Fig. IV.S2).

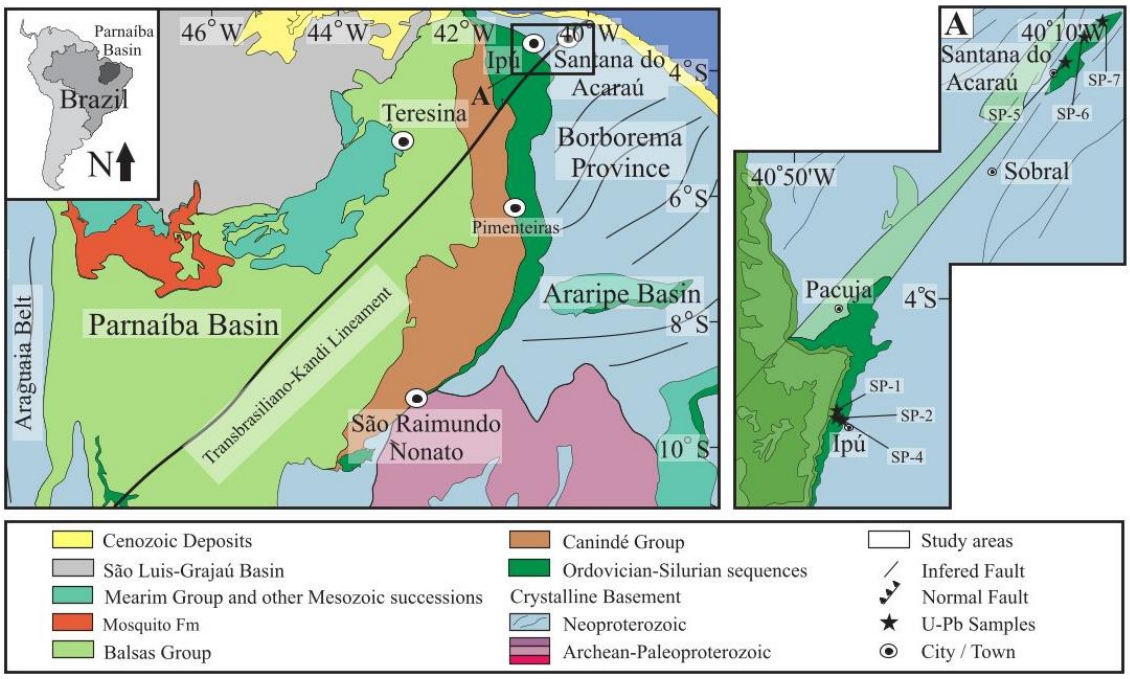

Figure IV.S1- The Parnaíba Basin in northern Brazil and the study area location. A: Geological map of the Ipueiras district shows the Serra de Ibiapaba and Santana de Acaraú regions with the locations of visited outcrops. Geological map at 1:100,000 of the Ipueiras district extracted from the database of the Geological Survey of Brazil (CPRM, 2013).

Sampling was done during fieldwork in the Serra do Ibiapaba (SI) and Santana de Acaraú (SA) regions (Fig. IV.S1). Six samples from outcrops were analyzed (Fig. IV.2). For the U–Pb zircon analysis, samples were crushed, and zircon crystals were separated through standard magnetic and hand-picking techniques at the Geosciences Institute of the Universidade Federal do Pará (UFPA), Brazil. Zircon grains were then mounted in an epoxy resin, ground and polished, and imaged by Scanning Electron Microscopy (SEM) microscope through the

cathodoluminescence technique. The resulting images emphasized the internal structure of zircon grains to identify zoning and fracturing aspects of each grain to aid in the location of laser spots.

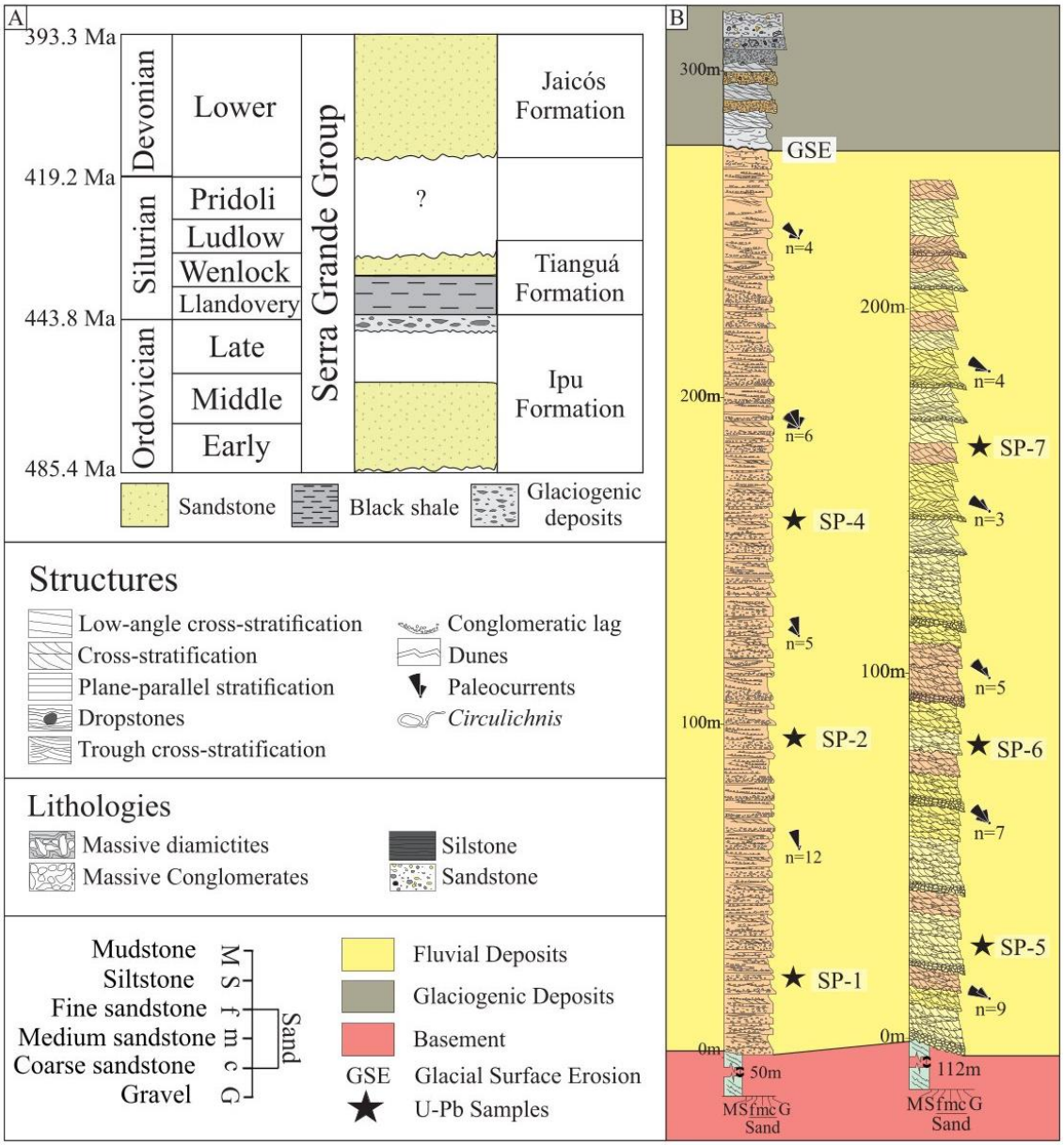

Figure IV.S2- A: Stratigraphy of the Serra Grande Group in the Parnaíba Basin, northern Brazil. Modified from Vaz et al. (2007). B: Sedimentary logs and descriptions of Ipu Formation in the Ipueiras region, eastern Parnaíba Basin, northeastern Brazil.

Zircon grains from samples were analyzed using a Finnigan Neptune ICP–MS coupled to an Nd–YAG laser ablation system at the Laboratory of Geochronological, Geodynamic, and Environment Studies of the Universidade de Brasília (UnB) following the analytical procedures outlined in Bühn et al. (2009) (Table S1). The accuracy of the procedures was controlled using the TEMORA-2, PEIXE, and 91500 standards. Corrections were made to the background, instrumental mass bias, and common Pb. U–Pb ages were calculated using Isoplot 3.6 (Ludwing, 2008). At least 120 grains were dated for each sample using a discordance filter of ca. 10% (Table

IV.S1). The ages of the analyzed detrital zircon are reported as 207Pb/206Pb for grains older than 1.5 Ga or 238U-206Pb ages for grains younger than 1.5 Ga. The data were graphically represented by Kernel Density Estimate plots (KDEs) using the R-package "Detzrcr." To better understand the tectonic setting and the similarity between samples, Cumulative Distribution Curves (CAD; Fig. IV.S3) were constructed using the CA-DA gap curve (Fig. IV.S3) (crystallization age - CA subtracted by the depositional age - DA; Cawood et al., 2012). A depositional age of ca. 490 Ma was used, corresponding to the Early Ordovician period for BTDR, while for the ATDR, a ca. 500 Ma was used.

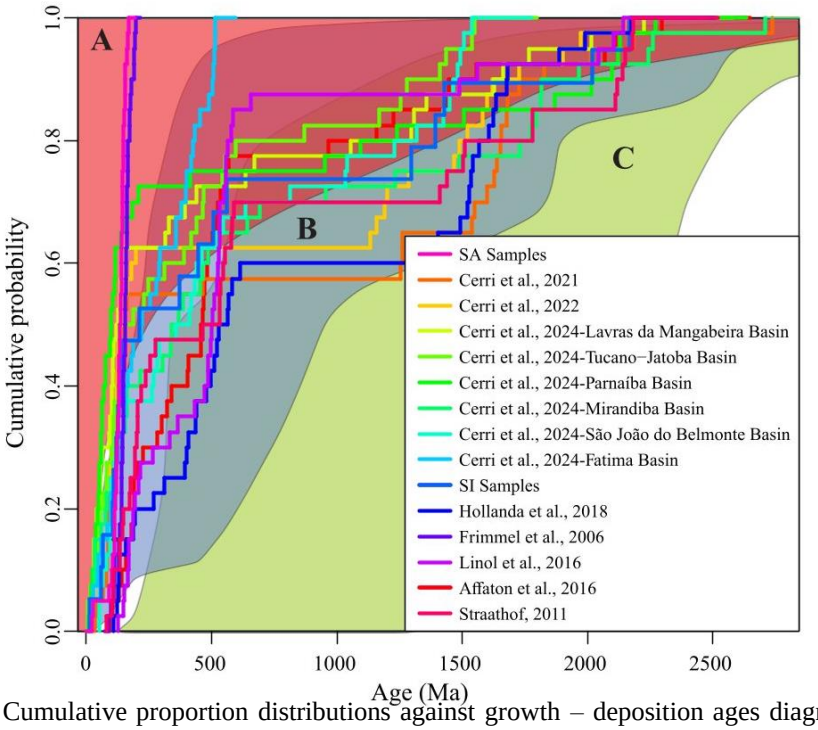

Figure IV.S3- Cumulative proportion distributions against growth – deposition ages diagram, modified from Cawood et al. (2012). Colored fields correspond to different depositional tectonic settings: A. convergent basins, B. collisional basins, C. extensional basins.

References

Bühn, B., Pimntel, M.M., Matteini, M., Dantas, E.L., 2009. High spatial resolution analysis of Pb and U isotopes for geochronology by laser ablation multi-collector inductively coupled plasma mass spectrometry (LA-MC-ICPMS). An Acad. Bras Ciˆ encias 81, 99–114.

Cawood, P.A., Hawkesworth, C.J., Dhuime, B., 2012. Detrital zircon record and tectonic setting. Geology 40 (10), 875–878.

Ludwig, K.R. 2008. Isoplot 3.60. Berkeley Geochronology Center, Special Publication No. 4, 77 p.

Vaz, P.T., Resende, N.G.A.M., Wanderley Filho, J.R., Travassos, W.A., 2007. Bacia do Parnaíba. Rio de Janeiro. 15(2). PETROBRÁS. Boletim de Geociências, pp. 253–263.

Supplementary Table IV.S1- U-Pb data for detrital zircon grains from SI and SA samples from the Ipu Formation.

Instituto de Geociências, Universidade de Brasília							Data for Tera-Wasserburg plot [b]						Data for Wetherill plot [c]						Dates [c]										
Identifier	f206c	^{206}Pb	U (µg g^{-1}) [a]	Th/U	^{206}Pb/^{204}Pb	1s (%)	^{238}U/^{206}Pb	1s (%)	^{207}Pb/^{206}Pb	1s (%)	^{208}Pb/^{206}Pb	1s (%)	^{207}Pb/^{235}U	1s (%)	^{206}Pb/^{238}U	1s (%)	Rho	^{208}Pb/^{232}Th	1s (%)	^{207}Pb/^{206}Pb	2s	2s$_{sys}$	^{206}Pb/^{238}U	2s	2s$_{sys}$	^{207}Pb/^{235}U	2s	2s$_{sys}$	^{208}Pb/^{232}Th	2s	2s$_{sys}$	% conc [d]
SP-1_49	-0.023	9864	39	0.7	260.42	38.14	11.06	2.0	0.062	4.42	0.130	5.109	0.767	4.2	0.092	2.0	0.48	0.027	3.916	569	215	220	569	22	24	568	39	41	530.875	41.119	69.373	100
SP-1_102	0.650	56766	223	0.8	1353.10	34.74	10.59	1.0	0.060	1.33	0.144	2.987	0.786	1.4	0.094	1.0	0.69	0.028	1.563	598	59	71	579	11	14	588	13	18	566.608	17.459	61.970	97
SP-1_4	-0.118	78770	195	0.8	-2421.66	-21.44	10.47	1.4	0.063	2.27	0.150	3.274	0.823	1.8	0.096	1.4	0.80	0.030	2.049	654	95	102	590	16	18	608	16	20	597.848	24.118	67.113	90
SP-1_17	1.121	69671	217	2.6	-12133.71	-33.87	10.59	1.8	0.063	2.82	0.426	2.536	0.817	2.2	0.096	1.8	0.84	0.028	1.868	622	126	133	590	21	23	604	20	24	550.851	20.323	61.337	95
SP-1_5	0.396	53081	139	0.6	-2217.78	-20.20	10.53	1.6	0.063	2.89	0.109	2.694	0.822	2.0	0.096	1.6	0.80	0.030	2.403	652	124	130	592	19	21	612	21	25	592.896	28.075	68.215	91
SP-1_37	0.094	123147	438	0.3	4684.00	35.57	10.10	1.4	0.061	1.83	0.056	2.280	0.838	1.7	0.099	1.3	0.79	0.030	1.814	616	75	84	610	15	18	617	15	20	602.074	21.532	66.744	99
SP-1_35	-1.166	13060	43	4.0	404.21	37.22	10.00	1.4	0.064	3.11	0.729	2.435	0.887	3.2	0.101	1.4	0.45	0.032	1.914	664	126	132	620	17	20	638	30	32	637.177	23.998	70.920	93
SP-1_69	1.515	19618	73	1.4	1203.72	26.26	10.12	2.3	0.064	2.87	0.243	5.841	0.862	3.3	0.101	1.8	0.54	0.030	2.865	684	127	133	620	21	23	634	27	29	590.280	33.348	70.364	91
SP-1_54	0.583	57694	201	2.3	749.66	66.07	9.93	1.4	0.063	2.17	0.546	4.698	0.879	1.9	0.101	1.5	0.76	0.030	1.359	673	95	103	620	17	20	638	18	22	597.622	15.993	64.621	92
SP-1_117	1.897	24617	92	1.5	513.04	32.90	9.88	1.1	0.061	2.36	0.263	3.416	0.859	2.3	0.102	1.0	0.46	0.029	2.009	602	100	107	624	12	16	627	21	24	579.669	22.939	64.958	104
SP-1_88	0.092	69062	262	0.4	2808.14	31.35	9.85	0.9	0.062	2.03	0.069	4.086	0.862	1.6	0.102	0.9	0.55	0.026	3.263	637	87	96	626	11	15	629	15	20	518.563	33.324	63.730	98
SP-1_81	1.067	42527	157	0.8	1391.31	41.38	9.88	1.3	0.061	2.60	0.163	6.602	0.862	2.5	0.102	1.2	0.50	0.023	3.631	599	115	122	626	15	18	628	23	26	460.147	32.975	58.476	104
SP-1_104	0.124	58559	207	0.6	1388.99	36.42	9.79	1.0	0.061	1.66	0.128	4.985	0.873	1.6	0.102	1.0	0.62	0.030	2.798	640	77	87	627	12	15	636	15	20	593.920	32.746	70.374	98
SP-1_27	0.478	125327	388	0.2	10685.69	28.83	9.77	1.2	0.062	1.94	0.050	6.909	0.881	1.3	0.103	1.2	0.91	0.025	5.526	660	80	89	629	15	18	640	13	18	499.447	54.583	75.769	95
SP-1_64	1.300	21648	76	1.0	387.58	53.25	9.75	1.5	0.062	2.49	0.173	3.318	0.870	1.9	0.103	1.4	0.74	0.031	2.489	627	106	113	629	17	20	637	20	24	623.454	30.562	72.103	100
SP-1_63	-2.145	14682	53	3.8	593.82	38.08	9.81	1.8	0.061	2.95	0.647	3.366	0.856	2.9	0.103	1.7	0.57	0.031	3.080	571	129	135	631	20	22	623	27	30	610.581	37.059	73.985	110
SP-1_118	-0.193	54012	198	0.2	647.33	53.18	9.69	0.8	0.063	1.69	0.040	2.542	0.880	2.5	0.103	0.8	0.33	0.029	3.007	700	69	78	634	10	14	655	25	28	587.192	34.762	70.663	91
SP-1_73	0.675	70813	241	1.5	3672.17	24.74	9.70	1.0	0.062	1.30	0.253	2.135	0.897	1.3	0.104	1.0	0.74	0.032	1.632	680	61	74	636	12	16	649	13	18	635.151	20.404	69.579	93
SP-1_100	1.215	20737	77	1.1	332.54	49.50	9.72	1.3	0.062	2.56	0.212	2.699	0.887	2.8	0.104	1.3	0.48	0.032	2.218	626	120	127	636	16	19	640	27	30	635.723	27.732	72.068	102
SP-1_38	0.451	47157	161	2.7	2825.50	23.89	9.66	1.1	0.061	2.25	0.495	2.986	0.868	1.8	0.104	1.1	0.63	0.032	1.790	607	99	107	638	14	17	632	17	21	645.118	22.716	71.234	105
SP-1_55	0.102	64998	217	0.4	3388.82	24.44	9.66	1.1	0.060	1.43	0.067	5.880	0.866	1.2	0.104	1.1	0.95	0.030	2.174	590	64	76	638	14	17	632	11	17	594.296	25.448	67.286	108
SP-1_70	0.364	105162	363	0.2	5272.74	27.03	9.61	0.8	0.060	1.55	0.037	2.017	0.868	1.1	0.104	0.8	0.69	0.032	1.967	596	68	78	640	10	14	634	11	17	634.811	24.587	70.916	107
SP-1_11	0.295	30877	82	2.6	-1984.30	-32.47	9.61	1.5	0.063	2.94	0.469	3.979	0.907	4.1	0.105	1.4	0.34	0.032	2.114	688	155	162	640	17	20	657	31	33	644.236	26.816	72.617	93
SP-1_30	0.203	84411	265	2.8	6342.03	26.84	9.56	0.6	0.059	1.45	0.465	1.371	0.856	1.3	0.105	0.6	0.47	0.031	1.327	591	63	74	641	8	13	630	14	20	616.839	16.127	66.648	109
SP-1_95	1.089	26721	96	1.1	925.87	29.78	9.55	1.1	0.062	2.28	0.199	2.269	0.893	1.8	0.105	1.1	0.64	0.032	2.126	639	99	107	642	14	17	646	17	21	635.426	26.586	71.661	100
SP-1_13	0.077	62063	163	1.0	-3325.31	-23.32	9.58	1.0	0.061	2.20	0.174	2.016	0.880	1.6	0.105	1.1	0.64	0.032	1.729	607	93	101	643	13	16	639	15	20	637.303	21.684	70.162	106
SP-1_36	-0.674	21140	75	2.0	50.86	396.80	9.63	2.5	0.063	4.16	0.352	3.941	0.918	3.8	0.105	2.8	0.74	0.031	3.157	663	174	178	645	34	35	658	36	39	616.604	38.306	75.067	97
SP-1_58	0.310	85511	289	0.3	2471.73	36.87	9.54	1.0	0.062	1.85	0.104	8.498	0.898	1.4	0.105	1.0	0.73	0.032	2.289	651	83	93	645	13	16	652	15	20	629.212	28.359	71.752	99
SP-1_94	0.907	34238	125	3.4	1244.42	31.35	9.55	1.3	0.061	2.25	0.596	2.728	0.886	2.0	0.105	1.2	0.61	0.031	1.395	597	97	105	646	15	18	642	19	23	619.570	17.029	67.120	108
SP-1_42	-4.384	8985	31	2.8	270.27	43.13	9.45	2.3	0.065	3.90	0.532	3.877	0.966	3.5	0.107	2.2	0.63	0.033	2.629	712	172	177	653	27	29	678	35	37	661.034	34.106	76.980	92
SP-1_28	0.068	65095	198	1.0	7800.61	24.28	9.41	1.2	0.061	1.87	0.162	2.394	0.905	1.5	0.107	1.2	0.81	0.032	1.619	611	86	96	655	15	18	653	14	19	634.454	20.203	69.399	107
SP-1_67	-0.166	58087	193	2.5	2510.87	31.54	9.27	1.1	0.062	1.72	0.408	1.501	0.930	1.5	0.108	1.0	0.65	0.033	1.228	657	74	83	661	12	16	666	15	20	648.193	15.669	69.633	101
SP-1_50	-0.034	49574	157	0.3	2239.32	32.86	9.22	1.4	0.062	2.44	0.063	13.283	0.933	2.0	0.109	1.3	0.67	0.030	4.661	649	115	122	669	17	20	666	19	23	589.001	54.343	82.468	103
SP-1_80	0.044	46767	157	0.8	3739.07	24.08	9.25	1.7	0.061	2.54	0.159	6.226	0.911	2.3	0.110	1.7	0.75	0.036	3.129	617	104	110	671	22	24	659	24	28	705.702	43.082	85.001	109
SP-1_87	0.251	81865	267	1.6	1910.56	43.62	9.10	1.1	0.063	1.84	0.301	3.551	0.951	1.5	0.110	1.2	0.78	0.034	1.756	696	81	91	673	15	18	677	15	20	677.070	23.362	74.634	97
SP-1_20	0.341	99201	273	0.1	163713.08	27.06	9.05	1.1	0.063	1.87	0.023	7.284	0.966	1.5	0.111	1.1	0.71	0.029	7.275	683	80	89	678	14	18	685	15	20	573.149	81.938	101.521	99
SP-1_60	1.252	32068	104	1.6	1694.52	25.82	8.95	1.1	0.062	2.11	0.257	1.755	0.950	1.9	0.111	1.3	0.67	0.033	1.714	629	96	105	681	16	20	675	19	23	648.878	21.892	71.385	108
SP-1_53	0.725	36640	113	1.2	1192.55	32.54	8.98	1.5	0.064	2.88	0.190	2.836	0.982	2.1	0.112	1.6	0.75	0.030	2.712	677	124	130	684	21	23	691	21	25	589.870	31.560	69.519	101
SP-1_52	0.358	44951	136	2.2	1292.49	36.29	8.87	1.3	0.064	2.44	0.400	3.257	1.001	1.8	0.114	1.3	0.71	0.033	1.435	710	111	119	693	17	20	706	20	25	661.929	18.689	71.740	98
SP-1_116	1.367	40411	133	0.9	770.69	34.50	8.78	1.2	0.064	1.60	0.172	11.472	1.003	1.5	0.115	1.2	0.79	0.032	2.191	705	72	82	699	16	19	704	15	20	627.622	27.068	71.089	99
SP-1_107	1.024	43471	151	1.2	976.20	35.48	8.64	1.5	0.063	2.30	0.252	5.344	1.004	2.2	0.117	1.5	0.66	0.039	2.983	663	96	103	713	20	23	702	22	26	768.550	44.922	91.842	108
SP-1_91	0.068	34280	98	1.3	857.87	40.12	7.57	0.9	0.067	2.27	0.224	3.332	1.218	2.1	0.132	0.9	0.43	0.037	1.670	790	90	97	802	14	19	812	26	31	731.413	24.006	80.176	101

SP-1_74	1.380	95555	245	1.1	1937.27	48.44	7.52	1.3	0.066	1.71	0.217	3.101	1.213	1.5	0.133	1.4	0.91	0.042	1.478	789	71	80	804	21	24	809	15	20	832.348	24.074	89.923	102
SP-1_96	1.222	68746	190	1.0	1837.40	35.85	7.18	1.3	0.067	1.78	0.161	2.265	1.292	1.7	0.140	1.2	0.72	0.039	3.000	811	73	82	846	19	23	840	19	24	777.220	45.819	93.289	104
SP-1_97	1.835	10454	13	0.7	207.03	46.02	3.57	4.0	0.108	2.97	0.129	4.574	4.275	4.2	0.293	2.7	0.64	0.093	5.113	1720	109	114	1650	81	85	1698	73	77	1830.572	192.482	277.799	96
SP-1_106	0.980	48975	51	0.9	1018.48	31.77	2.82	1.3	0.137	1.55	0.151	2.616	6.614	1.4	0.353	1.3	0.93	0.101	2.208	2169	54	63	1948	44	52	2057	26	36	1936.876	81.437	212.502	90
SP-1_6	0.126	139378	100	0.7	-2780.72	-45.26	2.77	2.1	0.136	3.29	0.124	5.294	6.769	2.3	0.365	2.2	0.96	0.107	1.956	2136	114	118	2003	76	81	2075	42	49	2049.495	76.832	222.696	94
SP-1_41	0.020	68166	65	1.1	1875.28	41.11	2.72	1.4	0.140	2.03	0.195	2.182	7.115	1.6	0.366	1.4	0.84	0.111	1.825	2200	70	77	2010	48	56	2126	27	35	2132.961	73.772	227.431	91
SP-1_93	0.309	148711	144	2.3	2737.92	58.67	2.69	1.1	0.129	1.24	0.289	2.275	6.709	1.1	0.372	1.1	0.96	0.082	1.752	2084	43	53	2037	37	47	2073	19	31	1583.858	53.532	171.212	98
SP-1_24	0.021	163949	137	0.5	31793.25	25.03	2.67	1.1	0.134	1.58	0.078	2.825	6.979	1.2	0.376	1.1	0.88	0.105	1.896	2140	56	65	2057	38	48	2110	21	31	2024.520	73.017	217.492	96
SP-1_51	0.050	55143	47	0.3	1442.43	39.93	2.54	1.3	0.141	1.56	0.088	8.689	7.739	1.5	0.395	1.3	0.87	0.117	2.850	2222	55	64	2143	46	55	2196	27	37	2233.541	119.968	254.094	96
SP-1_59	0.308	200307	147	0.4	3395.29	44.49	2.07	1.0	0.189	1.42	0.063	2.042	12.634	1.1	0.485	1.0	0.89	0.135	2.037	2720	47	56	2548	41	54	2650	21	33	2561.092	97.798	273.507	94
SP-1_15	0.190	102417	53	2.2	-6187.70	-26.78	1.93	1.4	0.191	1.90	0.335	2.177	13.798	1.5	0.523	1.4	0.93	0.140	1.710	2735	62	69	2707	61	72	2737	26	36	2650.746	85.042	277.882	99
SP-2_120	0.614	41042	178	0.7	1799.01	24.88	10.57	0.7	0.060	1.42	0.112	2.739	0.781	1.5	0.094	0.8	0.52	0.030	2.188	575	64	76	582	9	13	585	13	18	596.581	25.735	67.660	101
SP-2_5	2.350	15463	62	3.7	133.33	70.27	10.45	1.8	0.063	3.22	0.556	1.963	0.838	2.8	0.097	1.8	0.66	0.024	3.945	641	151	157	597	21	23	620	28	31	479.991	37.519	62.994	93
SP-2_103	2.634	11734	46	2.5	75.26	81.45	10.05	1.2	0.063	3.16	0.424	2.745	0.871	3.2	0.099	1.1	0.34	0.033	2.195	655	135	141	609	13	16	630	30	33	651.175	28.123	73.735	93
SP-2_19	0.555	68374	255	0.2	333.70	101.42	10.06	0.7	0.062	1.49	0.024	4.247	0.854	1.3	0.100	0.7	0.59	0.025	4.218	658	69	81	612	9	13	626	12	18	501.691	41.872	67.407	93
SP-2_94	-1.483	14917	60	1.5	-48.75	-132.72	10.02	1.4	0.063	2.51	0.473	41.040	0.875	2.3	0.100	1.5	0.65	0.034	2.484	666	109	116	612	17	20	635	22	26	666.661	32.558	76.951	92
SP-2_16	0.091	58730	230	1.9	742.50	44.53	10.01	0.8	0.063	1.36	0.312	2.515	0.869	1.3	0.100	0.9	0.69	0.027	2.001	681	58	70	613	10	14	634	12	18	539.769	21.351	60.657	90
SP-2_69	0.372	45466	187	1.1	1106.45	34.90	10.07	1.2	0.062	1.78	0.173	4.823	0.854	1.6	0.100	1.3	0.83	0.029	3.761	680	72	81	615	15	18	625	15	19	576.548	42.780	74.127	90
SP-2_2	0.154	86727	337	0.1	958.94	61.06	9.96	0.9	0.060	1.34	0.016	8.474	0.844	1.0	0.101	0.9	0.86	0.029	4.166	603	58	70	618	10	14	621	9	16	577.599	47.391	76.870	102
SP-2_32	0.199	48254	184	1.7	408.93	71.03	9.96	0.9	0.062	1.82	0.281	2.600	0.863	1.8	0.101	0.9	0.52	0.028	1.513	632	75	83	619	11	15	630	16	20	560.415	16.723	61.135	98
SP-2_37	1.805	14696	56	2.8	145.24	67.42	9.96	1.6	0.061	2.30	0.417	2.573	0.859	2.0	0.101	1.5	0.72	0.026	2.969	601	103	110	620	17	20	627	19	23	512.548	30.093	61.736	103
SP-2_109	0.493	100138	403	0.3	1988.84	38.22	9.91	0.7	0.062	1.29	0.055	3.167	0.868	1.3	0.101	0.7	0.56	0.033	1.922	662	55	67	620	9	13	633	12	18	657.977	24.882	73.212	94
SP-2_57	2.666	26235	111	1.5	683.32	49.85	10.00	2.2	0.061	3.52	0.175	8.113	0.870	3.6	0.101	2.4	0.67	0.020	9.192	635	171	177	622	29	30	632	33	36	393.778	71.702	82.852	98
SP-2_9	4.666	12955	49	2.0	-41.45	-109.45	9.89	1.5	0.063	2.87	0.334	2.511	0.880	2.6	0.102	1.4	0.56	0.029	2.193	649	131	138	623	17	20	637	24	27	570.145	24.658	64.716	96
SP-2_65	0.124	83261	332	0.9	1372.11	42.25	9.85	0.8	0.060	1.31	0.164	3.641	0.851	1.1	0.101	0.7	0.67	0.032	1.594	617	54	65	625	10	14	624	10	16	635.166	19.944	69.534	101
SP-2_71	0.154	139151	551	0.1	3974.16	29.71	9.85	0.9	0.060	1.19	0.013	3.843	0.848	1.2	0.102	0.9	0.72	0.032	3.804	596	52	66	625	11	15	622	12	17	640.031	47.994	82.524	105
SP-2_74	-0.151	37065	147	1.4	162.86	129.34	9.84	1.0	0.060	1.85	0.276	11.505	0.838	1.6	0.102	1.0	0.60	0.032	1.890	572	79	88	626	11	15	616	15	19	628.045	23.365	69.809	109
SP-2_24	0.329	58965	221	1.5	870.07	41.71	9.83	0.9	0.062	1.09	0.239	1.956	0.882	1.2	0.102	0.9	0.73	0.027	1.612	670	49	64	626	10	14	641	11	17	543.703	17.295	59.665	94
SP-2_70	0.310	66020	259	0.4	1124.03	42.20	9.81	1.0	0.061	1.58	0.061	2.490	0.852	1.4	0.103	1.0	0.75	0.032	2.301	608	67	77	629	12	16	625	13	18	628.130	28.462	71.702	95
SP-2_86	0.657	32973	130	0.9	209.05	94.16	9.79	1.1	0.063	1.39	0.156	3.328	0.887	1.5	0.103	1.1	0.73	0.033	1.784	680	59	71	630	13	16	643	14	19	663.778	23.292	73.290	93
SP-2_62	1.000	65664	279	1.2	4.23	12288.48	9.78	1.4	0.061	2.80	0.227	2.453	0.864	2.6	0.103	1.3	0.50	0.033	2.689	626	125	131	630	16	19	631	25	28	651.920	34.535	76.569	101
SP-2_10	0.587	43378	160	1.6	601.90	44.12	9.74	0.7	0.062	1.29	0.263	2.810	0.881	1.3	0.103	0.6	0.49	0.029	1.635	648	56	69	630	8	13	641	13	18	586.932	18.931	64.451	97
SP-2_54	0.003	73528	259	0.5	1587.33	61.00	9.78	1.6	0.062	2.33	0.073	5.344	0.872	1.8	0.103	1.6	0.89	0.027	6.046	639	103	110	631	19	22	641	14	17	543.464	65.011	86.608	99
SP-2_66	-0.389	18527	72	0.7	68.57	166.71	9.77	1.0	0.062	2.32	0.124	2.938	0.889	2.5	0.103	1.0	0.42	0.033	2.672	643	99	106	631	12	16	642	23	27	647.280	34.031	75.828	98
SP-2_79	0.334	41031	164	2.0	172.32	129.22	9.75	1.0	0.061	1.89	0.339	2.211	0.884	1.9	0.103	1.0	0.50	0.033	1.529	659	82	91	632	12	15	641	18	22	649.680	19.546	70.740	96
SP-2_47	1.107	10690	39	2.5	218.40	41.55	9.79	1.5	0.063	3.99	0.438	2.864	0.889	3.6	0.103	1.4	0.41	0.031	2.240	641	177	181	632	17	20	647	39	42	622.856	27.457	70.772	99
SP-2_68	0.018	8741	34	2.6	121.93	54.73	9.82	1.6	0.062	3.54	0.424	2.238	0.868	3.3	0.103	1.6	0.48	0.031	2.242	604	160	165	633	19	21	628	31	33	611.768	27.056	69.686	105
SP-2_22	-1.325	9213	33	1.8	1.60	2992.23	9.73	1.4	0.062	3.57	0.300	3.464	0.883	3.2	0.104	1.4	0.43	0.029	2.773	591	161	166	636	17	20	636	29	32	586.511	32.011	69.269	108
SP-2_52	0.930	39802	150	2.2	1066.45	31.89	9.66	1.0	0.064	1.64	0.346	2.324	0.915	1.5	0.104	0.9	0.63	0.029	2.769	704	67	77	637	11	15	658	14	19	571.209	31.334	67.855	90
SP-2_26	0.492	54348	200	1.1	637.59	50.82	9.64	0.8	0.060	1.39	0.185	1.952	0.873	1.3	0.104	0.9	0.63	0.029	1.507	611	65	78	638	10	15	639	14	20	583.361	17.324	63.555	104
SP-2_48	0.238	101521	426	1.8	3114.53	49.40	9.61	1.0	0.060	1.65	0.290	3.417	0.875	2.0	0.104	0.9	0.48	0.028	2.125	596	73	83	639	12	15	637	19	23	561.068	23.540	63.441	107
SP-2_30	-0.479	23623	92	0.5	422.33	53.39	9.63	1.4	0.062	2.91	0.091	5.904	0.913	3.6	0.104	1.4	0.39	0.030	4.117	665	141	148	639	17	20	655	34	36	600.505	48.697	79.577	96
SP-2_51	-0.104	35252	143	1.1	162.86	175.04	9.61	1.1	0.061	2.39	0.195	2.582	0.885	2.4	0.104	1.1	0.48	0.030	2.121	618	102	109	640	14	17	642	23	26	602.227	25.134	67.891	104
SP-2_106	-1.210	8631	34	1.8	99.56	62.48	9.64	1.9	0.062	3.33	0.300	4.673	0.895	3.1	0.105	1.7	0.54	0.033	2.814	630	137	142	640	21	23	643	29	32	647.469	35.894	76.779	102
SP-2_61	-0.042	90294	348	0.2	1045.31	64.75	9.58	0.7	0.060	1.35	0.046	5.364	0.873	1.3	0.105	0.7	0.57	0.033	2.206	597	59	71	641	9	13	636	12	18	650.457	28.226	73.711	107

SP-2_82	-1.035	18140	70	1.4	-35.80	-273.97	9.53	1.2	0.063	2.73	0.248	2.249	0.884	2.9	0.105	1.3	0.44	0.035	2.264	628	122	128	644	16	19	648	22	24	689.746	30.668	78.344	102
SP-2_40	0.481	59454	222	3.3	1040.43	41.29	9.54	0.8	0.061	1.55	0.555	1.356	0.885	1.6	0.105	0.8	0.48	0.030	0.947	614	67	78	644	9	14	642	15	20	603.265	11.261	64.305	105
SP-2_73	0.561	70966	301	2.6	1683.35	48.52	9.58	2.0	0.064	2.55	0.516	3.808	0.925	2.8	0.105	2.0	0.71	0.037	2.422	718	110	116	644	24	26	663	27	30	735.716	35.065	84.650	90
SP-2_96	0.325	46648	173	1.9	391.10	68.91	9.35	0.7	0.062	1.65	0.304	2.053	0.922	1.5	0.107	0.7	0.48	0.033	1.239	658	71	81	656	9	14	662	15	20	664.433	16.206	71.446	100
SP-2_93	0.485	60880	207	1.8	1205.17	41.57	9.37	1.8	0.061	2.03	0.290	2.386	0.904	2.4	0.108	1.9	0.78	0.035	2.751	622	85	94	658	23	26	652	23	26	691.577	37.379	81.408	106
SP-2_108	0.506	86033	307	1.8	1633.92	40.05	9.29	0.9	0.063	2.21	0.300	2.155	0.930	2.0	0.108	0.9	0.44	0.034	1.440	655	96	104	660	11	15	665	19	23	681.249	19.293	73.879	101
SP-2_25	0.578	44063	149	1.4	372.75	70.03	9.21	1.0	0.063	1.59	0.221	2.199	0.964	1.6	0.109	1.1	0.67	0.029	1.620	701	68	78	668	13	17	683	16	21	569.062	18.180	62.427	95
SP-2_75	0.151	35147	133	0.8	574.83	48.61	9.22	1.3	0.062	1.71	0.144	2.329	0.944	2.1	0.109	1.3	0.64	0.034	2.168	678	80	91	669	17	20	676	22	26	678.660	28.910	76.643	99
SP-2_97	0.758	43587	166	1.0	325.83	85.36	9.12	1.3	0.061	2.24	0.173	2.197	0.922	1.6	0.110	1.3	0.79	0.035	1.971	611	93	100	673	16	19	662	15	20	688.005	26.664	76.783	110
SP-2_115	0.126	63280	248	2.6	1209.43	54.15	8.98	0.9	0.064	2.17	0.430	4.054	0.990	2.2	0.111	0.9	0.41	0.034	1.664	729	91	98	681	11	16	697	22	26	684.657	22.423	75.180	93
SP-2_85	1.614	32215	120	2.1	90.02	179.51	8.89	1.7	0.064	2.45	0.358	3.360	0.993	2.4	0.112	1.7	0.72	0.034	2.176	735	103	110	682	22	25	702	22	25	679.610	29.068	76.822	93
SP-2_42	0.433	58341	201	2.5	1307.13	33.32	8.95	1.1	0.065	2.20	0.438	2.384	0.994	1.8	0.112	1.1	0.57	0.033	1.418	725	88	95	686	14	18	699	18	22	648.355	18.102	70.378	95
SP-2_98	0.689	55123	195	1.3	232.23	117.43	8.80	1.0	0.063	1.34	0.182	2.249	0.989	1.3	0.114	1.0	0.75	0.030	3.003	678	58	70	696	13	17	697	13	19	588.995	34.823	70.874	103
SP-2_49	-0.690	17733	48	1.6	345.36	55.09	7.77	1.3	0.067	3.30	0.242	3.411	1.181	2.9	0.129	1.3	0.44	0.036	3.429	819	163	170	784	19	23	788	32	36	705.017	47.574	87.825	96
SP-2_91	0.932	82627	268	0.4	1319.76	42.01	7.73	1.0	0.066	1.28	0.078	6.519	1.184	1.4	0.130	1.1	0.76	0.036	3.434	801	52	64	787	16	20	792	15	22	716.658	48.441	89.340	98
SP-2_33	1.671	25696	73	1.3	466.11	42.26	7.31	1.3	0.070	2.60	0.228	3.634	1.369	2.8	0.138	1.3	0.45	0.037	2.553	926	119	126	830	20	24	870	33	37	737.174	37.051	85.633	90
SP-2_72	0.030	52525	152	1.7	682.64	51.93	7.26	0.9	0.067	1.65	0.286	1.303	1.279	1.5	0.138	0.9	0.60	0.044	1.334	816	70	80	835	15	20	834	18	23	873.579	22.793	93.735	102
SP-2_7	3.837	14183	36	1.0	7.96	820.32	6.86	1.0	0.070	2.46	0.162	2.802	1.403	2.3	0.146	1.0	0.44	0.039	2.798	893	97	104	877	17	22	890	26	30	781.204	42.894	92.167	98
SP-2_114	0.063	35661	101	0.9	475.13	64.21	6.71	2.0	0.070	2.05	0.126	4.151	1.446	2.1	0.151	1.8	0.87	0.037	7.258	914	88	97	907	31	34	905	26	31	733.050	105.138	130.359	99
SP-2_83	0.020	127326	130	0.7	3353.73	37.51	2.65	1.1	0.129	1.17	0.109	2.691	6.810	1.4	0.378	1.1	0.83	0.111	2.443	2074	42	53	2066	39	49	2085	24	34	2133.081	98.454	236.003	100
SP-2_36	2.124	39311	40	1.5	240.34	89.15	2.57	1.1	0.143	1.66	0.266	2.863	7.682	1.6	0.388	1.3	0.78	0.113	2.428	2260	61	69	2110	46	55	2188	29	38	2169.244	99.572	239.946	93
SP-2_78	0.013	136221	142	1.6	1889.96	46.84	2.57	0.8	0.129	1.16	0.252	1.286	6.946	1.1	0.390	0.8	0.75	0.115	1.218	2070	40	51	2122	29	42	2102	19	31	2191.684	50.586	226.666	103
SP-2_21	0.219	100537	98	0.9	955.91	66.54	2.56	0.8	0.133	1.04	0.133	2.692	7.207	1.2	0.392	0.8	0.69	0.100	1.786	2128	37	49	2130	30	43	2141	19	28	1929.649	65.718	206.530	100
SP-2_31	-0.149	115188	109	0.7	184.70	352.81	2.56	1.0	0.133	1.09	0.112	1.791	7.251	1.3	0.392	1.0	0.75	0.108	1.617	2127	38	49	2132	35	46	2139	24	34	2066.083	63.376	217.918	100
SP-2_110	2.654	32600	33	1.0	550.00	45.43	2.43	1.1	0.146	2.36	0.205	4.825	8.173	2.1	0.410	1.3	0.60	0.144	2.503	2271	81	87	2210	48	57	2248	41	49	2712.046	125.724	295.363	97
SP-2_99	1.368	27539	21	2.4	336.79	43.88	1.92	1.1	0.191	1.59	0.389	2.202	13.793	1.6	0.523	1.2	0.77	0.158	1.787	2741	51	59	2709	54	65	2729	30	40	2961.895	97.854	307.438	99
SP4-79	-0.013	22593	114	1.4	251.44	49.12	10.80	1.4	0.060	2.61	0.314	18.483	0.768	2.4	0.093	1.3	0.53	0.030	2.089	532	112	112	573	14	15	575	21	21	602.324	24.781	115.903	108
SP4-62	0.023	50762	244	0.8	436.76	62.49	10.65	1.3	0.061	1.77	0.145	4.533	0.779	2.0	0.092	1.6	0.79	0.030	2.593	597	77	77	574	16	17	583	18	18	598.695	30.521	116.462	96
SP4-79	-0.013	22593	114	1.4	251.44	49.12	10.80	1.4	0.060	2.61	0.314	18.483	0.768	2.4	0.093	1.3	0.53	0.030	2.089	532	112	112	573	14	15	575	21	21	602.324	24.781	115.903	108
SP4-62	0.023	50762	244	0.8	436.76	62.49	10.65	1.3	0.061	1.77	0.145	4.533	0.779	2.0	0.092	1.6	0.79	0.030	2.593	597	77	77	574	16	17	583	18	18	598.695	30.521	116.462	96
SP4-61	-0.552	16704	77	2.3	31.78	252.61	10.16	1.1	0.062	2.71	0.402	2.819	0.849	2.8	0.098	1.1	0.39	0.029	1.601	645	116	116	600	13	14	619	26	26	584.137	18.435	111.423	93
SP4-44	0.629	52368	259	0.6	-146.31	-194.81	10.15	1.2	0.062	1.78	0.115	6.504	0.842	1.8	0.098	1.2	0.65	0.029	3.972	650	76	76	605	14	15	619	17	17	568.612	44.637	116.177	93
SP4-81	1.020	31131	152	1.3	183.58	79.64	10.10	1.7	0.062	1.97	0.170	4.758	0.840	2.3	0.100	1.4	0.59	0.020	4.413	641	88	88	612	16	17	616	22	22	404.158	35.397	84.334	96
SP4-58	-0.863	5532	24	1.9	-10.05	-241.58	10.13	2.1	0.064	4.66	0.399	8.374	0.876	4.7	0.100	1.9	0.41	0.033	3.704	602	235	235	616	23	24	624	47	47	651.941	47.404	131.022	102
SP4-13	0.004	97291	427	0.3	409.38	125.31	9.85	0.9	0.060	1.51	0.087	8.716	0.841	1.2	0.102	0.9	0.70	0.032	2.336	575	66	66	623	10	12	619	12	12	633.093	29.105	122.365	108
SP4-63	-0.246	76857	360	2.0	-353.50	-124.07	9.72	1.6	0.063	2.06	0.334	2.524	0.904	1.9	0.103	1.6	0.87	0.028	1.918	700	89	89	632	20	21	652	18	18	549.731	20.765	105.384	90
SP4-60	0.584	18652	85	2.5	57.59	195.07	9.67	1.3	0.062	3.45	0.435	2.136	0.882	3.0	0.104	1.3	0.43	0.030	1.810	590	157	157	635	15	17	638	28	28	602.118	21.473	115.276	108
SP4-97	0.911	48746	228	1.8	496.82	57.26	9.58	1.4	0.063	2.02	0.343	4.306	0.913	2.0	0.104	1.2	0.60	0.033	2.675	669	87	87	635	15	16	656	19	19	658.075	34.504	127.895	95
SP4-15	0.156	49944	209	1.1	767.35	44.14	9.61	1.4	0.063	1.85	0.196	2.300	0.904	1.9	0.104	1.3	0.70	0.028	2.479	679	80	80	637	16	17	652	18	18	555.573	27.110	107.840	94
SP4-115	1.203	28121	133	0.9	489.44	40.78	9.54	1.0	0.061	1.95	0.160	2.176	0.895	2.0	0.105	1.1	0.53	0.032	1.968	614	96	96	644	13	15	646	19	19	633.803	24.542	121.472	105
SP4-104	0.628	47686	195	2.5	129.73	291.35	9.49	1.2	0.060	2.84	1.031	58.423	0.881	2.8	0.105	1.1	0.40	0.036	6.406	585	125	125	645	14	15	639	27	27	711.203	87.862	157.658	110
SP4-27	1.058	53231	210	1.2	734.96	41.40	9.44	1.2	0.062	1.94	0.161	3.082	0.923	1.8	0.106	1.3	0.71	0.024	2.883	663	91	91	651	16	17	662	17	17	475.603	27.115	93.824	98
SP4-50	-0.872	29773	128	1.7	40.64	367.30	9.25	1.0	0.064	2.08	0.294	9.334	0.951	1.8	0.108	1.0	0.59	0.029	2.120	693	89	89	662	13	15	676	17	17	569.972	23.821	109.910	96
SP4-65	-0.501	19074	81	1.0	-106.55	-80.67	9.03	1.6	0.066	2.80	0.202	3.193	1.023	2.2	0.111	1.7	0.76	0.037	2.820	752	124	124	678	22	23	712	23	23	739.570	40.951	144.560	90
SP4-76	1.617	24384	99	1.1	127.66	96.01	8.82	1.6	0.062	2.75	0.209	8.971	1.010	2.5	0.114	1.7	0.67	0.034	3.437	683	114	114	698	22	24	704	25	25	675.424	45.538	134.449	102
SP4-48	-0.811	21314	73	1.2	-155.62	-64.79	8.25	2.0	0.063	3.44	0.118	4.054	1.054	2.9	0.121	1.8	0.61	0.022	8.644	709	151	151	733	25	26	736	36	36	441.490	75.560	112.558	103
SP4-64	0.656	63187	216	2.7	652.81	55.53	7.83	1.4	0.068	1.91	0.383	2.061	1.199	1.6	0.128	1.3	0.83	0.033	2.006	834	81	81	776	19	21	798	18	18	660.146	26.048	126.617	93

SP4-2	0.908	79430	262	1.3	-331.44	-109.67	7.64	1.3	0.066	1.69	0.211	3.984	1.203	1.6	0.131	1.3	0.82	0.033	2.969	794	78	78	792	19	21	800	17	17	661.309	38.479	129.420	100
SP4-3	0.797	70938	237	0.3	271.48	120.93	7.63	1.1	0.066	1.57	0.063	3.732	1.205	1.5	0.131	1.1	0.75	0.037	2.737	796	68	68	793	17	19	801	17	17	728.716	39.155	141.953	100
SP4-103	0.034	24326	92	1.4	168.66	89.15	7.62	1.1	0.065	2.11	0.248	3.138	1.181	2.0	0.131	1.1	0.54	0.042	2.046	731	92	92	795	16	18	788	22	22	831.429	33.321	158.878	109
SP4-66	-0.146	54633	182	0.3	654.28	49.00	7.52	1.0	0.066	1.57	0.049	4.166	1.214	1.4	0.133	0.9	0.69	0.039	3.826	786	66	66	803	14	16	809	17	17	777.492	58.157	156.329	102
SP4-17	0.335	69418	210	0.7	395.32	105.18	7.31	1.1	0.069	2.03	0.088	6.775	1.304	1.8	0.137	1.1	0.60	0.021	8.811	885	92	92	828	17	19	851	23	23	419.782	73.016	107.640	93
SP4-1	3.133	25402	62	2.8	348.94	47.39	5.63	3.7	0.077	2.26	0.307	3.652	1.957	2.8	0.182	2.2	0.78	0.036	5.951	1096	87	87	1091	50	52	1100	42	42	705.405	82.114	155.114	99
SP4-116	0.042	158318	243	1.1	1349.66	78.65	3.06	2.3	0.125	1.36	0.154	6.296	5.801	2.0	0.334	2.0	0.97	0.067	5.939	2020	47	47	1854	65	67	1937	38	38	1308.850	151.657	287.125	92
SP4-71	0.288	106070	146	0.7	-167.30	-291.82	2.89	1.2	0.127	1.19	0.117	2.210	6.098	1.2	0.346	1.1	0.94	0.096	2.142	2045	43	43	1915	37	41	1987	21	21	1858.332	75.677	345.504	94
SP4-12	0.307	114424	159	0.8	-276.62	-182.42	2.85	1.8	0.132	1.47	0.121	4.094	6.485	2.0	0.354	1.8	0.90	0.082	2.519	2115	51	51	1951	59	62	2038	36	36	1593.945	77.177	302.290	92
SP4-106	0.209	92110	129	1.2	1430.12	45.68	2.80	1.2	0.124	1.36	0.199	5.366	6.167	1.3	0.358	1.2	0.93	0.109	1.903	2008	47	47	1971	41	45	2006	22	22	2080.824	75.093	383.646	98
SP4-21	0.647	95244	125	0.8	86.76	562.74	2.81	2.1	0.130	1.69	0.140	3.127	6.563	2.4	0.363	2.2	0.92	0.098	4.145	2087	58	58	1993	75	77	2043	42	42	1878.773	147.819	371.220	96
SP4-35	0.237	65227	81	0.9	-62.54	-451.06	2.76	1.1	0.129	1.28	0.145	2.455	6.531	1.4	0.363	1.1	0.77	0.098	2.270	2075	45	45	1994	37	41	2047	24	24	1896.551	82.464	356.431	96
SP4-30	0.097	124063	151	0.9	-287.07	-203.81	2.75	0.9	0.124	1.20	0.157	4.056	6.274	1.0	0.364	0.9	0.86	0.096	1.678	2007	43	43	2001	31	36	2012	18	18	1856.513	59.330	342.917	100
SP4-40	0.249	91459	108	1.7	-232.23	-167.46	2.73	1.0	0.128	1.15	0.362	23.461	6.516	1.2	0.365	0.9	0.72	0.102	1.842	2058	41	41	2003	31	36	2045	22	22	1961.472	67.935	358.531	97
SP4-86	0.320	122745	150	1.5	-686.34	-78.44	2.71	1.7	0.130	1.51	0.222	3.129	6.703	1.8	0.367	1.6	0.89	0.107	2.950	2086	54	54	2014	56	59	2068	32	32	2048.868	114.354	387.353	97
SP4-119	-0.405	48524	62	1.3	316.32	100.16	2.74	1.4	0.132	1.46	0.167	3.824	6.706	1.5	0.368	1.4	0.88	0.086	4.365	2106	52	52	2016	47	51	2068	28	28	1655.178	139.188	334.528	96
SP4-94	0.108	79308	93	0.6	179.75	272.15	2.71	1.6	0.137	2.03	0.101	3.677	7.031	2.0	0.369	1.5	0.74	0.115	3.412	2175	71	71	2025	52	56	2110	36	36	2200.571	141.945	421.640	93
SP4-59	0.087	116414	151	1.2	-281.79	-204.74	2.72	1.5	0.128	1.24	0.230	4.968	6.595	1.5	0.367	1.3	0.90	0.100	1.737	2067	43	43	2026	52	56	2055	26	26	1925.567	63.497	354.569	98
SP4-73	0.501	77333	98	1.4	55.21	692.50	2.70	1.1	0.127	1.43	0.230	3.619	6.565	1.3	0.371	1.1	0.85	0.103	1.652	2047	51	51	2031	37	42	2051	22	22	1974.338	62.010	363.748	99
SP4-51	0.011	79736	87	0.9	-862.99	-39.48	2.70	1.5	0.130	2.13	0.143	2.217	6.649	1.6	0.371	1.5	0.98	0.107	1.824	2077	75	75	2031	53	57	2063	28	28	2049.323	70.948	377.971	98
SP4-55	-0.132	63637	82	1.4	-165.36	-220.60	2.69	1.1	0.131	2.05	0.250	6.165	6.745	1.6	0.371	1.1	0.67	0.100	2.100	2096	70	70	2034	38	42	2075	29	29	1924.566	76.850	357.719	97
SP4-83	0.971	35211	42	1.1	217.12	80.05	2.70	1.3	0.128	1.58	0.179	3.284	6.586	1.4	0.370	1.2	0.86	0.108	1.911	2049	56	56	2036	46	50	2053	25	25	2067.851	75.066	382.377	99
SP4-102	0.014	94129	125	0.9	2049.26	34.28	2.64	0.9	0.130	1.40	0.150	1.971	6.789	1.2	0.376	1.1	0.92	0.112	1.613	2089	49	49	2056	40	44	2085	20	20	2144.253	65.466	392.677	98
SP4-84	-0.136	31807	43	0.8	-133.62	-152.49	2.66	2.3	0.133	3.10	0.143	3.763	6.922	2.8	0.378	2.3	0.85	0.114	4.391	2120	103	103	2064	82	85	2095	51	51	2180.502	180.990	433.078	97
SP4-4	0.294	37162	37	0.8	-229.24	-79.80	2.57	1.6	0.139	2.44	0.144	5.935	7.568	2.9	0.387	1.8	0.62	0.106	5.611	2213	93	93	2107	65	68	2171	52	52	2028.635	217.292	428.656	95
SP4-52	2.884	26472	32	1.5	98.54	104.37	2.57	1.2	0.129	1.50	0.243	1.827	6.938	1.9	0.389	1.2	0.63	0.110	1.815	2065	52	52	2116	44	48	2094	35	35	2103.296	72.341	387.228	102
SP4-87	0.115	107956	132	1.4	665.05	76.90	2.56	1.0	0.131	1.26	0.218	2.081	7.089	1.2	0.389	1.0	0.88	0.112	1.512	2112	42	42	2118	38	42	2119	21	21	2144.563	61.483	393.168	100
SP4-10	0.759	47017	54	1.5	-74.37	-270.78	2.57	1.1	0.133	1.78	0.248	2.012	7.163	1.5	0.389	1.1	0.73	0.101	1.399	2117	61	61	2119	40	44	2127	27	27	1951.601	52.099	359.350	100
SP4-7	0.250	59379	67	1.4	30.13	858.81	2.56	1.0	0.134	1.48	0.220	1.961	7.259	1.4	0.391	1.1	0.76	0.103	1.662	2150	48	48	2123	38	43	2145	23	23	1978.998	62.497	364.104	99
SP4-100	-0.322	46255	52	1.0	590.06	65.90	2.55	1.5	0.135	2.32	0.149	2.692	7.340	1.6	0.393	1.5	0.90	0.124	2.738	2146	76	76	2135	53	56	2151	28	28	2356.555	121.697	441.428	99
SP4-88	0.276	57004	70	1.7	86.91	335.93	2.54	1.0	0.135	1.51	0.264	1.433	7.365	1.4	0.393	1.0	0.73	0.115	1.743	2156	51	51	2136	37	42	2152	25	25	2193.075	72.440	403.220	99
SP4-117	-0.129	90856	112	1.0	1291.49	51.32	2.49	0.9	0.137	1.39	0.154	2.025	7.634	1.1	0.401	0.8	0.77	0.110	1.441	2179	49	49	2171	30	36	2190	18	18	2103.682	57.706	386.126	100
SP4-9	0.792	33974	38	1.0	39.60	408.50	2.50	1.4	0.137	1.83	0.177	4.996	7.623	1.6	0.402	1.3	0.82	0.103	2.190	2173	65	65	2174	48	52	2183	28	28	1986.680	82.709	369.749	100
SP4-36	0.325	49587	55	1.3	4.96	4892.06	2.46	1.4	0.138	1.69	0.201	1.848	7.779	1.6	0.407	1.5	0.93	0.112	1.809	2183	59	59	2208	50	54	2200	28	28	2144.034	73.543	395.173	101
SP4-47	0.511	75567	88	0.7	-42.48	-868.22	2.43	1.3	0.138	1.44	0.115	3.503	7.836	1.3	0.411	1.3	0.96	0.108	2.359	2189	50	50	2219	48	52	2209	24	24	2071.757	92.548	385.638	101
SP4-114	0.353	47933	58	1.8	415.50	63.41	2.40	1.0	0.133	1.29	0.305	7.711	7.723	1.3	0.417	1.0	0.75	0.121	1.719	2130	46	46	2245	38	43	2195	24	24	2311.549	75.060	422.850	105
SP4-29	0.398	32938	33	2.6	327.55	65.63	2.12	2.1	0.178	2.07	0.476	2.787	11.645	2.4	0.476	2.0	0.85	0.131	2.275	2617	70	70	2506	84	87	2568	47	47	2488.342	106.118	457.759	96
SP4-109	-0.108	39051	42	2.2	-130.62	-145.67	2.04	1.1	0.187	1.93	0.381	3.781	12.569	1.9	0.488	1.3	0.66	0.140	2.649	2700	64	64	2561	54	59	2640	37	37	2649.693	130.417	487.445	95
SP4-19	0.229	112864	86	1.9	621.34	136.62	1.97	2.2	0.180	2.27	0.282	3.125	12.795	2.4	0.513	2.1	0.85	0.134	3.162	2644	77	77	2664	92	95	2658	46	46	2540.668	151.469	481.675	101
SP4-90	-0.120	84755	77	1.3	1149.08	44.77	1.89	1.1	0.189	1.43	0.255	7.759	13.847	1.1	0.528	1.1	0.93	0.136	1.964	2722	47	47	2733	48	53	2736	22	22	2574.355	94.761	470.606	100
SP4-24	0.454	154628	111	0.9	836.81	106.61	1.80	1.6	0.225	2.61	0.129	4.152	17.339	2.4	0.556	1.7	0.69	0.136	3.274	3000	85	85	2846	76	80	2948	47	47	2576.244	157.004	483.682	95
SP4-120	0.305	32919	30	0.6	277.50	72.47	1.77	1.7	0.207	1.68	0.109	3.288	16.347	1.7	0.573	1.7	0.97	0.168	3.169	2868	55	55	2915	78	82	2890	33	33	3127.846	184.057	584.055	102
SP4-75	2.269	138223	112	1.1	1530.54	37.95	1.72	1.3	0.225	1.50	0.235	4.910	18.345	1.8	0.583	1.3	0.74	0.218	6.706	3006	47	47	2957	62	67	3003	34	34	3936.605	477.790	830.982	98
SP4-67	-0.052	62678	50	0.5	167.92	200.40	1.70	1.2	0.232	1.72	0.081	6.610	18.876	1.4	0.585	1.1	0.81	0.155	2.779	3050	57	57	2968	53	59	3031	27	27	2908.950	150.291	537.705	97

SP4-32	-0.110	69985	51	0.3	434.53	88.86	1.72	1.5	0.231	1.49	0.082	8.356	18.757	1.4	0.588	1.4	0.99	0.163	3.226	3046	47	47	2975	67	72	3024	29	29	3073.465	193.223	603.659	98
SP4-101	-0.033	161235	127	1.1	2377.96	44.48	1.67	1.0	0.222	1.16	0.175	2.492	18.374	1.1	0.598	0.9	0.84	0.180	1.506	2984	37	37	3019	45	52	3006	22	22	3337.640	92.689	594.782	101
SP4-54	0.156	40077	31	1.2	-329.57	-43.73	1.67	1.7	0.240	1.64	0.191	3.130	20.035	1.5	0.603	1.4	0.98	0.158	2.127	3105	52	52	3037	71	76	3087	29	29	2955.455	116.092	533.769	98
SP4-57	0.629	47207	32	0.4	53.35	438.95	1.63	1.5	0.236	1.59	0.085	9.992	20.272	1.8	0.611	1.5	0.84	0.170	5.583	3086	50	50	3091	81	87	3099	34	34	3155.351	331.202	655.952	100

Instituto de Geociências, Universidade de Brasília							**Data for Tera-Wasserburg plot** [b]						**Data for Wetherill plot** [c]							**Dates** [c]											
Identifier	f206c	^{206}Pb	U (µg g^{-1}) [a]	Th/U	^{206}Pb/^{204}Pb	1*s* (%)	^{238}U/^{206}Pb	1s (%)	^{207}Pb/^{206}Pb	1s (%)	^{208}Pb/^{206}Pb	1s (%)	^{207}Pb/^{235}U	1s (%)	^{206}Pb/^{238}U	1s (%)	Rho	^{208}Pb/^{232}Th	1s (%)	^{207}Pb/^{206}Pb	2*s*	2s_{sys}	^{206}Pb/^{238}U	2*s*	2s_{sys}	^{207}Pb/^{235}U	2*s*	2s_{sys}	^{208}Pb/^{232}Th	2*s*	2s_{sys}	% conc [d]
SP7-31	-0.059	21022	97	1.2	73.102	168.025	12.34	1.5	0.058	2.81	0.249	6.366	0.664	2.6	0.081	1.4	0.53	0.027	2.856	491	142	142	502	13	14	514	21	21	530.11	29.88	104.20	102
SP7-41	0.779	15819	76	1.2	8.727	844.993	12.26	1.4	0.059	3.29	0.242	3.953	0.657	3.0	0.082	1.5	0.49	0.028	2.822	463	136	136	506	14	15	508	24	24	550.29	30.61	107.96	109
SP7-43	0.280	53228	214	0.9	83.595	272.727	10.85	1.3	0.060	1.78	0.143	2.724	0.770	1.7	0.093	1.3	0.75	0.026	2.202	581	81	81	571	14	15	578	15	15	519.48	22.58	100.44	98
SP7-57	0.593	58507	244	2.6	-217.991	-120.810	10.62	1.3	0.061	1.77	0.439	1.651	0.801	1.7	0.095	1.3	0.73	0.030	1.955	619	77	77	583	14	16	596	16	16	591.69	22.78	113.55	94
SP7-14	-0.386	53650	201	0.6	-99.272	-302.636	10.54	1.4	0.060	2.47	0.106	2.733	0.786	1.9	0.095	1.4	0.72	0.029	2.441	560	107	107	586	15	16	587	17	17	573.54	27.62	111.45	105
SP7-37	-0.146	31343	123	1.7	114.239	141.448	10.40	1.0	0.061	2.11	0.316	2.281	0.816	1.8	0.096	1.0	0.56	0.031	1.987	599	93	93	592	11	13	604	16	16	625.87	24.47	120.08	99
SP7-36	0.034	20467	80	1.1	-171.232	-43.935	10.38	1.2	0.063	3.81	0.191	3.116	0.837	3.1	0.096	1.2	0.41	0.030	2.316	626	138	138	592	14	15	612	27	27	593.56	27.12	115.03	95
SP7-101	1.268	7981	36	1.6	114.480	40.766	10.40	1.8	0.062	3.94	0.689	58.897	0.819	3.7	0.096	1.8	0.48	0.030	3.482	598	165	165	593	20	21	606	35	35	587.11	40.09	116.97	99
SP7-44	0.318	59470	239	1.5	27.770	977.737	10.39	1.4	0.061	1.72	0.246	4.486	0.815	2.0	0.097	1.3	0.64	0.028	2.399	613	73	73	595	15	16	603	19	19	549.98	26.05	106.89	97
SP7-39	0.908	36849	146	1.6	78.903	204.319	10.11	1.6	0.062	1.72	0.276	3.232	0.851	1.8	0.097	1.6	0.90	0.030	2.149	661	77	77	598	19	20	623	17	17	605.10	25.56	116.36	90
SP7-58	1.604	21971	88	0.8	72.488	138.910	10.19	1.4	0.062	2.29	0.148	6.877	0.842	2.1	0.098	1.3	0.66	0.032	3.124	660	97	97	600	15	17	618	19	19	635.43	39.08	125.65	91
SP7-97	-0.330	5337	22	1.3	146.429	60.391	10.42	2.6	0.066	6.06	0.247	7.770	0.886	4.6	0.098	2.6	0.57	0.031	5.163	644	260	260	603	30	30	634	43	43	617.70	62.71	131.81	94
SP7-63	2.044	34233	152	1.0	424.814	57.815	10.23	2.1	0.060	4.22	0.189	5.167	0.807	3.9	0.098	2.1	0.53	0.030	4.882	566	189	189	603	24	25	598	35	35	594.89	57.22	125.72	107
SP7-9	0.646	16344	56	1.3	243.177	41.935	10.26	1.7	0.061	3.01	0.232	2.556	0.823	2.5	0.099	1.7	0.68	0.031	2.437	565	129	129	606	20	21	606	23	23	618.61	29.69	120.03	107
SP7-54	2.062	10320	41	1.7	9.263	489.001	10.28	2.1	0.065	4.11	0.308	3.229	0.875	3.2	0.099	2.0	0.65	0.033	3.056	647	169	169	609	24	25	632	30	30	668.83	42.87	140.60	94
SP7-15	0.464	53986	190	0.7	15.566	1648.921	10.08	1.0	0.060	1.69	0.124	2.190	0.833	1.6	0.099	1.0	0.60	0.030	2.071	598	77	77	610	11	13	614	15	15	594.09	24.27	114.43	102
SP7-106	-1.750	3262	14	0.9	-6.170	-253.130	10.18	2.9	0.064	5.09	0.212	17.810	0.892	5.0	0.100	2.6	0.52	0.030	7.624	569	265	265	611	30	31	631	48	48	594.20	88.47	141.75	107
SP7-64	1.873	19470	77	0.8	-48.556	-152.752	10.13	1.7	0.063	2.84	0.156	2.885	0.846	2.6	0.100	1.5	0.58	0.031	2.772	624	123	123	611	18	19	618	24	24	625.76	34.09	122.22	98
SP7-73	1.005	29639	123	1.4	-40.065	-328.874	10.06	1.2	0.062	2.21	0.273	13.943	0.843	2.0	0.100	1.2	0.60	0.027	1.912	622	96	96	612	14	15	618	18	18	546.05	20.61	104.93	98
SP7-49	1.499	33478	127	0.9	340.978	44.096	10.10	1.6	0.061	2.26	0.162	5.248	0.842	1.6	0.099	1.5	0.95	0.032	2.112	626	110	110	614	19	20	618	15	15	630.17	26.22	121.36	98
SP7-2	0.132	40310	131	1.3	105.882	211.910	9.94	1.0	0.060	1.99	0.237	3.053	0.844	1.6	0.101	1.1	0.67	0.032	2.278	590	82	82	618	12	14	620	15	15	628.94	28.15	121.31	105
SP7-79	0.846	37853	152	1.2	-76.083	-204.818	9.95	1.1	0.061	2.13	0.198	2.120	0.847	1.9	0.101	1.1	0.58	0.027	1.942	593	99	99	619	13	15	621	18	18	544.00	20.83	104.42	104
SP7-99	-0.992	22701	93	1.4	-167.942	-55.937	9.88	1.0	0.060	2.85	0.249	2.347	0.850	2.3	0.101	1.0	0.44	0.032	2.188	572	122	122	621	12	14	621	22	22	628.91	27.06	121.21	109
SP7-70	1.623	22589	93	0.8	-72.905	-136.444	9.92	1.2	0.063	2.71	0.145	3.162	0.880	2.6	0.101	1.2	0.48	0.028	3.128	674	121	121	621	15	16	637	24	24	556.48	34.30	110.16	92
SP7-51	0.582	44068	168	1.9	-185.182	-87.324	9.84	1.0	0.063	1.88	0.365	7.089	0.879	1.7	0.101	1.0	0.60	0.033	1.765	666	80	80	622	12	14	638	16	16	655.13	22.72	124.97	93
SP7-88	0.164	72446	279	1.5	70.925	473.388	9.83	0.6	0.060	1.48	0.254	2.217	0.837	1.4	0.101	0.6	0.48	0.029	1.426	565	66	66	622	8	10	617	13	13	575.29	16.16	117.55	110
SP7-89	1.372	18521	77	1.4	107.120	84.318	9.89	1.4	0.060	2.59	0.246	3.163	0.836	2.2	0.102	1.3	0.60	0.030	2.840	570	111	111	623	16	17	614	21	21	588.67	32.95	115.57	109
SP7-61	0.371	60827	233	1.2	59.841	448.389	9.88	1.3	0.062	1.69	0.207	2.474	0.871	1.5	0.102	1.3	0.87	0.030	1.607	653	76	76	624	15	16	635	14	14	603.90	19.12	115.35	96
SP7-8	1.095	28940	93	1.3	385.018	44.751	9.86	1.4	0.061	2.24	0.235	3.528	0.855	1.8	0.102	1.4	0.79	0.031	2.592	609	100	100	626	16	18	626	17	17	624.50	31.80	121.36	103
SP7-62	0.651	75311	298	1.5	456.557	80.024	9.81	0.9	0.062	1.59	0.252	1.748	0.876	1.4	0.102	0.9	0.66	0.031	1.584	655	71	71	626	11	13	637	14	14	611.88	19.08	116.45	96
SP7-3	-0.725	22706	71	1.4	27.027	521.567	9.87	1.9	0.062	3.16	0.213	2.924	0.894	3.0	0.102	1.8	0.61	0.030	5.240	657	146	146	626	22	23	645	29	29	595.56	61.52	127.78	95
SP7-92	0.949	34406	150	1.6	135.789	182.415	9.74	1.6	0.063	3.93	0.416	26.979	0.894	3.4	0.103	1.6	0.46	0.029	3.568	652	193	193	629	19	20	646	33	33	573.85	40.40	115.39	96
SP7-55	0.898	23416	90	0.9	79.057	129.997	9.71	1.5	0.063	1.95	0.161	4.364	0.899	2.0	0.103	1.5	0.73	0.033	3.030	692	83	83	629	18	19	652	18	18	657.13	39.09	129.18	91
SP7-87	1.746	12037	47	1.9	61.840	106.362	9.77	1.4	0.063	2.78	0.347	4.687	0.896	2.6	0.103	1.4	0.56	0.028	2.496	651	130	130	631	17	19	645	25	25	561.97	27.64	109.23	97
SP7-112	0.207	15472	64	1.2	-14.156	-524.012	9.66	2.6	0.063	3.48	0.203	3.904	0.902	2.4	0.103	2.0	0.83	0.031	2.885	652	147	147	633	24	25	649	23	23	613.00	34.85	120.43	97

SP7-90	0.631	56471	235	0.7	449.528	62.016	9.67	1.0	0.061	1.92	0.125	2.532	0.862	1.7	0.103	1.0	0.58	0.028	2.200	590	83	83	633	12	14	629	16	16	566.21	24.56	109.33	107
SP7-1	-0.517	39589	127	1.2	-115.658	-226.456	9.58	1.4	0.061	2.03	0.213	2.774	0.889	1.9	0.104	1.4	0.73	0.033	1.797	610	88	88	640	17	18	644	18	18	646.89	22.88	123.75	105
SP7-120	-3.036	6080	25	1.0	-19.375	-145.234	9.60	1.8	0.064	4.19	0.207	11.564	0.925	4.0	0.106	1.9	0.47	0.033	6.071	622	179	179	647	23	24	654	39	39	661.16	78.39	146.08	104
SP7-100	0.068	21952	86	1.1	11.047	1290.587	9.45	1.2	0.062	1.88	0.190	16.748	0.910	1.7	0.106	1.2	0.69	0.028	2.362	655	85	85	649	15	16	655	17	17	566.49	26.36	109.75	99
SP7-93	0.739	43982	175	1.0	292.911	65.933	9.42	1.1	0.064	1.99	0.173	4.350	0.935	2.1	0.106	1.1	0.50	0.029	1.962	719	90	90	650	13	15	667	20	20	591.10	24.52	121.85	90
SP7-105	0.777	47905	192	1.9	164.527	143.762	9.45	1.3	0.063	1.68	0.317	1.784	0.929	1.6	0.106	1.3	0.79	0.032	1.392	694	70	70	650	16	17	665	16	16	636.44	17.42	120.73	94
SP7-67	2.602	16474	62	1.4	36.556	225.552	9.31	1.5	0.064	3.05	0.254	4.979	0.936	2.7	0.107	1.2	0.46	0.032	2.748	692	119	119	655	16	17	666	26	26	636.21	34.43	124.34	95
SP7-107	0.395	26585	109	1.2	27.613	513.213	9.38	1.5	0.063	2.36	0.198	2.908	0.933	2.2	0.107	1.5	0.70	0.031	2.219	684	103	103	655	19	20	667	21	21	624.30	27.30	120.54	96
SP7-117	-0.774	61187	262	1.3	-29.899	-1270.941	9.35	1.1	0.062	2.45	0.228	2.967	0.907	1.7	0.107	1.1	0.64	0.032	1.758	627	105	105	655	14	15	654	16	16	639.86	22.12	122.02	105
SP7-103	-0.495	20231	81	1.1	23.942	415.418	9.35	1.2	0.062	2.40	0.200	5.952	0.932	2.7	0.107	1.2	0.46	0.033	2.558	648	114	114	656	15	17	664	26	26	663.80	33.36	128.86	101
SP7-98	0.076	23269	92	1.0	263.027	50.172	9.18	1.6	0.062	2.46	0.148	4.772	0.917	2.6	0.108	2.0	0.78	0.025	5.556	617	108	108	661	25	26	656	26	26	513.51	59.95	119.16	107
SP7-115	1.566	29778	104	2.8	-116.345	-140.221	9.02	1.4	0.066	3.20	0.436	3.645	1.012	3.3	0.111	1.5	0.44	0.033	2.477	749	149	149	678	19	20	705	34	34	652.35	31.77	126.48	90
SP7-110	0.833	43045	173	1.1	39.976	716.274	8.79	1.2	0.062	2.45	0.200	5.464	0.969	2.1	0.113	1.0	0.49	0.031	2.282	632	105	105	689	14	15	685	21	21	620.40	27.88	119.90	109
SP7-68	0.484	106942	343	0.9	275.630	156.774	8.06	1.1	0.066	1.70	0.151	1.990	1.132	1.2	0.124	1.1	0.96	0.034	1.228	796	75	75	755	16	18	768	13	13	668.16	16.13	126.73	95
SP7-10	-0.410	17235	47	1.2	123.835	74.661	7.96	1.4	0.066	2.95	0.226	3.588	1.156	2.6	0.126	1.4	0.53	0.041	3.120	731	129	129	766	20	21	774	28	28	808.31	49.35	158.86	105
SP7-23	0.085	38531	50	1.1	256.244	82.725	3.56	1.1	0.103	1.47	0.189	2.058	4.002	1.5	0.280	1.2	0.82	0.086	2.172	1661	55	55	1591	34	37	1631	25	25	1658.60	68.92	310.73	96
SP7-84	1.019	66370	94	1.6	139.748	228.428	3.47	1.3	0.106	1.77	0.418	10.905	4.222	1.5	0.289	1.3	0.86	0.081	2.706	1716	65	65	1633	37	41	1674	24	24	1563.96	79.97	293.32	95
SP7-75	1.005	48565	65	0.9	-41.663	-461.452	3.26	1.1	0.111	1.67	0.142	2.549	4.673	1.6	0.307	1.1	0.67	0.080	1.751	1798	59	59	1723	32	36	1758	26	26	1548.59	52.02	287.86	96
SP7-4	0.946	50152	47	1.0	775.991	53.934	3.23	1.9	0.111	2.31	0.165	6.420	4.762	2.1	0.312	1.9	0.93	0.088	2.057	1787	82	82	1748	59	61	1773	35	35	1699.94	67.13	318.70	98
SP7-114	0.657	44154	53	1.9	-152.077	-117.100	2.80	1.1	0.121	1.68	0.297	1.847	5.946	1.3	0.358	1.1	0.84	0.099	1.467	1946	61	61	1969	38	42	1964	23	23	1914.49	53.60	352.82	101
SP7-28	-0.068	206745	211	0.7	-1075.871	-95.151	2.70	1.2	0.134	1.73	0.110	1.806	6.845	1.4	0.370	1.2	0.80	0.096	2.074	2131	62	62	2029	40	44	2088	25	25	1849.08	73.02	343.79	95
SP7-33	0.094	276110	310	1.0	118.539	2580.143	2.65	2.0	0.136	2.23	0.151	4.361	6.962	2.5	0.377	2.0	0.80	0.088	4.386	2172	78	78	2059	71	73	2104	45	45	1694.89	142.49	341.23	95
SP7-24	-0.189	50499	48	1.5	-183.833	-119.306	2.65	1.3	0.134	1.81	0.238	2.415	7.021	1.3	0.378	1.3	0.97	0.106	1.650	2129	63	63	2067	45	49	2110	23	23	2034.27	64.03	376.04	97
SP7-6	-0.199	90650	82	1.0	497.707	126.660	2.58	1.4	0.138	1.79	0.167	2.072	7.388	1.4	0.388	1.4	0.96	0.107	2.077	2184	62	62	2112	49	53	2156	25	25	2053.43	81.06	381.55	97
SP-5_58	0.221	63482	315	1.3	-500.903	-65.458	10.93	1.0	0.061	1.77	0.251	3.877	0.777	2.0	0.092	1.0	0.52	0.029	2.072	623	76	80	565	11	15	583	17	20	568.75	23.24	83.63	90.8
SP-5_42	0.493	42436	196	1.0	-361.631	-48.063	10.54	1.1	0.062	1.65	0.173	2.069	0.810	1.4	0.095	1.1	0.81	0.029	2.063	640	71	76	587	13	16	602	13	17	581.91	23.68	85.55	91.8
SP-5_33	1.274	38966	181	1.5	-107.551	-170.515	10.42	1.0	0.061	1.97	0.250	1.901	0.810	1.9	0.096	1.0	0.52	0.029	1.705	619	83	87	592	11	15	600	17	21	575.71	19.36	83.61	95.7
SP-5_104	1.045	18412	86	1.0	-60.960	-130.340	10.45	1.3	0.062	2.57	0.180	3.348	0.821	2.5	0.096	1.3	0.51	0.031	3.199	625	106	109	593	15	18	605	22	25	616.20	38.81	95.20	94.9
SP-5_96	0.470	40485	190	1.3	-380.689	-44.576	10.32	1.2	0.061	1.53	0.237	1.713	0.827	1.8	0.097	1.2	0.67	0.033	2.250	625	67	72	599	14	17	610	16	20	646.45	28.59	95.46	95.8
SP-5_7	0.202	42085	186	1.2	32.977	591.847	10.28	0.9	0.060	1.67	0.210	3.412	0.804	1.6	0.098	0.9	0.59	0.032	1.653	564	74	79	600	11	15	597	14	18	633.42	20.58	91.56	106.3
SP-5_93	1.358	11633	53	2.1	-108.753	-45.952	10.25	1.6	0.063	3.11	0.384	2.279	0.855	3.0	0.098	1.7	0.56	0.032	2.176	643	132	135	603	20	22	622	28	30	632.65	27.13	93.36	93.8
SP-5_15	2.762	7975	35	0.9	-19.728	-162.193	10.32	1.6	0.062	3.66	0.176	14.200	0.825	3.5	0.098	1.6	0.46	0.032	3.765	577	173	176	603	19	21	603	32	34	631.83	46.82	100.64	104.5
SP-5_48	0.203	105579	456	0.1	-671.366	-62.357	10.07	0.7	0.061	0.96	0.027	6.037	0.842	0.9	0.099	0.7	0.75	0.034	2.509	633	45	54	611	8	13	622	9	16	670.77	33.08	100.06	96.4
SP-5_26	0.096	46291	193	1.3	-494.221	-36.046	10.08	1.1	0.061	1.85	0.237	4.526	0.842	2.1	0.100	1.1	0.52	0.031	2.086	651	70	74	612	13	17	618	19	23	616.07	25.34	90.68	93.9
SP-5_28	-0.761	22533	97	0.9	-99.541	-102.556	10.06	1.0	0.061	2.82	0.155	2.322	0.841	2.4	0.100	1.0	0.41	0.032	2.247	591	117	119	613	11	16	616	21	24	639.77	28.29	94.54	103.6
SP-5_16	0.799	46811	197	0.9	-137.692	-162.874	10.05	1.5	0.063	2.23	0.144	4.734	0.871	2.2	0.100	1.4	0.63	0.031	2.945	681	99	102	614	16	19	634	21	24	622.07	36.10	94.96	90.3
SP-5_37	1.651	29723	140	0.8	-8.007	-2604.708	10.01	1.9	0.060	3.30	0.137	3.468	0.842	2.1	0.100	1.9	0.92	0.031	3.459	590	145	148	616	23	25	619	20	23	619.78	42.21	97.06	104.3
SP-5_94	3.440	9127	39	1.5	-85.661	-42.410	10.02	1.4	0.060	3.74	0.260	3.121	0.842	3.4	0.101	1.5	0.45	0.034	3.032	608	173	176	618	18	21	614	31	33	669.35	39.85	102.25	101.6
SP-5_61	-0.124	37127	158	0.8	-600.268	-21.052	9.93	0.7	0.062	1.76	0.132	1.779	0.863	1.6	0.101	0.7	0.42	0.030	1.678	634	77	81	619	8	13	630	15	19	596.48	19.73	86.51	97.6
SP-5_89	0.956	52538	227	1.1	-366.063	-51.963	9.89	0.9	0.062	1.30	0.182	2.027	0.862	1.4	0.101	0.9	0.66	0.031	1.657	643	56	62	622	11	15	630	13	18	616.27	20.09	89.17	96.7
SP-5_68	0.286	44379	193	1.6	-134.088	-142.306	9.90	1.0	0.062	1.16	0.285	1.581	0.870	1.3	0.101	1.0	0.76	0.031	1.513	655	53	60	622	12	16	635	12	17	625.12	20.02	96.87	95.0
SP-5_5	0.085	78184	325	1.1	-702.201	-45.190	9.86	0.8	0.061	1.28	0.176	2.549	0.854	1.0	0.101	0.8	0.78	0.032	1.576	633	60	66	623	9	14	629	10	16	629.12	19.50	90.76	98.4
SP-5_41	0.895	19482	84	1.0	-62.251	-130.831	9.83	1.2	0.060	2.01	0.180	3.467	0.850	2.0	0.102	1.1	0.54	0.033	2.578	571	89	94	625	13	17	622	19	22	653.05	33.05	97.60	109.4

SP-5_95	0.395	40892	173	2.2	-855.331	-47.948	9.85	1.0	0.062	1.70	0.417	4.661	0.878	1.7	0.102	1.0	0.58	0.034	1.710	645	75	80	625	12	16	638	16	20	667.26	22.39	96.51	96.9
SP-5_106	0.301	12852	56	1.3	-84.240	-63.288	9.82	1.4	0.062	3.11	0.225	2.399	0.872	3.2	0.102	1.3	0.40	0.032	2.617	638	132	134	625	15	19	630	31	33	645.59	33.25	96.92	97.9
SP-5_65	0.561	29275	124	0.8	-146.641	-78.120	9.86	1.2	0.061	2.32	0.143	3.155	0.856	2.2	0.102	1.2	0.56	0.031	2.376	607	101	105	626	14	18	630	21	25	626.54	29.32	93.14	103.2
SP-5_74	2.495	15728	67	1.1	-106.147	-57.127	9.82	1.3	0.062	3.23	0.212	4.738	0.881	3.1	0.102	1.2	0.40	0.032	2.984	594	139	141	626	15	18	636	28	31	633.21	37.19	96.71	105.5
SP-5_103	1.807	24853	106	1.8	-213.338	-44.362	9.78	1.1	0.060	2.29	0.289	1.909	0.859	2.3	0.102	0.9	0.41	0.031	1.730	573	99	103	627	11	15	626	21	24	625.70	21.32	90.82	109.4
SP-5_59	0.616	36051	157	1.6	-384.011	-38.933	9.82	1.2	0.062	1.80	0.278	1.644	0.884	1.8	0.102	1.1	0.60	0.032	1.293	648	82	87	627	13	17	642	17	21	628.64	16.02	90.15	96.9
SP-5_66	9.489	8837	35	2.4	-83.170	-45.973	9.91	2.4	0.064	4.60	0.388	2.770	0.874	4.7	0.103	2.0	0.43	0.030	2.061	667	192	194	629	24	27	628	46	47	605.43	24.60	88.96	94.3
SP-5_47	0.435	22349	94	0.9	-151.209	-57.147	9.79	1.0	0.064	2.06	0.151	2.600	0.903	2.2	0.103	1.1	0.48	0.031	2.214	694	88	92	629	13	17	650	20	24	617.02	26.91	91.12	90.7
SP-5_88	-0.014	46652	206	3.3	-718.520	-25.117	9.78	1.0	0.062	1.93	0.563	1.576	0.876	2.2	0.103	1.0	0.48	0.031	1.193	631	71	75	630	13	17	636	18	21	621.32	14.58	88.82	99.8
SP-5_21	-0.141	81840	322	0.9	-1048.106	-30.999	9.71	1.1	0.061	1.63	0.130	2.603	0.866	1.4	0.103	1.0	0.70	0.029	2.324	631	63	68	630	12	16	632	14	18	579.29	26.51	85.84	99.9
SP-5_1	-0.116	56018	236	0.5	-709.013	-32.647	9.73	0.9	0.060	1.81	0.101	13.880	0.862	1.5	0.103	0.9	0.60	0.033	2.423	591	77	82	631	11	15	630	14	18	650.70	31.03	96.84	106.9
SP-5_14	2.222	12392	51	1.3	-9.503	-558.967	9.62	1.5	0.062	2.87	0.210	2.649	0.893	2.6	0.105	1.5	0.58	0.033	2.546	623	129	132	643	19	22	644	25	28	651.80	32.69	97.60	103.3
SP-5_39	0.471	68322	289	1.0	-578.489	-42.931	9.56	1.1	0.060	1.24	0.178	1.943	0.886	1.6	0.105	1.1	0.67	0.033	1.755	616	57	63	644	13	17	643	15	19	647.57	22.35	93.90	104.5
SP-5_40	0.226	33516	140	3.1	-291.523	-42.422	9.54	0.9	0.061	1.61	0.541	1.291	0.891	1.7	0.105	0.9	0.52	0.033	1.347	640	68	73	644	11	16	645	16	20	651.70	17.28	93.48	100.6
SP-5_85	-0.444	21094	95	2.0	-306.003	-27.769	9.73	2.1	0.063	2.55	0.355	2.618	0.883	2.9	0.105	1.2	0.43	0.032	2.387	647	112	115	645	15	19	644	30	32	639.04	29.99	94.90	99.7
SP-5_38	0.186	48266	200	0.7	-809.833	-19.437	9.45	1.2	0.061	1.56	0.124	3.176	0.903	1.4	0.106	1.2	0.85	0.033	1.780	631	70	75	649	15	18	652	14	18	649.22	22.76	94.37	102.9
SP-5_45	1.909	22665	92	1.3	-234.703	-42.466	9.46	1.0	0.062	2.26	0.225	2.260	0.916	2.3	0.106	1.0	0.43	0.033	2.313	640	100	104	649	12	17	657	23	26	659.36	29.97	97.56	101.4
SP-5_112	0.379	40895	175	2.0	-539.701	-27.683	9.44	0.7	0.064	1.70	0.321	2.943	0.930	1.5	0.106	0.7	0.49	0.031	1.972	711	74	79	650	9	14	666	14	19	616.60	23.96	90.27	91.4
SP-5_36	1.116	59191	245	1.0	52.171	574.574	9.46	1.4	0.061	2.13	0.208	6.041	0.901	1.9	0.106	1.5	0.77	0.032	2.876	679	71	74	651	18	21	656	16	20	632.65	35.83	96.18	95.9
SP-5_82	0.203	50964	211	1.3	-421.696	-46.984	9.41	1.1	0.062	1.72	0.211	1.482	0.916	1.4	0.107	1.1	0.76	0.032	1.928	652	72	77	654	14	18	659	14	18	643.79	24.43	94.00	100.4
SP-5_19	-0.294	14855	57	2.1	-123.856	-55.402	9.31	1.2	0.063	2.91	0.362	4.010	0.918	2.7	0.107	1.3	0.47	0.034	2.320	651	122	124	657	16	19	658	26	29	678.01	30.90	100.26	100.9
SP-5_55	0.943	47318	173	1.1	-197.771	-119.321	9.11	1.0	0.062	1.68	0.180	4.267	0.947	1.6	0.110	1.0	0.62	0.033	2.368	665	73	78	672	12	17	676	15	20	653.27	30.40	96.87	101.0
SP-5_72	0.674	65643	259	1.3	-535.555	-49.326	8.78	0.9	0.063	1.71	0.219	2.422	1.001	1.7	0.114	0.9	0.50	0.034	1.549	696	65	70	696	12	17	703	16	20	677.89	20.63	97.61	100.0
SP-5_8	0.023	104952	289	0.1	-1033.902	-39.191	6.17	0.7	0.073	1.56	0.006	21.259	1.629	1.4	0.162	0.7	0.51	0.026	14.668	996	64	69	969	13	21	984	19	26	503.16	142.88	159.01	97.2
SP-5_54	0.330	13759	20	1.3	-134.975	-48.286	3.43	1.6	0.108	2.61	0.220	2.501	4.396	2.7	0.294	1.5	0.57	0.090	3.119	1738	100	103	1658	45	52	1702	46	51	1741.81	104.36	261.41	95.4
SP-5_24	-0.159	56373	88	1.1	-511.551	-63.775	3.47	3.0	0.102	1.68	0.195	3.132	4.172	3.1	0.294	2.7	0.88	0.099	3.522	1656	61	65	1659	80	84	1660	52	56	1908.81	128.36	290.85	100.2
SP-5_92	6.531	6946	10	2.7	-71.909	-34.667	3.35	2.4	0.104	3.81	0.424	2.791	4.296	3.4	0.302	2.5	0.73	0.088	2.665	1591	149	151	1726	73	78	1681	54	57	1699.80	86.91	249.33	108.5
SP-5_118	2.427	23738	32	1.9	-227.469	-44.583	3.25	1.7	0.110	1.88	0.330	4.296	4.729	2.3	0.311	1.6	0.71	0.098	2.679	1801	63	67	1742	50	57	1776	35	40	1888.83	96.54	275.58	96.8
SP-5_76	0.333	41821	56	1.2	-359.776	-51.637	3.23	1.4	0.109	1.57	0.195	1.816	4.718	1.5	0.312	1.5	0.99	0.094	2.017	1768	58	62	1749	46	53	1767	25	33	1808.74	69.65	257.01	98.9
SP-5_56	0.465	46410	58	1.3	-514.867	-42.207	3.18	1.2	0.110	1.75	0.201	2.182	4.827	1.7	0.316	1.2	0.69	0.094	2.300	1788	64	68	1767	37	46	1787	29	36	1819.33	80.09	261.93	98.8
SP-5_91	-0.005	236860	274	0.2	-2450.833	-48.533	2.92	1.5	0.127	1.44	0.027	3.617	6.004	1.9	0.345	1.5	0.81	0.071	3.553	2051	50	55	1907	51	59	1971	34	41	1379.50	94.63	212.94	93.0
SP-5_4	-0.283	81786	98	1.0	-1157.282	-32.982	2.71	1.3	0.136	1.19	0.165	4.312	6.910	1.4	0.368	1.2	0.91	0.110	1.784	2168	42	48	2018	43	53	2104	26	36	2111.71	71.56	296.09	93.1
SP-5_111	1.602	30457	36	1.6	-193.193	-64.701	2.68	1.0	0.142	1.49	0.279	8.388	7.338	1.3	0.372	1.1	0.84	0.112	1.853	2235	52	56	2039	39	50	2150	24	33	2151.95	75.65	302.11	91.2
SP-5_29	-0.108	142615	139	0.9	-1797.185	-31.774	2.25	0.8	0.157	0.86	0.131	1.400	9.706	0.9	0.445	0.8	0.91	0.123	1.138	2424	29	36	2373	32	48	2406	16	29	2343.49	50.22	319.94	97.9
SP-5_102	0.289	125059	94	0.2	-411.693	-146.155	1.88	1.0	0.229	1.12	0.017	3.182	16.937	1.2	0.533	1.0	0.83	0.107	5.289	3040	36	41	2753	43	59	2929	23	33	2045.06	206.18	347.11	90.6
SP-6_39	-0.171	31860	151	1.0	358.238	65.420	10.82	1.5	0.061	2.70	0.186	3.601	0.776	2.7	0.092	1.7	0.61	0.028	2.913	604	117	120	568	18	21	581	24	26	563.58	32.43	86.09	94
SP-6_17	0.718	35114	148	1.0	16.036	984.011	10.73	0.8	0.059	1.60	0.156	2.111	0.772	1.7	0.093	0.8	0.49	0.029	2.195	577	72	78	575	9	13	579	15	19	572.26	24.76	84.56	100
SP-6_118	0.731	36365	168	1.1	-155.939	-153.947	10.66	1.5	0.061	2.60	0.214	3.412	0.793	3.0	0.094	1.5	0.50	0.034	2.975	617	117	120	579	17	19	591	27	29	670.36	39.21	102.23	94
SP-6_112	1.289	42626	186	1.3	77.098	230.546	10.42	0.9	0.061	1.51	0.213	2.628	0.806	1.4	0.096	1.0	0.71	0.030	1.709	610	66	71	592	11	15	599	12	17	596.20	20.09	86.58	97
SP-6_34	3.872	8746	37	1.5	114.394	41.160	10.36	1.4	0.063	3.11	0.347	16.225	0.844	3.3	0.097	1.3	0.38	0.031	3.381	641	128	130	595	14	18	615	31	33	625.01	41.59	97.44	93
SP-6_67	0.388	92583	423	0.3	-1186.940	-41.683	10.35	1.3	0.061	2.59	0.086	16.021	0.802	1.6	0.097	1.3	0.80	0.030	6.795	622	105	108	595	15	18	598	14	18	592.02	79.58	115.64	96
SP-6_15	-0.155	43212	175	1.6	208.303	106.127	10.27	0.7	0.060	1.64	0.275	1.404	0.812	1.6	0.097	0.7	0.42	0.032	1.450	582	74	79	598	8	13	602	15	19	640.78	18.29	92.16	103
SP-6_28	0.458	45935	196	2.8	-47.573	-369.892	10.32	1.6	0.061	1.48	0.437	1.564	0.828	1.9	0.097	1.5	0.78	0.029	2.975	628	64	70	599	17	20	610	18	22	570.53	33.57	87.50	95
SP-6_65	2.392	15845	67	0.9	71.306	97.760	10.04	1.6	0.063	2.97	0.167	4.812	0.848	3.0	0.098	1.6	0.53	0.035	3.092	631	125	127	602	19	21	618	28	31	687.89	41.76	105.37	95

SP-6_100	0.660	59097	267	1.9	-282.027	-99.649	10.16	1.1	0.059	1.96	0.312	1.799	0.809	1.8	0.099	1.1	0.60	0.030	1.667	554	86	90	606	13	16	601	16	20	589.23	19.36	85.37	110
SP-6_88	0.647	8353	34	0.7	-15.187	-321.061	10.28	2.2	0.062	3.32	0.158	8.142	0.835	3.5	0.099	2.3	0.65	0.031	5.692	578	160	163	607	27	29	615	35	37	609.63	68.22	109.66	105
SP-6_48	2.529	24881	96	2.1	-89.860	-99.404	10.09	1.1	0.061	2.57	0.366	2.530	0.834	2.3	0.100	1.1	0.48	0.031	1.710	645	93	96	612	13	16	613	21	24	624.41	21.02	90.58	95
SP-6_80	0.122	19888	83	1.4	89.791	120.745	10.08	1.3	0.060	2.49	0.236	2.746	0.822	2.5	0.100	1.3	0.53	0.032	2.374	568	113	117	613	15	19	606	23	26	632.34	29.55	93.95	108
SP-6_92	0.162	69354	285	1.0	-236.959	-115.062	10.02	0.7	0.061	1.53	0.167	1.645	0.856	1.1	0.100	0.7	0.62	0.031	1.473	633	70	76	614	8	13	627	11	16	624.40	18.10	89.85	97
SP-6_50	-1.081	18358	78	1.0	-20.935	-448.684	10.07	1.4	0.061	2.43	0.191	9.676	0.838	2.4	0.100	1.3	0.54	0.031	2.956	576	108	111	615	15	19	615	22	25	618.32	35.96	94.29	107
SP-6_95	-0.700	42572	189	1.4	-242.872	-93.216	9.99	1.1	0.061	1.96	0.252	2.896	0.838	1.7	0.100	1.1	0.66	0.032	2.151	607	85	89	617	13	17	617	16	20	630.01	26.66	92.71	102
SP-6_43	0.651	55262	237	1.6	657.446	60.655	9.98	1.5	0.061	2.04	0.259	2.007	0.850	2.0	0.101	1.5	0.73	0.028	3.092	623	92	96	618	17	20	623	19	22	556.93	33.98	85.74	99
SP-6_81	-0.073	81424	347	2.6	-427.966	-82.719	9.85	1.0	0.061	1.47	0.444	3.319	0.847	1.3	0.102	0.9	0.73	0.032	1.269	609	64	70	623	11	16	622	12	17	645.82	16.14	92.48	102
SP-6_23	0.111	36883	148	0.6	-101.421	-145.871	9.93	1.4	0.060	1.69	0.113	10.236	0.846	2.2	0.102	1.2	0.56	0.030	4.295	602	73	78	623	15	18	620	21	24	592.14	50.40	98.02	103
SP-6_89	0.790	128878	508	0.2	1121.837	85.658	9.85	1.1	0.062	1.63	0.036	16.406	0.872	1.8	0.102	1.1	0.62	0.024	6.637	682	56	60	624	13	17	636	17	21	470.96	61.85	91.02	91
SP-6_44	0.528	21991	88	3.0	-8.235	-1139.563	9.86	1.0	0.060	2.19	0.491	1.747	0.847	1.8	0.102	0.9	0.51	0.030	1.398	584	88	92	624	11	15	621	17	20	602.79	16.59	86.61	107
SP-6_87	-0.279	17501	69	1.7	-78.285	-93.876	9.84	1.1	0.062	2.52	0.311	3.604	0.871	2.3	0.102	1.1	0.46	0.034	2.239	659	118	122	627	13	17	633	23	26	678.33	29.85	100.05	95
SP-6_33	1.193	32587	132	0.9	217.561	81.323	9.82	1.1	0.061	2.49	0.164	2.098	0.859	2.2	0.102	1.1	0.51	0.032	2.028	585	108	111	628	13	17	627	20	23	638.00	25.47	93.49	107
SP-6_40	1.049	11413	45	1.8	-2.802	-1806.896	9.82	1.2	0.063	3.14	0.284	2.545	0.895	2.8	0.102	1.2	0.42	0.029	2.152	646	142	145	629	14	18	644	26	29	586.62	24.85	86.40	97
SP-6_78	0.334	30090	119	1.1	-126.763	-96.902	9.77	0.8	0.060	1.69	0.177	2.000	0.853	1.7	0.103	0.8	0.46	0.033	1.831	576	78	83	629	9	14	624	16	20	657.98	23.71	95.71	109
SP-6_103	1.194	36544	154	1.0	171.750	109.617	9.75	1.0	0.062	1.87	0.171	2.412	0.886	1.7	0.103	1.0	0.57	0.033	2.303	662	81	86	631	12	16	643	16	20	653.98	29.63	96.80	95
SP-6_97	0.837	47198	191	1.0	-156.387	-118.624	9.73	0.7	0.061	1.55	0.165	2.222	0.875	1.4	0.103	0.7	0.52	0.032	2.024	629	66	71	631	9	14	637	13	18	637.67	25.38	93.33	100
SP-6_62	0.214	26078	105	0.9	85.976	159.917	9.74	1.0	0.063	2.15	0.142	3.053	0.877	1.6	0.103	1.0	0.63	0.033	2.545	659	94	98	632	12	16	645	18	23	658.07	32.98	98.50	96
SP-6_4	-0.008	31543	121	1.0	90.781	167.483	9.72	0.8	0.060	1.83	0.165	1.996	0.858	1.6	0.103	0.8	0.49	0.034	1.869	584	79	84	632	9	14	628	15	19	678.02	24.96	98.84	108
SP-6_32	-1.439	24433	97	1.1	-63.061	-197.833	9.74	1.1	0.061	2.17	0.195	2.827	0.857	2.0	0.103	1.1	0.56	0.031	2.014	583	95	99	633	13	17	630	20	24	621.09	24.61	90.93	109
SP-6_8	-0.615	11342	44	0.7	-18.278	-293.715	9.75	1.2	0.062	3.10	0.124	4.431	0.884	3.0	0.103	1.1	0.38	0.034	3.627	624	127	130	633	15	19	638	28	30	677.87	51.56	114.14	101
SP-6_101	0.389	13024	54	1.2	-53.100	-109.924	9.69	1.3	0.064	3.10	0.218	8.027	0.909	3.1	0.103	1.5	0.49	0.033	4.041	663	131	134	634	18	21	650	30	32	660.27	52.27	106.38	96
SP-6_29	0.411	33101	127	0.9	188.884	92.202	9.68	0.9	0.063	1.87	0.147	2.194	0.903	1.8	0.104	0.9	0.49	0.032	2.136	659	86	90	635	11	15	655	16	20	626.76	26.34	92.17	96
SP-6_71	-0.974	42227	171	1.1	-219.617	-107.951	9.68	1.1	0.061	1.76	0.192	3.192	0.870	1.6	0.104	1.1	0.67	0.034	2.241	608	78	83	635	13	17	635	16	20	676.65	29.83	99.91	104
SP-6_56	-0.159	43090	172	1.6	52.250	385.000	9.65	0.7	0.061	1.69	0.273	1.393	0.864	1.6	0.104	0.7	0.46	0.032	1.163	602	78	83	636	9	14	631	15	19	636.54	14.58	90.99	106
SP-6_58	0.500	42922	170	1.0	-289.918	-50.677	9.66	0.8	0.063	1.73	0.165	1.806	0.905	1.8	0.104	0.9	0.47	0.032	1.786	700	79	84	636	10	15	656	16	20	643.37	22.59	93.37	91
SP-6_52	-0.203	43639	179	1.3	126.365	188.332	9.67	1.2	0.062	1.89	0.216	1.602	0.888	1.8	0.104	1.2	0.65	0.032	2.024	646	83	88	636	14	18	644	17	21	636.94	25.40	93.42	98
SP-6_25	1.064	23238	95	1.7	-14.419	-982.980	9.68	1.6	0.062	2.99	0.342	4.790	0.894	2.8	0.104	1.6	0.58	0.035	2.304	644	130	133	637	20	23	646	27	30	698.06	31.61	103.23	99
SP-6_102	0.006	32911	136	0.6	-260.185	-51.852	9.67	1.1	0.062	2.11	0.108	3.152	0.892	1.8	0.104	1.1	0.60	0.033	2.676	652	89	93	637	13	17	646	17	21	653.08	34.42	98.38	98
SP-6_72	-0.337	19965	78	0.8	-41.592	-260.289	9.59	1.1	0.063	1.92	0.149	4.013	0.910	2.0	0.104	1.0	0.50	0.037	2.781	666	80	84	640	12	17	654	19	23	731.26	39.89	110.21	96
SP-6_73	0.183	18068	73	1.0	4.524	2429.754	9.61	1.2	0.061	2.70	0.183	4.926	0.883	2.6	0.104	1.1	0.44	0.033	2.659	625	110	113	640	14	18	639	26	29	663.59	34.70	99.68	102
SP-6_91	-0.893	15515	63	1.9	-210.786	-26.774	9.49	1.3	0.062	2.96	0.332	2.735	0.904	2.7	0.105	1.0	0.35	0.034	1.989	661	124	127	643	12	16	649	25	28	665.85	26.03	97.23	97
SP-6_63	0.113	43366	169	2.8	-243.851	-75.152	9.47	0.9	0.061	1.93	0.462	1.901	0.892	1.7	0.106	0.9	0.50	0.033	1.006	605	81	86	649	11	15	646	16	20	665.20	13.17	94.73	107
SP-6_49	0.500	52155	196	0.6	-270.065	-76.699	9.45	0.8	0.060	1.42	0.097	3.664	0.883	1.2	0.106	0.8	0.61	0.032	1.919	595	63	69	649	9	15	642	12	17	644.84	24.38	94.25	109
SP-6_116	4.330	20929	74	1.7	86.348	172.800	9.14	1.4	0.063	4.32	0.277	5.167	0.950	3.8	0.110	1.3	0.35	0.036	3.470	652	186	188	670	17	21	675	38	40	705.02	48.05	110.24	103
SP-6_82	0.519	92059	205	0.9	145.489	726.969	6.22	2.6	0.074	4.65	0.094	6.697	1.637	3.6	0.161	2.6	0.72	0.035	8.876	1013	191	192	964	47	50	983	46	49	690.27	120.28	154.56	95
SP-6_16	0.389	43901	59	0.9	430.680	55.982	3.29	0.9	0.109	1.20	0.150	1.822	4.631	1.4	0.305	0.9	0.62	0.093	1.672	1778	44	50	1714	27	38	1751	24	32	1802.14	57.64	253.52	96
SP-6_13	0.170	9899	13	1.8	-54.632	-82.721	3.30	1.8	0.110	3.03	0.297	3.813	4.627	2.6	0.307	1.9	0.72	0.092	3.110	1743	120	123	1724	56	62	1743	46	51	1793.68	116.25	291.86	99
SP-6_6	-0.051	138192	152	0.9	423.936	161.820	2.76	0.6	0.130	1.08	0.142	3.336	6.465	1.0	0.362	0.6	0.62	0.107	1.260	2089	37	43	1992	22	38	2039	18	28	2050.82	49.20	283.95	95
SP-6_41	0.219	270858	296	0.3	-789.192	-219.247	2.63	0.9	0.138	1.09	0.042	3.394	7.207	1.2	0.380	0.9	0.71	0.100	3.275	2199	38	44	2076	30	44	2143	17	25	1924.59	121.10	291.23	94
SP-6_30	-0.269	116160	97	1.2	-514.465	-123.728	2.15	0.8	0.171	1.15	0.182	3.101	11.060	1.1	0.466	0.8	0.76	0.128	1.579	2560	39	44	2466	33	49	2526	20	31	2426.37	72.21	335.27	96
SP-6_18	-0.016	214101	184	1.0	1658.740	72.308	2.12	0.6	0.169	0.79	0.157	1.089	11.083	0.8	0.470	0.7	0.86	0.134	0.863	2548	27	34	2485	27	46	2529	14	28	2539.36	41.24	344.30	98

[a] concentration uncertainty ca. 20%

[b] data not corrected for common-Pb

[c] data corrected/not corrected for common-Pb

[d] Concordance calculated as (206Pb-238U age/207Pb-206Pb age) * 100

Decay constants of Jaffey et al. (1971) used bd = below detection; #N/A = not available

Uncertainties quoted without components related to systematic error unless otherwise state

Total systematic uncertainties (ssys): 206Pb/238U = 1.0%, 207Pb/206Pb = 0.55% (2s

CAPÍTULO V SEDIMENTOLOGY FROM A PRE-VEGETATIONAL BIG RIVER SYSTEM: AN EXAMPLE FROM EASTERN PARNAÍBA BASIN, BRAZIL.

Artigo submetido em: Sedimentology (12/11/2024)

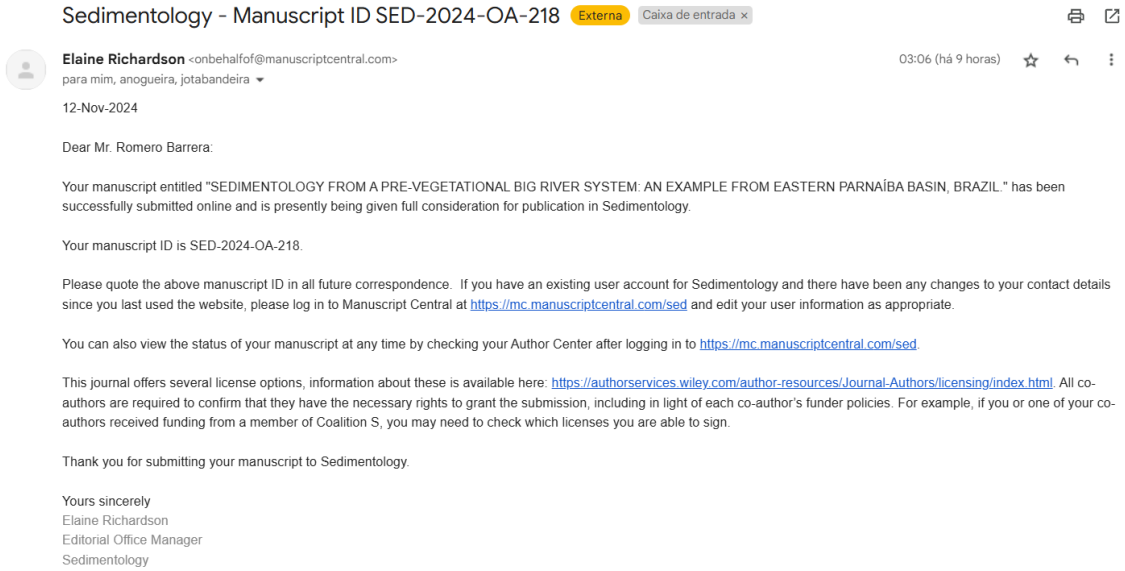

Sedimentology - Manuscript ID SED-2024-OA-218 Externa Caixa de entrada ×

Elaine Richardson <onbehalfof@manuscriptcentral.com> 03:06 (há 9 horas)
para mim, anogueira, jotabandeira

12-Nov-2024

Dear Mr. Romero Barrera:

Your manuscript entitled "SEDIMENTOLOGY FROM A PRE-VEGETATIONAL BIG RIVER SYSTEM: AN EXAMPLE FROM EASTERN PARNAÍBA BASIN, BRAZIL." has been successfully submitted online and is presently being given full consideration for publication in Sedimentology.

Your manuscript ID is SED-2024-OA-218.

Please quote the above manuscript ID in all future correspondence. If you have an existing user account for Sedimentology and there have been any changes to your contact details since you last used the website, please log in to Manuscript Central at https://mc.manuscriptcentral.com/sed and edit your user information as appropriate.

You can also view the status of your manuscript at any time by checking your Author Center after logging in to https://mc.manuscriptcentral.com/sed.

This journal offers several license options, information about these is available here: https://authorservices.wiley.com/author-resources/Journal-Authors/licensing/index.html. All co-authors are required to confirm that they have the necessary rights to grant the submission, including in light of each co-author's funder policies. For example, if you or one of your co-authors received funding from a member of Coalition S, you may need to check which licenses you are able to sign.

Thank you for submitting your manuscript to Sedimentology.

Yours sincerely
Elaine Richardson
Editorial Office Manager
Sedimentology

SEDIMENTOLOGY FROM A PRE-VEGETATIONAL BIG RIVER SYSTEM: AN EXAMPLE FROM EASTERN PARNAÍBA BASIN, BRAZIL.

Ivan Alfredo Romero Barrera[1], Afonso César Rodrigues Nogueira[1], José Bandeira[1].

[1] Programa de Pós-Graduação em Geologia e Geoquímica, Faculdade de Geologia, Instituto de Geociências, Universidade Federal do Pará, 66075-110, Belém, PA, Brazil, (ivan.barrera@ig.ufpa.br).

ABSTRACT

The extensive landmass of West Gondwana played a significant role in forming large rivers during the Ordovician period, largely preserved as siliciclastic deposits in the intracratonic basins along the northwestern margin of this supercontinent. Conglomerates and sandstones from the Ipu Formation in the Parnaiba Basin represent one of the most spectacular examples of transcontinental drainage with migration towards the Iapetus Ocean on the northwestern margin of Gondwana. This unit includes a 300-400-meter-thick succession comprising laterally continuous coarse-grained lithoarenites and conglomerate beds currently preserved on the eastern border of the Parnaíba Basin. The well-exposed outcrops from the Ordovician Ipu Formation allow for detailed pre-vegetational Big Rivers fluvial architectural analyses and interpretations of discharge pattern variations. This field-based study comprises a collection of high-resolution sedimentological, stratigraphic, and paleocurrent data from 300 m of integrated logs. These deposits are organized in meter-scale fining upward cycles that reflect the predominance of sheet flow with sporadic channel incisions filled by migrating small- to large-scale two and three-dimensional bedforms. Locally, small- to medium-scale humpback dunes and antidunes deposited by unstable, transcritical, and supercritical flows during non-periodic, peak-flood events were registered. Six architectural elements, including laminated sand sheets, sandy bedforms, Dune complexes, Frontal Accretion Macroforms, Channel Fill Sandy Forms, and conglomerate bars, reflect different fluvial dynamics and sedimentation stages. The Ipu Formation depositional record is consistent with braided fluvial systems formed under humid conditions, characterized by low-sinuosity drainage patterns and periodic discharge variability. The results emphasize the stability of the depositional environment, with high rates of channel amalgamation and minimal accommodation space creation, suggesting low tectonic activity during deposition. This research expands the understanding of pre-vegetation Big Rivers, providing insights into sedimentary processes that have shaped ancient large-scale river systems.

Keywords: Big Rivers, Western Gondwana, Parnaíba Basin, Ipu Formation, Serra Grande Group.

1. INTRODUCTION

Distinct sedimentary architectures and depositional features often characterize fluvial systems in pre-vegetation landscapes due to the absence of rooting structures and stabilizing vegetation, which typically influences riverbank stability and floodplain sedimentation in more recent depositional systems (Cotter, 1978; Hjellbakk, 1997; Davies et al., 2011). As a result, ancient fluvial systems were likely more prone to lateral migration and sediment reworking, leading to extensive channel-belt development with little to no fine-grained overbank deposits (Schumm, 1968; Cotter, 1978; Fuller, 1985; Mac Naughton et al., 1997; Long, 2004; Davies and Gibling, 2010). Understanding the architectural elements and bounding surfaces within these fluvial deposits is crucial for reconstructing their paleoenvironmental conditions and interpreting the processes that shaped their stratigraphy (Miall, 1988a; 1988b; 1992).

Bedforms and architectural elements interpretation are essential components of fluvial systems stratigraphic evolution understanding (Miall, 1985, 1996; Bridge, 2003). Detailed sedimentological analyses aid in reconstructing paleo-environments related to fluvial sedimentation. Fluvial sandy channel bodies characterized by planar and trough cross-bedding indicate low discharge variability (Fielding et al., 2018). Conversely, humpback dunes and antidunes are linked to more complex flow dynamics, often associated with transcritical and supercritical flows (Manna et al., 2021). Initially believed to have low preservation potential, these bedforms have gained recognition in the sedimentary record due to recent studies highlighting their prevalence (Fielding, 2006; Cartigny et al., 2014; Alexander et al., 2001). Their accumulation is linked to turbulent flows, indicating high discharge variability (Fielding, 2006; Plink-Björklund, 2015) and reflecting numerous bounding surface types. The concept of bounding surfaces serves as a valuable framework for analyzing the stratigraphic hierarchy within fluvial deposits. Categorizing surfaces based on their scale, geometry, and relation to other sedimentary features can identify different depositional elements and infer changes in river dynamics, such as discharge variability, channel migration, and sediment supply. In this study, we apply this hierarchical classification to describe the architectural elements of the Ipu Formation, delineating bounding surfaces that capture the depositional patterns of this ancient braided river system.

The Ipu Formation within the Parnaíba Basin in northeastern Brazil represents an essential sedimentary archive from the Ordovician-Silurian transition, marked by

significant global climate and biological evolution changes (Assis et al., 2019; Barrera et al., 2020; Cerri et al., 2024). Understanding the geological evolution of the Gondwana supercontinent and its sedimentary environments during the Ordovician period is paramount to comprehending paleogeographic dynamics and repercussions in Big Rivers fluvial morphodynamics. In this context, this study investigates extensive landmasses that stretched hundreds of kilometers in Western Gondwana during the Ordovician, serving as sites for developing large rivers. These fluvial systems are primarily preserved as siliciclastic successions in intracratonic basins and isolated grabens, notably exemplified by the Ipu Formation in the Parnaiba Basin (Fig. V.1). These deposits contain specific data on the behavior of ancient river systems before plants widespread colonization of land. As one well-preserved example of pre-vegetation Big Rivers, the Ipu Formation offers invaluable insights into how such river systems operated under vastly different ecological conditions than those of today.

2. GEOLOGICAL SETTINGS

The Parnaíba Basin is a Phanerozoic magmatic-sedimentary unit that spans over 600,000 km² and reaches a thickness of 3.5 km at its depocenter in northeastern Brazil (Góes & Feijó, 1994; Vaz et al., 2007; Tozer et al., 2017). This basin is classified as a sag type and exhibits low and localized subsidence rates, which are influenced by orogenic cycles associated with the Brasiliano-Pan-African cycle rather than tectonic plate boundaries (Milani & Zalán, 1999; Daly et al., 2014; Castro et al., 2016).

The origin and evolution of the Parnaíba Basin are primarily linked to tectonomagmatic events (De Oliveira & Mohriak, 2003; Daly et al., 2014). These events led to the sedimentation onset during the Early Paleozoic era, which began with an Ordovician depression caused by isostatic adjustments and cooling following the assembly of Gondwana (Brito Neves et al., 1984; De Castro et al., 2014). The basement of the basin consists mainly of igneous, metamorphic, and sedimentary rocks, with ages ranging from the Proterozoic to the Cambrian. These rocks were formed or reworked during the Brasiliano-Pan-African cycle (Vaz et al., 2007).

A broad erosive surface developed during the early Paleozoic, marking the transition from the basement to the sedimentary infill (Vaz et al., 2007; Daly et al., 2014; Porto et al., 2018). The stratigraphic framework of the Parnaíba Basin includes five depositional sequences, which are separated by regional, basin-scale unconformities (Fig.

V.1A). These sequences include the Ordovician-Silurian (Serra Grande Group), Middle Devonian-Lower Carboniferous (Canindé Group), Carboniferous-Lower Triassic (Balsas Group), Jurassic (Pastos Bons Formation), and Cretaceous (Codó, Corda, Grajaú, and Itapecuru formations) (Góes & Feijó, 1994; Vaz et al., 2007).

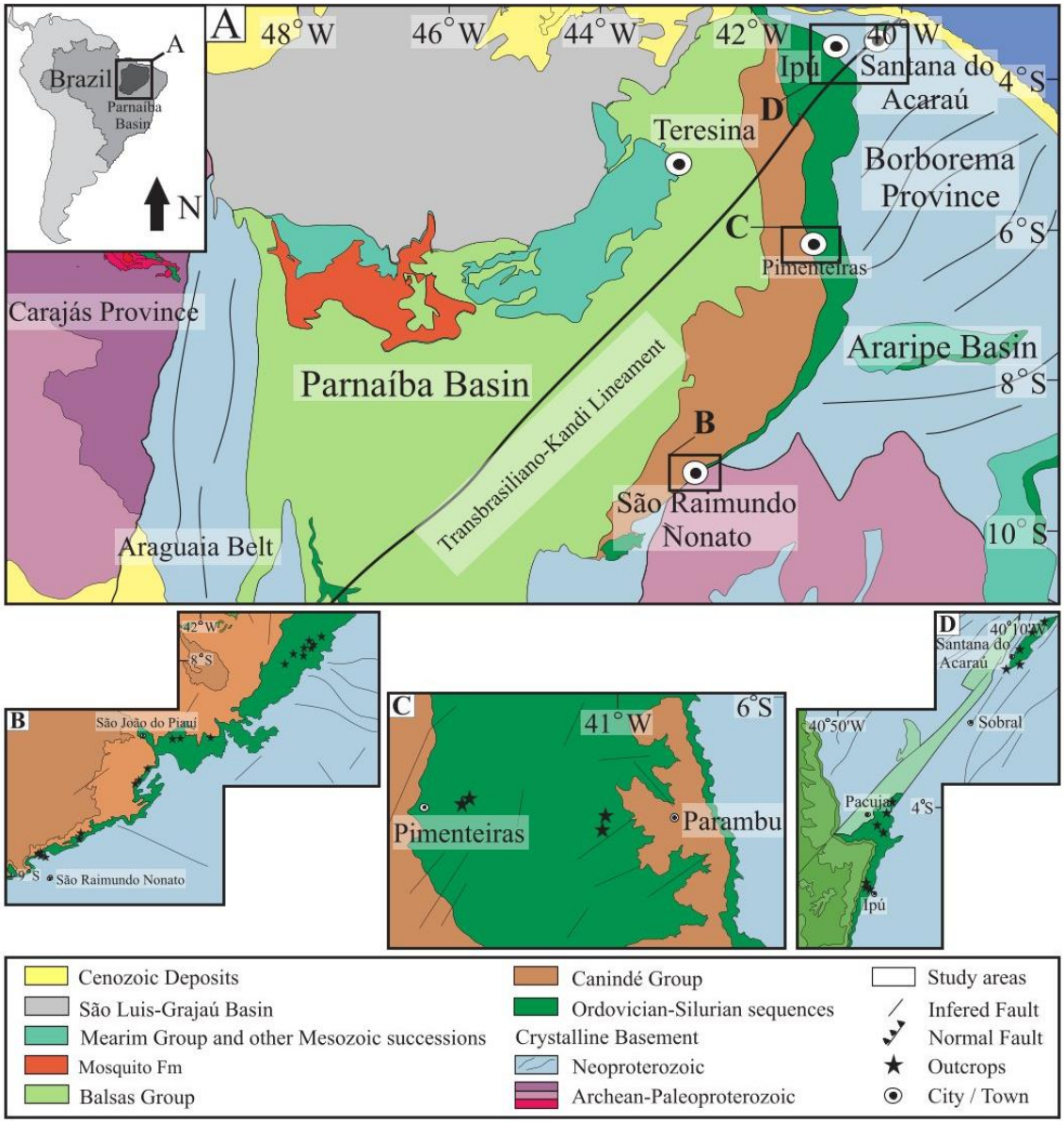

Figure V.1- Location map of the study area. A) Parnaíba Basin geological map containing stratigraphic sequences, surrounding geological units, and main lineaments. The study areas are in polygons. (B, C, and D) Detailed maps of the study areas.

This study is focused on the Ordovician-Silurian sequence, specifically the Ipu Formation, the lowermost unit of the Serra Grande Group. The Serra Grande Group outcrops in a restricted, narrow N-S area on the Parnaíba Basin eastern present-day edge, overlying Precambrian basement rocks. In the subsurface, the Serra Grande Group covers almost the entire basin (Vaz et al.,2007).

The Ipu Formation is discordantly deposited over the basin basement and exhibits a transitional contact with the overlying Tianguá Formation (Caputo & Lima, 1984). This formation primarily consists of sandstones, conglomerates, coarse sandstones, and diamictites, with thicknesses reaching up to 400 meters in the northeastern part of the basin (Caputo & Lima, 1984). Kegel (1953) described faceted pebbles found within the diamictites in the upper sections of the Ipu Formation, which were later interpreted as glacial in origin (Barrera et al., 2020). Basal and middle portions of the Ipu Formation were deposited within massive river systems that supplied sediment for marine environments in Western Gondwana (Cerri et al., 2024).

The Tianguá Formation has a maximum thickness of up to 270 meters in the subsurface and 150 meters as measured in outcrops on the basin eastern edge (Caputo & Lima, 1984). Rodrigues (1967) introduced the term "Tianguá" to identify a sedimentary succession composed of black shales, siltstones, and fine sandstones observed in outcrops within the Tianguá municipality in the northeastern basin. These sediments are interpreted as having been deposited in shallow marine and deltaic systems (Caputo & Lima, 1984; Grahn & Caputo, 1992; Le Hérissé et al., 2001; Grahn et al., 2005).

The Jaicós Formation, proposed by Plummer (1946), designates a sedimentary succession found on the slopes of the Serra Grande in the northeastern part of the basin. This unit mainly consists of coarse sandstones, which are believed to have been deposited in river and delta environments, with maximum thicknesses of up to 400 meters in the subsurface and 200 meters at the surface (Caputo & Lima, 1984; Vaz et al., 2007). The Jaicós Formation overlaps the Tianguá Formation, with its upper portion limited by a regional unconformity that separates it from the Devonian Itaim Formation (Canindé Group) (Caputo & Lima, 1984).

3. STUDY AREA AND METHODS

The study area is in the present-day eastern edge of the Parnaíba Basin in Ceará and Piauí states, northeast Brazil (Fig. V.1). The Ipu Formation crops out along highways and adjacent hills, in particular from the town of São Raimundo Nonato to São João do

Piauí, where most of the outcrops are situated.

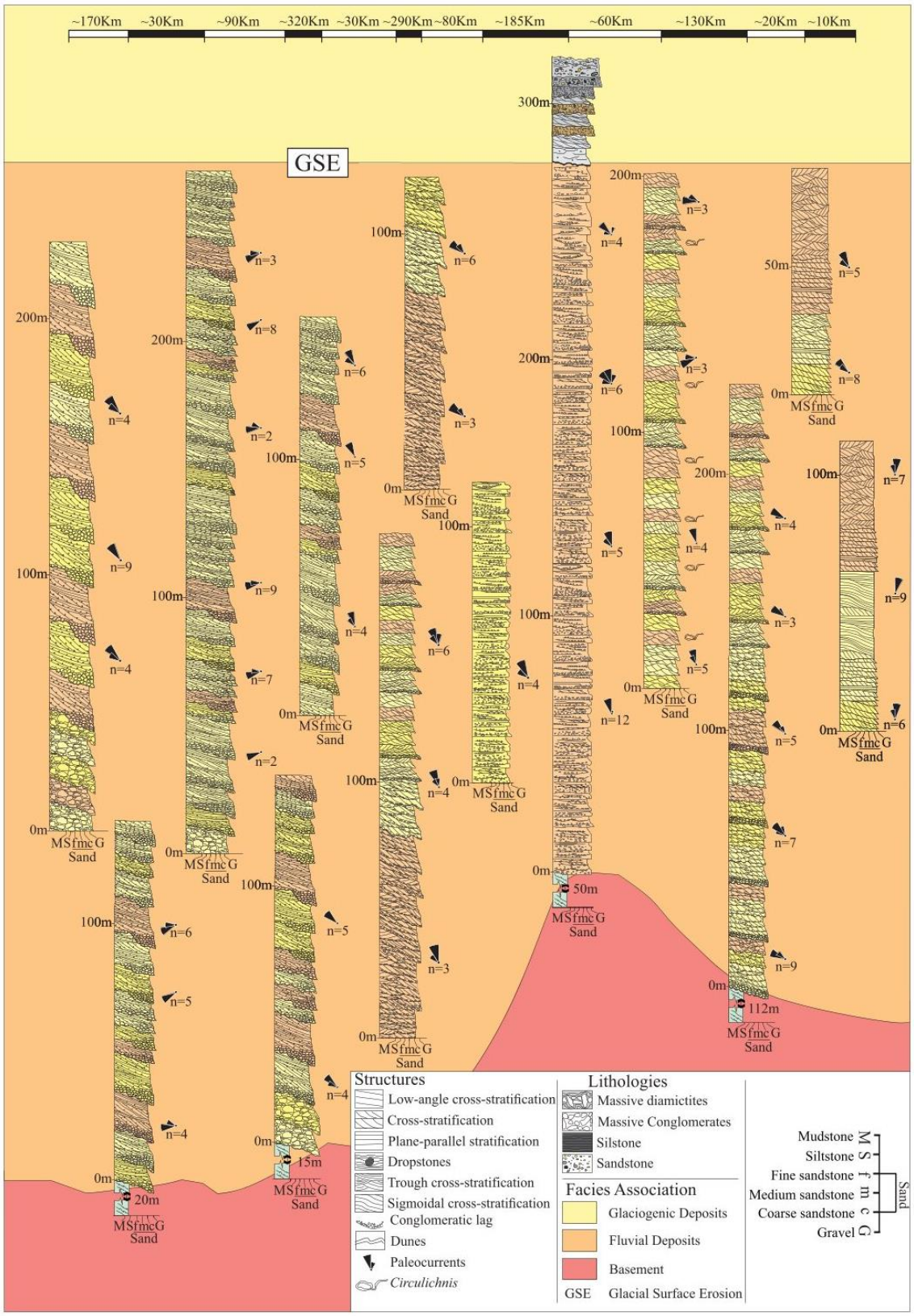

Figure V.2- Sedimentary logs and facies descriptions of the Ipu Formation in the eastern Parnaíba Basin, northeastern Brazil**.**

Also, extensive rock exposures of this unit were recognized and described in the Ipú, Sobral, and Santana de Acaraú regions. Thirteen stratigraphic sections were measured in the eastern portion of the Parnaíba Basin, encompassing the Ipu, Ipueiras, Pacuja, Santana de Acaraú, Sobral, Pimenteiras, Parambu, São João do Piauí, and São Raimundo Nonato regions (Fig. V.2). Each sedimentary succession was logged bed by bed using outcrop-based facies analysis techniques (lithologies, sedimentary structures, paleocurrent data, and lateral and vertical variations). The bed thicknesses were grouped as very thin-bedded (<1 cm), thin-bedded (1-10 cm), medium-bedded (10-30 cm), thick-bedded (30-100 cm), and very thick-bedded (>100 cm) (Ingram, 1954). Architectural elements were classified based on Miall (1988a, 1992) and Fielding (2006), with minor adaptations to better assign architectural elements to processes and geometry.

Paleocurrent data were collected by analyzing sedimentary structures formed under unidirectional flow conditions, each providing insights into the flow dynamics during deposition. Photomosaics were employed to create detailed visual representations of the architectural elements displayed in two-dimensional exposures to enhance the understanding of these geological features. This approach allows for a comprehensive examination of the sedimentary environments and their associated flow patterns.

4. RESULTS

4.1 FLUVIAL SEDIMENTOLOGIC ASPECTS

4.1.1 Massive to crudely bedding conglomerate

These facies correspond to 5 % of the total succession and are always the lowermost deposits at the base of each fining-upward cycle (Fig. V.2). It consists of hundred-meter to kilometric laterally continuous tabular bodies, with thicknesses ranging from 0.2 to 3m, commonly interbedded with sandy deposits. The contacts between the beds are mainly erosive with shallow undercuts; subordinate flat/non-erosive contacts were identified in the middle and upper portion of the succession. Gravel-dominated, lensoid lithosomes consist of massive, cross-bedded, and planar bedding (Fig. V.3). Subordinate levels of massive conglomerates change laterally to pebbly sandstone occurring preferentially at the bases of cycles (Figs. V.3A and B). Imbricate clasts are commonly observed (Fig. V.3C). Locally, disproportionate clasts occur in the pebbly conglomeratic facies (Figs. V.3D, E, and F). The clast population is poorly sorted, and the size varies from pebbly to boulder (Fig. V.3). The shape of the pebbles fluctuates from

spheroidal to elliptical to tabular, but most are well-rounded. These ortho conglomerates exhibit a medium- to coarse-grained, sub-angular to sub-rounded, poorly sorted sandstone matrix. Rock frameworks are predominantly quartz, metamorphic, and secondarily igneous and sedimentary rock fragments. Rock cement is mainly silica, with minor iron oxides and calcium carbonate. In most instances, these facies are overlain coarse-grained sandstone and interbedded siltstone and claystone (Fig. V.2). The siltstone and claystone interbed drape the conglomerate units and are 10 to 40 cm thick.

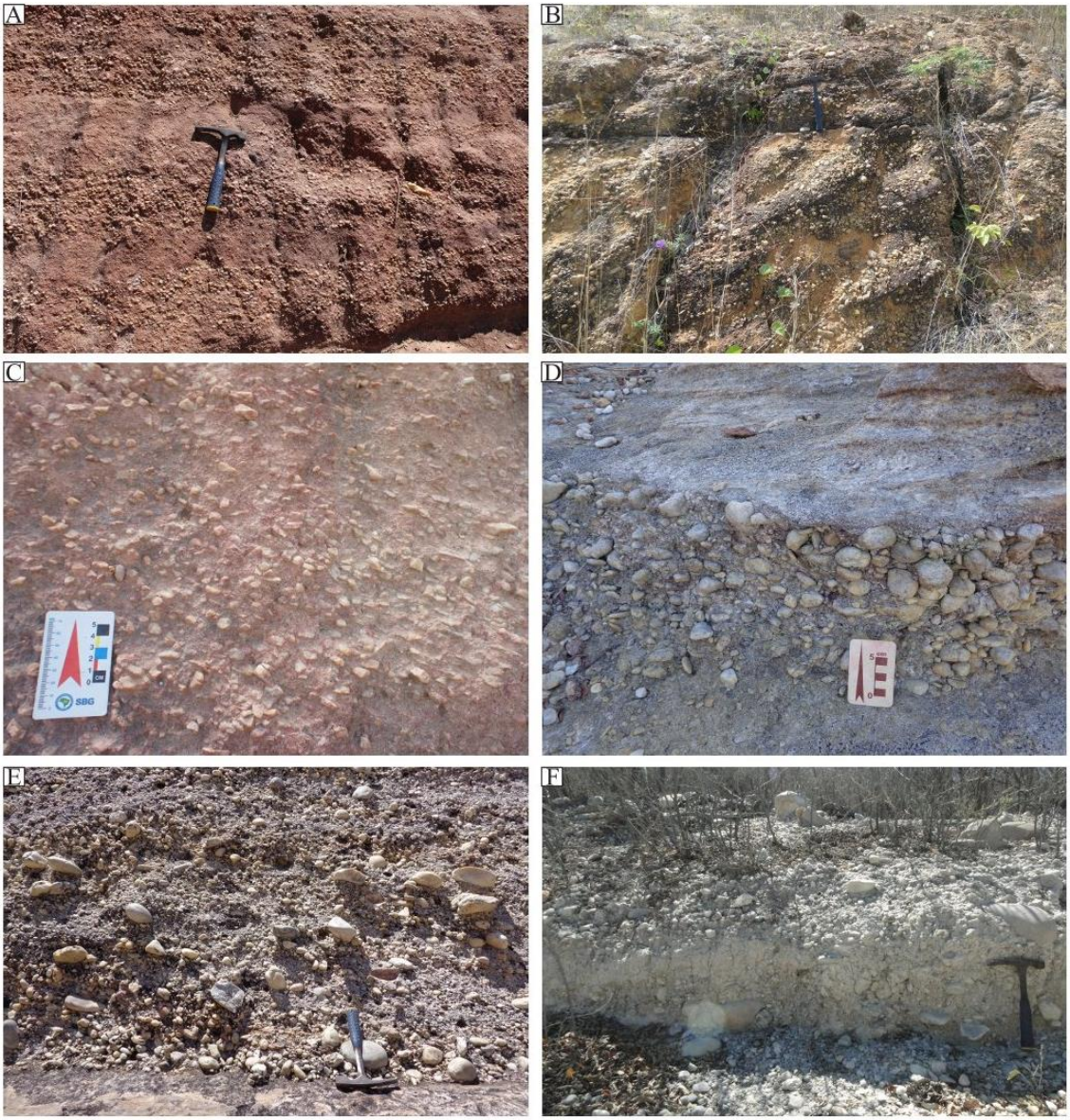

Figure V.3- Massive to crudely bedding conglomerates lithofacies aspects. A and B) Levels of massive conglomerates change laterally to pebbly sandstone, which occurs preferentially at the finning upward cycles bases. C) Imbricated clasts observed at the bottom of a fining-upward cycle. D, E, and F) Poorly-sorted, granule- to pebble-supported massive conglomerates consisting of subangular to sub-rounded clasts. The hammer length is 30 cm.

Interpretation

Conglomerate-dominated lithosomes represent active, gravel-bed fluvial channels filled by 3D dune deposition. The widespread massive form of the beds, the poor sorting of clasts, and the predominance of imbricated clasts suggest relatively rapid sedimentation from a high energy flow (Rust & Koster, 1984; Miall, 1996; Ghazi & Mountney, 2009). The prevalence of coarse-grained conglomerates with clasts reaching cobbles and boulders indicates an intermediary braided plain distant from the source area. Characteristics of these facies are consistent with deposition from high-velocity flows in the deepest part of the fluvial channel (Allen, 1970; Miall, 1988a; Collinson, 1996; Ghazi & Mountney, 2009). These facies represented a channel lag deposited under a lower flow regime, with sediment transport occurring by tractional currents. The common occurrence of crudely developed sets of crossbedding and planar bedding and the dominance of extraspinal clasts indicate that these facies were deposited either by downstream migrating 3D dunes or by obliquely migrating longitudinal bars within channels (Rust & Koster, 1984; Miall, 1996; Paredes et al., 2007; Ghazi & Mountney, 2009).

4.1.2 Trough cross-stratified sandstone

These facies represent 45 % of the total succession and most commonly overlies conglomeratic facies or are the lowermost deposits at the base of each fining-upward cycle (Fig. V.2). It compounds medium- to very coarse-grained sand, granules, and small pebble-sized, moderately to poorly sorted, arranged into trough cross-bedded sets and cosets (Fig. V.4). Sets consist of hundred-meter to kilometric laterally continuous tabular bodies, with thicknesses ranging from 0.4-4m, commonly interbedded with conglomerates or tabular cross-bed sandstones (Fig. V.4A). The contacts between the sandstone beds are mainly flat/non-erosional, and subordinate erosive contacts have been identified (Figs. V.4B and C). The rock framework exhibits angular to subangular grains with low sphericity. The grains are predominantly quartz and metamorphic, igneous and sedimentary rock fragments, and secondarily feldspars and heavy minerals. The trough cross-bedded units mostly form large-scale (2 m thick, 5-10 m wide), though some small-scale types are also evident (0.4 m thick, 0.8 m wide) (Fig. V.4). These facies occur in solitary sets or cosets with unimodal paleocurrent patterns. The inclination of forests varies from 15 to 30° and is generally towards the north or northwest. Isolated pebbles are observed following the forest dips (Fig. V.4D). Coarse grains up to 2 cm are segregated in the foresets and at the base of sets, forming lags (Fig. V.4E). Sporadically,

subrounded to rounded extraformational lithic pebbles of quartz, schist, and gneiss, up to 50 mm occur as isolated clasts within the bodies of sets. Thin siltstone layers usually mark sharp boundaries between sets and costs (Fig. V.2). Geometrically, these facies occur as tabular bodies commonly arranged into stacked, cross-bedded sets extending laterally for several hundreds of meters. The lower boundary is either gradational with conglomeratic facies or erosional with sandy facies of the underlying cycle. The upper contact is sharp and flat with overlying crossbred sandstone facies.

Figure V.4- Trough cross-stratified sandstone lithofacies aspects. A) Panoramic section depicting the trough cross-bedding tabular sandstone beds. Note a 1.85 m-tall person for scale. B and C) Varieties of sandstone bed contacts D) Cross-stratified sandstone facies with coarse particle size segregation in the foresets. 4D). E) Imbricated coarse grains up to 5 cm segregated at the cross-stratified sandstone sets base. Note a 1.75 m-tall person for scale. The hammer length is 30 cm, and the switchblade length is 8 cm.

Interpretation

Trough cross-stratified sandstone is interpreted as the product of 3D dunes migrating in channels under the conditions of the upper part of the lower flow regime (Cant & Walker, 1976; Miall, 1996; Capuzzo and Wetzel, 2004; Hjellbakk, 1997). The low inclined dip of the larger forests and the coarse sand grain size suggest that major sets of these facies probably formed low-angle-inclined fronts of bars (Smith, 1970; Ghazi & Mountney, 2009). Dunes that migrated over or across the lee faces of the bars probably generated smaller troughs (Collinson, 1996; Ghazi & Mountney, 2009). The basal conglomeratic lags, with ripples at the top, suggest progressive bar build-up and water-depth shallowing (Stear, 1983; Ielpi & Rainbird, 2015). The considerable lateral extent of trough crossbedding, the relationship to other facies, and the spread of cross-bed orientations suggest that these deposits were deposited across a broad, sandy river plain. The moderately to poorly sediment sorting, the tabular geometry, and the predominance of an unimodal orientation of trough cross strata favor a fluvial bedform interpretation (Collinson, 1996; Miall, 1996; Eriksson et al., 1998; Ghazi & Mountney, 2009).

4.1.3 Tabular cross-stratified sandstone

These facies, which represent 35% of the total succession, consist of medium- to coarse-grained, poorly sorted lithoarenite sandstone arranged into kilometric-wide tabular sets with thicknesses ranging from 0.3-3m, commonly interbedded with conglomerates or trough cross-stratified sandstone (Figs. V.2 and V.5). The contacts between the beds are mainly flat/non-erosional, and subordinate erosive contacts have been identified in the middle portion of the association (Fig. V.5A). The lithofacies are moderately well-sorted and texturally mature. The rock framework exhibits angular to subangular grains with low sphericity, predominating medium- to coarse-grained sand, granules, and small pebble-sized. The grains are predominantly quartz, metamorphic, sedimentary rock fragments, and secondarily feldspars and heavy minerals. Coarse grains are segregated in the foresets and at the base of sets, forming lags (Fig. V.5B). The cross-strata dips show preferential paleocurrent trends toward NW. The thickness of planar cross-bedded sets typically decreases with decreasing grain size (Fig. V.5C). Cosets of these facies generally form kilometric-wide tabular bodies (Fig. V.5D).

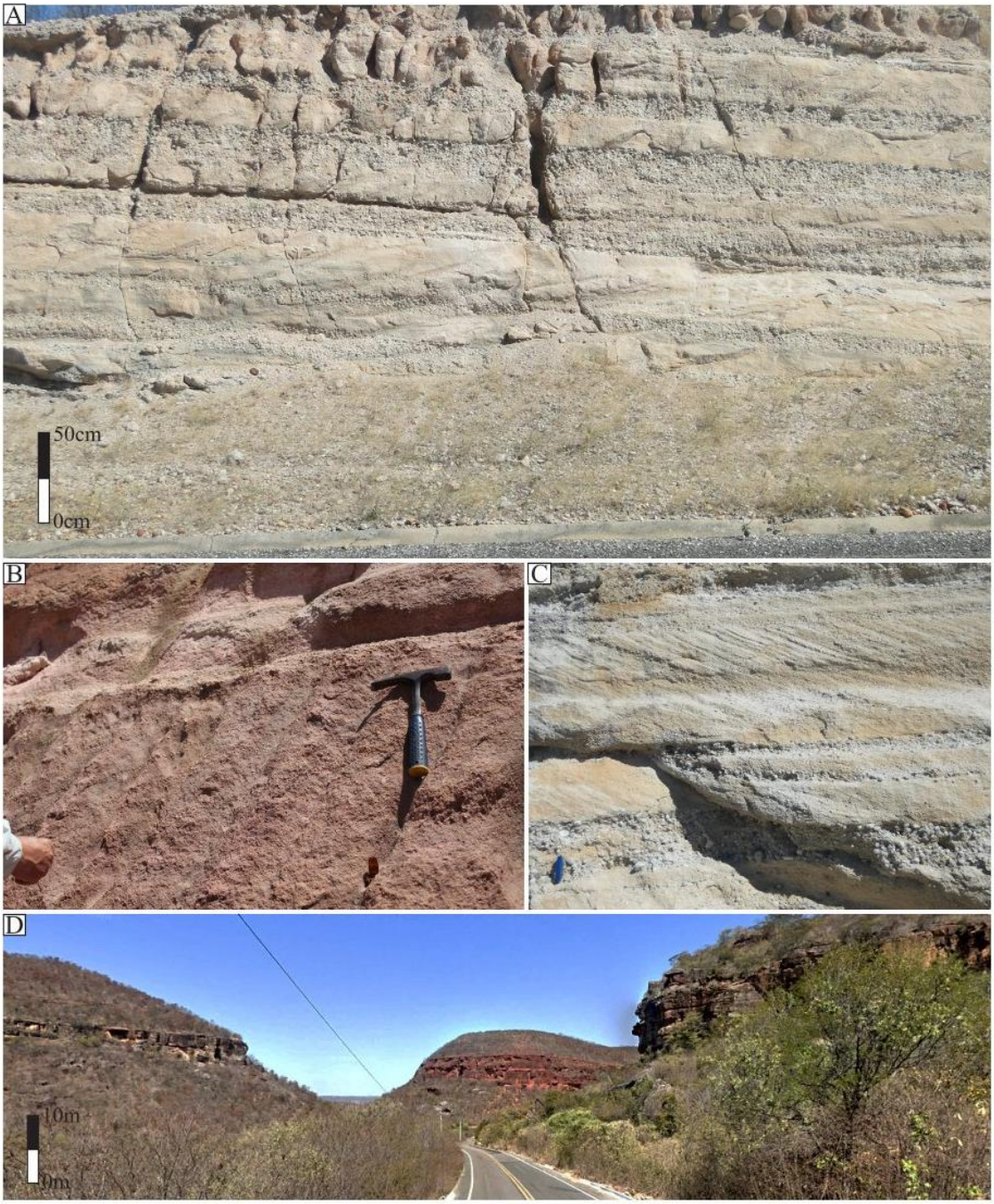

Figure V.5- Tabular cross-stratified sandstone lithofacies aspects. A) Tabular bed geometries. B and C) Tabular cross-stratified sandstone interbedded with massive sandstone and conglomerate facies. D) The panoramic section depicts the wide continuity of the tabular cross-bedding sandstone beds. The hammer length is 30 cm, and the switchblade length is 8 cm.

Interpretation

These facies are interpreted as forming by the migration of straight-crested dunes or bars deposited under conditions of a lower flow regime (Collinson, 1996; Miall, 1996; Hjellbakk, 1997; Capuzzo & Wetzel, 2004). The predominance of tabular beds laterally continuous for hundreds of meters suggests sand deposition from unconfined flows on

planar surfaces. Planar foresets geometry and the grain size indicate deposition during periods of low water level or waning flow in channels (Hjellbakk, 1997). The deposition of large-scale tabular crossbedding suggests that these larger sets are a product of bar migration (Cant & Walker, 1976; Sharma et al., 2002). The minor groups of these facies show a divergent paleocurrent orientation, which most likely indicates that they were deposited in front of or on the lower flanks of oblique bars present in major channels and transverse bars of subsidiary channels. These areas had avalanche faces of bedforms that were oblique to the predominant orientation of the channel tract (see. Cant & Walker, 1976).

4.1.4 Planar horizontally stratified sandstone

These facies encompass 5% of the studied sections (Figs. V.2 and V.6). It consists dominantly of low-angle (<10°) to horizontally stratified lithoarenites compounds by medium- to coarse-grained sandstone, commonly interbedded with cross-stratified sandstone (Figs V.6A and B). The bed geometry is tabular with parallel bounding surfaces locally defined by thinly interbedded mudrocks (Fig. V.6C). The exposed bounding surfaces can be traced for tens of meters. The planar-stratified sandstone is in single beds of 0.1-0.8 meters thick with tens of meters wide (Figs. V.6D and E). Horizontal stratification is often laterally traced into areas of massive sandstone in places with disturbed stratification or convolutions. The lithofacies are moderately well-sorted and texturally mature. The rock framework exhibits angular to subangular grains with low sphericity, predominating medium- to coarse-grained sand. The grains are predominantly quartz, metamorphic, sedimentary rock fragments, and secondarily feldspars and heavy minerals.

Interpretation

These sediments were deposited by bed-load turbulent migration of low-amplitude bedforms (Bridge & Best, 1988; Paola et al., 1989; Hjellbakk, 1997). Planar traction structures in these deposits form by a persistently bed-load high sediment concentration.Bed-load layers beneath highly concentrated suspended loads receive most sediment from suspended sediment clouds, which collapse abruptly rather than gradually as flow intensity decreases (Lowe, 1988; Hjellbakk, 1997). A sediment fallout rate exists where input exceeds the bed-load layer's ability to move and sort the falling debris (Hjellbakk, 1997). The absence of laminations may indicate that the sediment fallout rate

was high enough to prevent sorting mechanisms. Therefore, these facies are interpreted as the deposition record on large, flat bar-top areas controlled by vigorous currents (Hjellbakk, 1997).

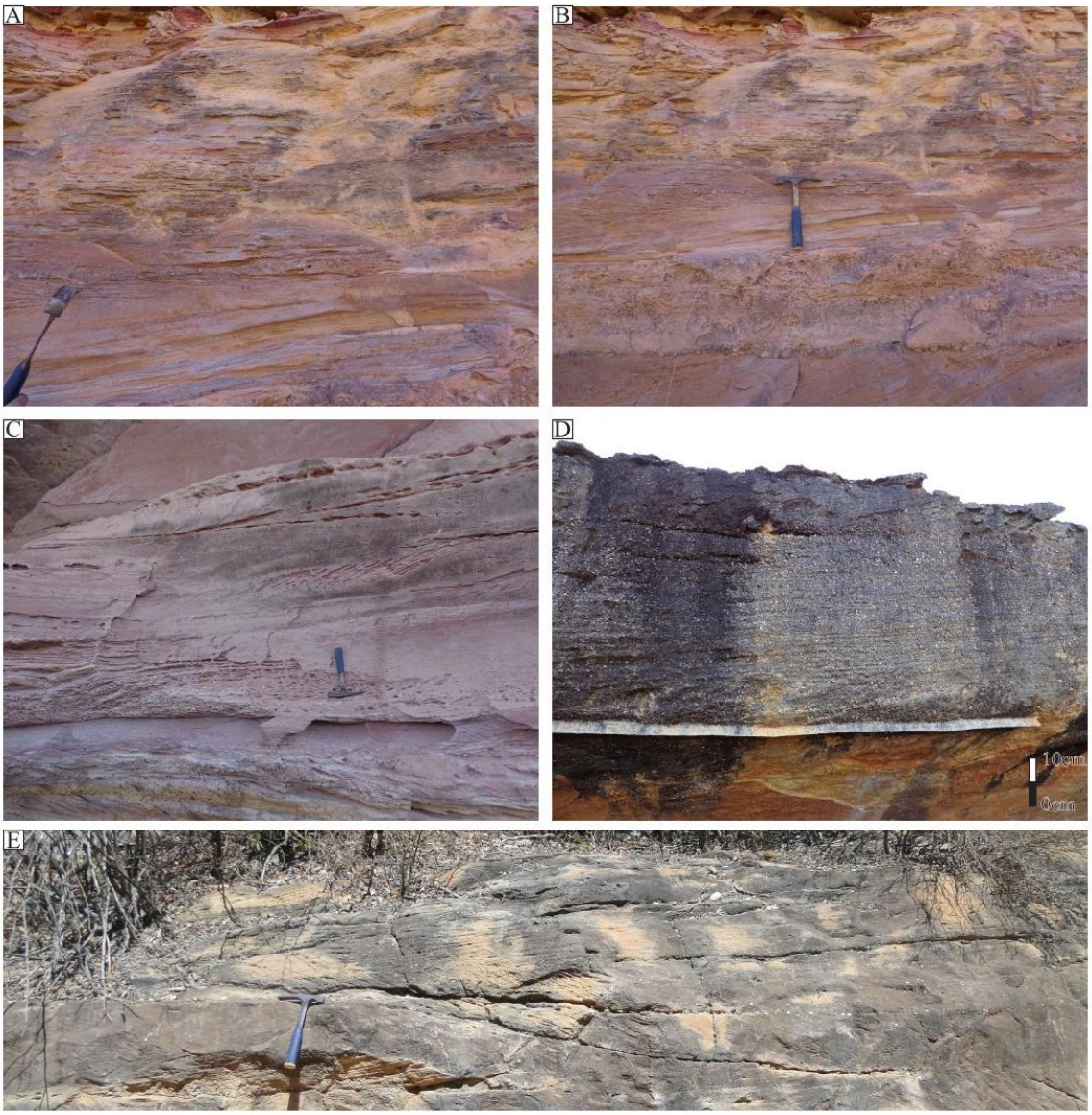

Figure V.6- Planar horizontally stratified sandstone lithofacies aspects. A and B) Low-angle (<10°) to horizontally stratified lithoarenites. C) Planar horizontally stratified sandstone interbedded with cross-stratified sandstone horizons. D) Solitary set of planar-stratified sandstone. E) The planar-stratified sandstone tens of meters broad continuity. The hammer length is 30 cm.

4.1.5 Massive sandstone

These facies comprise 6% of the measured sections (Fig. V.2). It includes massive medium- to coarse-grained sandstone beds without apparent organization (Fig. V.7). The thickness of these lithoarenites single beds varies between 0.4 and 1.5 m (Figs. V.7A to D). The contacts between the beds are mainly flat/non-erosional, and these facies are commonly interbedded with conglomerates (Figs. V.7B and C). The lithofacies are

moderately well-sorted and texturally mature. The rock framework exhibits angular to subangular grains with low sphericity, predominating medium- to coarse-grained sand (Fig. V.7E). The grains are predominantly quartz, metamorphic, igneous, sedimentary rock fragments, and secondarily feldspars and heavy minerals.

Figure V.7- Massive sandstone lithofacies aspects. A to D) Varieties of massive sandstone thickness beds observed in outcrops interbedded with massive conglomerate horizons. E) Detail of massive sandstone lithofacies clasts morphologies. The hammer length is 30 cm.

Interpretation

Massive beds may form in response to depositional processes or by post-depositional deformation. In the present interpretation, deformational processes are considered less important based on the absence of stratification or the remaining transitional structures to the massive sandstone. Minor velocity changes may reduce dispersive stress and turbulence below a critical value, allowing an accelerated bedload deposition (Lowe 1982). Hence, the massive beds are interpreted as resulting from the

transport and deposition of a sudden discharge of sediments by fast-moving flow, which hindered the effectiveness of hydraulic sorting procedures (Hjellbakk, 1997).

4.1.6 Undulatory laminated, planar cross-stratified, and rippled sandstone

These facies correspond to 2% of the total succession and usually overlie cross-bed sandstone and conglomerates (Figs. V.2 and V.8). The beds are fine- to medium-grained sandstone compounds, generally well-sorted and interlaminated with thin mudrock horizons (Fig. V.8A and B). It occurs as thin wedge-shaped bodies that pinch out laterally within tens of meters. These facies contain asymmetrical ripple marks and flat bedding (Figs. V.8C and D). Subordinately alternations of parallel lamination with ripple cross-laminated sets and asymmetrical ripple marks are present (Figs. V.8A and B). Solitary sets of small-scale cross-laminae sandstone occur intercalated with the laminated sandstones and build up 0.2-1.2 m thick cosets superimposed on cross-bed sandstone (Fig. V.8E).

Interpretation

The asymmetrical current ripples and cross-lamination draped by clay lamination indicate deposition by alternating subaqueous traction and suspension processes (Miall, 1996; Ghazi & Mountney, 2009). The characteristic sedimentary structures and the grain size range indicate formation by processes operating in the lower flow regime lower to middle part (Hjellbakk, 1997). Under controlled sediment supply conditions, sinuous trains of asymmetrical ripples migrated down current in a lower flow regime of low intensity, resulting in these facies (Allen, 1963; Ghazi & Mountney, 2009). The structures suggest deposition over bar-top during periods of low water level or waning flow in channels (Hjellbakk, 1997).

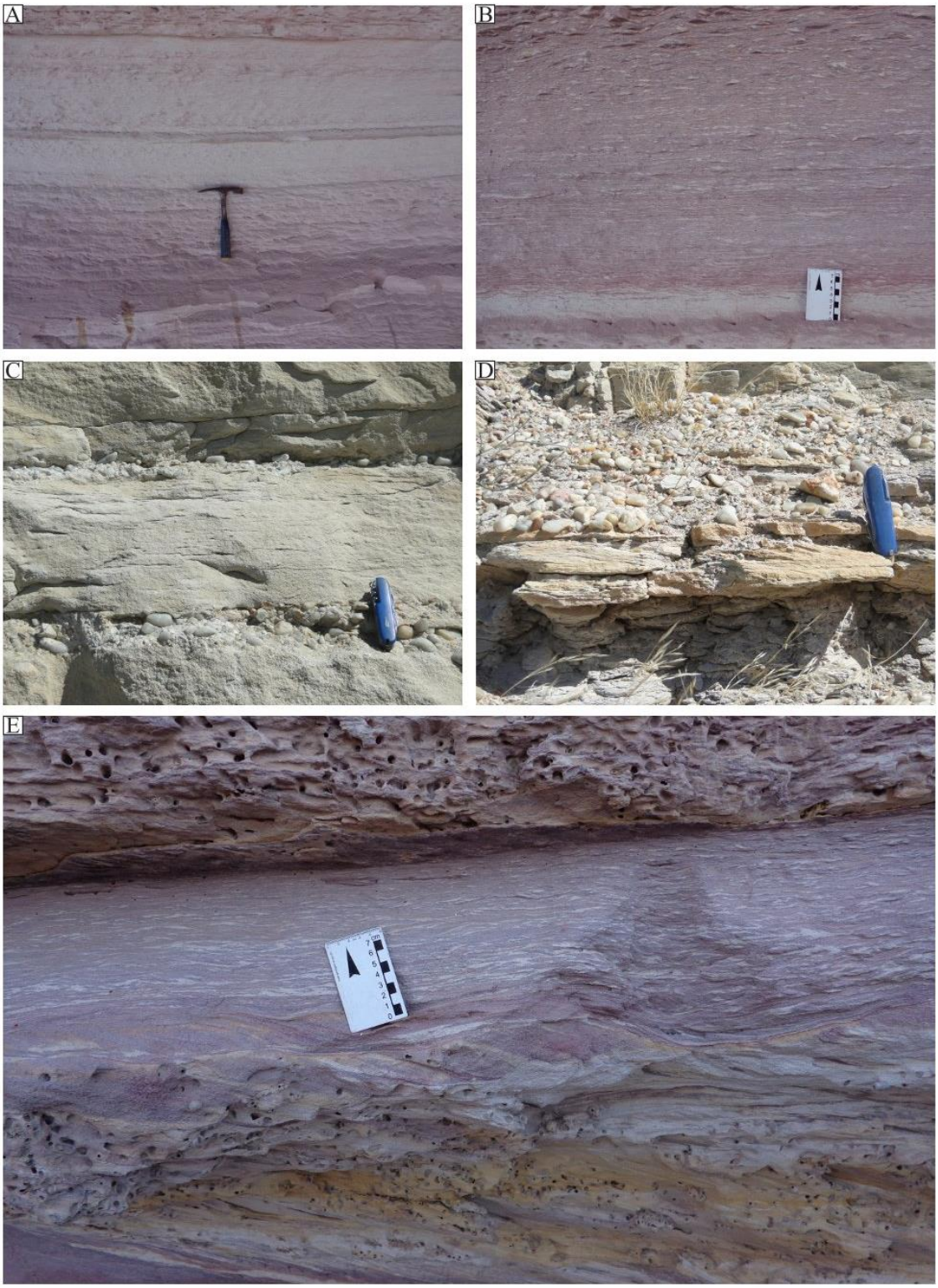

Figure V.8- Undulatory laminated, planar cross-stratified, and rippled sandstone lithofacies aspects. A and B) Fine- to medium-grained sandstone beds show undulatory laminated to ripple marks structures interbedded with siltstone lenses. C and D) Fine- to medium-grained sandstone beds exhibit asymmetrical ripple marks and flat bedding interbedded with massive conglomerates. E) Solitary sets of small-scale cross-laminae sandstone intercalated with laminated and crossbedded sandstones. The hammer length is 30 cm, and the switchblade length is 8 cm.

4.1.7 Massive to crossbedded conglomerates and sandstone

These facies comprise 1% of the measured sections (Fig. V.2). It includes horizontally stratified sandstone, crossbedded sandstone and conglomerate, massive clast-supported conglomerate, and massive sandstone (Fig. V.9). A coarsening upward pattern marks the transition from sandstone to conglomerate beds with oversized clasts (Figs. V.9A to C). The lithosomes predominately consist of lenticular beds (~0.2-0.4 m thick) with erosional bases of massive clast-supported conglomerates interbedded with massive to crossbedded sandstones (Figs. V.9D and E). Gradational grain size changes delineate the lens boundaries. Clast-supported conglomerate lenses truncate and superimposed on one another and over sandstone beds (Fig. V.9F). In primary lenses, the long axis of gravel clasts is inclined towards the lens center, forming a concave-up pattern (Fig. V.9G). The lowermost conglomerate lenses cut into antidunes bedform sandstones preserved morphologies (Fig. V.9G). The wave crests of antidune beds display downflow, while the internal lamination shows upflow or offsets. Wavelengths range from 0.2 to 0.4 m in pebbly sandstones, with amplitudes ranging from 0.1 to 0.3 m (Fig. 9G). The beds pinch and swell (Fig. V.9). Thin layers (<0.5 m) of medium to very coarse sand at the base of most conglomerate lenses show wavy bedding, lens-like structures with erosional bases, and convex upward bedding (Fig. V.9G). The lens-like structures are sandwiched between slightly wavy sandstone beds. Discontinuous beds of planar horizontally stratified sandstone are up to 0.2 m thick. Large clasts (>0.3m) disturb the bedding (Fig. V.9). The measured sections are parallel to the main channel flow. Locally, muddy to silt intraclasts were identified within basal conglomeratic beds (Fig. V.9G).

Interpretation

Basal sandstone facies with wavy bedding, lens-like structures with erosional bases, and convex upward bedding are interpreted as antidune deposits (Cheel, 1990; Russell & Arnott, 2003; Lang & Winsemann, 2013; Cartigny et al., 2014). Wavy to slightly wavy stratification may indicate a high rate of aggradation by stable quasi-steady supercritical flows, allowing for the preservation of both the stoss and lee sides of stable antidunes (Ito and Saito, 2006; Ito, 2010; Lang & Winsemann, 2013). Antidune waves in density flow form interfacial instabilities at the boundary between the flow and the ambient water or, in stratified density flows, at internal density interfaces (Prave & Duke, 1990; Mulder et al., 2009; Ito, 2010). Lateral truncations, Sub-horizontal stratification, and low-angle internal cross-stratification in sandstone indicate deposition by upflow- or

downflow-migrating stable antidunes, causing discontinuous aggradation (Fielding, 2006; Duller et al., 2008; Ito, 2010; Lang & Winsemann, 2013). The antidunes wavelength suggests this bedform's genesis is related to a stratified density flow's thin basal high-density layer (cf. Lang et al., 2017).

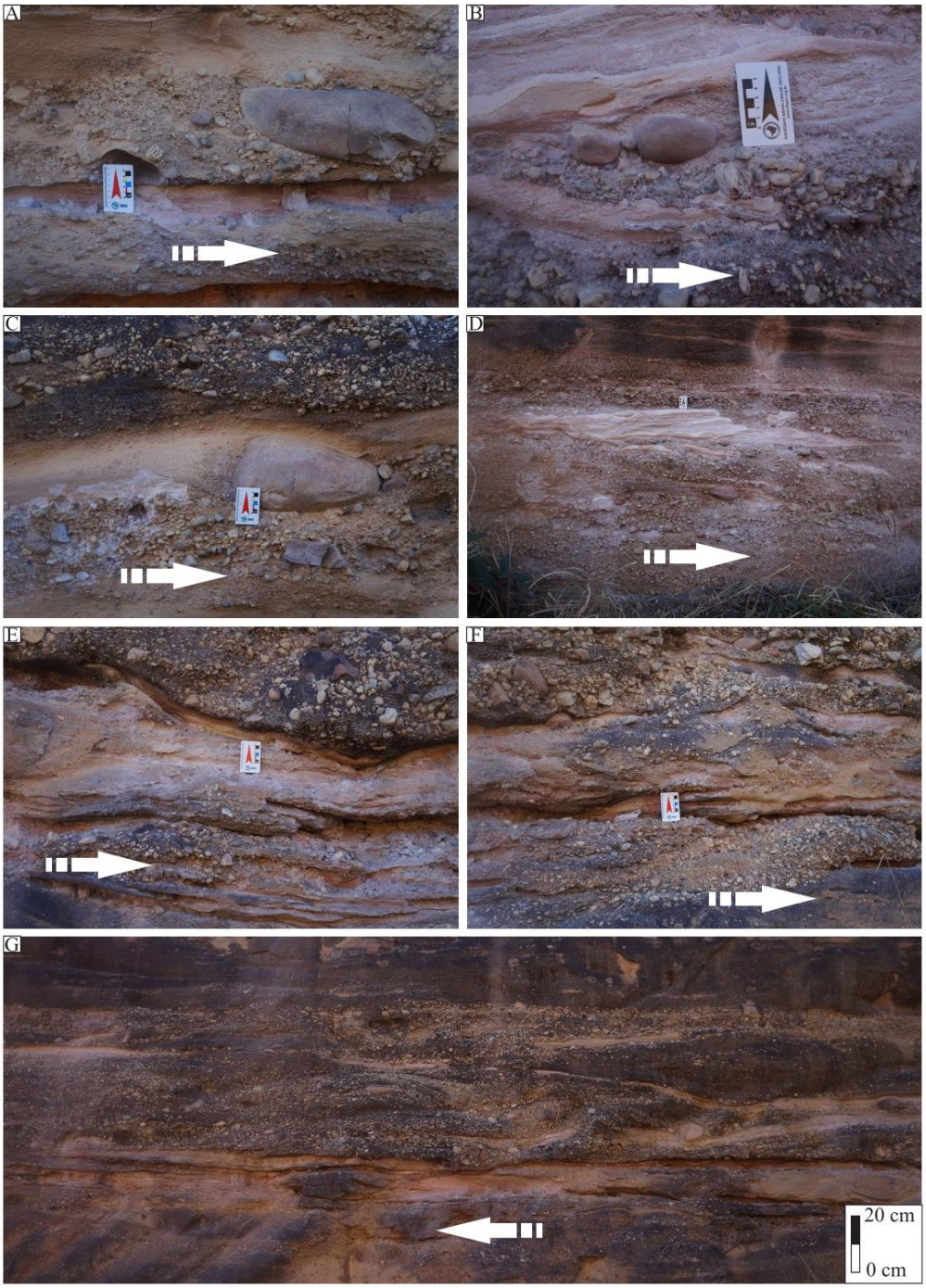

Figure V.9- Massive to crossbedded conglomerates and sandstone lithofacies aspects. A to D) Massive to crudely stratified clast-supported conglomerates interbedded with sandstone and siltstone lenses. Oversized clasts are present and disturb the coarsening upward pattern. E to G) Clast-supported gravel lenses and massive to weakly planar laminated sand and gravel conglomerate lenses truncate and superimposed on one another and over sandstone beds. Note the preserved antidune wave crests at the bed bottom in Fig. 9G. White arrows represent paleoflow direction.

Conglomeratic deposits are dominated by lenses interpreted as structures formed by antidunes developing and changing during the growth, breaking, and dissipation of stationary water-surface wave trains (Froude et al., 2017). The lenses and associated strata described above are comparable to gravel and sand-bed structures developed from stationary and upstream migrating waves in flume and field experiments, corroborating the diagnostic value of these structures (cf. Alexander et al., 2001; Yokokawa et al., 2010; Froude et al., 2017). This confirms that even where the antidune bedforms are not preserved, diagnostic structures may be recognized, and lens architecture can be related to antidunes in sandstone and conglomeratic deposits (cf. Froude et al., 2017). These facies are interpreted as the record of a flash flood event, and deposition is associated chiefly or entirely after the peak flow (cf. Froude et al., 2017).

4.1.8 Sigmoidal cross-stratified sandstone

These facies correspond to 1% of the total succession and usually overlie cross-bed sandstone (Fig. V.2). The beds are composed of fine—to medium-grained sandstone, generally well-sorted. Sigmoidal bedding shows normally graded foresets in single or multiple sets with topset preservation (Fig. V.10). These sandstones have tabular geometries in flow-parallel sections (Fig. V.10). The tabular cosets are usually more than 50 m long with thicknesses up to 2 m (Fig. V.10A). Sets are generally smaller, 10 to 130 cm thick (Fig. V.10B). Typically, the foresets angle slope varies between 15 ° and 30 ° (Fig. V.10). It is commonly observed that planar strata are transitional up- and down-current to sigmoidal cross-strata (Fig. V.10B).

Interpretation

Preserving sigmoidal cross-bedding structures within cross-bedded and flat-stratified sandstone intervals reflects fluctuating flow conditions (Fielding, 2006). These facies are interpreted as deposited by washed-out dunes and humpback dunes, related to transitory conditions between dune to upper plane-bed stability fields (Røe, 1987; Fielding & Webb, 1996). Flat-laminated top-set preservation implies formation under rising flow power conditions (Fielding, 2006). These bedforms are linked to settling large volumes of sediments transported by bed- and suspended-load (Røe, 1987; Fielding, 2006).

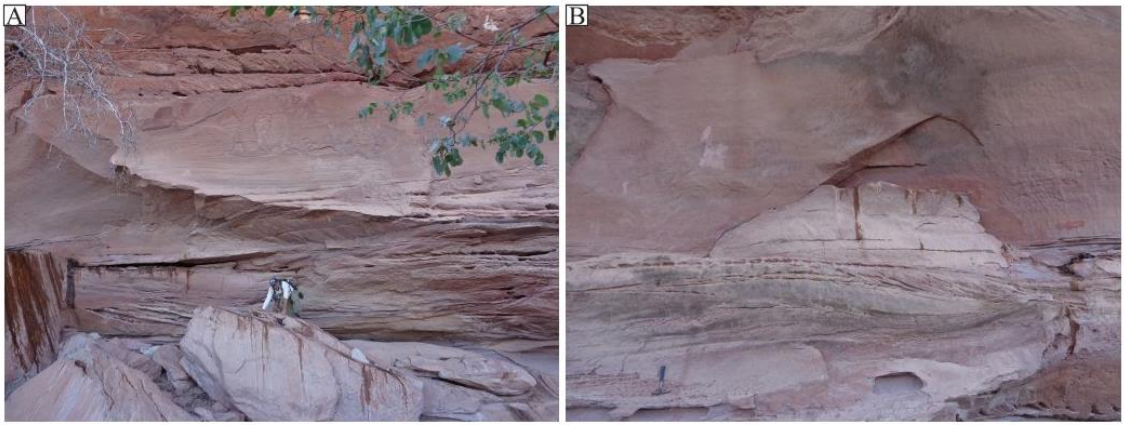

Figure V.10- Sigmoidal cross-stratified sandstone lithofacies aspects. A and B) Fine- to medium-grained sandstone shows compound vertical stacking by cross-stratified overlain by sigmoidal cross-stratified set, passing laterally to low-angle cross-stratification. Planar horizontally stratified sandstone and cross-stratified sets cover the sigmoidal beds. Note a 1.70 m-tall person for scale. The hammer length is 30 cm.

4.2 FLUVIAL DEPOSITIONAL ARCHITECTURE

4.2.1 Hierarchization of bounding surfaces

Seven different bounding contacts are defined for the measured successions (Fig. V.11). These contacts have been interpreted as bounding surfaces of five separate orders (1st to 5th). The theoretical framework proposed by Miall (1988a, 1988b, 1992) for developing this methodology has been used as a general guideline in discussions regarding bounding surfaces. Nevertheless, the interpretation of these surfaces in geological literature is primarily based on works developed within fluvial systems, significantly different from pre-vegetation systems. Consequently, understanding characteristics such as high discharge rates and denudation of pre-vegetation drainage becomes crucial, in addition to considering these factors when discussing the significance of individual bounding surfaces and their temporal relationships.

4.2.1.1 1st-Order Surfaces

These represent laterally continuous tabular surfaces for tens of meters with nonexistent to limited erosion, separating layers composed of sets of cross-bedding (Fig. V.11). They symbolize the ongoing migration of bedforms, exhibit minimal morphological variations, and remain within constant flow regimes and sedimentary conditions (Miall, 1988a, 1988b, 1992). Allen (1983) defined 1st-order surfaces as contacts separating genetically related sedimentary rock layers within migrating macroforms.

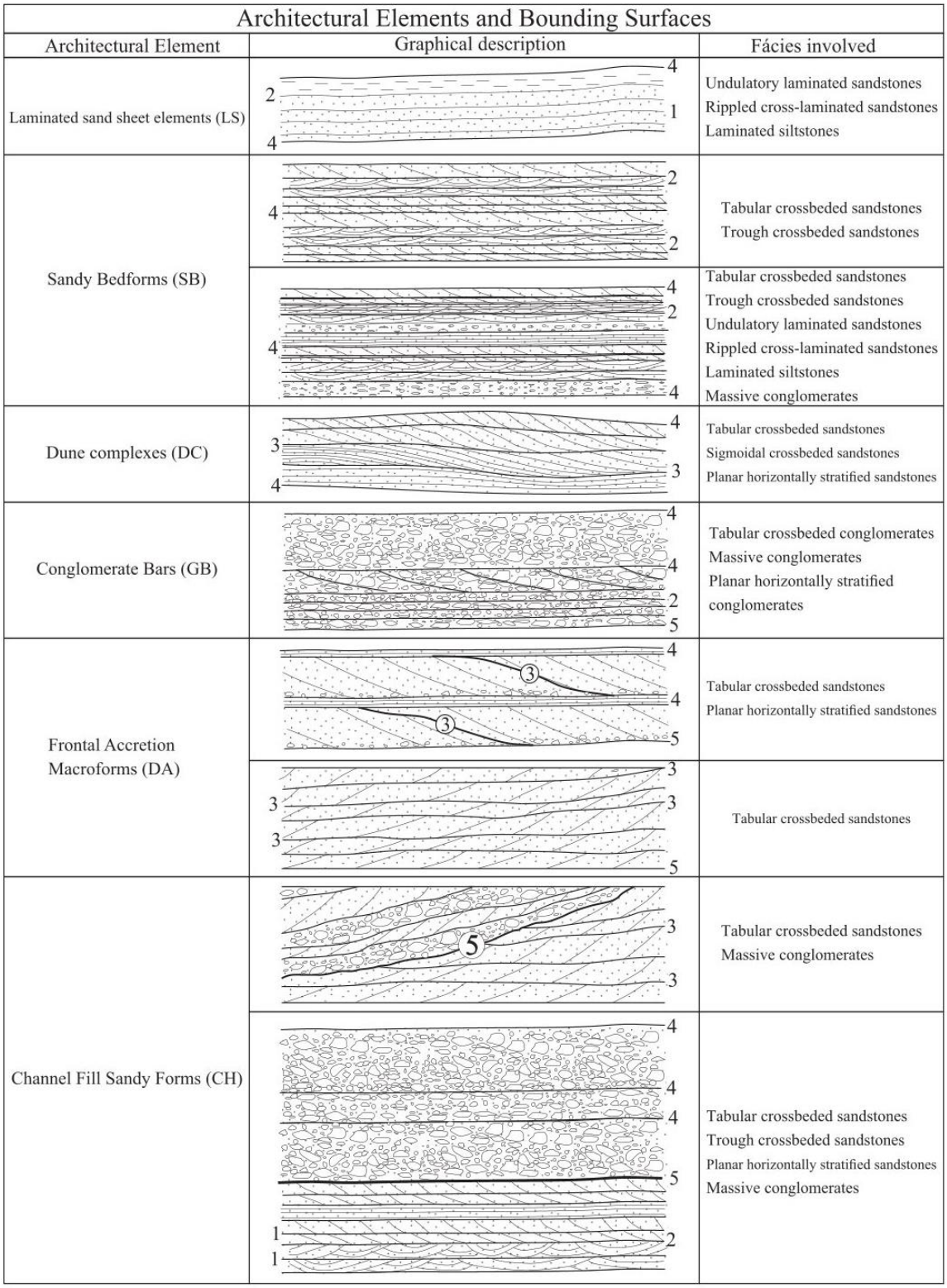

Figure V.11- Summary of architectural elements recognized within the Ipu Formation.

4.2.1.2 2nd-Order Surfaces

They are characterized by laterally continuous flat to undulating surfaces, separating cosets of cross-bedding. The lithofacies above and below the surface differ but generally lack significant truncations of stratification or other erosion evidence (Fig. V.11). These surfaces result from changes in flow regime and do not involve a significant depositional hiatus (Miall, 1988a, 1988b, 1992). According to Miall (1988a, 1988b, 1992), 2nd-order surfaces in fluvial systems are produced by events in which a large amount of debris is transported over short intervals, indicating flow regime or flow direction changes. Standard processes in pre-vegetation fluvial systems where small precipitation events could lead to large flash floods (Hjellbakk, 1997).

4.2.1.3 3rd-Order Surfaces

Correspond to two different surface types. The first type represents planar contacts with limited erosion, separating individual crossbed sandstone sets into major macroforms and surfaces separating minor macroforms like simple bars and laminated sand sheet elements (Fig. V.11). The second type is identified as a reactivation surface within simple bars. These erosional surfaces within macroforms dip at a low angle and truncate the underlying stratification. They represent small incisions produced by the lateral migration of high-energy fluvial channels during a flood cycle (Miall, 1988a, 1988b; Hjellbakk, 1997). According to Miall (1988a, 1988b), 3rd-order surfaces are erosional, have a low dip angle, and generally truncate adjacent cross-strata. They indicate changes in macroform direction, but the facies assemblages above and below exhibit similar characteristics (Miall, 1988a, 1988b).

4.2.1.4 4th-Order Surfaces

Two types of contacts have been recognized as 4th-order surfaces (Fig. V.11). The first type consists of erosive, concave-up surface bounding sandy units and conglomerate fill minor channel deposits. The second type corresponds to a flat surface bounding individual complex bar. They represent incisions produced by the lateral migration of high-energy fluvial channels and the migration of macroforms during flood periods (Miall, 1992). Miall (1988a, 1988b) defines 4th-order surfaces as boundaries between architectural elements of distinct lithosomes. However, Hjellbakk (1997) argues that the definition of this type of surface is ambiguous and could fit into another context, being defined as an erosional boundary separating architectural elements generated by similar

processes. Here, we use it to separate architectural elements created by similar and different processes.

4.2.1.5 5th-Order Surfaces

The 5th-order contact corresponds to large, nearly planar erosive surfaces laterally continuous for hundreds of meters, not associated with low and moderate deep incisions (Fig. V.11). These surfaces are always covered by large-scale conglomerate layers, cutting through complexes of sandy bars. The aggradation of the fluvial system reduces the gradient within areas occupied by interlocking floodplains, causing the migration of the channel belt to steeper slopes and generating this surface (Hjellbakk, 1997). According to Miall (1988a, 1988b), the 5th-order contact would correspond to critical laterally extensive erosive surfaces, generally not associated with deep incisions. These surfaces bound large sand bodies, such as channel-fill complexes.

4.2.2 Architectural Elements

Six architectural elements have been interpreted based on sediment textures, sedimentary structures, geometry, paleocurrent indicators, and lateral and vertical arrangement of lithofacies (Fig. V.11). The recognized architectural elements are separated by the definition and hierarchization of bounding surfaces and have a hierarchical account whereby smaller elements are nested and stacked within more significant elements. The defined architectural element's hierarchical description from minor to major corresponds to 1) Laminated sand sheet elements (LS), 2) sandy bedforms (SB), 3) dune complexes (DC), 4) conglomerate bars (GB), 5) downstream accretion macroforms (DA), and 6) channel fills (CH) (Fig. V.11).

4.2.2.1 Laminated sand sheet elements (LS)

These elements comprise tabular sheets of fine- to medium-grained sandstone, generally well-sorted and interlaminated with thin mudrock horizons (Fig. V.12). It involves undulatory laminated and rippled cross-laminated sandstone facies. The lamination is usually laterally continuous for about 100 m (Fig. V.12). Structureless or faintly parallel laminated sandstone rarely occurs. This element is in the basal and medium portions of the measured successions. Its principal occurrence is in the upper part of the fining-upward cycles, commonly associated with elements SB and DA (Fig. V.12). The LS elements are bounded at their bottom and top by sharp horizontal fourth-order

surface contacts (Fig. V.11). Typically, LS elements are up to 1.2 m thick and hundreds of meters wide and long (Fig. V.12).

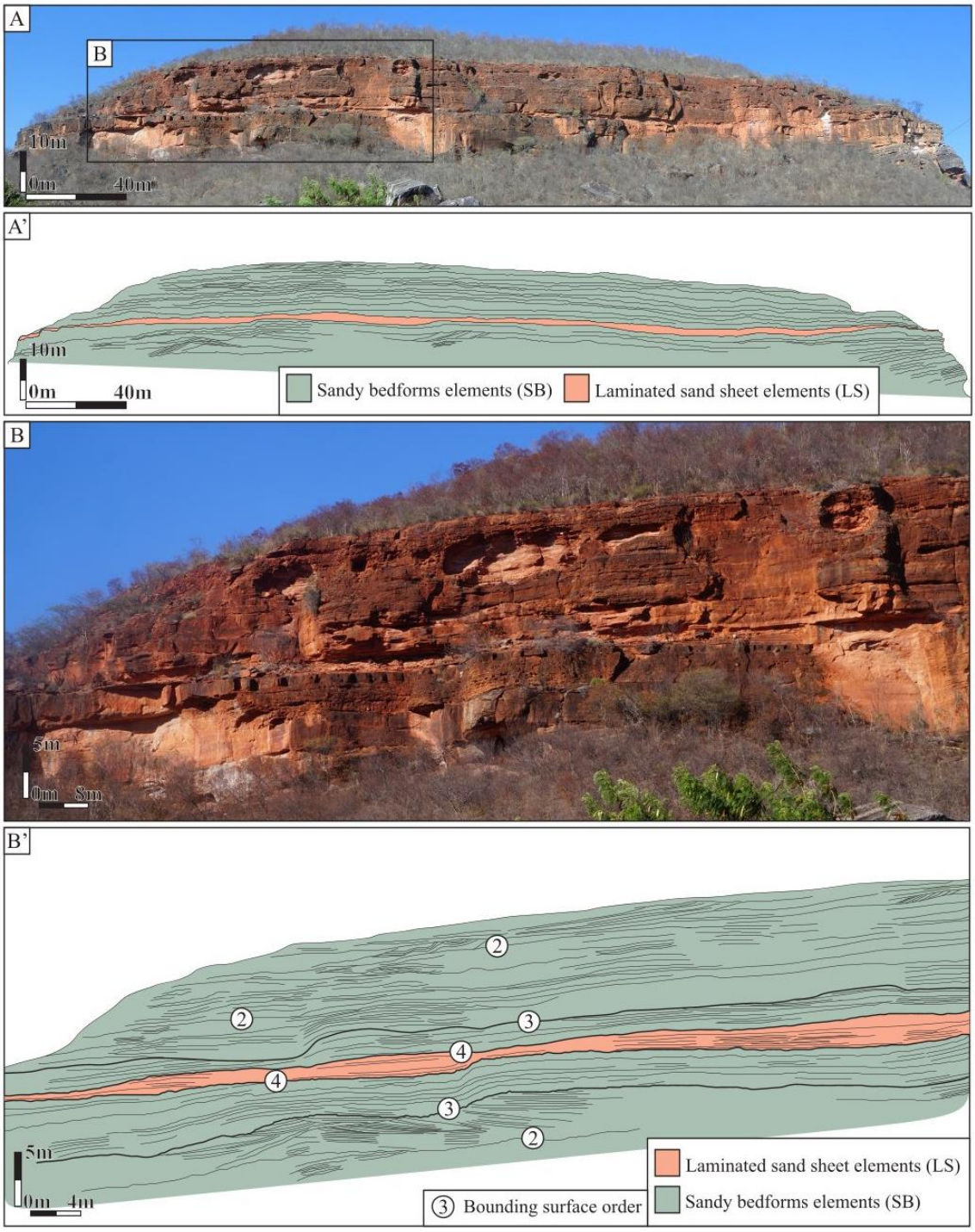

Figure V.12- A and interpreted panel A') Photomosaics show the architectural elements interpretation: typical intercalation of elements of sandy bedforms (SB) and laminated sand sheets (LS). B and interpreted panel B') Detail of A.

Interpretation

The thin, sheet-like geometry, small-scale sedimentary structures, and fine-grained lithology suggest deposition in bar-top settings (Miall, 1985; Ghazi & Mountney, 2009). These elements accumulated over a pre-existing vast flat topography in areas of flow expansion, commonly at channel junctions or places where channels widen during periods of low water level or waning flow in channels (cf. Cant and Walker, 1978; Hjellbakk, 1997). The genesis of this element in the measured sections may be attributed to deposition by alternating subaqueous traction and suspension processes. The presence of laminations and small-scale structures indicates that the sediment fallout rate was lower than the sorting mechanisms. The close vertical association of the LS and DA elements discards the deposition by overbank sheet flows (cf. Olsen, 1988).

4.2.2.2 Sandy Bedforms (SB)

Sandy bedforms are characterized by laterally continuous tabular external morphology for hundreds of meters, with flat erosional surfaces (Fig. V.13). Two variations of this element have been identified. The first variation consists of simple sandy bars composed solely of tabular or trough crossbedding with thicknesses of up to 2.5m (Fig. V.13). The second variation corresponds to complex bars consisting of massive conglomerate layers, cross-bedded sandstone, planar cross-bedded sandstone, sandstone with asymmetric ripple marks, and laminated siltstone, with thicknesses of up to 5m (Fig. V.12). Conglomeratic lags are at the base of cross-stratified sets or parallel to the stratification. Cross-stratified sandstone sets from 0.3 to 0.80 m contain well-developed normal grading within the foresets, varying from very coarse- to medium-grained sand. Massive conglomerates or conglomeratic sandstone lenses overlie irregular erosive surfaces at the base of the elements (Fig. V.11). Locally channelized basal erosional surfaces are identified in the two SB element variations.

Interpretation

These simple sandy bars are interpreted as deposits generated by periodic to quasi-periodic migration of bedforms (Røe, 1987; Hjellbakk, 1997). This element is primarily formed by local coalescence and vertical aggradation of 2D and 3D dunes (Hjellbakk, 1997). Small- to medium-scale planar and trough cross-stratified cosets, separated by laterally extensive surfaces, indicate downstream migration and climbing of 2D and 3D subaqueous dunes (Miall, 1996).

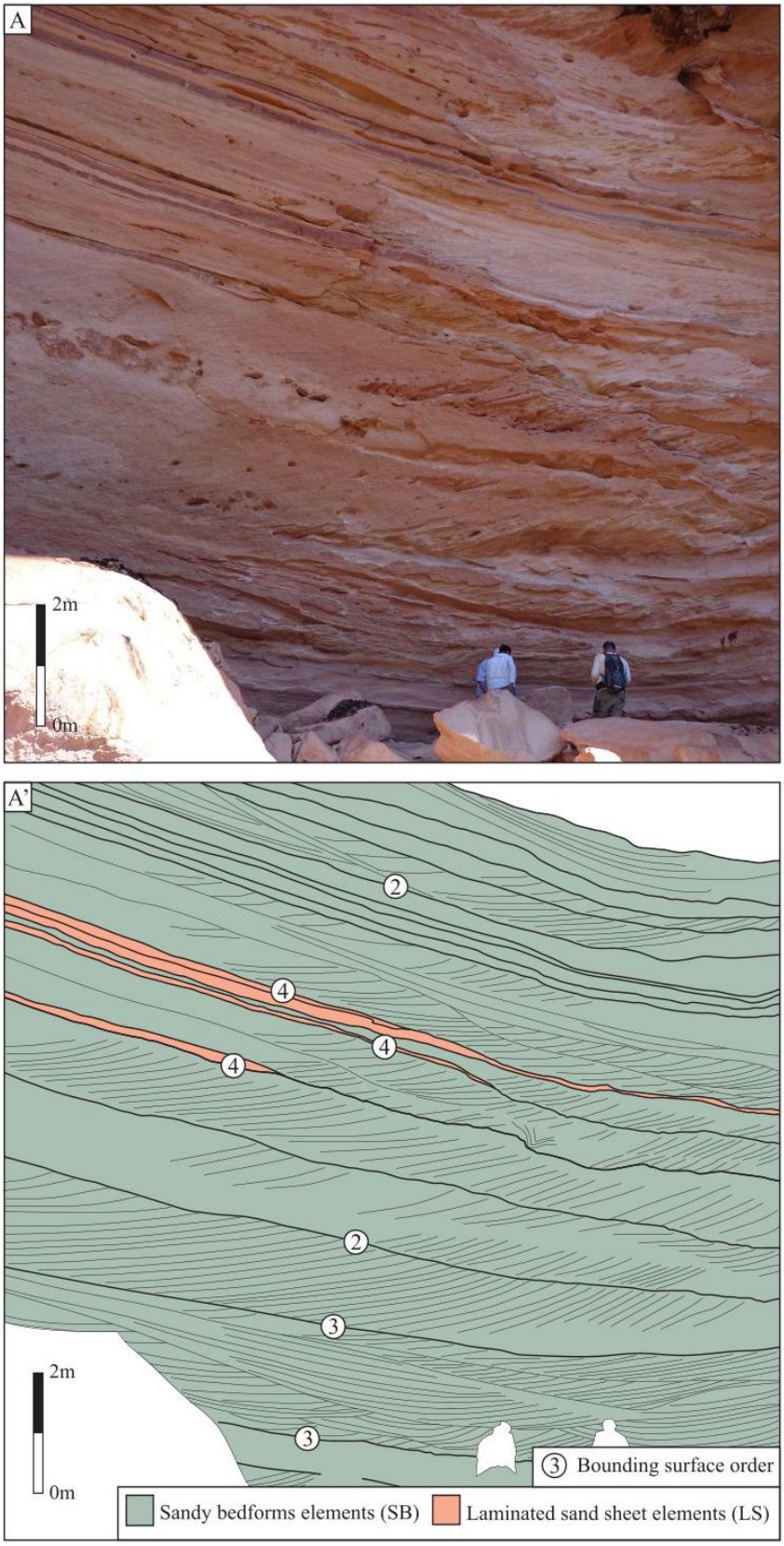

Figure V.13- A and interpreted panel A') Photomosaic of the architectural elements interpretation: sandy bedform and laminated sand-sheet elements. The outcrop is organized into stacked multi-story cross-stratified sandstone beds comprising sandy bedform elements (SB) bounded by laterally extensive laminated sand sheet elements (LS) located at the SB element top.

4.2.2.3 Dune complexes (DC)

The DC architectural element comprises tabular beds with flat to undulating top and base, up to 10 m thick, and are laterally extensive for hundreds of meters (Fig. V.11). It consists of medium- to very coarse-grained sandstones and conglomerates with various sedimentary structures (Figs. V.14 and V.15). Sigmoidal and tabular cross-strata comprise the most common lithofacies within these deposits and occur as small- to medium-scale stacked sets, 0.2 to 2 m thick, separated by planar to slightly undulated surfaces (Fig. V.15). Planar horizontally stratified sandstone sets, 0.15 to 0.30 m thick, exhibit thin, slightly undulated laminations. Lenses of massive sandstones and conglomerates, up to 0.3 m thick, are also present (Fig. V.14). A fining upward pattern marks the transition from conglomerate to sandstone beds with oversized clasts at the element base (Fig. V.14). The long axis of gravel clasts is inclined towards the main flow direction (Fig. V.14).

Interpretation

The DC element is interpreted as formed by the local coalescence and vertical aggradation of dunes on a wide and flat channel floor, which is washed out when flow velocity increases and generates a group of sedimentary structures deposited in transitional conditions between the dune and upper-plane bed stability fields (cf. Fielding, 2006). Preserving topsets, foresets, and bottom sets within sigmoidal bedforms is linked to high sedimentation rates under transcritical flow conditions. Undulating bedforms and conglomerate beds are antidune deposits generated under supercritical flows (Cartigny et al., 2014).

4.2.2.4 Gravel Bars (GB)

GB elements are characterized by a laterally continuous tabular external morphology for hundreds of meters, with a flat to undulating erosional base surface (Fig. V.16). This element consists of simple conglomerate bars composed solely of massive conglomerates or coalescence of stratified conglomerates with thicknesses of up to 3 meters. Massive sandstone lenses are 0.35 to 0.50 m thick and present in GB tops and inclined accretionary surfaces (Figs. V.16).

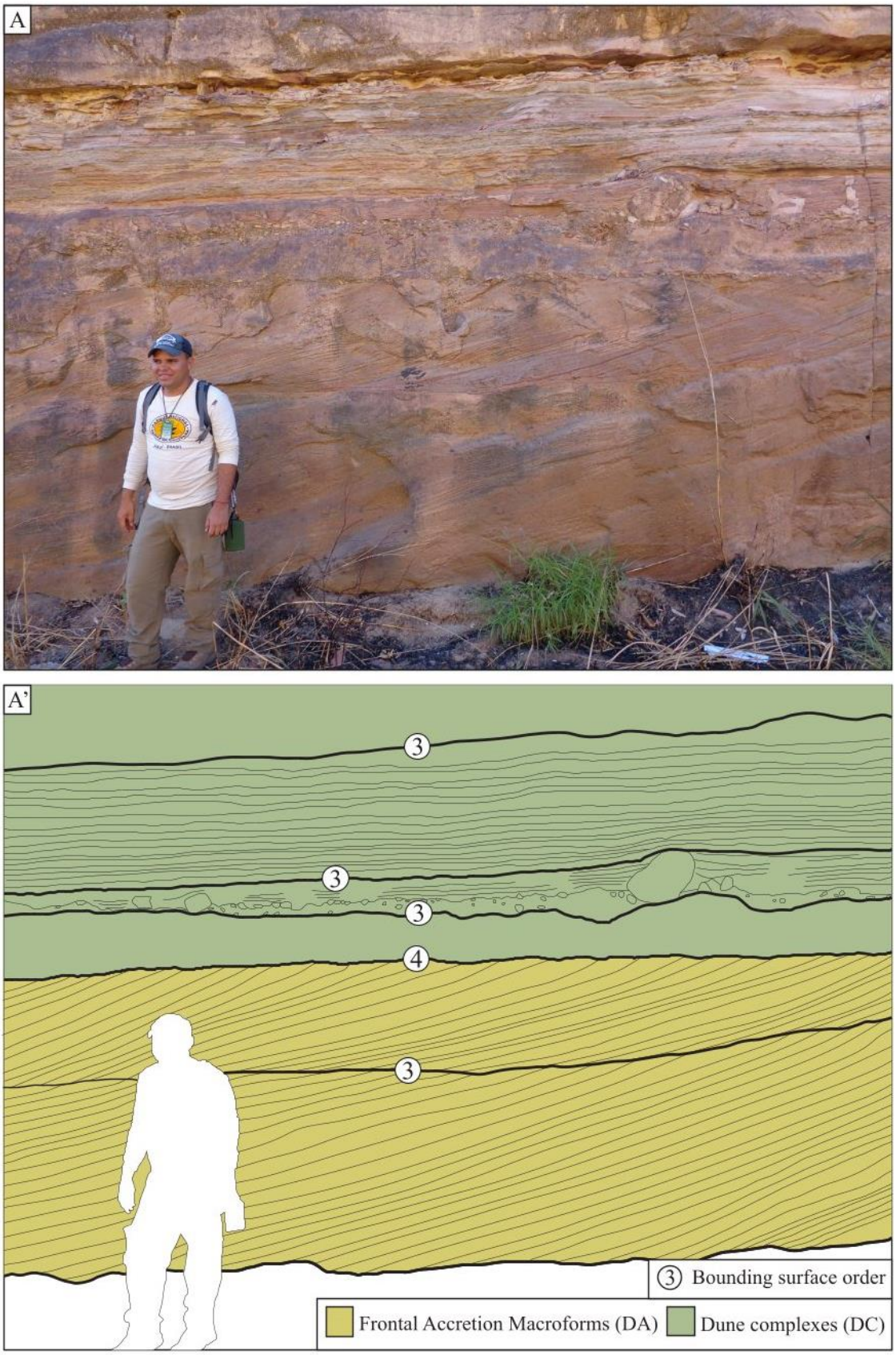

Figure V.14- A and interpreted panel A') Photomosaic of the architectural elements interpretation shows vertical stacked of simple frontal accretion macroform (DA) and dune complexes (DC). Note a 1.70 m-tall person for scale.

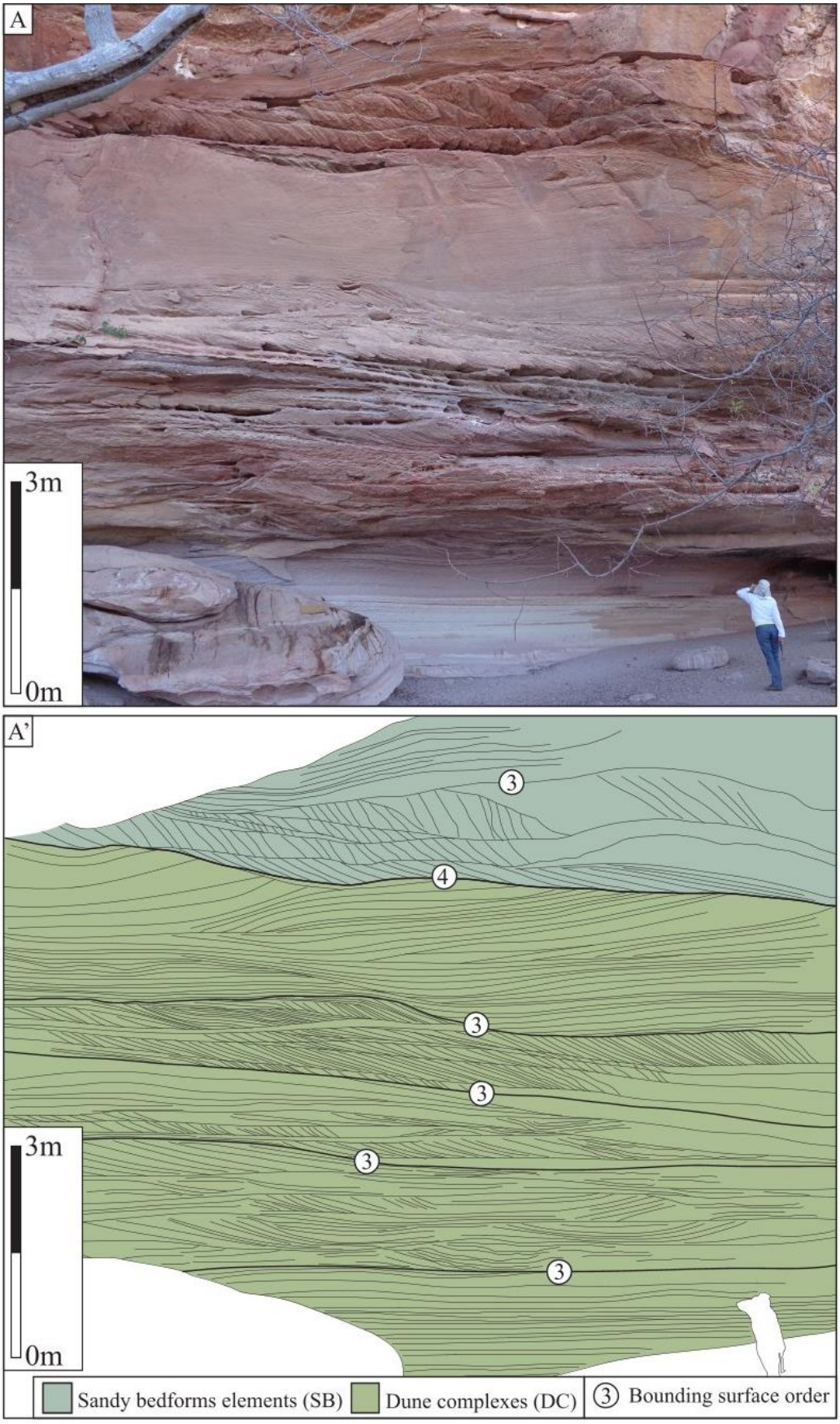

Figure V.15- A and interpreted panel A') Photomosaic of the architectural elements interpretation: typical vertical stacking of dune complexes (DC) and sandy bedforms (SB) elements.

Interpretation

These deposits are interpreted as the product of the migration of longitudinal or transverse conglomerate bars (Miall, 1988a). The horizontally bedded conglomerates upstream of the avalanche face represent accretion in the earlier and more proximal stages of bar evolution (Smith, 1990). Bar growth occurs in several stages, so sandstone lenses abruptly cover the bar faces. These contact types probably reflect waning flows, which either wholly stranded the bar so muddy sands were deposited in low-stage pools or remained sufficiently strong to carry sand over the avalanche face (Smith, 1990). During subsequent floods, the bar was reactivated, leading to partial erosion of the sands and the deposition of fresh foresets. Transitions into horizontally bedded and massive conglomerates possibly reflect increases in the proportion of downstream to vertical accretion caused by high discharges (Hein & Walker, 1977).

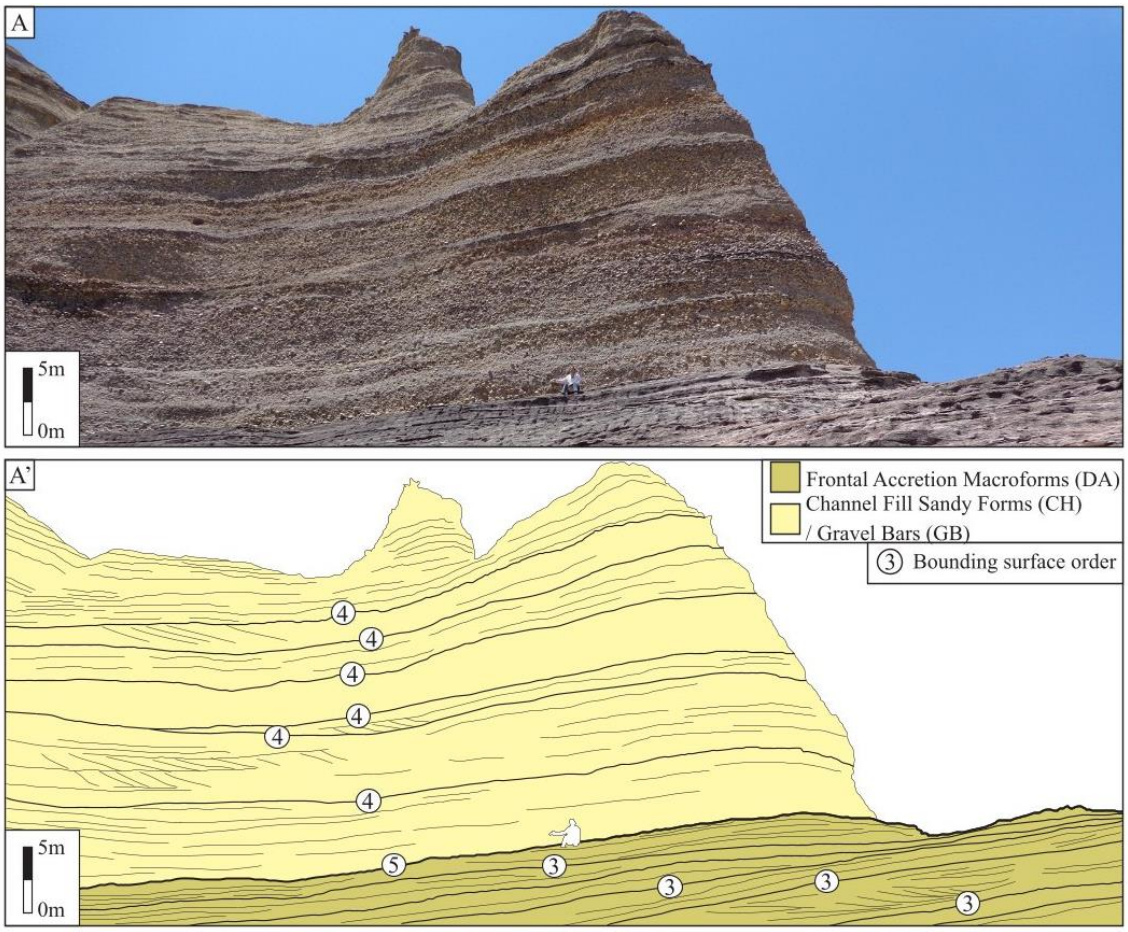

Figure V.16- A and interpreted panel A') Photomosaic of the architectural elements interpretation: example of channelized form. The fifth-order bounding surface separates the channel fill (CH) of the complex frontal accretion macroforms (DA) elements.

4.2.2.5 Frontal Accretion Macroforms (DA)

Frontal accretion macroforms are characterized by laterally continuous tabular external morphology for hundreds of meters and thicknesses up to 7 meters (Figs. V.17 and V.18). Internally, this element includes segments comprising solitary sets of large-scale tabular cross-bedded sandstones or cosets of medium- to small-scale cross-bedded and planar cross-bedded sandstones (Figs. V.17 and V.18). The upper portions within each complex generally include a series of smaller-scale structures and planar strata. The presence of conglomerate lags highlights the bounding surfaces of each segment of layers or simple sandy bars (Fig. V.17).

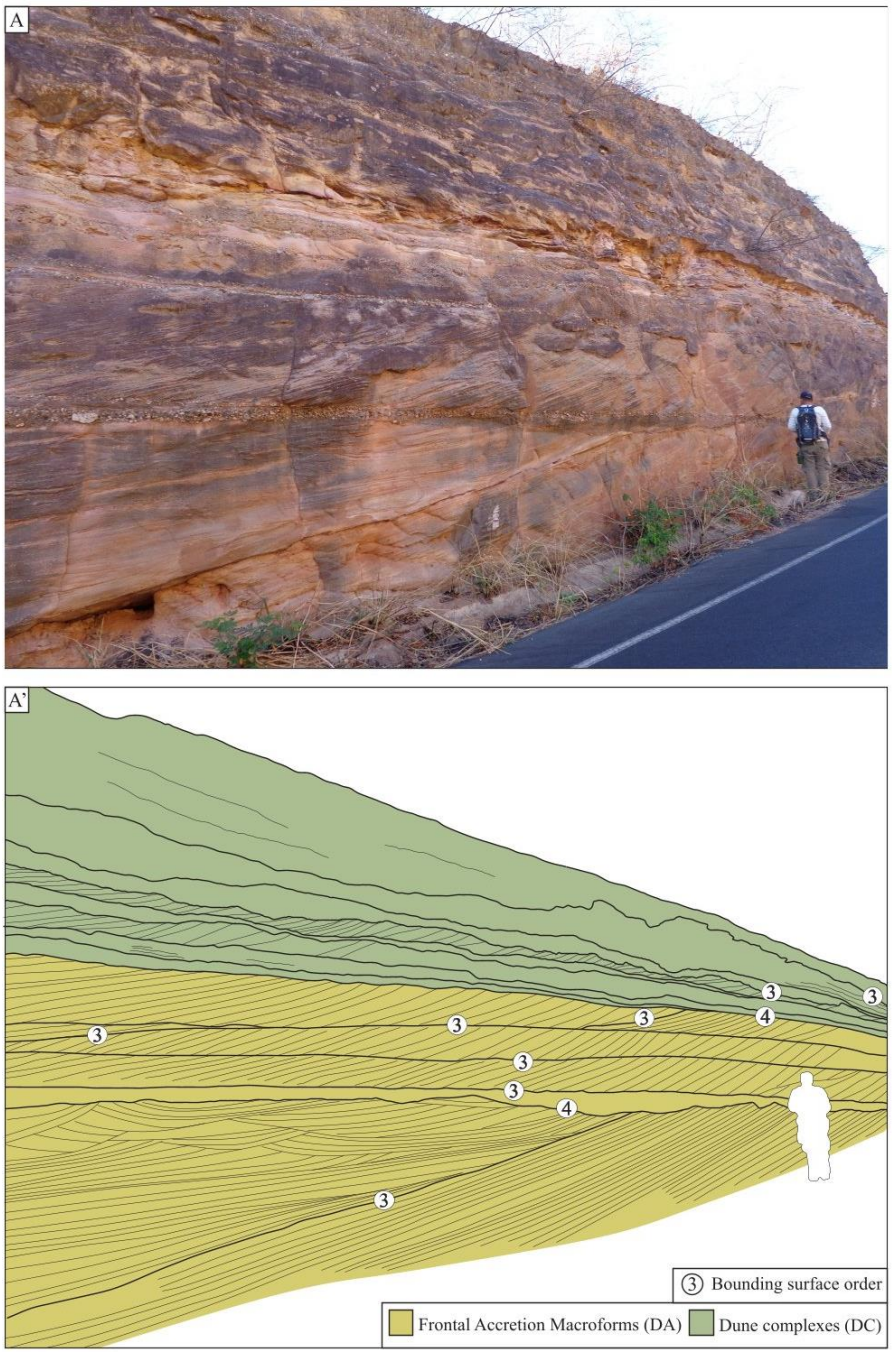

Figure V.17- A and interpreted panel A') Photomosaic of the architectural elements interpretation shows vertical stacked of complex frontal accretion macroform (DA) and dune complexes (DC). Complex frontal accretion macroform (DA) exhibits a bed upward thinning pattern accompanied by a diminution of third-order surface size. Note a 1.70 m-tall person for scale.

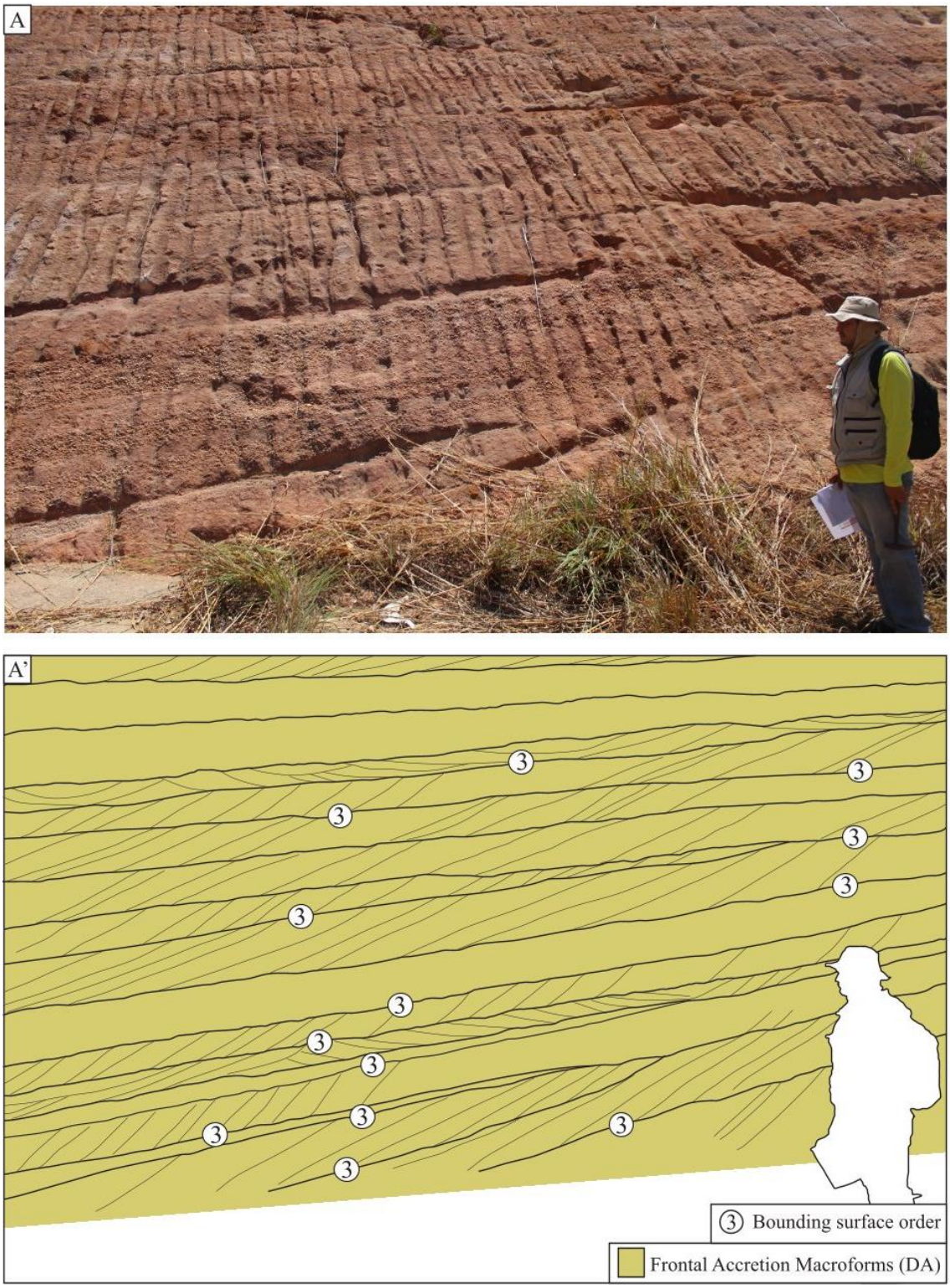

Figure V.18- A and interpreted panel A') Photomosaic of the architectural elements interpretation: an example of a complex frontal accretion macroform (DA) element.

Interpretation

These deposits are interpreted as the axial or quasi-axial section through the record of a large sandy plain that grew by frontal accretion (Allen, 1983; Miall, 1988a, 1988b; Hjellbakk, 1997). They likely represent sediments of active and non-periodic macroforms that grew during periods of high inflow in the fluvial system. These bars originate from unidirectional, subcritical flows characterized by the emergence of frontal single facies (Miall, 1996). These features suggest downstream accretionary mid-channel bars with periodic growth associated with stable, perennial rivers (Allen, 1983; Bridge, 2003). Large-scale cross-stratified sets are interpreted as the product of downstream migrating subaqueous simple sandy bars with well-developed slip faces (Allen, 1983; Bridge, 1993). Small—to medium-scale, cross-stratified cosets that dip in the same direction as the bounding surfaces represent the migration of 2D and 3D dunes along the compound bars lee face in the same direction of downstream bar accretion (Allen, 1983; Miall, 1996). Lenses of massive conglomerates and conglomeratic sandstones in basal portions of the DA element indicate non-extensive channel bottom deposits deposited by hyperconcentrated flows (Miall, 1996).

4.2.2.6 Channel Fill Sandy Forms (CH)

Two variations of this element have been identified, primarily distinguished by differences in scale and sedimentary fill composition (Fig. V.11). The first variation is characterized by an extended external morphology, laterally continuous for kilometers, with a flat to semi-undulating erosional base surface (Figs. V.16 and V.19). The sedimentary fill comprises dune complex, simple to compound sandy, and conglomerate bars up to 15 meters thick (Figs. V.16 and V.19). The second variation is an architectural element characterized by a lenticular external shape (Fig. V.11). Bounded by a concave-up erosional basal surface separating complex channel fill bars from simple sandy bars. Conglomerate layers highlight this transition. The channel-fill deposits consist of cross-bedded sandstones and massive conglomerates (Fig. V.11). The thickness of these deposits does not exceed three meters and exhibits lateral continuities of tens of meters.

Interpretation

This element is interpreted as the migration of simple and complex bars within a broad interlocking fluvial plain, allowing for the development of the different scales described for this element (Cf. Allen, 1983; Miall, 1988a, 1988b; Hjellbakk, 1997).

Laterally extensive geometries and sedimentary fill from upper and lower flow regime structures are interpreted as unconfined sheet-like deposits (Miall, 1985; North & Davidson, 2012). Each dune complex succession represents an individual flood event. The arrangement of facies in a vertical section with upper and lower flow regime structures and an evident fining upward trend suggests deposition within a highly variable flow in a dominantly aggradational setting.

Elements with lenticular external shapes are interpreted as fluvial channels of a multi-story, low-sinuosity, braided system (Miall, 1985). Conglomeratic basal units represent channel lag deposits formed with high flow velocities and dominantly bedload transport. Cross-bedding sets represent the migration of 2D and 3D dune trains along the bases of channels during times of lower sediment load.

5. DISCUSSION

The sedimentary evolution from the Cambrian to Ordovician periods after the Western Gondwana final amalgamation featured extensive transcontinental alluvial deposition systems (Squire et al., 2006; Meinhold et al., 2013). In this paleogeographic context, these transcontinental rivers flowed northward and northwestward across slightly tilted vast continental platforms, forming thick siliciclastic deposits along the margins of West Gondwana (Cerri et al., 2024). Dissected Paleoproterozoic rocks and uplifted Neoproterozoic orogenic terrains allowed the catchment of these massive depositional systems (Cerri et al., 2024). Geological mapping of this fluvial depositional unit suggests uniform subsiding rates along the Parnaíba Basin Eastern contouring, as demonstrated by the substantial lateral continuity of this succession (~650km). The tectonic stability defined for these deposits during the deposition suggests that climatic factors mainly control the sedimentological vertical and lateral variations.

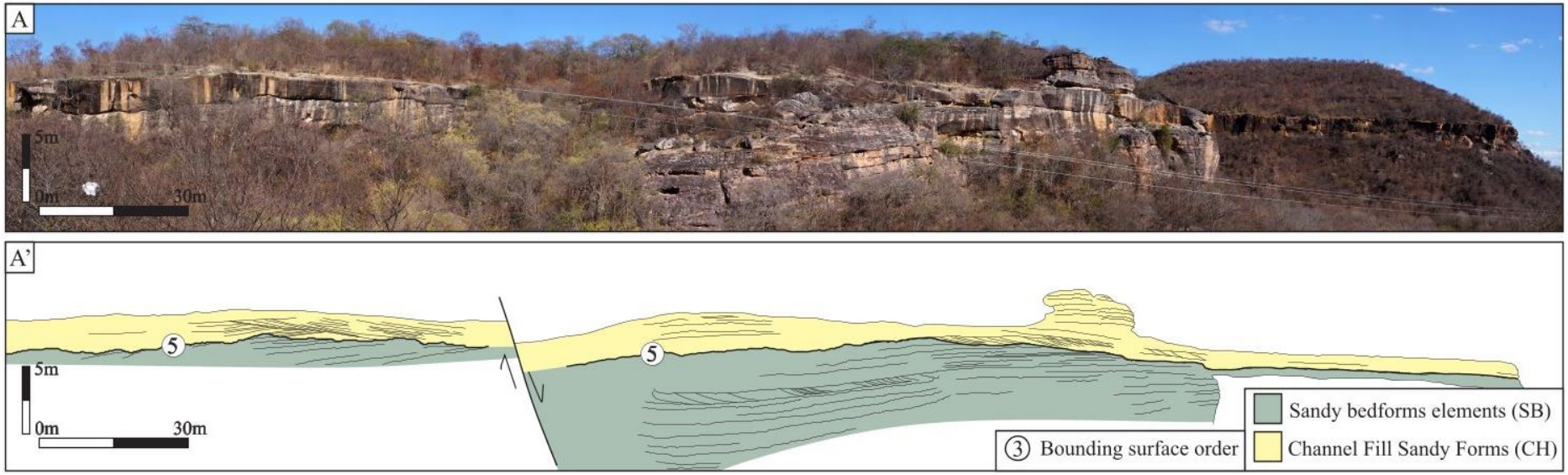

Figure V.19- A and interpreted panel A') Photomosaic of the architectural elements interpretation: example of incised channelized form. The fifth-order bounding surface separates the channel-fill sandy forms (CH) of the sandy bedforms (SB) elements.

Regarding facies models, the succession presented here is consistent with deposits of braided fluvial systems that proliferated in humid climatic settings (Fig. V.20). Paleocurrents data show minimal paleoflow variations related to low-sinuosity drainage patterns along the record. Midchannel bars present more potential to be preserved in low-sinuosity channel belts than bank-attached bars, probably associated with reworking extra-channel-belt areas (Kollmann et al., 1999). The Ipu Formation record mainly comprises mid-channel bars and subcritical, aggradational dunes that record deposition under a low discharge variability fluvial system. These deposits require consistent maintenance of subcritical flow conditions, ensuring permanent flow to facilitate dune migration and bar growth (Miall, 1996; Fielding et al., 2009). Downstream accretion surfaces within simple bars indicate bar migration local pauses, which resume when discharge increases during peak-discharge events (Miall, 1996; Long, 2006). Subcritical aggradational dune deposition and accumulation over the channel floor are laterally associated with simple and compound bars in deeper portions of the channel (Bristow, 1987; Miall, 1996). Dunes can also overlie bar tops and flanks, recorded by interbedded cross-strata in simple and compound bars, and may be related to low stages of flood events with permanent steady flows (Fielding et al., 2018).

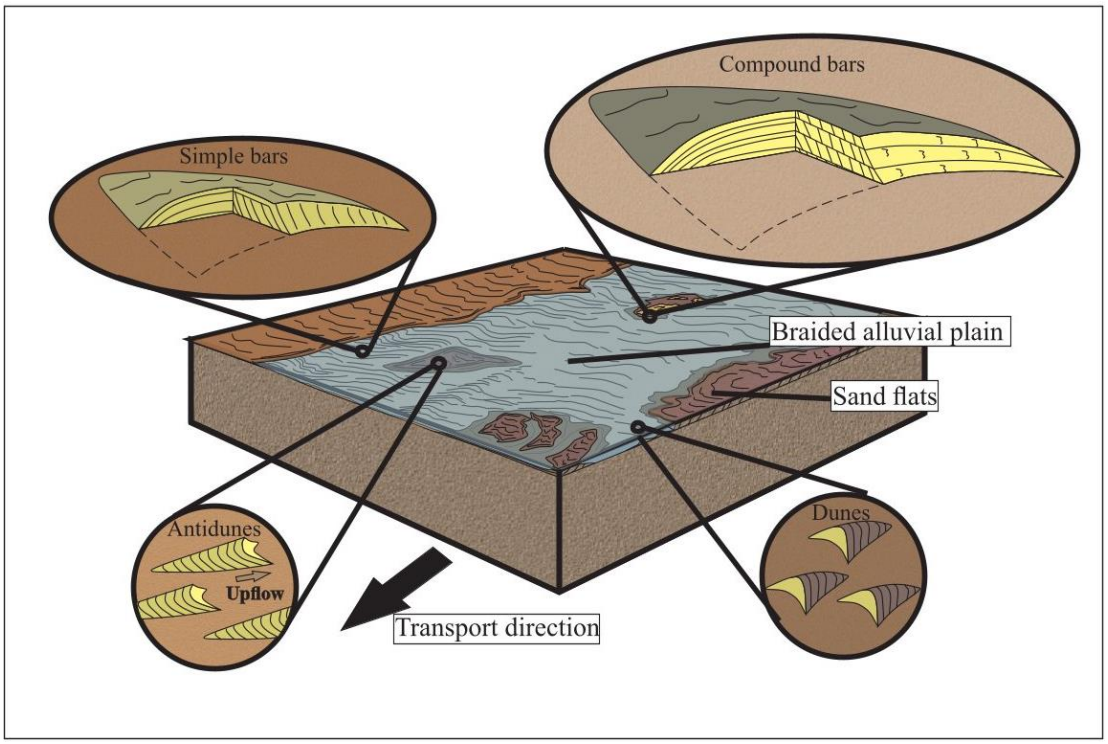

Figure V.20- Depositional model of a perennial fluvial system based upon field data collected from the Ipu Formation. The model highlights the interaction between the lower and upper flow regime bedforms and high sediment load structures within the fluvial environment. Major architectural elements were presented.

The sheet-like channel geometry and lateral persistence of the compound bars suggest deposition along vast, unconfined alluvial plains (Fig. V.20) (Cotter, 1978; Ielpi & Rainbird, 2015). Sheet-flood processes are widely present, with locally minor evidence for channelized flows. Vertical stacking patterns indicate build-up during the high-flood stage and reworking of large foreset bars during the waning-flood stage (Horn et al., 2012). Upper flow regime currents shaped bar tops, producing extensive sand flats (Fig. V.20) (Cant & Walker, 1978). Preserving upper flow regime deposits implies highly variable discharge, conditions attested by frequent alternations in preserved strata between deposits of upper and lower flow regime conditions. High-flood stages allow the submersion of extensive portions of the channel belt, with sediment bypass along bar heads and downstream accretion along bar fronts (Fig. V.20) (Todd & Went, 1991; Ielpi & Rainbird, 2015).

Locally, the fluvial stacking pattern comprises basal deposits of subcritical aggradational dunes within channel bodies, overlain by transcritical to supercritical bedforms. Various subcritical, transcritical, and supercritical bedforms coalesce, indicating a high discharge variability, highly aggradational settings, high sediment supply, and fluctuating flow conditions (Fielding, 2006; Winsemann et al., 2009). Flow strength and velocity variation can be a response to nonperiodic, multi-stage peak-discharge floods (Manna et al., 2021). During peak discharge episodes, channels widen and experience unstable flows, leading to accelerated flow variations and significant sediment transport by bed- and suspended load, followed by quick deposition. The channel floor is initially eroded during flooding events, followed by dune migration. With the increase in water discharge, turbulent and unstable flow produces a laterally widening of channel belts, and large sediment amounts are remobilized, covering broad overbank areas. Transcritical to supercritical flow conditions are reached during this stage, and bedforms are deposited. Sigmoidal bedforms are associated with traction and fallout processes linked primarily to sediment-laden unidirectional stream flows (Tinterri, 2011). These bedforms indicate transitory flow conditions between dune and upper plane-bed stability fields (Hjellbakk, 1997; Fielding, 2006). Fast flow acceleration changes produce the transition between stability fields under highly aggradational settings (Fielding, 2006; Winsemann et al., 2009, 2011; Lang & Winsemann, 2013). Accretionary surfaces within high discharge variability deposits and intercalation with subcritical aggradation dunes indicate bedforms developed within multistage flood events.

The results presented here show a fluvial style for the Ipu Formation containing no changes in paleoflow direction, no remarkable change in the mean grain size, and low rates of accommodation space creation, inferred by the high amalgamated channels degree (Fig. V.20). This evidence suggests that the basin topography was not significantly modified during the fluvial proliferation and deposition. Additionally, basin subsidence rates remained consistent over time. Fluvial records development in low discharge variability settings with permanent water flow provides ideal conditions for macroforms to be constructed and preserved (Allen, 1983). Fine-grained overbank deposits were not found. The only evidence of their previous existence is a few localized and dispersed, muddy to silty thin lenses interbedded with cross-strata and muddy to silty intraclasts within basal conglomeratic beds. The channel/floodplain ratio could indicate accommodation space creation rates in fluvial deposits (Martinsen et al., 1999). Thus, the multi-story channel belts predominance and the lack of preserved overbank deposits suggest high rates of channel amalgamation during low rates of accommodation space creation (Martinsen et al., 1999; Weissmann et al., 2013).

6. CONCLUSION

This investigation into the fluvial sedimentary evolution of ancient Big Rivers on intracratonic basins in Western Gondwana during the Ordovician has revealed a compelling narrative regarding the dynamic processes that shaped this supercontinent. The extensive landmasses that hosted the development of large rivers, notably exemplified by the Ipu Formation in the Parnaiba Basin, provide insights into Western Gondwana paleogeography and geological history during this period.

The Ipu Formation in the Parnaíba Basin analyses offers a detailed reconstruction of an Ordovician fluvial system, providing valuable insights into the depositional dynamics and sedimentary architecture of pre-vegetation braided rivers. The high-resolution analysis of facies and architecture indicates that the Ipu Formation consists of a fluvial stratigraphic framework deposited under distinct discharge regimes. Six architectural elements, including laminated sand sheets, sandy bedforms, Dune complexes, Frontal Accretion Macroforms, Channel Fill Sandy Forms, and conglomerate bars, were observed and reflect different fluvial dynamics and sedimentation stages. This record is characterized by downstream accretion bars and subcritical, aggradational dunes formed in a low discharge variability regime. Locally, architectural elements resulting from subcritical, transcritical, and supercritical flows reveal significant flow strength and

velocity variations. These bedforms suggest deposition in an environment with high discharge variability. Fluvial Succession is organized in meter-scale fining upward cycles that reflect the predominance of sheet flow with sporadic channel incisions filled by migrating small- to large-scale two and three-dimensional bedforms. Locally, small- to medium-scale humpback dunes and antidunes are described and deposited by unstable, transcritical, and supercritical flows.

The fluvial architecture was minimally influenced by tectonics, as evidenced by minor changes in paleoflow direction and no significant alteration in mean grain size. Additionally, the succession displays a high degree of amalgamated channels due to the limited generation of accommodation space and subsidence. Consequently, changes in discharge regimes were predominantly driven by climatic conditions. The fluvial record was produced by a steady, perennial system operating in a warm, humid climate, with bedforms accumulating during non-periodic, multi-stage peak discharge events.

This research expands the understanding of pre-vegetation Big Rivers, providing insights into sedimentary processes that have shaped ancient large-scale river systems. Additionally, this study provides the first research to explore how factors such as tectonic stability and climate variability influenced the morphodynamics and architectural evolution of ancient Big Rivers in Western Gondwana post-amalgamation geological settings.

ACKNOWLEDGMENTS

This paper is a part of the Ph.D. thesis of the first author, who is thankful to the Programa de Pós-Graduação em Geologia e Geoquímica (PPGG) of the Federal University of Pará (UFPA) for logistic and financial support. The first author acknowledges the CAPES – Fundação Coordenação de Aperfeiçoamento de Pessoal de Nível Superior (Brazil) - Grant 88887.508135/2020-00.

REFERENCES

Alexander, J., Bridge, J.S., Cheel, R.J. and Leclair, S.F. (2001). Bedforms and associated sedimentary structures formed under supercritical water flows over aggrading sand beds. *Sedimentology*, 48, 133–152.

Allen, J.R.L. (1963) The classification of cross-stratified units, with notes on their origin. *Sedimentology*, 2, 93-114.

Allen, J.R.L. (1970) Studies in fluviatile sedimentation: a comparison of fining-upward cyclothems, with special reference to coarse-member composition and interpretation. *J. Sed. Petrol*, 40, 298-323

Allen, J.R.L. (1983). Studies in fluviatile sedimentation: bars, bar-complexes and sandstone sheets (low-sinuosity braided streams) in the Brownstones (L. Devonian), Welsh Borders. *Sed. Geol*, 33, 237–293.

Assis, A.P., Porto, A.L., Schmitt, R.S., Linol, B., Medeiros, S.R., Martins, F.C. and Silva, D.S. (2019). The Ordovician-Silurian tectono-stratigraphic evolution and paleogeography of eastern Parnaiba Basin, NE Brazil. *J. S. Am. Earth Sci*, 95, 102241.

Barrera, I.A.R., Nogueira, A.C.R. and Bandeira, J. (2020). The Silurian glaciation in the eastern Parnaíba Basin, Brazil: paleoenvironment, sequence stratigraphy and insights for the evolution and paleogeography of West Gondwana. *Sed. Geol*, 406, 105714.

Bridge, J.S. and Best, J.L. (1988) Flow, sediment transport and bedform dynamics over the transition from dunes to upper-stage plane beds: implications for the formation of planar laminae. *Sedimentology*, 35, 753–763.

Bridge, J.S. (1993) Description and interactions of fluvial deposits: a critical perspective. *Sedimentology*, 40, 801– 810.

Bridge, J.S. (2003). Rivers and Floodplains: Forms, Processes, and Sedimentary Record. Blackwell, Oxford, 489 pp.

Brito Neves, B.B., Fuck, R.A., Cordani, U.G. and Thomaz. A.F. (1984). Influence of basement structures on the evolution of the major sedimentary basins of Brazil: a case of tectonic heritage. *J. Geodyn*, 1, 495–510.

Bristow, C.S. (1987) Brahmaputra river: channel migration and deposition. In: *Recent developments in fluvial sedimentology* (Eds. Ethridge, F.G., Flores, R.M. and Harvey, M.D.). Soc. Econ. Paleontol. Mineral. Spec. Publ. 39: 63-74.

Cant, D.J. and Walker, R.G. (1976) Development of a braidedfluvial facies model for the Devonian Battery Point Sandstone, Quebec. Can. *J. Earth. Sci*, 13: 102-119.

Cant, D.J. and Walker, R.G. (1978) Fluvial processes and facies sequences in the sandy braided South Saskatchewan River, Canada. *Sedimentology*, 25: 625-648.

Caputo, M.V. and Lima, E.C. (1984). Estratigrafia, idade e correlação do Grupo Serra GrandeBacia do Parnaíba. Anais do XXXIII Congresso Brasileiro de Geologia, pp. 228–241.

Capuzzo, N. and Wetzel, A. (2004). Facies and basin architecture of the Late Carboniferous Salvan-Dorénaz continental basin (Western Alps, Switzerland/France). *Sedimentology*, 51, 675–697.

Cartigny, M.J., Ventra, D., Postma, G. and van Den Berg, J.H. (2014). Morphodynamics and sedimentary structures of bedforms under supercritical-flow conditions: new insights from flume experiments. *Sedimentology*, 61, 712–748.

Castro, D., Bezerra, F., Fuck, R. and Vidotti, R. (2016). Geophysical evidence of pre-sag rifting and post-rifting fault reactivation in the Parnaíba basin, Brazil. *Solid Earth Discussions*, pp. 1–38.

Cerri, R.I., Warren, L.V., Luvizotto, G.L., Spencer, C.J. and Assine, M.L. (2024). The Early Paleozoic sedimentary record in northeastern Brazil: Unravelling the sedimentary provenance and evolution of fluvial systems after the Western Gondwana assembly. *Gondwana Res*, 131, 237-255.

Cheel, R.J. (1990). Horizontal lamination and the sequence of bed phases and stratification under upper-flow-regime conditions. *Sedimentology*, 37, 517–529.

Cotter, E. (1978) The evolution of fluvial style, with special reference to the central Appalachians Paleozoic. In: *Fluvial Sedimentology* (Ed. A.D. Miall), Can. Soc. Petrol. Geol. Mem., 5, 361–384.

Collinson, J.D. (1996). Alluvial sediments. In: *Sedimentary Environments: Processes, Facies and Stratigraphy* (Ed. H.G. Reading) 3rd ed. Blackwell, Oxford, pp. 37-82.

Davies, N.S. and Gibling, M.R. (2010) Cambrian to Devonian evolution of alluvial systems: the sedimentological impact of the earliest land plants. *Earth-Sci. Rev*., 98, 171–200.

Davies, N.S., Gibling, M.R. and Rygel, M.C. (2011) Alluvial facies evolution during the Palaeozoic greening of the continents: case studies, conceptual models and modern analogues. *Sedimentology*, 58, 220–258.

Daly, M.C., Andrade, V., Barousse, C.A., Costa, R., McDowell, K., Piggott, N. and Poole, A.J. (2014). Brasiliano crustal structure and the tectonic setting of the Parnaíba basin of NE Brazil: results of a deep seismic reflection profile. *Tectonics*, 33, 2102–2120.

De Castro, D.L., Fuck, R.A., Phillips, J.D., Vidotti, R.M., Bezerra, F.H.R. and Dantas, E.L. (2014). Crustal structure beneath the Paleozoic Parnaiba Basin revealed by airborne gravity and magnetic data, Brazil. *Tectonophysics*, 614, 128–145.

De Oliveira, D.C. and Mohriak, W.U. (2003). Jaibaras trough: an important element in the early tectonic evolution of the Parnaıba interior sag basin, Northern Brazil. *Mar. Pet. Geol.* 20 (3–4), 351–383.

Duller, R.A., Mountney, N.P., Russell, A.J. and Cassidy, N.C. (2008) Architectural analysis of a volcanistic jokulhaups deposit, Southern Iceland: sedimentary evidence for supercritical flow. *Sedimentology*, 55, 939–964.

Eriksson, P.G., Condie, K.C., Tirsgaard, H., Mueller, W.U., Altermann, W., Miall, A.D., Aspler, L.B., Catuneanu, O. and Chiarenzelli, J.R. (1998) Precambrian clastic sedimentation systems. *Sed. Geol.*, 120, 5–53.

Fielding, C.R. and Webb, J.A. (1996). Facies and cyclicity of the Late Permian Bainmedart Coal Measures in the northern Prince Charles Mountains, MacRobertson Land, Antarctica. *Sedimentology*, 43, 295–322.

Fielding, C.R. (2006). Upper flow regime sheets, lenses and scour fills: extending the range of architectural elements for fluvial sediment bodies. *Sed. Geol.*, 190, 227–240.

Fielding, C.R., Allen, J.P., Alexander, J. and Gibling, M.R. (2009). Facies model for fluvial systems in the seasonal tropics and subtropics. *Geology*, 37, 623-626.

Fielding, C.R., Alexander, J. and Allen, J.P. (2018) The role of discharge variability in the formation and preservation of alluvial sediment bodies. *Sed. Geol.*, 365, 1–20.

Froude, M. J., Alexander, J., Barclay, J. and Cole, P. (2017). Interpreting flash flood palaeoflow parameters from antidunes and gravel lenses: An example from Montserrat, West Indies. *Sedimentology*, 64(7), 1817–1845.

Fuller, A.O. (1985). A contribution to the conceptual modelling of pre-Devonian fluvial systems. *Geol. Soc. S. Aft. Trans.*, 88, 189-194.

Ghazi, S. and Mountney, N. P. (2009). Facies and architectural element analysis of a meandering fluvial succession: The Permian Warchha Sandstone, Salt Range, Pakistan. *Sed. Geol.*, 221(1-4), 99–126.

Góes, A.M.O. and Feijó, F.J. (1994). Bacia do Parnaíba. Boletim de Geociências da Petrobras, 8, 57–67.

Grahn, Y. and Caputo, M.V. (1992). Early Silurian glaciations in Brazil. *Palaeogeogr. Palaeoclimatol. Palaeoecol.*, 99, 9–15.

Grahn, Y., De Melo, J.H.G. and Steemans, A.P. (2005). Integrated chitinozoan and miospore zonation of the Serra Grande group (Silurian-Lower devonian), Parnaíba Basin, northeast Brazil. *Rev. Esp. Micropaleontol*., 37, 183–204.

Hein, F.J. and Walker, R.G. (1977). Bar evolution and development of stratification in the gravelly, braided, Kicking Horse River, British Columbia. Canada. *J. Earth. Sci.*, 14: 562-570

Hjellbakk, A. (1997). Facies and fluvial architecture of a high-energy braided river: the Upper Proterozoic Seglodden Member, Varanger Peninsula, northern Norway. *Sed. Geol.*, 114, 131–161.

Horn, J.D., Fielding, C.R. and Joeckel, R.M. (2012). Revision of Platte River alluvial facies model through observations of extant channels and barforms, and subsurface alluvial valley fills. *J. Sed. Res.*, 82, 72–91.

Ielpi, A. and Rainbird, R.H. (2015). Architecture and morphodynamics of a 1.6 Ga fluvial sandstone: Ellice Formation of Elu Basin, Arctic Canada. *Sedimentology*, 62, 1950–1977.

Ito, M. and Saito, T. (2006). Gravel waves in an ancient canyon: analogous features and formative processes of coarse-grained bedforms in a submarine-fan system, the lower Pleistocene of the Boso Peninsula, Japan. *J. Sed. Res.*, 76, 1274–1283.

Ito, M. (2010). Are coarse-grained sediment waves formed as downstream-migrating antidunes? Insight from an early Pleistocene submarine canyon on the Boso Peninsula, Japan. *Sed. Geol.*, 226(1-4), 1–8.

Kegel, W. (1953). Contribuição para o estudo do Devoniano da Bacia do Parnaiba. Dept. Nac. Prod. Min., Div. de Geol. e Min., Rio de Janeiro, Brazil, p. 38 Boletim no 135.

Kollmann, J., Vieli, M., Edwards, P.J., Tockner, K. and Ward, J.V. (1999). Interactions between vegetation development and island formation in the Alpine river Tagliamento. *Appl. Veg. Sci.*, 2, 25–36.

Lang, J. and Winsemann, J. (2013). Lateral and vertical facies relationships of bedforms deposited by aggrading supercritical flows: from cyclic steps to humpback dunes. *Sed. Geol.*, 296, 36–54.

Lang, J., Brandes, C. and Winsemann, J. (2017). Erosion and deposition by supercritical density flows during channel avulsion and backfilling: Field examples from coarse-grained deepwater channel-levée complexes (Sandino Forearc Basin, southern Central America). *Sed. Geol.*, 349, 79–102.

Le Hérissé, A., Melo, J.H.G., Quadros, L.P., Grahn, Y. and Steemans, P. (2001). Palynological characterization and dating of the Tianguá Formation, Serra Grande Group, northern Brazil. In: Correlaçâo de Seqüências Paleozóicas Sul Americanas (Eds. J.H.G, Melo, G.J.S. Terra). *Ciência-Técnica-Petróleo*. 20, pp. 25–41.

Long, D.G.F. (2004). Precambrian Rivers. In: The Precambrian Earth: Tempos and Events: Developments in Precambrian Geology 12 (Eds. Eriksson, P.G., et al.), *Elsevier, Amsterdam*, pp. 660–663.

Long, D.G.F. (2006) Architecture of pre-vegetation sandy braided perennial and ephemeral river deposits in the Paleoproterozoic Athabasca Group, northern Saskatchewan, Canada as indicators of Precambrian fluvial style. *Sed. Geol.*, 190, 71–95.

Lowe, D.R. (1982). Sediment gravity flows, II. Depositional models with special reference to the deposits of high density turbidity currents. *J. Sediment. Petrol.*, 52, 279-297.

Lowe, D.R. (1988). Suspended-load fallout rate as an independent variable in the analysis of current structures. *Sedimentology*, 35, 765-776.

Mac Naughton, R.B., Dalrymple, R.W. and Narbonne, G.M. (1997). Early Cambrian braid-delta deposits, Mac Kenzie Mountains, north-western Canada. *Sedimentology*, 44, 587–609.

Manna, M. O., Scherer, C. M. dos S., Bállico, M. B., Reis, A. D. dos, Moraes, L. V., Ferrari, L. A. B. and Oliveira, V. G. de. (2021). Changes in fluvial architecture induced

by discharge variability, Jaicós Formation (Silurian-Devonian), Parnaíba Basin, Brazil. *Sed. Geol.*, 420, 105924.

Martinsen, O., Ryseth, A., Hansen, W.H., Fleshe, H., Torkildsen, G. and Idil, S. (1999). Stratigraphic base level and fluvial architecture: Ericson Sandstone (Campanian), Rock Springs Uplift, SW Wyoming, USA. *Sedimentology*, 46, 235–259.

Meinhold, G., Morton, A.C. and Avigad, D. (2013). New insights into peri-Gondwana paleogeography and the Gondwana super-fan system from detrital zircon U-pb ages. *Gondwana Res.*, 23 (2), 661–665.

Miall, A.D. (1985). Architectural-element analysis: a new method of facies analysis applied to fluvial deposits. *Earth Sci. Rev.*, 22, 261-308.

Miall, A.D. (1988a). Reservoir heterogeneities in fluvial sandstones: lessons from outcrop studies. *Am. Assoc. Petr. Geol. Bull.*, 72, 682-697.

Miall, A.D. (1988b) Architectural elements and bounding surfaces in fluvial deposits: anatomy of the Kayenta Formation (Lower Jurassic), southwest Colorado. *Sed. Geol.*, 55, 233-262.

Miall, A.D. (1992). Alluvial deposits. In: Facies Models in Response to Sea Level Change (Eds. Walker, R.G., James, N.P.), *Geological Association of Canada, Toronto*, pp. 119-142.

Milani, E. and Zalán, P. (1999). An outline of the geology and petroleum systems of the Paleozoic interior basins of South America. *Episodes-Newsmagazine of the International Union of Geological Sciences*, 22, 199–205.

Mulder, T., Razin, P. and Faugeres, J.-C. (2009). Hummocky cross-stratification-like structures in deep-sea turbidites: Upper Cretaceous Basque basins (Western Pyrenees, France). *Sedimentology*, 56, 997–1015.

North, C.P. and Davidson, S.K. (2012). Unconfined alluvial flow processes: recognition and interpretation of their deposits, and the significance for palaeogeographic reconstruction. *Earth-Sci. Rev.*, 111, 199–223.

Olsen, H. (1988) The architecture of a sandy braided-meandering river system: an example from the Lower Triassic Solling Formation (M. Buntsandstein) in W-Germany. *Geol Rundsch,* 77, 797-814.

Paredes, J.M., Foix, N., Pinol, F.C., Nillni, A., Allard, J. and Marquillas, R.A. (2007). Volcanic and climatic controls on fluvial style in a high-energy system: the Lower Cretaceous Matasiete Formation, Golfo San Jorge basin, Argentina. *Sed. Geol.*, 202, 96–123.

Paola, C., Wiele, S.M. and Reinhart, M.A. (1989). Upper-regime parallel lamination as the result of turbulent sediment transport and low amplitude bedforms. *Sedimentology*, 36, 47–60.

Plink-Björklund, P. (2015). Morphodynamics of rivers strongly affected by monsoon precipitation: Review of depositional style and forcing factors. *Sed. Geol.*, 323, 110–147.

Plummer, P.D. (1946). Geossinclíneo do Parnaíba. Conselho Nacional do Petróleo. Relatório de 1946. Rio de Janeiro, 1948. *PETOBRAS*, pp. 87–134.

Porto, A., Daly, M.C., La Terra, E. and Fontes, S.L. (2018). The pre-Silurian Riachão Basin: a new perspective on the basement of the Parnaiba Basin, NE Brazil. Cratonic Basin Form. A case Study Parnaiba Basin Brazil. 472. *Geol. Soc. London Spec. Publ.*, pp. SP472–2.

Prave, A.R. and Duke, W.L. (1990). Small-scale hummocky cross-stratification in turbidites: a form of antidune stratification? *Sedimentology*, 37, 531–539.

Rodrigues, R. (1967). Estudo sedimentológico e estratigráfico dos depósitos silurianos e devonianos da Bacia do Parnaíba. *PETROBRAS*. RENOR, Belém, Brasil Relatório Interno no 273M.

Røe, S. (1987). Cross-strata and bedforms of probable transitional dune to upper stage plane bed origin from Late Pre-Cambrian fluvial sandstone, northern Norway. *Sedimentology*, 34, 89–101.

Russell, H.A.J. and Arnott, R.W.C. (2003). Hydraulic-jump and hyperconcentrated-flow deposits of a glacigenic subaqueous fan: Oak Ridges Moraine, southern Ontario, Canada. *J. Sediment. Res.*, 73, 887–905.

Rust, B.R. and Koster, E.H. (1984). Coarse alluvial deposits. In: Facies models, 2nd edn (Ed. Walker R.G.) *Geosci Ca. Reprint Ser* 1: 53-69.

Sharma, M., Sharma, S., Shukla, U. K. and Singh, I. B. (2002). Sandstone body architecture and stratigraphic trends in the Middle Siwalik Succession of the Jammu area, India. *J. Asian Earth Sci.*, 20(7), 817–828.

Schumm, S.A. (1968). Speculations concerning paleohydrologic controls of terrestrial sedimentation. *Geol. Soc. Am. Bull.*, 79, 1573–1588.

Smith, N.D. (1970). The braided stream depositional environment: comparison of the Platte River with some Silurian clastic rocks, north central Appalachians. *Geol Soc Am Bull*, 81, 2993-3014.

Smith, S.A. (1990). The sedimentology and accretionary style of an ancient gravel-bed stream: the Budleigh Salterton Pebble Beds (Lower Triassic), southwest England. *Sed. Geo1.*, 67, 199-219.

Squire, R.J., Campbell, I.H., Allen, C.M. and Wilson, C.J. (2006). Did the transgondwanan supermountain trigger the explosive radiation of animals on Earth? *Earth Planet. Sci. Lett.*, 250, 116–133.

Steer, W.M. (1983). Morphological characteristics of ephemeral stream channel and overbank splay sandstone bodies in the Permian Lower Beaufort Group, Karoo Basin,

South Africa. In: Modern and ancient fluvial systems (Eds. Collinson JD, Lewin J) . *Int Assoc Sedimentol Spec Publ*, 6, 405-420

Tinterri, R. (2011). Combined flow sedimentary structures and the genetic link between sigmoidal- and hummocky cross stratification. *GeoActa*, 10, 1–43.

Todd, S.P. and Went, D.J. (1991). Lateral migration of sand-bed rivers: examples from the Devonian Glashabeg Formation, SW Ireland and the Cambrian Alderney Sandstone Formation, Channel Islands. *Sedimentology*, 38, 997-1020.

Vaz, P.T., Resende, N.G.A.M., Wanderley Filho, J.R. and Travassos, W.A. (2007). Bacia do Parnaíba. Rio de Janeiro. PETROBRÁS. *Boletim de Geociências*, 15(2), 253–263.

Tozer, B., Watts, A.B. and Daly, M.C. (2017). Crustal structure, gravity anomalies, and subsidence history of the Parnaíba cratonic basin, Northeast Brazil. *J. Geop. Res. Sol. Earth.*, 122, 5591–5621.

Winsemann, J., Hornung, J.J., Meinsen, J., Asprion, U., Polom, U., Brandes, C., Bußmann, M. and Weber, C. (2009). Anatomy of a subaqueous ice-contact fan and delta complex, Middle Pleistocene, NW Germany. *Sedimentology*, 56, 1041–1076.

Winsemann, J., Brandes, C. and Polom, U. (2011). Response of a proglacial delta to rapid high amplitude lake-level change: an integration of outcrop data and high-resolution shear wave seismics. *Basin Res.*, 23, 22–52.

Weissmann, G.S., Hartley, A.J., Scuderi, L.A., Nichols, G.J., Davidson, S.K., Owen, A., Atchley, S.C., Bhattacharyya, P., Chakraborty, T., Ghosh, P., Nordt, L.C., Michel, L. and Tabor, N.J. (2013). Prograding distributive fluvial systems – geomorphic models and ancient examples. In: New Frontiers in Paleopedology and Terrestrial Paleoclimatology (Eds. Driese, S.G., Nordt, L.C.), *SEPM Spec. Publ.*, 104, 131–147.

Yokokawa, M., Hasegawa, K., Kanbayashi, S. and Endo, N. (2010). Formative conditions and sedimentary structures of sandy 3D antidunes: an application of the gravel step-pool model to fine-grained sand in an experimental flume. *Earth Surf. Proc. Land.*, 35, 1720–1729.

CAPÍTULO VI CONSIDERAÇÕES FINAIS

O presente trabalho contribuiu significativamente para o entendimento dos depósitos siliciclásticos de idade Cambriana/Ordoviciana-Siluriana no norte e nordeste do Brasil e suas conexões com a evolução tectônica e paleogeográfica do Gondwana Ocidental durante o Paleozoico Inferior. A partir de uma abordagem integrada que envolveu análises sedimentológicas, estratigráficas e multiproxies de proveniência, foi possível redefinir o arcabouço estratigráfico do Grupo Paredão e da Formação Gorotire da PMC, bem como explorar suas correlações com as formações Ipu, Cariri e Tacaratu no nordeste do Brasil e equivalentes na África Central.

A Formação Gorotire, com cerca de 400 m de espessura, foi interpretada como resultado de sedimentação em sistemas fluviais por carga de fundo, enquanto o Grupo Paredão foi dividido em dois membros. O membro inferior corresponde a conglomerados maciços de leques aluviais (~90 m de espessura), e o membro superior inclui diamictitos maciços glaciomarinhos e arenitos deltaicos organizados em ciclos granodecrescentes ascendentes (~140 m de espessura). Sendo a Formação Gorotire anexada ao Grupo Paredão como pertencente ao seu membro inferior.

As análises de proveniência realizadas, baseadas em dados isotópicos Sm-Nd, petrografia de arenitos, proveniência macroscópica, assembleia de minerais pesados e química mineral de granadas, reforçam que o Grupo Paredão não está geneticamente relacionado à evolução Arqueana-Neoproterozóica da PMC. A sedimentação desta unidad só ocorreu após a estabilização da região sudeste do Cráton Amazônico no Neoproterozóico. Adicionalmente, o registro sedimentar foi associado ao evento glacial da passagem entre os períodos Ordoviciano e Siluriano.

A descoberta de depósitos paleozoicos em uma região tradicionalmente considerada como exclusivamente pré-cambriana amplia as perspectivas de compreensão do Cráton Amazônico. Estes novos resultados indicam que esta área sofreu subsidência em diferentes intervalos temporais, preservando a superposição de diferentes tipos de bacias ao longo do tempo. As reativações Mesozoicas da plataforma Sul-Americana tiveram um papel importante na preservação de depósitos paleozoicos em áreas de extensão frágil da crosta superior.

Os resultados deste trabalho não apenas revisam e simplificam a estratigrafia da PMC, mas também trazem implicações significativas para a prospecção mineral. A

exclusão do Grupo Paredão e da Formação Gorotire como possíveis alvos prospectivos no PMC elimina interpretações equivocadas relacionadas à mineralização Precambriana, contribuindo para um melhor direcionamento de futuros estudos geológicos e econômicos.

A investigação dos registros sedimentares Cambrianos/Ordovicianos no Nordeste do Brasil e na África Central revelou importantes dinâmicas geológicas do Gondwana Ocidental. A partir de análises detalhadas da arquitetura fluvial e idades U-Pb em zircões detríticos, identificou-se a existência de imensos sistemas de drenagem transcontinentais que moldaram a paisagem após a amalgamação do Supercontinente Gondwana. Os depósitos siliciclásticos analisados, com espessuras variando entre 300-400 m e extensões laterais superiores a 300.000 km², revelam a atuação de grandes sistemas aluviais e fluviais transcontinentais que fluíram em amplas peneplanícies no limite Cambriano-Ordoviciano. Estruturas deposicionais, como leitos tabulares de conglomerados e arenitos organizados em ciclos granodecrescentes ascendentes, refletem uma dinâmica de fluxo em lençol e preenchimentos de canais esporádicos. Os registros da Formação Ipu, caracterizados por elementos arquiteturais como lençóis de areia laminados, formas de leito arenosas, dunas complexas, macroformas de acreção frontal, preenchimentos de canal e barras conglomeráticas, refletem sistemas de rios entrelaçados pré-vegetação em contextos climáticos quentes e úmidos. A arquitetura fluvial foi pouco influenciada por tectônica, mas fortemente modulada por variações climáticas que controlaram os regimes de descarga. Este registro amplia o entendimento sobre grandes sistemas fluviais pré-vegetação e fornece diversas perspectivas sobre como estabilidade tectônica e variabilidade climática influenciaram a morfodinâmica desses rios em contextos pós-aglutinação do Gondwana Ocidental.

Por fim, esta pesquisa reforça a relevância de abordagens integradas para interpretar ou reinterpretar registros sedimentares complexos, estabelecendo bases para estudos futuros sobre a evolução paleoambiental e paleogeográfica de supercontinentes, como o Gondwana, e ampliando as possibilidades de correlações globais no Paleozoico Inferior.

REFERÊNCIAS

Adams A.E., Mackenzie W.S., Guilford C. 1984. *Atlas of sedimentary rocks under the microscope*. Longman, Harlow, 140 p.

Adôrno R. R. 2014. *Estudo cronobioestratigráfico da Formação Vila Maria: litoestratigrafia e paleontologia do limite ordoviciano-siluriano da Bacia do Paraná, estados de Goiás e de Mato Grosso, Brasil Central*. MS Dissertation, Instituto de Geociências, Universidade de Brasília, Brasília. 94.

Afonso, J. & Nogueira, A. 2018. Sedimentology and stratigraphy of Neoproterozoic-lower 765 Paleozoic carbonate-siliciclastic succession of the southwesternmost Amazon Craton, 766 state of Rondônia, Brazil. *Brazilian Journal of Geology*. **48**. 10.1590/2317-767 4889201820170002.

Allen, P. A. & Heller, P. L. 2011. Dispersal and preservation of tectonically generated aluvial gravels in sedimentary basins. *Tectonics of Sedimentary Basins: Recent Advances*, 111-130.

Almeida F.F.M., Hasui Y., Brito Neves B.B., Fuck R.A. 1981. Brazilian Structural Provinces: an introduction. *Earth-Science Reviews*, **17**: 1–29.

Araujo O.J.B & Maia R.G.N. 1991. *Serra dos Carajás, Folha SB.22-Z-A: Estado do Pará.* Projeto especial mapas de recursos minerais, de solos e de vegetacao para a area do Programa Grande Carajas; Subprojeto Recursos Minerais. Brasilia, Companhia de Pesquisa de recursos Minerais ‑ CPRM (Relatorio, 136 p).

Araújo O.J.B., Maia R.G.N., Jorge João X.S., Costa J.B.S. 1988. A megaestruturação arqueana da Folha Serra dos Carajás. In: 7º Congresso Latino-americano de Geologia. Belém. *Anais*. v.1, p. 324-333.

Araújo, R. & Nogueira, A. 2019. Serra Sul diamictite of the Carajás Basin (Brazil): A Paleoproterozoic glaciation on the Amazonian craton. *Geology*, **47**:1166-1170.

Araújo, R., 2020. *Estratigrafia e eventos da transição Neoarqueano-Paleoproterozóico da Bacia de Carajás, sudeste do Cráton Amazônico*. PhD Thesis, Universidade Federal do Pará, Brazil, pp. 215.

Araujo Filho R.C., Nogueira A.C., Araujo R.N. 2020. New stratigraphic proposal of a Paleoproterozoic siliciclastic succession: Implications for the evolution of the Carajas Basin, Amazonian craton, Brazil. *Journal of South American Earth Sciences*, **102**:102665.

Assine M.L., Alvarenga C.J.S., Perinotto J.A.J. 1998. Formação Iapó: glaciação continental no limite Ordoviciano/Siluriano da Bacia do Paraná. *Revista Brasileira de Geociências*, **28**(1): 51-60.

Avigad, D., Sandler, A., Kolodner, K., Stern, R.J., McWilliams, M., Miller, N., Beyth, M. 2005. Mass-production of Cambro-Ordovician quartz-rich sandstones as a consequence of chemical weathering of Pan-African terranes: environmental implications. *Earth and Planetary Science Letters*, **240**, 818–826.

Barnes, C.R., 2004. Ordovician oceans and climates, in Webby, B.D., Droser, M.L., Paris, F., and Percival, I., eds., The Great Ordovician Biodiversification Event: New York, Columbia University Press, p. 72–76.

Barrera I.A.R., Nogueira A.C.R., Bandeira J. 2020. The Silurian glaciation in the eastern Parnaíba Basin, Brazil: paleoenvironment, sequence stratigraphy and insights for the evolution and paleogeography of West Gondwana. *Sedimentary Geology*, **406**.

Berner, R. A. & Kothavala, Z. 2001. GEOCARB III: A revised model of atmospheric CO2 over Phanerozoic time. *American Journal of Science*, **301**(2), 182–204.

Bettencourt, J.S., Juliani Xavier, R.P., Monteiro, L.V.S., Bastos-Neto, A.C., Klein, E.L., Assis, R.R., Leite-Jr, W.P., Moreto, C.P.N., Fernandes, C.M.D., Pereira, V.P., 2016. Metallogenetic systems associated with granitoid magmatism in the Amazon Craton: an overview of the present understanding and exploration significance. *Journal of South American Earth Sciences*, **68**, 22–49.

De Brito Neves, B. B., Fuck, R. A., Cordani, U. G., & Thomaz F, A. 1984. Influence of basement structures on the evolution of the major sedimentary basins of Brazil: A case of tectonic heritage. *Journal of Geodynamics*, **1**(3-5), 495–510.

Buhn B., Pimentel M.M., Matteini M., Dantas E.L. 2009. High spatial resolution analysis of Pb and U isotopes for geochronology by laser ablation multi-collector inductively coupled plasma mass spectrometry (LA-MC-ICP-MS). *Anais da Academia Brasileira de Ciências*, **81**:99-114.

Burke, K., MacGregor, D.S., Cameron, N.R., 2003. Africa's petroleum systems: four tectonic 'Aces' in the past 600 million years. In: Arthur, T.J., MacGregor, D.S., Cameron, N.R. (Eds.), *Petroleum geology of Africa*: new themes and developing technologies: Geological Society of London, p. 21–60. (Special Publication, vol. **207**).

Busfield M.E. & Le Heron D.P. 2013. Glacitectonic deformation in the Chuos Formation of northern Namibia: Implications for Neoproterozoic ice dynamics. *Proceedings of the Geologists' Association*, **124**:778-789.

Busfield M.E. & Le Heron D.P. 2018. Snowball Earth under the microscope. *Journal of Sedimentary Research*, **88**:659-677.

Cabral A.R., Creaser R.A., Nägler T., Lehmann B., Voegelin A.R., Belyatsky B., Pašava J., Seabra Gomes Jr. A.A., Galbiatti H., Böttcher M.E., Escher P. 2013. Trace-element and multiisotope geochemistry of Late-Archean black shales in the Carajás iron-ore district, Brazil. *Chemical Geology*, **362**:91-104.

Caputo, M. V. 1984. *Stratigraphy, tectonics, paleoclimatology and paleogeography of Northern Basins of Brazil*. PhD Thesis, University of Califórnia, Santa Bárbara. USA. pp. 586.

Caputo, M. V. & Lima, E. C. 1984. Estratigrafia, idade e correlação do Grupo Serra Grande – Bacia do Parnaíba. SBG 33º Congresso Brasileiro de Geologia, Rio de Janeiro, *Anais* [...]. v. **2**, p. 740-759.

Carozzi A.V., Falkenhein F.U.M., Carneiro R.G., Esteves R.P., Contreiras C.J.A. 1975. Análise ambiental e evolução tectônica sinsedimentar da seção siluro-eocarbonífera da Bacia do Maranhão. Rio de Janeiro, Brasil, Petrobras, **48.** (*Série Ciência-Técnica-Petróleo. Seção Exploração de Petróleo n. 7*).

Cerri, R.I., Warren, L.V., Varejão, F.G., Silva, A.J.C.A., Lana, C., Assine, M.L., 2021. So close and yet so far: U-pb geochronological constraints of the Jaibaras Rift Basin and the intracratonic Parnaíba Basin in SW Gondwana. *Geological Magazine*, **121**.

Cerri, R.I., Warren, L.V., Spencer, C.J., Varejão, F.G., Promenzio, P., Luvizotto, G.L., Assine, M.L., 2022. Using detrital zircon and rutile to constrain sedimentary provenance of Early paleozoic fluvial systems of the Araripe Basin, Western Gondwana. *Journal of South American Earth Sciences*, **116**, 103821.

Cerri, R.I., Warren, L.V., Luvizotto, G.L., Spencer, C.J., Assine, M.L., 2024. The Early Paleozoic sedimentary record in northeastern Brazil: Unravelling the sedimentary provenance and evolution of fluvial systems after the Western Gondwana assembly. *Gondwana Research,* **131**, 237-255.

Chemale Jr. F., Dussin I.A., Alkmim F.F., Martins M.S., Queiroga G., Armstrong R., Santos M.N. 2012. Unravelling a Proterozoic basin history through detrital zircon geochronology: the case of the Espinhaço Supergroup, Minas Gerais, Brasil. *Gondwana Research*, **22**:200-206.

Cocks, L.R.M. & Torsvik, T.H., 2002. Earth geography from 500 to 400 million years ago: a faunal and palaeomagnetic review. *Journal of the Geological Society of London*, **159**, 631–644.

Collins, A.S. & Pisarevsky, S.A., 2005. Amalgamating eastern Gondwana: the evolution of the Circum-Indian Orogens. *Earth-Science Reviews*, **71**, 229–270.

Daly M.C., Andrade V., Barousse C.A., Costa R., McDowell K., Piggott N., Poole A.J. 2014. Brasiliano crustal structure and the tectonic setting of the Parnaíba basin of NE Brazil: results of a deep seismic reflection profile. *Tectonics*, **33**: 2102–2120.

De Castro D.L., Fuck R.A., Phillips J.D., Vidotti R.M., Bezerra F.H.R., Dantas E.L. 2014. Crustal structure beneath the Paleozoic Parnaiba Basin revealed by airborne gravity and magnetic data. Brazil. *Tectonophysic*, **614**: 128–145.

Díaz-Martínez, E. 1997. Facies y ambientes sedimentarios de la Formación Cancañiri (Silúrico inferior) en La Cumbre de La Paz, norte de la Cordillera Oriental de Bolivia. *Geogaceta*, **22**: 55–57.

Díaz-Martínez, E. 1998. Silurian of Peru and Bolivia: recent advances and future research. 6th International Graptolite Conference and Field Meeting of the International Subcommission on Silurian Stratigraphy, Madrid. *Temas Geológico-Mineros del Instituto Tecnológico Geominero de España*, **23**: 69–75.

Díaz-Martínez E., Acosta H., Cárdenas J., Carlotto V., Rodríguez R. 2001. Paleozoic diamictites in the Peruvian Altiplano: evidence and tectonic implications. *Journal of South American Earth Sciences*, **14**: 587–592.

Díaz-Martínez, E. & Grahn, Y. 2006. Early Silurian glaciation along the western margin of Gondwana (Peru, Bolivia and northern Argentina): paleogeographic and geodynamic setting. *Paleogeography, Paleoclimatology, Paleoecology*, **245**: 62–81.

Dreher A.M. 2004. *O depósito primário de Cu-Au de Igarapé Bahia, Carajás: rochas fragmentarias, fluidos mineralizantes e modelo metalogenético*. PhD Thesis, Universidade Estadual de Campinas, São Paulo, 221 p.

Dreher A.M., Xavier R.P., Martini S.L. 2005. Fragmental rocks of the Igarapé Bahia Cu-Au deposit, Carajás mineral province, Brazil. *Revista Brasileira de Geociências*, **35**:359-368.

Dreher A.M., Xavier R.P., Taylor B.E., Martini S.L. 2008. New geologic, fluid inclusion and stable isotope studies on the controversial Igarapé Bahia Cu-Au deposit, Carajás Province, Brazil. *Mineral Deposita*, **43**:161-184.

Faure G. 1986. *Principles of Isotope Geochemistry*. 2nd edition. New York. John Wiley & Sons, 464 p.

Fedo, C.M., Sircombe, K., Rainbird, R. 2003. Detrital zircon analysis of the sedimentary record. In Hanchar, J.M., Hoskin, P.W.O.

Fernandes, C.A.S., Da Fonseca, V. M. M., Ponciano, L. C. M. (ed.). *ICNOFÓSSEIS DA BACIA DO PARNAÍBA: AS CONTRIBUIÇÕES DE WILHELM KEGEL*. Reviews in Mineralogy and geochemistry, v. 53, p. 277-303. Rev. bras. paleontol. 15(2):153-163, Maio/Agosto 2012 Sociedade Brasileira de Paleontologia.

Feio, G.R.L., Dall'Agnol, R., Dantas, E.L., Macambira, M.J.B., Gomes, A.C.B., Sardinha, A. S., Oliveira, D.C., Santos, R.D., Santos, P.A., 2012. Geochemistry, geochronology, and origin of the Neoarchean Planalto Granite suite, Caraj´as, Amazonian craton: Atype or hydrated charnockitic granites? *Lithos*, **151**, 57–73.

Feio, G.R.L., Dall‟‟Agnol, R., Dantas, E.L., Macambira, M.J.B., Santos, J.O.S., Althoff, F.J., Soares, J.E.B. 2013. Archean granitoid magmatism in the Canaã dos Carajás area: implications for crustal evolution of the Carajás province, Amazonian craton, Brazil. *Precambrian Research*, **227**: 157-185.

Ferguson, R., Hoey, T., Wathen, S., Werritty, A. 1996. Field evidence for rapid downstream fining of river gravels through selective transport. *Geology*, **24**(2), 179-182.

Fernández-Suárez, J., Gutiérrez Alonso, G., Cox, R., Jenner, G.A., 2002. Assembly of the Armorican microplate: a strike–slip terrane delivery? Evidence from U–Pb ages of detrital zircons. *Journal of Geology*, **110**, 619–626.

Finnegan, S, Bergmann, K., Eiler, J.M., Jones, D. S., Fike, D. Eisenman, I., Hughes, N., Tripati, A., Fischer, W. 2011. "The Magnitude and Duration of the Late Ordovician-Early Silurian Glaciation". *Science*, **331**(6019), 903–906.

Galarza M.A., Macambira M.J.B., Villas R.N. 2008. Dating and isotopic characteristics (Pb and S) of the Fe oxide–Cu–Au–U–REE Igarapé Bahia ore deposit, Carajás mineral province, Pará state, Brazil. *Journal of South American Earth Sciences*, **25**:377-397.

Garzanti, E. 2019. Petrographic classification of sand and sandstone. *Earth-Science Reviews*, **192**.

Ghienne, J.-F., Desrochers, A., Thijs, R.A., Vandenbroucke, A.A., Asselin, E., Dabard, M-P., Farley, C., Loi, A., Paris, F., Wickson, S., Veizer, J., 2014. A Cenozoic-style scenario for the end-Ordovician glaciation. *Nature Communications*, **5**, 4485.

Ghienne, J-F., Abdallah, H., Deschamps, R., Guiraud, M., Gutiérrez-Marco, J. C., Konaté, M., Meinhold, G., Moussa, A., and Rubino, J-L. 2023. The Ordovician record of North and West Africa: unravelling sea-level variations, Gondwana tectonics, and the glacial impact. *Geological Society, London, Special Publications*, **533**, 199 – 252.

Gibbs A.K., Wirth K.R., Hirata W.K., Olszewski W.J. 1986. Age and composition of the Grão Pará group volcanics, Serra dos Carajás. *Revista Brasileira de Geociências*, **16**:201-211.

Góes, A.M.O.; Souza, J.M.P.; Teixeira, L.B. 1990. Estágio exploratório e perspectivas petrolíferas da Bacia do Parnaíba. *Boletim de Geociências da Petrobras*, **4**(1): 55-64.

Grahn, Y. 1991. The Ordovician-Devonian biostratigraphy of Brazil. *Anais da Academia Brasileira Ciencias*. Resumo Comun. **94.**

Grahn, Y. 1992. Revision of Silurian and Devonian strata of Brazil. *Palynology*, **16**:35-61.

Grahn, Y., 2005. Ordovician and Silurian chitinozoan biozones of western Gondwana. *Geological Magazine*, **143**.

Grahn, Y. & Caputo, M.V. 1992. Early Silurian glaciations in Brazil. *Palaeogeography, Palaeoclimatology, Palaeoecology*, **99**, 9–15.

Grahn, Y. & Paris, F. 1992. Age and correlation of the Trombetas Group, Amazonas Basin, Brazil. *Revue de Micropaléontologie*, **35**, 197–209.

Grahn, Y., De Melo, J.H.G., Steemans, A.P., 2005. Integrated chitinozoan and miospore zonation of the Serra Grande group (Silurian-Lower Devonian), Parnaíba Basin, northeast Brazil. *Revista Espanola Micropaleontologia*, **37**, 183–204.

Haughton, P. D. W., Todd, S. P., Morton, A. C. 1991. Sedimentary provenance studies. *Geological Society, London, Special Publications*, **57**(1), 1-11.

Howard, J. L. 1993. The statistics of counting clasts in rudites: a review, with examples from the upper Palaeogene of southern California, USA. *Sedimentology*, **40**(2), 157-174.

Jacobsen, S.B. & Kaufman A.J. 1999. The Sr, C and O isotopic evolution of Neoproterozoic seawater. *Chemical Geology*, **161,** 37– 57.

Johnson, P.R., Andresen, A., Collins, A.S., Fowler, A.R., Fritz, H., Ghebreab, W., Kusky, T., Stern, R.J., 2011. Late Cryogenian-Ediacaran history of the Arabian-Nubian Shield: a review of depositional, plutonic, structural, and tectonic events in the closing stages of the northern East African Orogen. *Journal of African Earth Sciences*, **61**, 167–232.

Kegel, W. 1953. *Contribuição para o estudo do Devoniano da Bacia do Parnaiba*. Rio de Janeiro, Departamento Nacional da Produção Mineral, Divisâo de Geologia e Mineralogia, 38p. (Boletim,135)

Knoll, A.H. 1991. *Scientific American*, pp. 42– 49.

Le Hérissé, A., Melo, J.H.G., Quadros, L.P., Grahn, Y., Steemans, P. 2001. Palynological characterization and dating of the Tianguá Formation, Serra Grande Group, northern

Brazil. In: Melo, J.H.G., Terra, G.J.S. (Eds.), Correlaçâo de Seqüências Paleozóicas Sul-Americanas. *Ciência-Técnica-Petróleo*, **20:** 25–41.

Lima F.D. & Pinheiro R.V.L. 2001. Formação Gorotire: Considerações Sobre uma Unidade Siliciclástica Particular da Serra dos Carajás - PA. In: Reis N.J. e Monteiro M.A.S. (ed.). *Contribuições à Geologia da Amazônia, 1. Manaus, SBG/NO*, **2**: 201-224.

Luz B.R. & Crowley J.K. 2012. Morphological and chemical evidence of stromatolitic deposits in the 2.75 Ga Carajás banded iron formation, Brazil. *Earth and Planetary Science Letters*, **355**:60-72.

Macambira J.B. 2003. *O ambiente deposicional da Formação Carajás e uma proposta de modelo evolutivo para a Bacia Grão Pará*. Ph.D Thesis, Universidade Estadual de Campinas, São Paulo, 217 p.

Macambira J.B., Ramos J.F.F., Assis J. F. P., Figueiras A. J. M. 1990. *Projeto Serra Norte*. Conv. Seplan/DOCEGEO/UFPa. Projeto Pojuca. Convênio DNPM/DOCEGEO/UFPa. Relatório final. 150 p.

Machado N., Lindenmayer Z., Krogh T.E., Lindenmayer D. 1991. U-Pb geochronology of Archean magmatism and basement reactivation in the Carajás area, Amazon shield, Brazil. *Precambrian Research*, **49**:329-354.

Mange, M.A. & Maurer, H.F.W. 1992. *Heavy Minerals in Color*. London, Chapman and Hall. 147p.

Marangoanha, B. 2018. *Petrologia e evolução crustal da porção central do Domínio Canaã Dos Carajás, Província Carajás*. PhD Theses, Universidade Federal do Pará, Belém, 224 pp.

Martins P.L.G., Toledo, C.L.B., Silva A.M., Chemale Jr F., Santos J.O.S., Assis L.M. 2017. Neoarchean magmatism in the southeastern Amazonian Craton, Brazil:

Petrography, geochemistry and tectonic significance of basalts from the Carajás Basin. *Precambrian Research*, **302**:340–357.

McCulloch M. T. & Wasserburg G. J. 1978. Sm-Nd and Rb-Sr Chronology of Continental Crust Formation. *Science*, **200** (4345), 1003-1011.

Meinhold, G., Morton, A. C., & Avigad, D. 2013. New insights into peri-Gondwana paleogeography and the Gondwana super-fan system from detrital zircon U–Pb ages. *Gondwana Research*, **23**(2), 661–665.

Melchin, M. J., Sadler, P. M., Cramer, B. D. 2012. The Silurian Period. With contributions by R. Cooper, O. Hammer and F. M. Gradstein. *In*: Gradstein, F. M., Ogg, J. G., Schmitz, M., Ogg, G. et al. (Eds.), *The Geological Time Scale*. Elsevier. pp. 525–59.

Melo J.H.G. 1997. *Resultados de solicitação de análise palinológica em amostras de superfície da região da represa Balbina (AM), Bacia do Amazonas*. Comunicação técnica SEBIPE 10/97. Petrobrás. (Relatório interno).

Melo J.H.G. & Steemans P. 1997. *Resultados de investigações palinoestratigráficas em amostras de superfície da região de Presidente Figueiredo (AM), Bacia do Amazonas*. Comunicação técnica SEBIPE 048/97. Petrobrás. (Relatório interno).

Melo G.H.C, Monteiro L.V.S, Xavier R.P, Moreto C.P.N, Arquaz R.M., Silva M.A.D. 2019. Evolution of the Igarapé Bahia Cu-Au deposit, Carajás Province (Brazil): Early syngenetic chalcopyrite overprinted by IOCG mineralization. *Ore Geology Reviews*, **111**:102993.

Miall, A.D. 1985. Architectural-element analysis: a new method of facies analysis applied to fluvial deposits. *Earth Science Reviews*, **22**(4), 261-300.

Miall, A.D. 1996. *The Geology of Fluvial Deposits: Sedimentary Facies, Basin Analysis, and Petroleum Geology*. Springer Verlag; 582p.

Miall, A.D. & Tyler, N. 1991.The Three-Dimensional Facies Architecture of Terrigenous Clastic Sediments and Its Implications for Hydrocarbon Discovery and Recovery. Tusla, *SEPM research Symposium*, Concepts in Sedimentology and Paleontology.

Mizusaki A.M.P., Melo J.H.G., Vignol-Lelarge M.L., Steemans P. 2002. Vila Maria Formation (Silurian, Paraná Basin, Brazil): integrated radiometric and palynological age determinations. *Geological Magazine*. **139** (4): 453–463.

Moreto C.P.N., Monteiro L.V.S., Xavier R.P., Creaser R.A., DuFrane S.A., Tassinari C.C.G., Sato K., Kemp A.I.S., Amaral W.S. 2015. Neoarchean and Paleoproterozoic iron oxide-copper-gold events at the Sossego Deposit, Carajas Province, Brazil: Re-Os and U-Pb geochronological evidence. Econ. Geol. 110: 809-835.Morris R.C. 1993. Genetic modeling for banded iron-formation of the Hamersley Group, Pilbara Craton, Western Australia. *Precambrian Research*, **60**(1-4): 243-286.

Morton A. C. 1985. Heavy minerals in provenance studies. *In*: Zuffa, G. G. ed. *Provenance of Arenites*. Dordrecht, Reidel Publishing Company, p. 249-277.

Morton A.C. & Hallsworth C.R. 1994. Identifing provenance-specific features of detrital heavy mineral assemblages in sandstones. *Sedimentary Geology*, **90**, 241-256.

Morton A.C. & Hallsworth C.R. 1999. Processes controlling the decomposition of heavy mineral assemblages in sandstones. *Sedimentary Geology*, **124**, 3-29.

Morton, A.C., Hallsworth, C.R., Chalton, B., 2004. Garnet compositions in Scottish and Norwegian basement terrains: a framework for interpretation of North Sea sandstone provenance. *Marine and Petroleum Geology*, **21**, 393–410.

Munnecke, A., Calner, M., Harper, D., Servais, T. 2010. Ordovician and Silurian Sea–water chemistry, sea level, and climate: A synopsis. *Palaeogeography, Palaeoclimatology, Palaeoecology*, **296**, 389-413.

Nogueira A.C.R. 1995. *Análise faciológica e aspectos estruturais da Formação Águas Claras, Região Central da Serra dos Carajás-Pará.* MS Dissertation, Instituto de Geociências, Universidade Federal do Pará, Belém, 168 p.

Olszewski W.J., Wirth K.R., Gibbs A.K., Gaudette H.E. 1989. The age, origin, and tectonics of the Grão Pará Group and associated rocks, Serra dos Carajás, Brazil: Archean continental volcanism and rifting. *Precambrian Research*, **42,** 229-254.

Pereira, R. M. P., 2009. *Geologia da Região Sul da Serra Norte e Características do Minério de Ferro do Depósito N8, Província Mineral Carajás*. MS dissertation, Universidade Federal de Minas Gerais, Brazil, pp.131.

Pinheiro R.V.L., 1997. *Reactivation history of the Carajás and Cinzento Strike Slip Systems, Amazon, Brazil.* Ph.D Thesis, Durham, Inglaterra, 408p.

Pinheiro, R.S.de C., 2019. *Evolução paragenética e regime de fluidos no sistema Cu-Co Tarzan, Província Carajás.* MS dissertation, Universidade Estadual de Campinas (UNICAMP), Brasil, 122p.

Plummer, P.D. 1946. *Geossinclíneo do Parnaíba*. Conselho Nacional do Petróleo. Relatório de 1946. Rio de Janeiro, 1948. *PETOBRAS*, pp. 87–134.

Pohl, A., Donnadieu, Y., Le Hir, G., Ladant, J.-B., Dumas, C., Alvarez-Solas, J., Vandenbroucke, T.R.A., 2016. Glacial onset predated Late Ordovician climate cooling, *Paleoceanography*, **31**, 800–821.

Porto A., Daly M.C., La Terra E., Fontes S.L. 2018. The pre-Silurian Riachão Basin: a new perspective on the basement of the Parnaiba Basin, NE Brazil. In: Daly M. C., Fuck R. A., Julià J., MacDonald D.I.M., Watts A. B. Cratonic basin form. A case study Parnaiba basin Brazil. London, *Geological Society of London*, **472**, 127-145.

Ramos, J.F. da F.; Moura, C.A.V.; Melo, CF.de; Pereira, J.L.; Serique, J.S.C.; & Rodrigues, R.M. 1984. Uma discussão sobre sequencias sedimentares tidas como Formação Rio Fresco, Sudeste do Para. In: SBG 33°, Congresso Brasileiro de Geologia, Rio de Janeiro, *Anais* [...]. v. 2, p. 862-872.

Rodrigo L.A., Castaños A., Carrasco R. 1977. La formación cancañiri: sedimentología y paleogeografía. *Revista de Geociencias de la Universidad Mayor de San Andrés*. **1**, 1–22.

Rodrigues R. 1967. *Estudo sedimentológico e estratigráfico dos depósitos silurianos e devonianos da Bacia do Parnaíba*. Petrobras. RENOR, Belém, Brasil. (Relatório Interno no 273M).

Rossignol, C., Antonio, P., Narduzzi, F., Siciliano Rego, E., Teixeira, L., Almeida de Souza, R., Ávila, J., Silva, M., Lana, C., Trindade, R., Philippot, P., 2022. Unraveling one billion years of geological evolution of the southeastern Amazonian Craton from detrital zircon analyses. *Geoscience Frontiers*. **13**, 101202.

Scotese, C. 2016. *Some Thoughts on Global Climate Change*: The Transition for Icehouse to Hothouse Conditions.

Scotese, C.R.; Boucot, A.J., Mckerrow, W.S. 1999. Gondwana palaeogeography and palaeoclimatology. *Journal of African Earth Sciences*, **28**(1):99-114.

Serique, J.S.C.B, & Ramos, J. F. da F. 1984. Aspectos petrograficos dos sedimentos Precambrianos da Serra do Paredao. SBG, 33° Congresso Brasileiro de Geologia, Rio de Janeiro, *Anais* [...]. 2, p. 886-893.

Sheehan, P. M. 2001. The Late Ordovician Mass Extinction. *Annual Review of Earth and Planetary Sciences*, **29** (1): 331–364.

Small, H. 1914. *Geologia e suprimento d'água subterrânea no Piauí e parte do Ceará*: Brasil. Rio de Janeiro, Inspectoria Federal de Obras contra as Secas. 146 p (Série 1- D, publ. 32).

Soares E. A. A. 1998. *Fáceis litorâneas glaciais da formação Nhamundá (Siluriano inferior), na região de Presidente Figueiredo, AM, Bacia do Amazonas*. MS Dissertation, Centro de Geociências, Universidade Federal do Pará, Belém, 74p.

Sproson, A., Pogge, S., Selby, D., Jarochowska, E., Fryda, J., Hladil, J., Loydell, D., Slavík, L., Calner, M., Maier, G., Munnecke, A., Lenton, T., 2022. Osmium and lithium isotope evidence for weathering feedbacks linked to orbitally paced organic carbon burial and Silurian glaciations. *Earth and Planetary Science Letter,* **577**. 117260.

Squire, R. J., Campbell, I. H., Allen, C. M., & Wilson, C. J. L. 2006. Did the Transgondwanan Supermountain trigger the explosive radiation of animals on Earth? *Earth and Planetary Science Letters*, **250**(1-2), 116 - 133.

Stacey J.S. & Kramers J.D. 1975. Approximation of terrestrial lead isotope evolution by a two-stage model. *Earth and Planetary Science Letter,* **26,** 207–221.

Stampfli, G.M. & Borel, G.D. 2002. A plate tectonic model for the Paleozoic and Mesozoic constrained by dynamic plate boundaries and restored synthetic oceanic isochrones. *Earth and Planetary Science Letters*, **196**, 17–33.

Stampfli, G.M., von Raumer, J., Wilhem, C., 2011. The distribution of Gondwana-derived terranes in the early Paleozoic. *In*: Gutiérrez-Marco, J.C., Rábano, I., García-Bellido, D. (Eds.), *The Ordovician of the World*. Madrid. Instituto Geológico y Minero de España, p. 567–574. (Cuadernos del Museo Geominero, v. 14).

Stern, R.J., 1994. Arc assembly and continental collision in the Neoproterozoic East African Orogen: implications for the assembly of Gondwanaland. *Annual Review of Earth and Planetary Sciences*, **22**, 319–351.

Tallarico F.H.B., Figueiredo B.R., Groves D.I., Kositcin N., McNaughton N.J., Fletcher I.R., Rego J.L. 2005. Geology and SHRIMP U-Pb geochronology of the Igarapé Bahia deposit, Carajás copper-gold belt, Brazil: an Archean (2.57 Ga) example of iron-oxide Cu-Au-(UREE) mineralization. *Economic Geology*, **100**, 7-28.

Tavares, F. M., Trouw, R. A. J., da Silva, C. M. G., Justo, A. P., & Oliveira, J. K. M. (2018). The multistage tectonic evolution of the northeastern Carajás Province, Amazonian Craton, Brazil: Revealing complex structural patterns. *Journal of South American Earth Sciences*, **88**, 238–252.

Timothée, M., Florent, B., Hardy Meddry Dieu-Veill, N., Damien, D. 2024. The Cambro-Ordovician Gondwana alluvial megafan in Central Africa: Insights from the Paleozoic sandstones of the Inkisi group, Congo Republic and Democratic Republic of the Congo. *Journal of African Earth Sciences*, **209**, 105109.

Trendall A.F., Basei M.A.S., De Laeter J.R., Nelson D.R. 1998. SHRIMP U-Pb constraints on the age of the Carajas Formation, Grao Para Group, Amazon Craton. *Journal of South American Earth Sciences,* **11**:265-277.

Vaz, P.T., Resende, N.G.A.M., Wanderley Filho, J.R., Travassos, W.A. 2007. Bacia do Parnaíba. Rio de Janeiro, PETROBRÁS, *Boletim de Geociências*, **15**(2):253-263.

von Raumer, J.F., & Stampfli, G.M. 2008. The birth of the Rheic Ocean—Early Palaeozoic subsidence patterns and subsequent plate tectonic scenarios. *Tectonophysics,* **461**, 9–20.

Walker R.G. 1992. Facies, facies models and modern stratigrahic concepts. *In*: R.G. Walker, N.P. James. (ed). *Facies Models - Response to Sea Level Change*. Ontario, Geological Association of Canada, p. 1-14.

Wetherill, G.W. 1956. Discordant uranium-lead ages, I. Transactions. *American Geophysical Union*, **37**, 320-326.

Whittaker, A. C., Attal, M., Allen, P. A. 2010. Characterizing the origin, nature and fate of sediment exported from catchments perturbed by active tectonics. *Basin Research*, **22**(6), 809-828.

Wizevic, M.C. 1991. Photomosaic of outcrops: useful photomographic techniques. *In*: Miall A.D. e Tyler N. (ed). *The three-dimensional facies architecture of terrigenous clastic sediments and its implications for hydrocarbon discovery and recovery*. Oklahoma, SEPM, Society for Sedimentary Geology, p. 22-24.

Ziegler, A.M., Hutver, M.L., Rowley, D.B. 1997. Permian world topography and climate. *In*: Martini, I.P. (ed.) *Late glacial and postglacial environmental changes - quaternary, Carboniferous-Permian and Proterozoic*. New York: Oxford University Press, p.111-146.

Zucchetti, M. 2007. *Rochas máficas do Grupo Grão-Pará e sua relação com a mineralização de ferro dos depósitos N4 e N5, Carajás, PA*. PhD Theses, Belo Horizonte, MG, Brazil, 125p.

UNIVERSIDADE FEDERAL DO PARÁ
INSTITUTO DE GEOCIÊNCIAS
PROGRAMA DE PÓS-GRADUAÇÃO EM GEOLOGIA E GEOQUÍMICA

ATA/PARECER

Sobre a Defesa Pública da Tese de Doutorado de IVAN ALFREDO ROMERO BARRERA

Aos dezoito dias do ano de dois mil e vinte e quatro, às 14h, reuniu-se a banca examinadora para a apresentação da Tese de Doutorado de **IVAN ALFREDO ROMERO BARRERA** orientando do Prof. Dr. Afonso Cesar Rodrigues Nogueira (UFPA) e composta pelos professores doutores Gelson Luís Fambrini (UFPE), Renato Sol Paiva de Medeiros (UFPA), Francisco Romério Abrantes Junior (UFF) e Candido Augusto Veloso Moura (UFPA**),** após apresentação por vídeo conferência da tese intitulada **"A SUCESSÃO CAMBRIANA-SILURIANA DA BACIA DO PARNAÍBA E PROVÍNCIA MINERAL DE CARAJÁS: PALEOAMBIENTE, PROVENIÊNCIA E EXTENSÃO DA GLACIAÇÃO SILURIANA NO GONDWANA OESTE"** emite o seguinte parecer:

O candidato realizou sua apresentação de forma clara, bem-organizada e segura no tempo estipulado. Na arguição mostrou domínio da temática abordada e respondeu às perguntas formuladas pela banca. O trabalho escrito foi apresentado na forma de três artigos, todos submetidos a periódicos de impacto internacional. Dessa forma, o documento apresentado atende às exigências básicas para uma tese de doutorado.

Finalmente, a banca examinadora decidiu por unanimidade aprovar **COM DISTINÇÃO** a tese de doutorado.

Belém, 18 de dezembro de 2024

Prof. Dr. AFONSO CESAR RODRIGUES NOGUEIRA (Orientador-UFPA)

Prof. Dr. GELSON LUÍS FAMBRINI (Membro-UFPE)

gov.br Documento assinado digitalmente
GELSON LUIS FAMBRINI
Data: 18/12/2024 20:54:00-0300
Verifique em https://validar.iti.gov.br

Prof. Dr. RENATO SOL PAIVA DE MEDEIROS (UFPA)

gov.br Documento assinado digitalmente
RENATO SOL PAIVA DE MEDEIROS
Data: 19/12/2024 14:36:00-0300
Verifique em https://validar.iti.gov.br

Prof. Dr. FRANCISCO ROMÉRIO ABRANTES JUNIOR (UFF)

gov.br Documento assinado digitalmente
FRANCISCO ROMERIO ABRANTES JUNIOR
Data: 19/12/2024 10:43:32-0300
Verifique em https://validar.iti.gov.br

Prof. Dr. CANDIDO AUGUSTO VELOSO MOURA (UFF)

gov.br Documento assinado digitalmente
CANDIDO AUGUSTO VELOSO MOURA
Data: 20/12/2024 10:00:56-0300
Verifique em https://validar.iti.gov.br

UNIVERSIDADE FEDERAL DO PARÁ
INSTITUTO DE GEOCIÊNCIAS
PROGRAMA DE PÓS-GRADUAÇÃO EM GEOLOGIA E GEOQUÍMICA

UNIVERSIDADE FEDERAL DO PARÁ
PROGRAMA DE PÓS-GRADUAÇÃO EM GEOLOGIA E GEOQUÍMICA
TESE APROVADA COM DISTINÇÃO
Instituto de Geociências

ATA/PARECER

Sobre a Defesa Pública da Tese de Doutorado de IVAN ALFREDO ROMERO BARRERA

A banca examinadora da Tese de Doutorado de **IVAN ALFREDO ROMERO BARRERA** orientando do Prof. Dr. Afonso Cesar Rodrigues Nogueira (UFPA) e composta pelos professores doutores Gelson Luís Fambrini (UFPE), Renato Sol Paiva de Medeiros (UFPA), Francisco Romerio Abrantes Junior (UFF) e Candido Augusto Veloso Moura (UFPA), após apresentação da sua tese intitulada **"A SUCESSÃO CAMBRIANA-SILURIANA DA BACIA DO PARNAÍBA E PROVÍNCIA MINERAL DE CARAJÁS: PALEOAMBIENTE, PROVENIÊNCIA E EXTENSÃO DA GLACIAÇÃO SILURIANA NO GONDWANA OESTE"** emite o seguinte parecer:

O candidato realizou sua apresentação de forma clara, bem-organizada e segura no tempo estipulado. Na arguição mostrou domínio da temática abordada e respondeu às perguntas formuladas pela banca. O trabalho escrito foi apresentado na forma de três artigos, todos submetidos a periódicos de impacto internacional. Dessa forma, o documento apresentado atende às exigências básicas para uma tese de doutorado.

Finalmente, a banca examinadora decidiu por unanimidade aprovar COM DISTINÇÃO a tese de doutorado.

Belém, 18 de dezembro de 2024

gov.br Documento assinado digitalmente
AFONSO CESAR RODRIGUES NOGUEIRA
Data: 26/12/2024 17:26:46-0300
Verifique em https://validar.iti.gov.br

Prof. Dr. AFONSO CESAR RODRIGUES NOGUEIRA (Orientador-UFPA)

Prof. Dr. GELSON LUÍS FAMBRINI (Membro-UFPE) gov.br Documento assinado digitalmente
GELSON LUIS FAMBRINI
Data: 18/12/2024 20:54:00-0300
Verifique em https://validar.iti.gov.br

Prof. Dr. RENATO SOL PAIVA DE MEDEIROS (UFPA) gov.br Documento assinado digitalmente
RENATO SOL PAIVA DE MEDEIROS
Data: 19/12/2024 14:36:00-0300
Verifique em https://validar.iti.gov.br

Prof. Dr. FRANCISCO ROMÉRIO ABRANTES JUNIOR (UFF) gov.br Documento assinado digitalmente
FRANCISCO ROMERIO ABRANTES JUNIOR
Data: 19/12/2024 10:43:32-0300
Verifique em https://validar.iti.gov.br

Prof. Dr. CANDIDO AUGUSTO VELOSO MOURA (UFPA) gov.br Documento assinado digitalmente
CANDIDO AUGUSTO VELOSO MOURA
Data: 20/12/2024 10:00:56-0300
Verifique em https://validar.iti.gov.br